Using Mathematical Modelling and Electrochemical Analysis to Investigate Age-Associated Disease

Thesis submitted in accordance with the requirements of the University of Chester for the degree of Doctor of Philosophy
By

Amy Elizabeth Morgan
MRes, BSc (Hons), PGCertLTHE, FHEA

March 2019

University of Chester
Thornton Science Park
Pool Lane
Ince
Chester
CH2 4NU

Declaration

The material being presented for examination is my own work and has not been submitted for an award of this or another HEI except in minor particulars which are explicitly noted in the body of the thesis. Where research pertaining to the thesis was undertaken collaboratively, the nature and extent of my individual contribution has been made explicit.

Signed: ……………………………………………………..

Date: …………………………………………………….

Acknowledgements

Abbreviations

ABC-A1: Adenosine triphosphate binding cassette subfamily A member 1

ABCG5/G8: Adenosine triphosphate binding cassette subfamily G5/G8

AC: Alternating current

ACAT1: Acetyl-coenzyme A: cholesterol acetyltransferase 1

ACAT2: Acetyl-coenzyme A: cholesterol acetyltransferase 2

AD: Alzheimer's disease

Akt (PKB): Protein kinase B

apo: Apolipoprotein

ASBT: Apical sodium dependent bile acid transporter

ATP: Adenosine triphosphate

Au-RDE: Gold rotating disk electrode

Au-SPE: Gold screen printed electrode

BMI: Body mass index

BSEP: Bile salt export pumps

BSH: Bile salt hydrolase

CAD: Coronary artery disease

CALERIE: Comprehensive Assessment of Long-Term Effects of Reducing Calorie Intake

CEH: Cholesterol ester hydrolase

CETP: Cholesteryl ester transfer protein

CHD: Coronary heart disease

CKK: Cholecystokinin

CpG: Cytosine-guanine dinucleotide

CR: Caloric restriction

CRP: C-reactive protein

ctDNA: Circulating tumour DNA

CV: Cyclic voltammetry/voltammogram

CV50: Cyclic voltammetry/voltammogram at 50mV/s

CV200: Cyclic voltammetry/voltammogram at 200mV/s

CVD: Cardiovascular disease

CYP7AI: Cholesterol 7-alpha-hydroxylase

DASH: Dietary Approaches to Stop Hypertension

DCE: Dietary cholesterol esters

ΔE_p: Peak to peak separation

DFC: Dietary free cholesterol

DNA: Deoxyribonucleic acid

dNTPs: Deoxynucleotide triphosphates

DPV: Differential pulse voltammetry

dsDNA: Double stranded DNA

EIS: Electrochemical impedance spectroscopy

EMEM: Eagle's minimal essential medium

EN1: engrailed homeobox 1 gene

E_p^{ox}: Peak oxidation potential against Ag/AgCl reference electrode

E_p^{red}: Peak reduction potential against Ag/AgCl reference electrode

FBA: Foetal bovine serum

FFA: Free fatty acid

GH: Growth hormone

FoxO3: Forkhead box O 3

HCBA: Hepatic conjugated bile acid

HCE: Hepatic cholesterol esters

HDL: High density lipoprotein

HDL-C: High density lipoprotein cholesterol

HFC: Hepatic free cholesterol

HL: Hepatic lipase

HLDLRs: Hepatic low density lipoprotein receptors

HMG-CoA: 3-hydroxy-3-methylglutaryl CoA

HSL: Hormone sensitive lipase

HSP: Heat shock protein

HUBA: Hepatic unconjugated bile acid

ICBA: Ileocytic conjugated bile acid

IDL: Intermediate density lipoprotein

IDL-C: Intermediate density lipoprotein cholesterol

IHD: Ischemic heart disease

i_{bp}: Current before pulse

i_p: Current at pulse

i_{pa}: Peak anodic current

i_p^{ox}: Peak oxidation current

i_p^{red}: Peak reduction current

IUBA: Ileocytic unconjugated bile acid

KO: Knock out

LCAT: Lecithin-cholesterol acyltransferase

LCBA: (Intestinal) Lumen conjugated bile acid

LDL: Low density lipoprotein

LDL-C: Low density lipoprotein cholesterol

LDLr: Low density lipoprotein receptor

LPL: Lipoprotein lipase

LRP: Low density lipoprotein receptor-related protein

LUBA: (Intestinal) Lumen unconjugated bile acid

LVC: Longevity village communities

LXRα: Liver X receptor α

MCP-1: Monocyte chemotactic protein 1

MTHFR: Methylenetetrahydrofolate reductase

mTOR: Mechanistic target of rapamycin

mTORC1: Mechanistic target of rapamycin complex 1

mTORC2: Mechanistic target of rapamycin complex 2

MTP: Microsomal triglyceride transfer protein

MUFA: Monounsaturated fatty acid

ndHDL: Nascent HDL

NEAA: Non-essential amino acids

NO: Nitric oxide

NPC1L1: Niemann-pick C1-like 1

ODE: Ordinary differential equation

OTU: Operational taxonomic unit

ox-HDL: Oxidised high density lipoprotein

ox-LDL: Oxidised low density lipoprotein

PAMP: Pathogen associated pattern

PBS: Phosphate buffered saline

PCE: Peripheral cholesterol esters

PCR: Polymerase chain reaction

PDGF: Mitogen platelet derived growth factor

P-DMRs: Prenatal malnutrition-associated differentially methylated regions

PFC: Peripheral free cholesterol

P_H: Pulse height

PI3K: Phosphatidylinositol 3-kinase

PLTP: Phospholipid transfer protein

PSCK9: Proprotein convertase subtilisin kexin-9

PUFA: Polyunsaturated fatty acid

P_W: Pulse width

RCT: Reverse cholesterol transport

R_{ct}: Charge transfer resistance

Reg3g: Regenerating islet-derived 3 gamma

ROS: Reactive oxygen species

RSD: Relative standard deviation

SA: Sensitivity analysis

SAH: S-adenosyl homocysteine

SAM: S-adenosyl methionine

SBML: Systems biology markup language

SCS: Seven Countries Study

SD: Standard devation

SFA: Saturated fatty acid

S_H: Step height

S_i: Sensitivity coefficient

Sirt6: Sirtuin 6

SNP: Single nucleotide polymorphism

SR-BI: Scavenger receptors of class B type I

SREBP-2: Sterol-regulatory element binding protein 2

ssDNA: Single stranded DNA

S_T: Step time

TC: Total cholesterol

TG: Triglyceride

TNF-α: Tumour necrosis factor α

T2DM: Type II diabetes mellitus

UTC: Urbanised town communities

VLDL: Very low density lipoprotein

VLDL-C: Very low density lipoprotein cholesterol

WGA: Whole genome amplified

Z: Impedance

Abstract

People are living longer. With this rise in life expectancy, a concomitant rise in morbidity in later life is observed; with conditions including cardiovascular disease (CVD), and cancer. However, ageing and the pathogenesis of age related disease, can be difficult to study, as the ageing process is a complex process, which affects multiple systems and mechanisms. The aim of this research was two-fold. The first aim was to use mathematical modelling to investigate the mechanisms underpinning cholesterol metabolism, as aberrations to this system are associated with an increased risk for CVD. To better understand cholesterol from a mechanistic perspective, a curated kinetic model of whole body cholesterol metabolism, from the BioModels database, was expanded in COPASI, to produce a model with a broader range of mechanisms which underpin cholesterol metabolism. A range of time course data, and local and global parameter scans were utilised to examine the effect of cholesterol feeding, saturated fat feeding, ageing, and cholesterol ester transfer protein (CETP) genotype. These investigations revealed: the model behaved as a hypo-responder to cholesterol feeding, the robustness of the cholesterol biosynthesis pathway, and the impact CETP can have on healthy ageing. The second aim of this work was to use electrochemical techniques to detect DNA methylation within the engrailed homeobox 1 (EN1) gene promoter, which has been implicated in cancer. Hypermethylation of this gene promoter is often observed in a diseased state. Synthetic DNA, designed to represent methylated and unmethylated variants, were adsorbed onto a gold rotating disk electrode for electrochemical analysis by 1) electrochemical impedance spectroscopy (EIS), 2) cyclic voltammetry (CV) and 3) differential pulse voltammetry (DPV). The technique was then applied to bisulphite modified and asymmetrically amplified DNA from the breast cancer cell line MCF-7. Results indicated that electrochemical techniques could detect DNA methylation in both synthetic and cancer derived DNA, with EIS producing superior results. These non-traditional techniques of studying age related disease were effective for the investigation of cholesterol metabolism and DNA methylation, and this work highlights how these techniques could be used to elucidate mechanisms or diagnose/monitor disease pathogenesis, to reduce morbidity in older people.

Contents

Figures

Tables

Chapter 1 Introduction

Ageing is described as the accumulation of detrimental changes at the cellular and tissue levels, which result in an increased risk of disease and premature death (Tosato et al., 2007). It is a complex process, and thus there are several theories as to how ageing occurs (Lipsky and King, 2015; Mercado-Sáenz et al., 2010). For instance, the cross linking theory of ageing suggests that glucose binds to proteins as we age, impairing biological function (Bjorksten, 1968), while another theory suggests that the accumulation of intracellular waste products is responsible for cellular ageing (Hirsch, 1986). The free radical theory of ageing, proposed by Harman in 1956, suggests the gradual accumulation of free radical damage on cell components and connective tissue is the cause of ageing (Harman, 1956; Harman, 1972). Alternatively, the shortening of telomeres with each cell division, has also been implicated in ageing (Harley et al., 1990; Shammas, 2011). From these, and many other examples it is clear ageing is a complex process that is likely underpinned by changes to multiple aspects of cellular biology. Its complexity is further compounded by evidence that suggests ageing is regulated by both genetic and lifestyle factors. It is estimated that approximately 25% of the variation in human longevity is genetically controlled, while the remainder is associated with lifestyle factors (Passarino et al., 2016).

There are numerous diseases associated with ageing (Niccoli and Partridge, 2012), such as CVD (Dhingra and Vasan, 2012), neurodegeneration (Hindle, 2010), type II diabetes mellitus (T2DM) (Papier et al., 2016), and various forms of cancer (White et al., 2014). It is estimated that if the rate of chronic disease in older people continues to increase as it has done from 2010, there will be a 54% rise in older people with moderate to severe disability, and a 56% increase in public spending on continued care for these individuals by 2022 (Wittenberg et al., 2012). Therefore, reducing the risk of age related disease is vital, through lifestyle changes, the development of superior medication, and early diagnosis of disease. However, as ageing affects multiple systems and mechanisms, it is a problematic area of investigation that requires numerous complex and expensive analytical techniques to study it (Mooney et al., 2016).

Systems biology provides a suitable framework for dealing with the complexities of the ageing process (Borgqvist et al., 2017; Ideker et al., 2001). It aims to holistically investigate a system, by incorporating all mechanisms involved; through biological, mathematical and computational techniques (Breitling, 2010). Conversely, often in biological fields, biological systems are analysed in a reductionist way, focusing on one element of a system. However, as ageing is associated with the dysregulation of multiple pathways, which in turn, synergistically disrupt the normal biological mechanisms, and lead to the accumulation of detrimental changes, it would be short-sighted to focus on a single aspect of ageing. Using the systems biology approach, two key areas associated with ageing and disease are investigated using non-traditional techniques. Firstly, cholesterol metabolism is investigated using mathematical modelling. It is hoped this work will enable the elucidation of pathways associated with CVD, and highlight the role of ageing on the dysregulation of cholesterol metabolism. Furthermore, by examining the effect of system perturbations on LDL-C levels, it is possible that ways of ameliorating these changes, to reduce the risk of CVD, can be identified. Secondly, an electrochemical sensor is developed to detect DNA methylation changes in a gene promoter, because of its close association with cancer. With additional optimisation and validation, this inexpensive sensor could be used to rapidly detect early-stage cancer from a non-invasive blood test, thus enabling early treatment and long term survival for patients.

It is important to note, that although this work focuses on the use of mathematical modelling on cholesterol metabolism, and the use of electrochemistry in detecting DNA methylation, these techniques could be applied to other biological systems. For instance, electrochemical techniques could be used to determine changes to cholesterol metabolism or detect the onset of CVD, and DNA methylation could be mathematically modelled.

For instance, Valencia-Morales et al. (2015) reported that aortic lesion progression, from donors with atherosclerosis, was correlated with DNA methylation. Thus, it was proposed this marker of lesion severity, could act as a biomarker for atherosclerosis diagnosis and could potentially serve as a target

to ameliorate the lesion progression (Valencia-Morales et al., 2015). In another example, Guay et al. (2014) showed methylation of the ATP-binding cassette subfamily A member 1 (ABCA1) gene promoter was associated with ageing and coronary artery disease (CAD) risk. Methylation of the gene promoter for the ABCA1 receptor, which plays a key role in reverse cholesterol transport, was also associated with higher levels of cholesterol, a risk factor for CVD. Moreover, it was reported that methylation was reduced when acetylsalicylic acid therapy was administered (Guay et al., 2014). From these examples, it is clear that DNA methylation may be a way of monitoring CVD and the effect of treatment. Furthermore, as electrochemistry has been utilised in the detection of DNA methylation in cancer (Sina et al., 2018), it is possible this technique could be applied to other diseases such as CVD, by analysing a different gene promoter.

Additionally, there are several examples of DNA methylation being mathematically modelled (Jeltsch and Jurkowska, 2014; Pfeifer et al., 1990; Riggs and Xiong, 2004). The most recent of which, was published by Zagkos et al. (2019), who produced linear and nonlinear models of DNA methylation. The linear model was able to account for the overall epigenetic inheritance of DNA methylation, while the nonlinear model could predict hyper- and hypomethylated states within gene promoters (Zagkos et al., 2019). A Bayesian algorithm was later applied to the models for parameter estimation (Larson et al., 2019). In another example, McGovern et al. (2012) created a six compartment model of DNA methylation, based on DNA methyltransferase (dnmt) and ten-eleven translocation (tet) enzymatic activity, using a series of partial differential equations. The model included hydroxymethylcytosine, a newly discovered intermediate of the demethylation pathway, and could accurately predict DNA methylation, when compared to published experimental data of haematological malignancies (McGovern et al., 2012). Thus, from the examples outlined, it is clear that mathematical modelling can be employed to investigate DNA methylation, a regulatory system which is closely intertwined with the ageing process.

It is important to recognise the integrated nature of ageing and the techniques used to study it. The systems biology paradigm provides a suitable mechanism for studying the complexities of the ageing process (Borgqvist et al., 2017). In this work, cholesterol metabolism was explored through mathematical modelling, while electrochemical techniques were employed to detect aberrant DNA methylation as a sensor for cancer. Below is a list of the publications associated with each chapter.

Related publications

Chapter 1 - Part 1

Morgan, A.E., Mooney, K.M., Wilkinson, S.J., Pickles, N.A., Mc Auley, M.T., 2016. Cholesterol metabolism: A review of how ageing disrupts the biological mechanisms responsible for its regulation. Ageing Research Reviews 27, 108-124.

Morgan, A.E., Mooney, K.M., Wilkinson, S.J., Pickles, N.A., Mc Auley, M.T., 2016. Investigating cholesterol metabolism and ageing using a systems biology approach. Proceedings of the Nutrition Society 76(3), 378-391.

Chapter 1- Part 2

Morgan, A.E., Davies, T.J., Mc Auley, M.T., 2018. The role of DNA methylation in ageing and cancer. Proceedings of the Nutrition Society 77(4), 412-422.

Chapter 3

Morgan, A.E., Mooney, K.M., Wilkinson, S.J., Pickles, N.A., Mc Auley, M.T., 2016. Mathematically modelling the dynamics of cholesterol metabolism and ageing. Biosystems 145, 19-32.

1.1 PART 1: Cholesterol metabolism and ageing

1.1.1 Introduction

Life expectancy is increasing at a phenomenal rate, as shown in Figure 1.1 (Clio-Infra, 2016). If one examines life expectancy in the UK in 1982 and compares it to the projected value for 2082, then this demographic shift in favour of older people is truly emphasized (UNSD, 2016). Males and females born in 1982, had a life expectancy of 71.1 and 77.0 years respectively, while the projected values for 2082 are 89.7 and 92.6 years (OFNS, 2013). This has resulted in an ageing population (Figure 1.2). It is anticipated that the percentage of individuals in the UK over 60 years will double to 22% by 2050, when compared to 2000 (WHO, 2014). Moreover, by 2050 it is anticipated the number of individuals >80 years will quadruple (WHO, 2014).
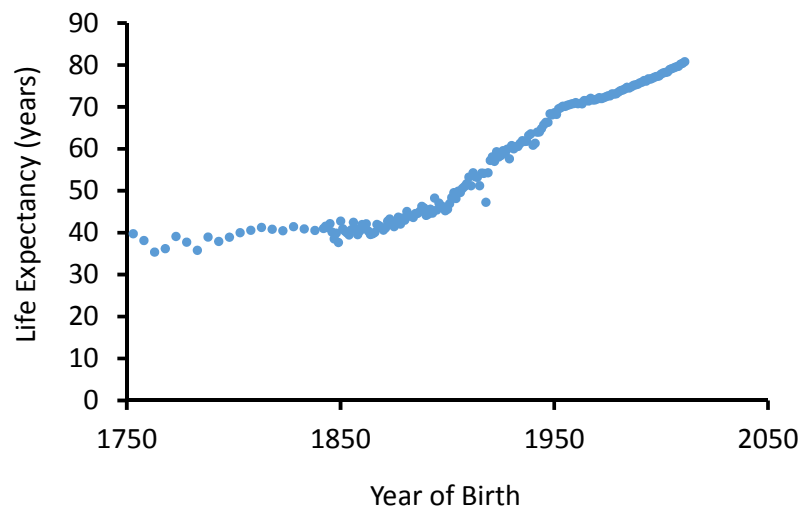
Figure 1.1 Life expectancy by year of birth.
Data taken from Clio-Infra (2016).

This increase in life expectancy comes with significant challenges. Most significant of these is maintaining health status by remaining disease free. Ageing is associated with increased CVD mortality and morbidity (Figure 1.3 and 1.4). Of the diseases which burden older people in the UK, CVD is the leading cause of morbidity (30.3%) in individuals ≥60 years of age (Prince et al., 2015). Additionally,

26

CVD is the leading cause of mortality in individuals over the age of 85 in the UK (Townsend et al., 2015). CVD has many risk factors, however plasma levels of total cholesterol (TC), low density lipoprotein cholesterol (LDL-C) are long established gold standard risk factors for CVD (Appelman et al., 2015). Specifically, increases in both total and LDL-C result in an elevated CVD risk due to the association of LDL-C with atherosclerotic plaque formation (Austin et al., 1988). Conversely, raised levels of high density lipoprotein cholesterol (HDL-C) are associated with a decreased CVD risk, due to its role in removing cholesterol deposits from the tissues (Cooney et al., 2009).
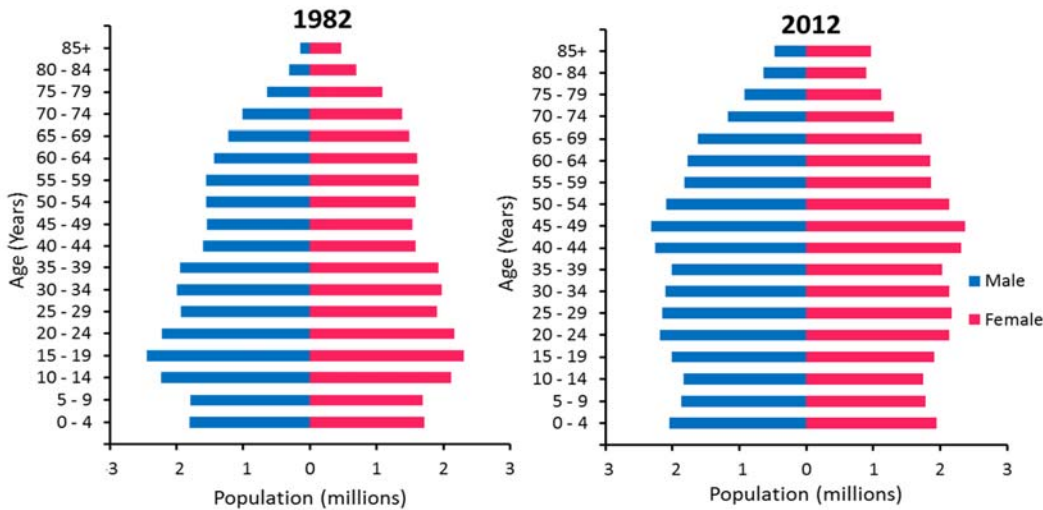
Figure 1.2 UK population by age group and gender in 1982 and 2012.
Data taken from UNSD (2016).
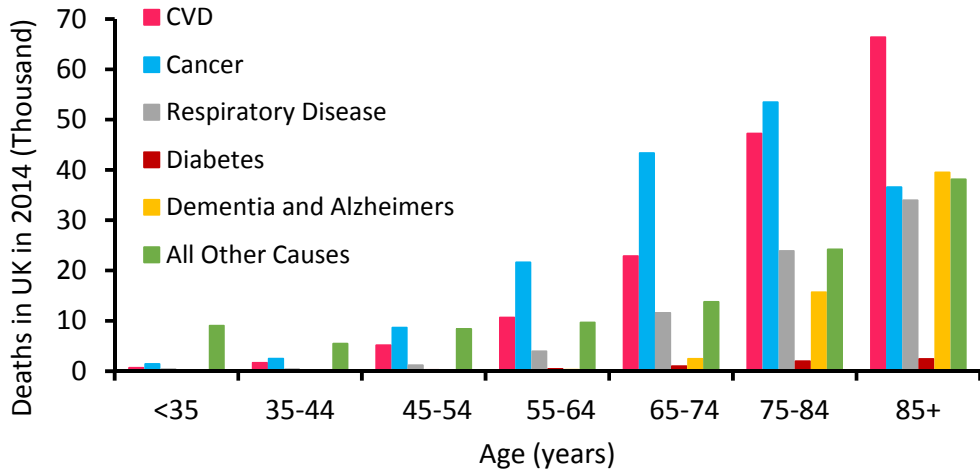
Figure 1.3 Disease mortality by age.
Data taken from Townsend et al. (2015).
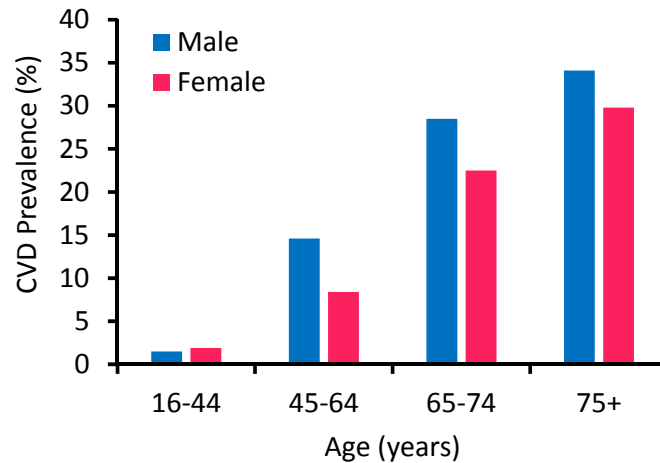
Figure 1.4 CVD morbidity by age and gender.
Data from Prince et al. (2015).

An intriguing feature of ageing, is that it is often accompanied by the dysregulation of whole body cholesterol metabolism (Mc Auley and Mooney, 2014). Whole body cholesterol metabolism is regulated by a number of factors including cholesterol synthesis, intestinal cholesterol absorption, hepatic cholesterol uptake (known as reverse cholesterol transport), cholesterol excretion, bile acid production, and deconjugation by intestinal microflora and subsequent excretion. Changes to any of these mechanisms can dysregulate cholesterol metabolism (Morgan et al., 2016a). A clinical manifestation of this dysregulation, is an age-related rise in the plasma levels of LDL-C (Abbott et al., 1983). On a population basis, ageing has been shown to result in a rise in both total and LDL-C in males and females (McQueen et al., 2008). For example, as shown in Figure 1.5, data from the Framingham Study demonstrates there is a gradual rise in LDL-C from an initial value of ~100mg/dL (2.59mmol/L) in 15-19 year olds (males and females), to 143mg/dL (3.70mmol/L) and 159mg/dL (4.11mmol/L) in 60-64 year olds, males and females respectively. Beyond the 6th decade, LDL-C levels continue to rise in females, however they marginally decline in males within this population (Abbott et al., 1983). The rise in LDL-C has a significant impact on CVD risk, due to the association elevated plasma LDL-C has with the mechanisms which underpin atherosclerotic plaque formation (Gould et al., 2007). Therefore, the slight decline in LDL-C observed in males in this study, could be because those susceptible to the

effect of higher levels of LDL-C have already died, and thus cannot be included in the study (Lv et al., 2015).
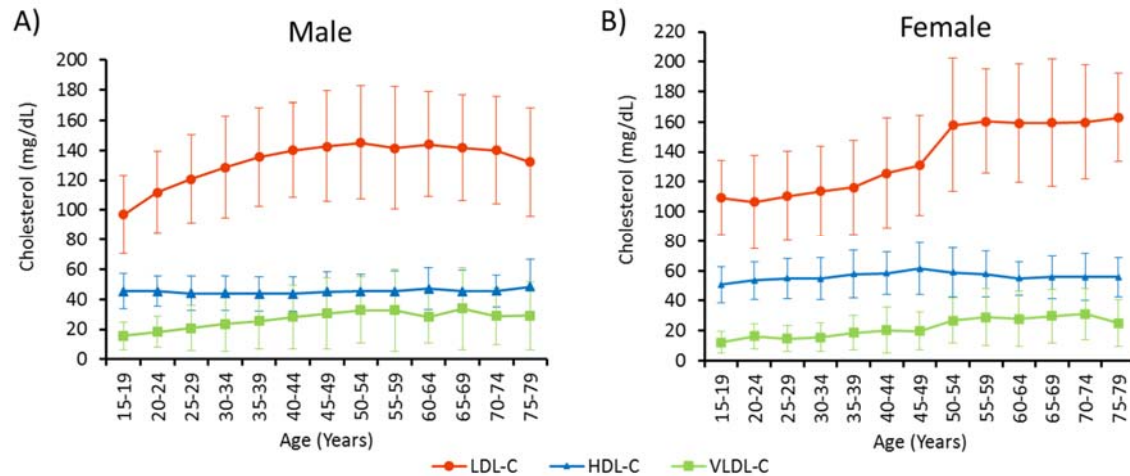
Figure 1.5 LDL-C, HDL-C, and VLDL-C trend with age.
Data taken from Abbott et al. (1983), of trends in cholesterol for A) males and B) females. LDL-C, low density lipoprotein cholesterol; HDL-C, high density lipoprotein cholesterol; VLDL-C very low density lipoprotein cholesterol.

Conversely, one prospective study, which followed 2,222 men and 2,677 women over 8 years, showed that HDL-C levels diminish with age (Wilson et al., 1994). However, Figure 1.5 demonstrates data from the Framingham study show the level of HDL-C is unaffected by ageing (Abbott et al., 1983). HDLs are central to reverse cholesterol transport (RCT) (Groen et al., 2004). This process, which results in the trafficking of HDL-C, or the so-called 'good cholesterol' to the liver for subsequent removal via the intestine, represents the only way of eliminating excess cholesterol from peripheral tissue. There is a plethora of epidemiological evidence supporting an inverse relationship between HDL -C levels and CVD risk, and evidence has consistently shown that HDL-C levels are correlated with longevity in several population groups (Ferrara et al., 1997). It is therefore not surprising, that a healthy ageing phenotype has regularly been associated with the fine tuning of cholesterol metabolism, within certain cohorts of individuals who possess particular genetic variants in tandem with exceptional longevity (Milman et al., 2014). For example, a three-fold increase in the prevalence of homozygosity

for the favourable I405V polymorphism, a mutation in the cholesteryl ester transfer protein (CETP), has been observed in those exhibiting exceptional longevity (Barzilai et al., 2003). Caused by a missense A>G mutation at exon 14 of chromosome 16, the isoleucine substitution for valine at codon 405, is associated with a 17% reduction in CETP; the enzyme which facilitates the 1:1 exchange of esterified cholesterol from HDL with TAGs from LDL and VLDL. Barzilai et al. (2003) found that the offspring of long lived individuals had significantly larger HDL and LDL particle sizes than their control counterparts. It was suggested that the reduced risk of atherosclerosis development, as a result of the diminished ability of the larger LDL particle to cross the arterial endothelium, could in part be responsible for the exceptional longevity displayed (Barzilai et al., 2003; Kulanuwat et al., 2015).

Many key mechanisms involved in cholesterol metabolism are affected by ageing (Figure 1.6). For instance, ageing has been associated with a decline in the hepatic expression of cholesterol 7-alpha-hydroxylase (CYP7AI), a key regulator of bile acid synthesis. This decline results in a decrease in the amount of cholesterol being converted to bile acids for excretion. Thus there is a reduced demand for cholesterol to be transported from plasma to the liver for this conversion (Bertolotti et al., 2007). Furthermore, there is a decline in hepatic LDL receptors (LDLr) with age, leading to a reduction in LDL-C clearance (Ericsson et al., 1991; Millar et al., 1995). Within the small intestine, there is an increase in the number of the sterol transporter Niemann-pick C1-like 1 (NPC1L1), a key mediator of cholesterol absorption (Duan et al., 2006). In addition, there is a decline in the predominant bacterial populations that play a role in the enterohepatic circulation of bile acids (Hopkins and Macfarlane, 2002). Moreover, dysregulation of cholesterol biosynthesis is associated with two key intracellular pathways which are thought to underpin intrinsic ageing and health-span. These pathways are defined by the mammalian/mechanistic target of rapamycin (mTOR) and by the NAD^+-dependent deacetylase silent information regulator proteins (sirtuins). The former of these pathways has been suggested as a central regulator of intracellular cholesterol homeostasis (Wang et al., 2011), while mammalian sirtuin 6 (Sirt6), has been identified as a critical controller of sterol-regulatory element binding protein (SREBP)-2 in rodents (Tao et al., 2013). These recent findings suggest that it is not one mechanism that

is the central driver of cholesterol dysregulation with age, but rather a number of mechanisms interacting with one another to disrupt cholesterol metabolism. Therefore, it is important to view cholesterol metabolism and its relationship with ageing in an integrated way.
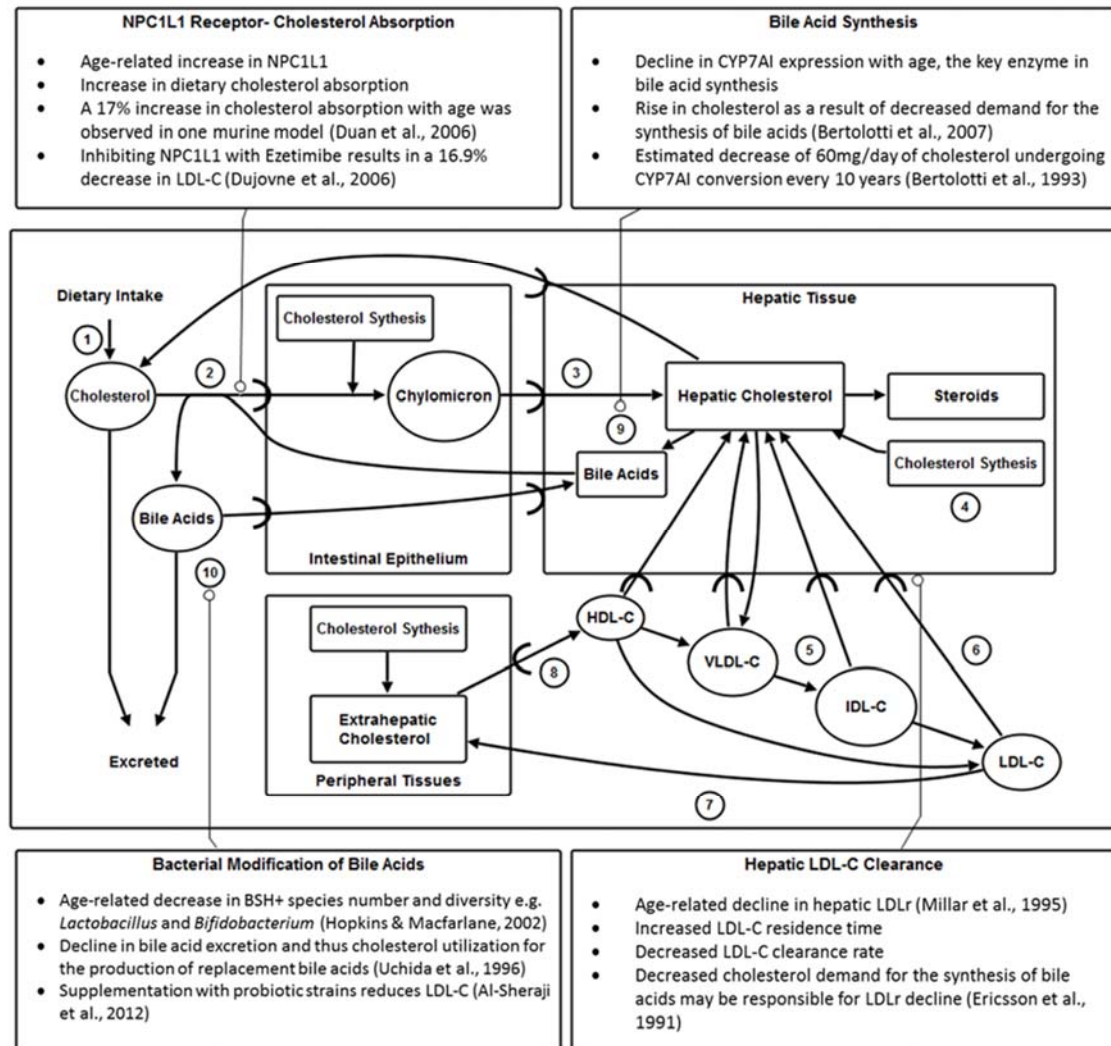
Figure 1.6 Overview of cholesterol metabolism and age associated changes to its mechanisms.
Briefly, outlined is 1) ingestion of dietary cholesterol, 2) intestinal absorption, 3) chylomicron transport, 4) cholesterol biosynthesis, 5) VLDL-C production and hydrolysis to IDL-C and LDL-C, 6) hepatic uptake of LDL-C, 7) peripheral uptake of LDL-C, 8) reverse cholesterol transport, 9) bile acid synthesis, and 10) enterohepatic circulation of bile acids and bacterial modification. The age-related changes highlighted centre on some of the mechanisms responsible for the rise in LDL-C with age; the increase in intestinal absorption of cholesterol, the reduction of bile acid synthesis, the decrease in LDL-C clearance, and the decrease in BSH[+] species in the digestive microbiome.

1.1.2 Overview of cholesterol metabolism

Cholesterol plays a vital role in the human body, as it is an essential component of all cell membranes. In addition, it is the precursor of steroid hormones, which control a range of physiological functions. Cholesterol is also the precursor to bile acids, which are necessary for the intestinal absorption of cholesterol, fats and lipophilic vitamins. Cholesterol can be obtained from the diet, as well as being endogenously synthesised, the latter being the main source in humans (Gylling, 2004). The average UK male consumes ~300mg of cholesterol daily (Henderson et al., 2003), while cholesterol can be endogenously synthesised at a rate of 9.8mg/kg/day in healthy adults (Renfurm et al., 2004). Jones and Schoeller (1990) demonstrated that in men with an average weight of 69.8kg, 710mg of cholesterol could be synthesised (Jones and Schoeller, 1990). These intake and synthesis values balance with excretion rates; with 500mg per day of cholesterol excreted, and 500mg per day converted to bile acids for excretion (Lu et al., 2010). Thus, subtle balancing act between ingestion, absorption, synthesis and excretion is required whole body cholesterol metabolism. Figure 1.7 gives an overview of cholesterol metabolism (Morgan et al., 2016b):
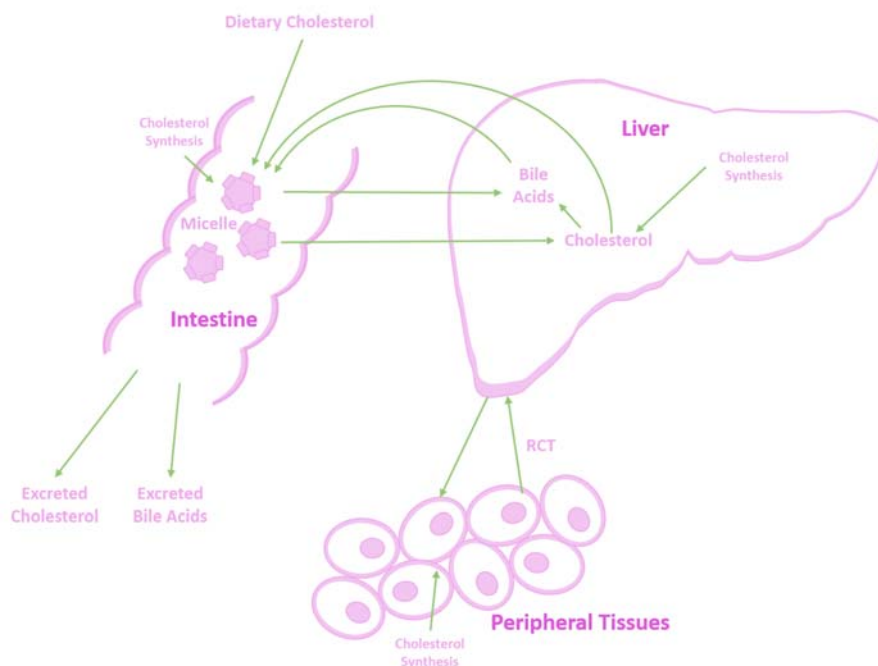
Figure 1.7 Overview of cholesterol metabolism.
Adapted from Morgan et al. (2016b).

1) The average daily intake of cholesterol is 304 ±127.7mg/day and 213 ±94.5mg/day, for males and females respectively, living in the UK (Henderson et al., 2003). Of this, 85-90% is free cholesterol while 10-15% is in the esterified form (Iqbal and Hussain, 2009). Ingested cholesterol then enters the small intestine, where it is absorbed (Tancharoenrat et al., 2014).

2) Cholesterol in the free form is more readily incorporated into a bile acid micelle for absorption. Therefore, cholesterol ester hydrolase (CEH)/cholesterol esterase/bile salt-dependent lipase (BSDL) converts the esterified cholesterol into free cholesterol, which can then be incorporated into a bile acid micelle, as shown in Figure 1.8 (Ikeda et al., 2002). This enables NPC1L1 to absorb the cholesterol by clathrin-mediated endocytosis (Betters and Yu, 2010). Plant sterols can also be absorbed via NPC1L1, although the majority of these are effluxed out by the heterodimer ATP-binding cassette (ABC) G5/G8 (Yu et al., 2014). Upon entry to the enterocyte, acetyl CoA:acetyltransferase 2 (ACAT2) converts the cholesterol into the esterified form in order to maintain the concentration gradient (Chang et al., 2009). Microsomal triglyceride transfer protein (MTP) then shuttles the esterified cholesterol with apo B-48, while triacylglycerol and phospholipids are also incorporated to form a nascent chylomicron (Jamil et al., 1995).
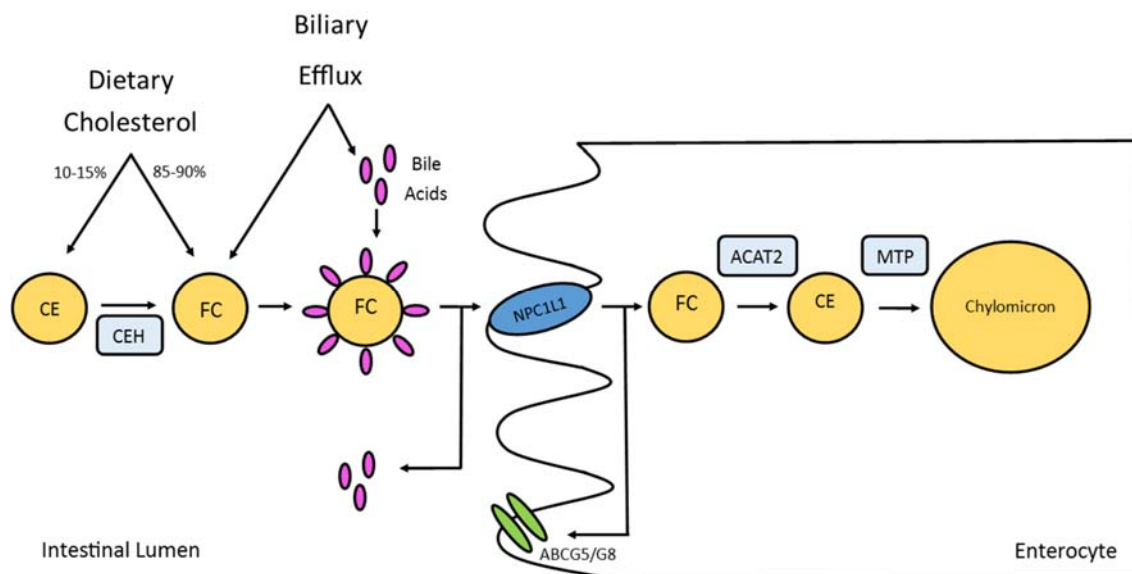
Figure 1.8 Overview of cholesterol absorption.

3) The nascent chylomicron exits the enterocyte via exocytosis and enters the lacteal. At this point, it exits the lymphatic system via the thoracic duct and enters the blood stream (Van Dyck et al., 2007). The acquisition of apo C-II and E from HDL converts the nascent chylomicron to a mature chylomicron. When delivered to adipose or muscle tissues, apo C-II enables the activation of lipoprotein lipase (LPL) found on the capillary endothelium. This catalyses the hydrolysis of the internalised TAG releasing glycerol and free fatty acids (FFAs) for the surrounding cells (Kersten, 2014; Olivecrona and Beisiegel, 1997). The chylomicron remnant returns the apo C-II to HDL and hepatocytes recognise apo B-48 and E, causing remnant receptors, LDLr and low density lipoprotein receptor-related protein (LRP), to uptake the chylomicron remnants for degradation (Cooper, 1997).

4) Cholesterol is also synthesised endogenously in all nucleated cells in the body, including the hepatocytes and enterocytes from acetyl CoA (Bloch, 1965). As outlined in Figure 1.9, acetoacetyl CoA thiolase catalyses the interconversion of acetyl CoA and acetoacetyl CoA. This interconversion allows one molecule of acetyl CoA and one molecule of acetoacetyl CoA to undergo a condensation reaction by 3-hydroxy-3-methylglutaryl-coenzyme A (HMG CoA) synthase to form a molecule of HMG CoA. HMG CoA reductase, with the addition of 2 nicotinamide adenine dinucleotide phosphate (NADPH) molecules then catalyses the conversion of HMG CoA to mevalonate. As the rate limiting enzyme of cholesterol biosynthesis, HMG CoA reductase is a target for therapeutically treating high levels of cholesterol for the prevention of atherosclerosis; namely statins (Sirtori, 2014). Phosphorylation of mevalonate by the enzyme mevalonate kinase forms mevalonate-5P, which then undergoes further phosphorylation to form mevalonate-5PP via the enzyme phosphomevalonate kinase. Decarboxylation and dehydration by mevalonate-5PP decarboxylase forms isopentenyl-PP (IPP), and thus its isoform dimethylallyl-PP (DMAPP) via isopentenyl diphosphate delta isomerase. Farnesyl diphosphate synthase initiates the condensation of DMAPP with one molecule of IPP and NADPH to create geranyl-PP. Further condensation and the addition of another molecule of IPP and NADPH creates farnesyl-PP. Condensation of 2 farnesyl-PP molecules by squalene synthase and NADPH forms squalene, which is then converted to squalene epoxide by squalene epoxidase, NADPH, and O_2, before

undergoing cyclisation by oxidosqualene cyclase to form lanosterol (Hoshino et al., 2012). A series of reactions, including the branching of 7-dehydrodesmosterol to either desmosterol or 7-dehydrocholesterol, both of which can then be converted to the end product cholesterol via the enzymes 24-dehydrocholesterol reductase (DHCR24) and 7-dehydrocholesterol reductase (DHCR7) concludes the *de novo* synthesis of cholesterol (Luu et al., 2015; Risley, 2002).
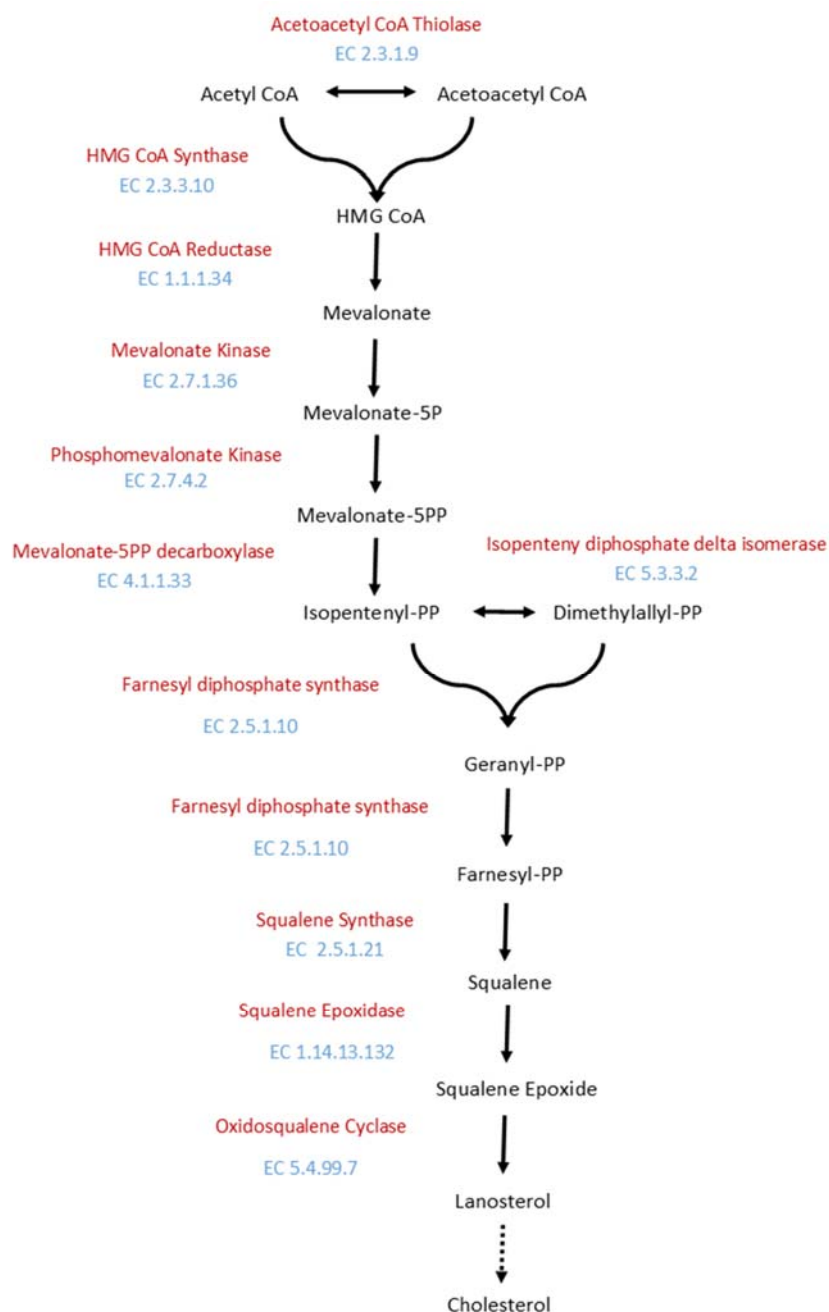
Figure 1.9 Cholesterol biosynthesis.

5) From the hepatic cholesterol pool, very low density lipoprotein cholesterol (VLDL-C) is formed, to enable the transport of endogenously synthesised triacylglycerol to the tissues. Partial hydrolysis of VLDL-C by lipoprotein lipase (LPL) forms the LDL-C precursor, intermediate density lipoprotein cholesterol (IDL-C). IDL-C is further hydrolysed by hepatic lipase to form LDL-C (Havel, 1984).

6) Following this, VLDL-C, IDL-C and LDL-C are removed from the circulation by hepatic LDLr (Veniant et al., 1998). In addition, LDL-C can also be absorbed by receptor independent means (Spady et al., 1985).

7) LDL also has the ability to return these cholesterol esters to the peripheral tissues. Accumulation of LDL-C can develop into atherosclerosis, the major clinical manifestation of CVD (Baigent et al., 2010).

8) Cholesterol can be removed from the tissues by HDL during RCT. RCT removes intercellular cholesterol from the peripheral tissues and transports it to the liver for excretion in bile or conversion to bile acids (Ohashi et al., 2005; Scheibner et al., 1994). This process reduces the risk of the development of atherosclerosis by removing excess cholesterol from peripheral tissue (Shen et al., 2015). To remove cholesterol stored in tissues, intracellular cholesterol firstly needs to be effluxed to nascent HDLs, a lipoprotein containing apo A-I, and phospholipids (Lund-Katz et al., 2013). Cholesterol efflux can occur via the receptors ABC-A1 (He et al., 2015) or scavenger receptor class B type 1 (SR-B1) (Ji et al., 2011), or via passive diffusion (Gillotte et al., 1998). Lecithin-cholesterol acyltransferase (LCAT) then esterifies the incorporated cholesterol, converting the nascent HDL to HDL_3 (Sorci-Thomas et al., 1990). The assembly of two small, dense, HDL_3 molecules, in the presence of phospholipid transfer protein (PLTP), induces the formation of a larger HDL_2 molecule (Chirackal Manavalan et al., 2014). This conversion can be reversed in the presence of hepatic lipase (HL) (Patsch et al., 1987). Once transported to the liver, the cholesterol and cholesterol ester rich HDL_2, needs to deposit the cholesterol and esters before recirculating (Patsch et al., 1987). Cholesterol esters have the ability to enter the liver directly via the receptor SR-B1, or via the enzyme CETP, which facilitates the 1:1 exchange of cholesterol esters from HDL_2 with TAGs from very low density lipoprotein (VLDL) and LDL

(Zhang et al., 2015). These lipoproteins then return the esterified cholesterol to the liver, for conversion to bile acids or excretion (Brown and Goldstein, 1984)

9) Cholesterol can be removed from the body by two mechanisms; directly via the ATP-binding cassette subfamily G5/G8 (ABCG5/G8) receptor and effluxed to the gall bladder (Repa et al., 2002), or alternatively, it can be converted to bile acids for faecal excretion. Primary bile acids are produced from cholesterol in the liver via either the neutral (classical) pathway, or the acidic (alternative) pathway (Björkhem et al., 2002; Schwarz et al., 2001). However, it has been suggested other pathways, initiated by 24-hydroxylase and 25-hydroxylase may also be involved (Fuchs, 2003). Secondary bile acids, such as deoxycholic acid and lithocholic acid are formed by structural modification of the bile acids by bacterial enzymes found in the small intestine (Ridlon et al., 2006). In the classical pathway of primary bile acid synthesis, hydroxylation of cholesterol by cholesterol 7α- hydroxylase (CYP7A1) creating 7α- hydroxycholesterol initiates bile acid synthesis (Figure 1.10). Modification of the sterol ring by cholest-5-ene-3β, 7α-diol 3β-dehydrogenase (HSD3B7) then forms 7α-hydroxy-5β-cholesten-3-one before the classical pathway splits, to enable the formation of either cholic acid (CA) or chenodeoxycholic acid (CDCA). For the formation of cholic acid, modification of the sterol ring by 12α-hydroxylase (CYP8B1) must occur before further modification by aldo-keto reductase family 1 member D1 (AKR1D1). The side chain of 4-cholesten-7α, 12α- diol-3-one is then acted upon by sterol 27-hydrolase (CYP27A1) by a series of progressive oxidation steps leading to its shortening. Further modification by several enzymes then takes place to form cholic acid. Taking the other route in the classical pathway the same steps are undertaken in the absence of 12α- hydroxylation catalysed by CYP8B1 - this route concludes with the generation of chenodeoxycholic acid (Russell, 2003). In the alternative pathway of primary bile acid synthesis, side chain shortening by CYP27A1 occurs first, creating 27α- hydroxycholesterol, before hydroxylation by 25-hydroxycholesterol 7α-hydroxylase (CYP7B1) creates 3β-7α-dihydroxy-5-cholestenoate. HSD3B7, CYP8B1 and AKR1D1 modification of the sterol ring can then occur, and upon further modification, CA and CDCA can then be formed (Thomas et al., 2008), although CDCA is considered its main product (Fuchs, 2003). This is followed by

conjugation of 98% of these bile acids. Conjugation is necessary as it increases polarity, therefore lowering the bile acids ability to move into the enterocyte from the intestinal lumen via passive transport. This allows the movement of bile acids to be tightly regulated, and under receptor control (Aldini et al., 1996). Additionally, conjugation improves solubility. This is important for their role in forming the mixed micelle, for the absorption of cholesterol. It also reduces the likelihood of precipitate being formed in the presence of calcium, thus lowering the chances of gallstone formation (Hofmann and Mysels, 1992). For conjugation to occur, firstly bile acid: CoA synthase (BACS) generates bile acid- CoA, before bile acid CoA: amino acid N-acyltransferase (BAT) conjugates the bile acid to either glycine or taurine, usually observed in a 3:1 ratio (Hardison, 1978).
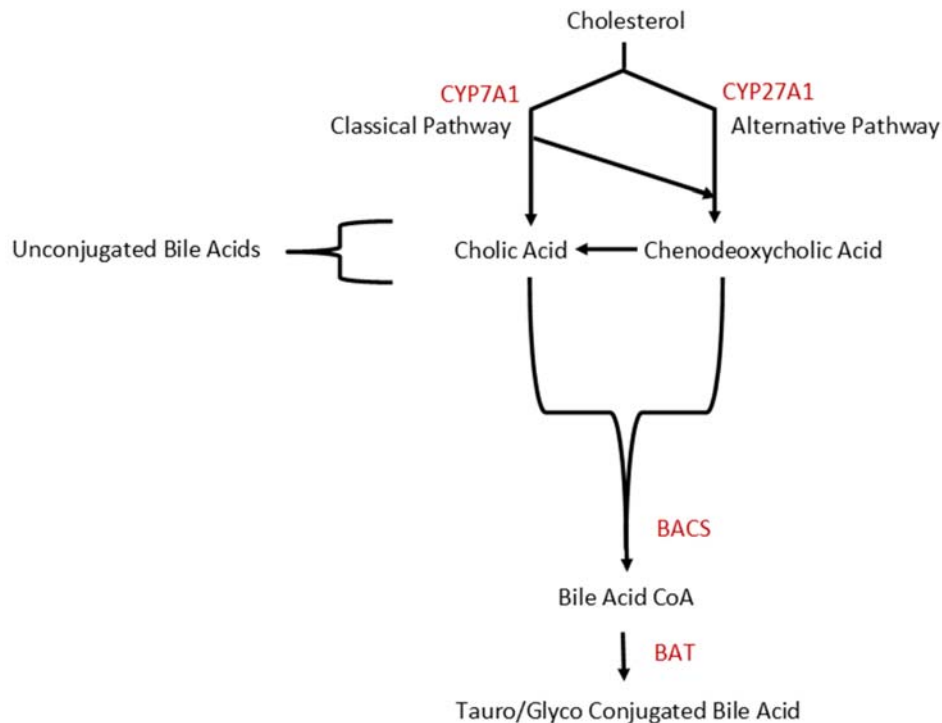
Figure 1.10 Bile acid synthesis.

Bile acids are then effluxed to the gallbladder by receptors, including the bile salt export pump (BSEP) which has a preference for unconjugated bile acids and glycine conjugates > taurine conjugates (Soroka and Boyer, 2014). The secondary receptors multidrug resistance-associated protein 2 (MRP2), and multidrug export pump (MDR1A) also play a role in the transportation of bile acids from the liver.

Bile acids are secreted into the bile canaliculi along with cholesterol, phospholipids, and bilirubin, for storage in the gall bladder, before release into the small intestine postprandially in response to cholecystokinin (CKK), produced in response to ingested fats (Marciani et al., 2013; Schjoldager, 1994). Entry into the small intestine then enables bile acid micelle formation (Birru et al., 2014; Garrett and Young, 1975; Woollett et al., 2006). Once the bile acids have enabled the absorption of the variety of lipids, including cholesterol, the bile acids themselves must be reabsorbed. Conjugated bile acids are absorbed into ileocytes via the apical sodium dependent bile acid transporter (ASBT) (Weinman et al., 1998). These are absorbed with a higher efficiency than unconjugated bile acids (Craddock et al., 1998). Created by bacterial modification, unconjugated bile acids have a decreased polarity. This allows them to freely diffuse across the apical membrane of enterocytes the length of the small intestine and colon (Dawson et al., 2009). Once the bile acids have made their way across the apical membrane, they are shuttled across the enterocyte to the basolateral membrane and expelled into circulation by the heterodimeric organic solute transporter α and β (OSTα/β) (Ballatori et al., 2005). From the portal vein, bile acids are primarily absorbed into hepatocytes via Na^+- taurocholate cotransporting polypeptide (NTCP) which has a preference of tauro-conjugates > glyco-conjugates > unconjugated bile acids (Meier et al., 1997; Mita et al., 2006) and accounts for 75% of conjugated and 40% of unconjugated bile acid Na^+ dependent transportation into the liver (Kouzuki et al., 1998). The secondary receptor, organic anion transporting polypeptide 2 (OATP2) also plays a role in the inflow of bile acids into the hepatocyte (Thomas et al., 2008). The majority of returning unconjugated bile acids are reconjugated, along with the newly synthesised bile acids, before they are effluxed out of the hepatocyte for another circuit of enterohepatic circulation. This enterohepatic circulation of bile acids occurs between 4-12 times per day.

10) On average, 500mg/day of both cholesterol and bile acids are excreted (Lu et al., 2010). Of the 5% of circulating bile acids that are excreted daily, 98% are in the unconjugated form due to a lower reabsorption efficiency in the ileum (Batta et al., 1999; Gérard, 2014). Conjugated bile acids are deconjugated by bacterial modification, as outlined in Figure 1.11 (Joyce et al., 2014). Bacterial species

such as *Lactobacillus* and *Bifidobacterium* produce bile acid hydrolase (BSH) in order to remove the associated amino acid (Oner et al., 2014). *Lactobacillus* species are responsible for 86% of the BSH activity in the ileum, and 74% in the caecum (Tannock et al., 1989). BSH preferentially hydrolyses glyco-conjugated bile acids than tauro-conjugated bile acids. There are several survival-promoting motives for bacteria to respond in this way; these include providing a nutrition source and bile acid detoxification (Begley et al., 2006). This modulation of bile acid circulation indicates that the gut microbiome also plays an important role in maintaining cholesterol metabolism. Collectively the mechanisms discussed coordinate together to maintain whole body cholesterol balance and age-related changes to such mechanisms have important implications for health.
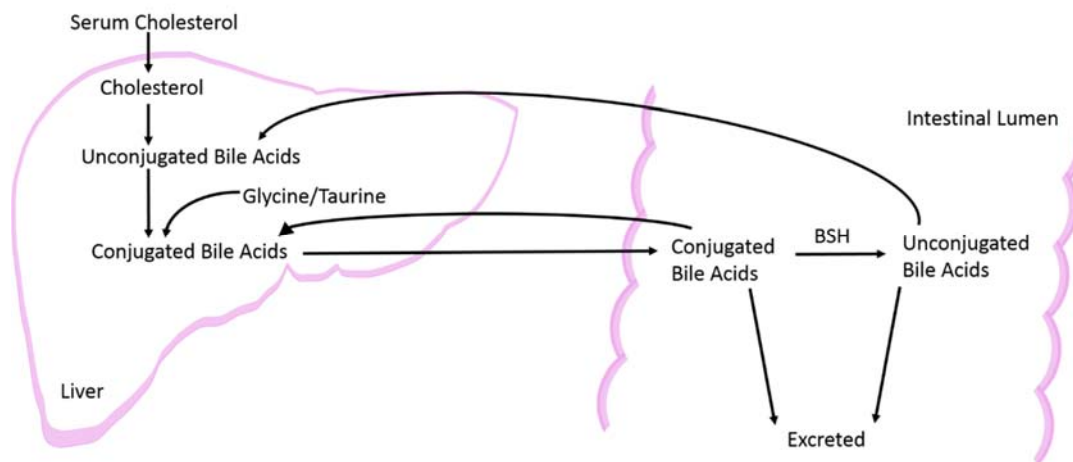
Figure 1.11 Role of BSH in deconjugating bile acids.

1.1.3 Impact of ageing on cholesterol metabolism

1.1.3.1 Lipoprotein dynamics and ageing

It is well established that LDL-C levels rise with age (Abbott et al., 1983). Evidence from the Framingham Study demonstrates LDL-C steadily rises from 97.08mg/dL (2.51mmol/L) and 100.44mg/dL (2.60mmol/L) in 15-19 year olds, to 132.25mg/dL (3.42mmol/L) and 156.91mg/dL (4.06mmol/L) in 75-79 year olds in males and females, respectively (Abbott et al., 1983). An increase in LDL-C is correlated with an increased risk of CVD; every 1mmol/L (38.6mg/dL) of LDL-C is associated with a 28% increased risk of coronary heart disease (CHD)-mortality (Gould et al., 2007). Paradoxically, this is not always the case, as higher levels of LDL-C were associated with a lower risk of all-cause mortality in a Chinese cohort of 935 ≥80 year old males and females. In this cohort each 1mmol/L increase in LDL-C reflected a 19% decrease in mortality (Lv et al., 2015). Furthermore, abnormally high LDL-C (≥3.37mmol/L) resulted in a 40% reduction in mortality. Participants that survived the three year survey-based study were also found to have a higher prevalence (39.0% vs. 27.7%) of central obesity (Lv et al., 2015). This phenomenon in the oldest old (≥80 years old) could be explained by several factors. Firstly, it is possible that individuals susceptible to the effects of increased LDL-C levels had already died before the age of 80 years, and are consequently not included in studies of the oldest old. It has also been suggested increased LDL-C enhances the immune response to pathogens (Biswas et al., 2015; Netea et al., 1996).

A mechanistic explanation for the correlation between advancing age and increased LDL-C is that over time there is a reduction in its rate of clearance from the circulation. Under normal circumstances, apo B-100 containing lipoproteins, LDL-C and VLDL-C, are removed from the circulation by hepatic LDLr (Veniant et al., 1998). From the hepatic pool, cholesterol can be directly effluxed to the small intestine for excretion, or first be converted to bile acids. This process occurs in order to maintain the levels of circulating cholesterol, by counteracting the synthesis and ingestion of cholesterol. Deficiency in LDLr results in severe hypercholesterolaemia (type II), as cholesterol cannot be removed from the

plasma and into the liver for excretion (Hasan et al., 2014; Kowala et al., 2000). Murine models have shown LDLr deficiency increases the residence time of LDL-C and VLDL-C by decreasing the clearance rate (Ishibashi et al., 1993). For example, Ishibashi et al. (1993) demonstrated LDLr deficiency increased the half-life of ^{125}I-LDL and ^{125}I-VLDL by 2.5- and 30-fold respectively, while the half-life of ^{125}I-HDL was unaffected. Furthermore, LDLr deficiency induced a 2-fold increase in TC, a 7- and 9-fold increase in IDL-C and LDL-C respectively, in addition to a modest 1.3-fold rise in HDL-C (Ishibashi et al., 1993). In humans the number of hepatic LDLr decrease with age, thus reducing the rate of LDL-C clearance, and augmenting LDL-C residence time (Millar et al., 1995). Furthermore, the rate of VLDL apo B-100 synthesis increases (Millar et al., 1995). This age-related decline in LDLr is possibly a contributing factor to LDL-C accumulation. It is likely there are several factors influencing the decline in LDLr with age, the primary factor being the decline in the rate of bile acid synthesis, as discussed in section 3.2. Briefly, a decline in bile acid synthesis, results in a decline in cholesterol utilisation from the hepatic pool. Thus, less cholesterol is required to maintain the hepatic pool, resulting in down regulation of LDLr and plasma cholesterol accumulation. More recently, proprotein convertase subtilisin kexin-9 (PSCK9) has also been associated with LDLr degradation (Mousavi et al., 2009). PCSK9, a serine protease regulated by SREBP-2, acts by binding to the epidermal growth factor like repeat A domain of LDLr leading to receptor degradation. Levels of PCSK9 have been shown to rise with age, and may account for the age-related reduction in LDLr and LDL-C clearance (Cui et al., 2010; Dubuc et al., 2010).

HDL-C levels are also affected by the ageing process (Wilson et al., 1994). Typically, HDL-C is observed to decrease by 1% per year (Ferrara et al., 1997). The age-related decline of the atheroprotective HDL-C is linked with the pathogenesis of CVD (Cooney et al., 2009). For instance, a favourable HDL-C profile is often observed in the offspring of centenarians (Barzilai et al., 2001). Due to the lack of controls, to compare the lipoprotein protein of long lived individuals with age-matched controls, offspring studies are utilised. By using this approach, inherited elevated HDL-C levels can be observed (Barzilai et al., 2001). Therefore, increased levels of HDL-C have been highlighted as a potential mechanism

conferring exceptional longevity. This is substantiated by evidence detailing individuals with familial hyperalphalipoproteinaemia, whereby the production rate of apo A-I is markedly increased. These individuals display increased HDL-C levels, and exhibit reduced rates of CHD, which may play a role in promoting exceptional longevity (Rader et al., 1993).

1.1.3.2 Cholesterol absorption and the synthesis & enterohepatic circulation of bile acids

Cholesterol from both the diet and bile is absorbed in the small intestine (Repa et al., 2002; Tancharoenrat et al., 2014). Cholesterol absorption is regulated by two receptors on the apical membrane, NPC1L1 and ABCG5/G8. NPC1L1 is predominantly located in the jejunum, although is found the length of the small intestine, and is responsible for the absorption of sterols from the intestinal lumen into the enterocytes (Masson et al., 2010; Sane et al., 2006). ABCG5/G8 is located primarily in the jejunum and ileum and to a lesser extent, the duodenum, and is responsible for the efflux of non-cholesterol sterols from the enterocyte into the intestinal lumen (Masson et al., 2010; Wang et al., 2007). Murine models have demonstrated that NPC1L1 expression significantly increases in the duodenum and jejunum with age, while ABCG5/G8 expression is suppressed. These age-related changes to receptor expression represented a 19-40% increase in cholesterol absorption between young adult and aged adult mice. This effect was amplified in response to high levels of oestrogen (Duan et al., 2006). These findings are intriguing, as it has long been suggested that an increase in cholesterol absorption is an important factor in the rise in LDL-C which accompanies ageing (Hollander and Morgan, 1979). Thus inhibiting NPC1L1 is one strategy that has been adopted in the treatment of hypercholesterolaemia (Dujovne et al., 2002)

Bile acid synthesis declines with age in humans (Bertolotti et al., 2007; Einarsson et al., 1985). This is due to a reduction in the hepatic expression of the rate limiting enzyme for bile acid synthesis, CYP7AI (Bertolotti et al., 2007). This in turn reduces cholesterol utilisation, which is accompanied by a rise in

plasma cholesterol (Uchida et al., 1996). Significantly, it has been estimated that with every 10 years, there is a decrease of 60mg/day in cholesterol converted to bile acids (Bertolotti et al., 1993). Thus, a decline in bile acid synthesis is another factor which could contribute to the dysregulation of whole body cholesterol metabolism with age.

In rodents a mechanistic explanation for the decline in CYP7AI activity has been postulated. It is suggested the reduction in its activity is in part, due to neuroendocrine dysfunction which causes an age dependent decrease in growth hormone, which is known to act pleiotropically on lipoprotein metabolism (Parini et al., 1999). Similar studies have also illustrated that sex hormones play a role in the decline of CYP7AI, as gender differences are often observed. For example, aged female rodents often have an increased concentration of serum bile acids, whereas levels remain constant in males with age (Fu et al., 2012). This is in addition to alterations to the composition of bile acids (Trautwein et al., 1999). Synthesised bile acids are effluxed from the liver primarily by BSEP, and stored in the gall bladder, with BSEP expression remaining fairly consistent with age in mice (Fu et al., 2012). Following release into the small intestine postprandially, bile acids aid in the absorption of dietary lipids, and undergo bacterial modification before being reabsorbed or excreted. Therefore, any age related alterations to these processes will have consequences for whole body cholesterol metabolism.

Digestive microflora play a vital role in the enterohepatic circulation of bile acids, by modifying bile acids and influencing feedback mechanisms. For example, conventionally raised mice have a 71% reduction in the size of their bile acid pool compared to germ free mice. Furthermore, these conventionally raised mice excrete over four times the amount of bile acids (Sayin et al., 2013). This emphasises the comprehensive role of the gut microbiota in regulating enterohepatic circulation. It is therefore logical that changes to the gut microbiota with age will have an impact on overall cholesterol metabolism. Within the digestive tract, bile acids are metabolised by the digestive microbiota and converted to secondary bile acids. Deconjugation of primary bile acids by bacterial BSH is essential for this conversion to secondary bile acids. Deconjugated bile acids are more readily excreted than

conjugated bile acids, as they are less readily reabsorbed by ASBT (Dawson, 2011). The excreted bile

acids need to be replenished from the conversion of cholesterol (Joyce et al., 2014). With age, the rise

in LDL-C can in part be explained by the decline in BSH+ species, such as *Lactobacillus* and

Bifidobacterium species (Hopkins and Macfarlane, 2002). A decline in BSH results in fewer bile acids

being deconjugated, and thus more are reabsorbed, and fewer are excreted. This results in a decline

in the need for bile acid synthesis, and thus cholesterol utilisation is reduced (Joyce et al., 2014). One

way to combat this decline in BSH is via the administration of probiotic strains (Al-Sheraji et al., 2012).

This has also been associated with improved gut health (Tuohy et al., 2003) and increased immunity

in human subjects (Moro-Garcia et al., 2013). However, caution is needed when suggesting this

strategy as a therapeutic intervention for the treatment of hypercholesterolaemia, as increased

concentrations of secondary bile acids can increase inflammation and cancer risk in the colon

(Salemans et al., 1993). This is emphasized in older individuals, where intestinal transit time is

elevated, and reabsorption of conjugated bile acids is decreased, thus increasing the exposure of the

intestinal mucosa to bile acids (Salemans et al., 1993). This elevated exposure time results in the

promotion of colorectal cancer in the elderly (Ajouz et al., 2014).

1.1.4 Impact of genetic variation on cholesterol metabolism and healthy ageing

There are several key genes involved in cholesterol metabolism: mutations to these genes can impact

on plasma cholesterol levels; the response to pharmaceutical intervention; and the pathogenesis of

age-related disease. In this section several of the key genetic polymorphisms responsible for the

dysfunction of cholesterol metabolism, as well as those promoting exceptional longevity are

discussed. Asselbergs et al. (2012) describe 122 single nucleotide polymorphisms (SNPs) which could

account for ~9.9% of the variance in HDL-C levels. Furthermore, 104 SNPs could explain ~9.5% of the

variance in LDL-C, 142 SNPs could explain 10.3% of variance in TC, while 110 SNPs could explain 8.0%

of the variance associated with triglyceride levels (Asselbergs et al., 2012). In addition, genetic factors can also influence the lipoprotein response to extrinsic factors, such as pharmaceutical intervention or diet. For example, in response to increases in dietary cholesterol, individuals can be categorised as either a hypo-responder, where plasma TC increases <0.05mmol/L, or as hyper-responders, where there is an increase of ≥0.06mmol/L per each additional 100mg dietary cholesterol, respectively (Herron et al., 2003). Likewise, Herron et al. (2003) demonstrated ingestion of ~640mg/day resulted in a 30% increase in LDL-C and an 8% increase in HDL-C in individuals classified as hyper-responders, whereas LDL-C and HDL-C were unaffected in individuals classed as hypo-responders. Thus, it is not surprising that previously Bosner et al. (1999) demonstrated cholesterol absorption varies from 29.0 to 80.1% in healthy subjects aged between 17 and 80 years of age. Ethnicity also plays a role in this variation, with African-Americans on average absorbing larger amounts of cholesterol than Caucasians or those from Asian descent (63.4% vs. 56.2%). Although, dietary intake, rather than absorption efficiency, appeared to be the dominant factor in cholesterol absorption (Bosner et al., 1999). In addition, the response to pharmaceutical intervention, such as the administration of cholesterol biosynthesis inhibitors or cholesterol absorption inhibitors is highly variable (Barber et al., 2010; Simon et al., 2005). For example, the presence of at least one minor allele at g.-18C>A resulted in a 15% improved reduction in LDL-C in response to ezetimibe + statin therapy (Simon et al., 2005).

1.1.4.1 Cholesteryl ester transfer protein

Mutations to the gene encoding for the CETP enzyme can influence CETP activity and size (Cefalu et al., 2009). This affects both the amount of esterified cholesterol transported from HDL to LDL and VLDL, as well as lipoprotein size and number (Wang et al., 2002). There are a number of mutations within the CETP gene that have been discovered. Of these polymorphisms, several have been associated with lower CETP levels, reduced risk of CVD, and increased longevity. Murine models transfected with CETP undergo extensive lipid profile remodelling resulting in an increased risk for

CVD (Westerterp et al., 2006). Therefore, any mutation resulting in decreased CETP, is thought to reduce CVD risk and increase life-span. For example, homozygosity for the common I405V polymorphism is associated with exceptional longevity (Barzilai et al., 2003). In one case, a three-fold increase in homozygosity for the I405V genotype was observed in long lived individuals (24.8% vs. 8.6%). This homozygous amino acid substitution of 405 isoleucine for valine reflected a 17% reduction in CETP levels, elevated HDL concentrations by 3.63%, and decreased LDL levels by 7.31%, in comparison to individuals homozygous for the isoleucine codon. Furthermore, LDL and HDL particles were significantly larger (Barzilai et al., 2003). These larger lipoproteins have been associated with a decreased incidence of CVD, hypertension, metabolic syndrome and neurodegeneration (Barzilai et al., 2006; Barzilai et al., 2003). It is likely that larger LDL molecules are less readily able to penetrate the arterial tissue, and therefore result in a decreased risk for atherosclerosis pathogenesis (Barzilai et al., 2003). Homozygosity for the I405V polymorphism is therefore regarded as a protective phenotype for healthy ageing (Atzmon et al., 2005; Barzilai et al., 2006).

The missense D442G mutation in exon 15 of the CETP gene, has also been described as an atheroprotective genotype, as the D442G mutation has been shown to increase LDL-C particle size, and HDL-C levels (Wang et al., 2002). In addition, this mutation which reduces CETP mass, activity and secretion, has been associated with a decreased risk of CVD mortality (Arashiro et al., 2001; Koropatnick et al., 2008). However, Zhong et al. (1996) demonstrated an increase in HDL-C associated with this genotype, was correlated with an increase in CHD risk (Zhong et al., 1996). Alternatively, Hirano et al. (1997) demonstrated that a G to A mutation in intron 14, which induced a rise in HDL-C exhibited a U-shaped curve of the incidence risk of ischemic change (Hirano et al., 1997). Moreover, Agerholm-Laren et al. (2000) demonstrated the A373P/R451Q genotype resulted in a decrease in HDL-C in both males and females from the Danish general population. Homozygosity for the mutation resulted in the effect being more pronounced than in heterozygotes, with HDL-C levels of 1.19 and 1.38mmol/L in males and females respectively compared to 1.26 and 1.62mmol/L. Non-carrier males and females had HDL levels of 1.4 and 1.74mmol/L, respectively. Although this CETP genotype induced

lower levels of HDL-C, potentially due to an increase in CETP activity, they were not associated with ischemic heart disease (IHD). Furthermore, when the authors adjusted for a group of risk factors in addition to HDL-C, the mutation resulted in a 36% reduction in risk of IHD (Agerholm-Larsen et al., 2000).

1.1.4.2 Niemann-Pick C1-like 1

Intestinal absorption of cholesterol varies significantly from person to person. In healthy individuals, cholesterol absorption can range from 29.0-80.1% (Bosner et al., 1999). This is due, in part to the genetic variation in the genes encoding for the NPC1L1 receptor, which is responsible for the clathrin-mediated endocytosis of cholesterol from the digestive tract. Cohen et al. (2006) discovered 20 polymorphisms within individuals classified as hypo-absorbers, compared to only five for the hyper-absorber category. Of the 20 mutations conferring a low cholesterol absorption efficiency, 18 were observed in African-Americans. This reflected the findings that these hypo-absorber phenotypes were more prevalent in African Americans (6.2%) than white (1.8%) or Hispanic (1.7%) populations. These hypo-absorber phenotypes conferred an average 8.6% reduction in LDL-C (Cohen et al., 2006).

In individuals with autosomal dominant hypercholesterolaemia, lacking LDLr or apo B mutations, NPC1L1 mutations may play a role in the hypercholesterolaemic phenotype displayed. For example, it has been shown that the -133A>G polymorphism, significantly increases NPC1L1 promoter activity (Martín et al., 2010). More recently, NPC1L1 SNPs have been linked with CVD. For instance, Polisecki et al. (2010) demonstrated that homozygous carriers for the minor alleles at -18A>C, L272L, V1296V or U3_28650A>G exhibited a 2-8% increase in LDL-C, while the risk of developing a fatal or nonfatal CHD event escalated by 50-67% (Polisecki et al., 2010). Muendlein et al. (2015) determined that 24 variants, particularly rs55837134 were associated with future cardiovascular events. Homozygosity for the rare rs55837134 variant was associated with a 3-fold increase in cardiovascular event incidence, compared with carriers homozygous for the common allele (Muendlein et al., 2015). In

contrast, Stitziel et al. (2014) demonstrated that the presence of 1 of 15 NPC1L1 inactivating mutations, as observed in 1/650 individuals, corresponded to a 12mg/dL (0.31mmol/L) decline in LDL-C, and a 53% reduction in cardiovascular event risk (Stitziel et al., 2014). In addition to affecting baseline lipoprotein characteristics, mutations to the NPC1L1 gene also influence the lipoprotein profile response to therapeutic intervention. For example, Simon et al. (2005) demonstrated that individuals homozygous for the common allele g.-18C>A exhibited a 24.2% decline in LDL-C from baseline levels with ezetimibe treatment, compared with 27.8% for individuals heterozygous for the minor allele. Thus, heterozygosity for the minor allele represented a 15% increased response to ezetimibe treatment (Simon et al., 2005). In addition to NPC1L1 mutations leading to an altered response to the NPC1L1 inhibitor ezetimibe, statin treatment efficiency is also affected. Polisecki et al. (2010) demonstrated the -133A>G SNP influenced the LDL-C response to Pravastatin treatment. Males homozygous for the minor -133A>G allele had the greatest decline in LDL-C with pravastatin treatment, while females with the major -133A>G allele exhibited the greatest response to treatment (Polisecki et al., 2010).

1.1.4.3 Apolipoprotein E

Apolipoprotein E is present on chylomicrons, VLDL, IDL, and HDL and acts as a ligand for hepatic LDLr and LRP to enable lipoprotein uptake. There are three major alleles associated with the *APOE* gene. These are, ε2, ε3, and ε4, which have a population frequency of 6.9, 76.2 and 16.9%, respectively in a Belgian cohort (Engelborghs et al., 2003). The ε3 allele is most commonly observed, and is considered as the 'neutral' apo E genotype. Along with ε2, ε3 preferentially binds to HDL-C, while the ε4 allele has a preference for VLDL-C (Dong and Weisgraber, 1996). The presence of the ε4 allele confers a 15 and 25% decline in plasma apo E in males and females, respectively, compared to those with the ε3 allele. This decline in apo E is associated with a 2 and 5% increase in LDL-C in males and females, respectively. In comparison, those with the ε2 allele exhibit a 27 and 32% increase in apo E, which is associated with

a 10% decrease in LDL-C levels (Larson et al., 2000). The presence of an ε4 allele is considered a risk factor for the development of many conditions including atherosclerosis (Zende et al., 2013), Alzheimer's Disease (AD) (Rhinn et al., 2013), and multiple sclerosis (Horakova et al., 2010), in addition to accelerating telomere shortening (Wikgren et al., 2012). On the other hand, this allele has been associated with a higher vitamin D status (Huebbe et al., 2011), and has been identified as a possible protective genotype against age related macular degeneration (Kovacs et al., 2007). The ε2 allele in contrast has been associated with an increased risk for the disease, or for its earlier onset (Tikellis et al., 2007). Furthermore, homozygosity for the ε2 allele is found in 90% of individuals with hyperlipoproteinaemia type III (Mahley and Rall, 2000). The ε2 isotope results in defective lipoprotein binding to LDLr, which in turn leads to incomplete catabolism of chylomicrons and VLDL-C, resulting in an accumulation of cholesterol rich lipoprotein remnants (Phillips, 2014). However, only 5% of ε2 homozygotes have this disease, and therefore there are other factors involved in the development of the disease (de Beer et al., 2002). With the exception of hyperlipoproteinaemia type III, this ε2 allele has been associated with a protective phenotype against CHD (Bennet et al., 2007). Furthermore, the ε2 allele is positively associated with exceptional longevity in Italian, Danish, US, and Japanese cohorts. In contrast, the presence of the ε4 allele reduced the chance of reaching exceptional longevity in Spanish, Italian, Danish, US and Japanese cohorts (Garatachea et al., 2014; Schupf et al., 2013).

1.1.4.4 Lipoprotein and hepatic lipase

Another enzyme that is affected by genetic mutation is LPL. LPL is primarily found on the endothelial wall of capillaries and is responsible for the hydrolysis of triacylglycerol in chylomicrons and VLDL into FFA and monoacylglycerol (Goldberg et al., 2009). A common polymorphism in the LPL gene is S447X, which results in a truncated protein due to a serine to stop codon change at amino acid 447, as a result of a C>G mutation at nucleotide 1595. In a cohort of American subjects, 44.0 and 50.6% of males and females, respectively exhibited homozygosity for the common allele, which is associated with reduced

LPL activity, while only 12.6 and 7.6% were homozygous for the rare allele (Larson et al., 1999).

Heterozygosity was displayed in 43.4 and 41.8% of males and females respectively. Females, but not

males, exhibiting homozygosity for the rare allele had lower TC and LDL-C levels, when compared to

heterozygotes and homozygotes for the common allele (Larson et al., 1999). This alteration to

cholesterol metabolism could play a role in the association of this genotype with age-related

conditions such as hypertension, T2DM, and coronary artery disease (CAD) (Daoud et al., 2013;

Muñoz-Barrios et al., 2012). Hepatic lipase is responsible for the conversion of IDL to LDL, and can also

be affected by genetic mutation. In contrast, the –C480T polymorphism in the hepatic lipase gene, has

been shown to elevate HDL-C levels (Murtomäki et al., 1997). While it is known that this polymorphism

is associated with reduced postheparin HL activity, the precise mechanism for this phenotypic change

is unknown. Homozygosity for the common allele was observed in 53.2% of control individuals, while

40.3% of these individuals were observed to be heterozygous. Homozygosity for the –C480T

polymorphism was observed in 6.5% of healthy individuals, whereas, this was reduced to 4.7% for

individuals with a paternal history of myocardial infarction before the age of 55 years, although this

was not statistically significant (Murtomäki et al., 1997). Furthermore, McCaskie et al. (2006) found

that although HDL-C levels were raised in an Australian population with this polymorphism, it was not

associated with a decrease in CHD risk (McCaskie et al., 2006). In contrast, Fan et al. (2006) found that

this polymorphism was associated with a lower coronary flow reserve, which is an early indicator of

atherosclerosis (Fan et al., 2006).

1.1.4.5 HMG CoA reductase

HMG CoA reductase is the enzyme responsible for the rate limiting step in cholesterol biosynthesis,

and is therefore the main target for pharmaceutical intervention by statins (Istvan and Deisenhofer,

2001). Chasman et al. (2004) demonstrated that two genetic polymorphisms were not only able to

influence the baseline characteristics of the lipoprotein profile, but also influence the efficacy of statin

treatment. The presence of one copy of SNP 12 (rs17244841) induced an 18.9% reduction in LDL-C and 4.6% increase in HDL-C, compared with individuals homozygous for the major allele. Whereas, heterozygotes for SNP 29 (rs17238540), exhibited 18.9 and 2.4% reduction in LDL-C and HDL-C, respectively. The presence of one of the SNPs also resulted in the diminished efficacy for cholesterol lowering treatment by pravastatin. For individuals with either SNP, the TC and LDL-C lowering efficacy was reduced 22 and 19% respectively (Chasman et al., 2004). The authors postulate these findings could be due to these SNPs affecting expression, activity, or drug binding. The authors also suggest that a close linkage between these SNPs and a third SNP, which is responsible for influencing HMG CoA reductase RNA stability, may also play a role in altering LDL-C and HDL-C levels, in addition to statin treatment efficacy (Chasman et al., 2004).

Thus, genetic polymorphisms in certain enzymes and receptor genes associated with cholesterol biosynthesis can provoke the dysregulation of cholesterol metabolism, lipoprotein profile, alter CVD risk, and the response of cholesterol metabolism to pharmaceutical intervention.

1.1.5 Oxidative stress and cholesterol metabolism

The free radical theory of ageing is underpinned by the belief, that the gradual accumulation of oxidative damage with time is responsible for the ageing process (Harman, 1956, 2009). Oxidative stress is the result of redox imbalance, due to an increase in damaging free radicals, such as reactive oxygen species (ROS). This in turn leads to detrimental changes including DNA damage, lipid oxidation, and impaired protein function. It is this accumulation of oxidative damage that manifests as ageing. (Kandola et al., 2015). ROS are produced during mitochondrial oxidative phosphorylation, and by cells exposed to xenobiotics (Berthiaume and Wallace, 2007), pathogen associated patterns (PAMPs) (Tassi et al., 2009) or pro-inflammatory cytokines (Yang et al., 2007). Despite the perceived role ROS may play in the ageing process, ROS also have useful roles in processes such as phagocyte derived bactericidal and tumouricidal activity (Li et al., 2013; Vatansever et al., 2013), nitric oxide (NO)

production (Shen et al., 2014), and insulin signalling (Bashan et al., 2009). Atherosclerosis is suggested to be a condition mediated by ROS, LDL-C and intrinsic ageing (Vogiatzi et al., 2009). Briefly, LDL-C migrate across a damaged artery endothelium into the tunica intima, where an accumulation of LDL-C, immune cells, and proliferative smooth muscle cells occlude the artery lumen restricting blood flow (Hansson and Hermansson, 2011). This endothelial damage and dysfunction can be influenced by a variety of factors including smoking (Ambrose and Barua, 2004), hypertension (Li and Chen, 2005), hyperglycaemia (Popov, 2010), hyperlipidaemia (Kerenyi et al., 2006), ageing (Wang and Bennett, 2012), infection (Rosenfeld and Campbell, 2011), and hyperhomocysteinaemia (Guthikonda and Haynes, 2006). This damage results in increased ROS production, and a more permeable membrane in which LDL-C and immune cells can more freely migrate. Oxidation of LDL by ROS forms the cytotoxic and immunogenic oxLDL (Mahmoudi et al., 2011). Release of monocyte chemotactic protein-1 (MCP-1) by endothelial smooth muscle cells and macrophages that have already localised in the tunica intima, leads to the migration of monocytes across the endothelium where they differentiate into macrophages (Dewald et al., 2005). These macrophages then engulf oxLDL via scavenger receptors SR-A and CD36, forming lipid-laden foam cells (Korporaal et al., 2007). Meanwhile, T cells, mainly Th1, migrate across the endothelium and release pro-inflammatory cytokines such as IL-2, IL-12 and IFN-γ to intensify the immune response (Baidya and Zeng, 2005). Foam cells, macrophages, and T-cells then combine to form a fatty streak. The macrophages also secrete the pro-inflammatory cytokines TNFα, IL-1β, IL-6, and IL-12, in addition to the mitogen platelet derived growth factor (PDGF), which induces the proliferation of smooth muscle cells of the tunica media forming a cap for the plaque (Ross et al., 1990). This segregates the plaque from the blood, however the plaque cause the artery to harden and narrow, restricting blood flow. Subsequent instability in the plaque can result in it rupturing; which can block the supply of blood to the heart causing a myocardial infarction, or to the brain, triggering an ischaemic stroke (Bentzon et al., 2014). In addition to the effects of ROS on LDL, it has also been shown to interact with the atheroprotective particle HDL. It has been suggested HDL is oxidised during the pathogenesis of atherosclerosis, causing HDL to lose its protective properties and transform into

a proinflammatory and proatherogenic mediator. These oxidised HDL, oxHDL, have been shown to promote smooth muscle cell proliferation and migration in a dose dependent manner, thus aiding in the progression of atherosclerosis pathogenesis (Wang et al., 2014). Further to this, oxHDL, have also been shown to induce ROS production, upregulate the expression of the proinflammatory cytokine TNF-α, and upregulate the expression of prothrombotic cyclooxygenase-2, COX-2, and plasminogen activator inhibitor-1, PAI-1 (Callegari et al., 2006; Norata et al., 2004; Soumyarani and Jayakumari, 2012).

1.1.6 Caloric restriction

Caloric restriction (CR), a dietary regime defined by a 20-40% reduction of calories, which does not induce malnutrition (Taormina and Mirisola, 2014), has been demonstrated to extend life-span in a diverse range of organisms, however its effect on humans has not be fully established (Barzilai et al., 2012; Guarente, 2013). CR has been associated with many metabolic effects linked to ageing and longevity. For example, CR has been associated with a reduction in the release of ROS from complex I of mitochondria within the cardiac tissue of rodents (Gredilla et al., 2001). Therefore, there is a prevailing hypothesis within gerontology, that the positive effects of this dietary regime are mediated through a reduction in ROS. However, it is possible that the beneficial effects of CR on health-span extend beyond this particular aspect of ageing, as evidence suggests, that metabolic rate is unaffected by CR in murine models (Hempenstall et al., 2010). Moreover, it is considered that ageing is associated with the accumulation of oxidative damage. Conversely, recent evidence has suggested that low grade oxidative damage may be beneficial. As an example, glucose restriction has been associated with an increase in oxidative stress in *Caenorhabditis elegans*, which is thought to increase resistance to further oxidative stress, and thus extend life-span via mitochondrial hormesis (Schulz et al., 2007). Alternatively, murine models have demonstrated that CR can prevent the age-related decline of heat shock proteins (HSPs), which are induced following exposure to stress to protect cells and organs from

the stressor (Colotti et al., 2005). CR has also been shown to have a positive effect on cholesterol metabolism in mammals. For instance, Edwards et al. (1988) investigated the effect of CR on LDL-C over a five year period in Rhesus monkeys and found this regime reduced LDL-C levels when compared to a control group (Edwards et al., 1998). Much more recently, it has also been suggested CR improves metabolic health generally (Ristow and Zarse, 2010). For instance, Colman et al. (2014) demonstrated a 2.9 times increased risk for all age-related causes of death, in Rhesus monkeys undertaking a control diet, when compared to those undertaking a 30% CR diet. CR also increased the survival rate of those animals by 3.63 times (Colman et al., 2014). The Comprehensive Assessment of Long-Term Effects of Reducing Calorie Intake (CALERIE) study provides information on the effect of CR in humans. Phase one of this program examined healthy, but overweight individuals (BMI 25-29.9kg/m^2) from three centres across America who underwent 20-25% CR. From these studies it was determined two biomarkers of longevity, fasting insulin and body temperature were reduced following 6 months of 25% CR. The authors of this study postulated that CR increases longevity via a reduction in metabolic rate (Heilbronn et al., 2006). In terms of a direct impact on lipid metabolism, CR was shown to decrease weight, fat mass and visceral adipose tissue in participants. These changes were associated with an increase in insulin sensitivity (Larson-Meyer et al., 2006). The project has recently progressed to phase 2 trials, to examine the effects of CR on healthy nonobese (BMI 22-28kg/m^2) individuals (Stewart et al., 2013).

The effects of CR in humans has also been investigated by Fontana et al. (2004). In this study, the lipoprotein profile and carotid artery intima-media thickness of 18 members of the Caloric Restriction Society, whose members practice long term self-imposed CR (3-15 years), was compared with 18 control individuals. This investigation revealed a number of interesting findings about the interaction of CR with lipid metabolism, including a decline in TC, LDL-C, and triacylglycerol by 19.1, 29.5 and 63.8%, respectively. HDL-C was also affected by CR, with a 51.2% elevation in levels. This was in addition to a reduction in other risk factors associated with CVD including, blood pressure and the inflammatory marker C-reactive protein (CRP). Together with the carotid intima-media thickness

reduction of approximately 40%, CR appears to have an atheroprotective effect (Fontana et al., 2004).

It can be concluded from these studies, although it is clear that CR increases life-span in many species,

the underlying mechanisms are still ambiguous. However, in mammals a favourable lipid profile could

be one component of a much broader cardioprotective protective effect brought on by CR which

ultimately contributes to life span extension.

1.1.7 mTOR, sirtuins, and cholesterol biosynthesis

Mechanistic target of rapamycin (mTOR) is an evolutionarily conserved serine/threonine protein

kinase of the phosphatidylinositol-3-OH kinase (PI(3)K)-related family that regulates an array of

anabolic and catabolic pathways at the mRNA expression level (Johnson et al., 2013). mTOR acts as a

key metabolic sensor in a wide range of biological activities, both at a cellular and organism level. This

ability to act as a regulator causes it to respond to a plethora of both intrinsic and extrinsic cellular

signals (Mc Auley et al., 2015b). These metabolic cues include changes to oxygen, nutrient and

hormonal levels. mTOR forms the catalytic subunit of two discrete signalling complexes, known as

mTOR complexes 1 and 2 (mTORC1 and mTORC2). The mTOR pathway impacts cell growth and

proliferation by provoking anabolic processes, including biosynthesis of proteins, lipids and organelles,

and by restricting catabolic processes, such as autophagy. There is a large body of evidence which has

been generated from several animal models that link the activities of mTORC1 to the beneficial effects

of CR, and thus longevity. Discussing these studies is beyond the scope of this thesis, rather the focus

will be on how mTOR impacts cholesterol biosynthesis. Central to the regulation of cholesterol

biosynthetic gene expression is the SREBP family of transcription factors (Horton et al., 2002). It has

been observed that silencing of SREBP inhibits Akt (Protein kinase B (PKB)) dependent lipogenesis. Akt

is an upstream regulator of mTOR, and it has been suggested PI3K/Akt/TOR pathway regulates protein

and lipid biosynthesis in an orchestrated manner (Porstmann et al., 2008). More recently, Peterson et

al. (2011) demonstrated mTORC1 regulates SREBP by controlling the nuclear entry of lipin 1, a

phosphatidic acid phosphatase. It was found that inhibition of hepatic mTORC1 impaired SREBP function and resulted in mice becoming tolerant in a lipin 1-dependent fashion, to hepatic steatosis and hypercholesterolemia induced by a high-fat and cholesterol diet (Peterson et al., 2011). Moreover, a recent study that examined non-alcoholic fatty liver disease under conditions of inflammation in apolipoprotein E knockout mice, demonstrated the inhibition of mTORC1 activity blocked the translocation of SCAP/SREBP-2 complex from the endoplasmic reticulum to the Golgi, and decreased the expression of LDLr and SREBP-2. These effects were accompanied by an increase in LDLr degradation (Liu et al., 2015). Thus, this study suggests that there could be an important link between mTOR and LDLr turnover, which has significant implications for whole body cholesterol balance and healthy ageing.

Sirtuins have also been shown to impact cholesterol biosynthesis. There are seven known mammalian sirtuins, that function as NAD^+-dependent deacetylases, which are involved in a wide range of cellular activities including nutrient sensing and DNA repair (Chang et al., 2009; de Magalhães et al., 2012). The most well studied of the sirtuins, SIRT1, plays a role in various metabolic processes that enable the cell to adapt to changes in nutrient levels. For instance, SIRT1 plays a part in modulating hepatic gluconeogenesis, insulin secretion, fat mobilisation, and stress responses (Satoh et al., 2011; Wei et al., 2011). SIRT1 also deacetylates the nuclear receptor liver X receptor α (LXRα) to induce synthesis of the transporter ABCA1, a mediator of HDL and RCT. SIRT1 KO mice display reduced plasma HDL-C levels in addition to an accumulation of cholesterol in the liver (Li et al., 2007). SIRT1 has also been suggested to be cardioprotective. For instance, evidence indicates it has a role in preventing cardiac hypertrophy (Planavila et al., 2011). In contrast, it has been demonstrated that inhibition of SIRT2 can reduce sterol biosynthesis by decreased trafficking of SREBP-2, as a mechanism of neuroprotection in cellular and invertebrate models of Huntingtons Disease (Luthi-Carter et al., 2010). Moreover, Tao et al. (2013) have suggested that Sirt6 is a critical factor for Srebp2 gene regulation. Hepatic deficiency of Sirt6 in mice resulted in elevated serum and hepatic cholesterol levels. Sirt6 is recruited by forkhead box O (FoxO)3 to Srebp2, where Sirt6 deacetylates histone H3 at lysines 9 and 56, thus promoting a

repressive chromatin state. It was found that Sirt6 or FoxO3 overexpression improved hypercholesterolemia in diet-induced or genetically obese mice (Tao et al., 2013). Therefore, Sirt6 and FoxO3 could have a crucial role to play in the regulation of cholesterol homeostasis

1.1.8 Can diet mitigate the effect ageing has on cholesterol metabolism?

During the 1950s, the Seven Countries Study (SCS) began exploring the role of diet and lifestyle on disease rates in populations from various countries. Amongst the findings reported from these studies were the causal association between, serum cholesterol, blood pressure and smoking, and CHD mortality rates (Menotti et al., 1998; Menotti et al., 2004a; Menotti et al., 2004b), whereas, diets high in saturated fat, and trans fats were associated with higher serum cholesterol and thus CHD risk (Kromhout et al., 1995). Conversely, diets high in vegetables, rich in fibre and antioxidants, promoted significant reductions in CHD risk (Buijsse et al., 2008; Streppel et al., 2008). Dietary regime is therefore an important factor that should be analysed and adjusted in order to reduce CHD risk and promote longevity. The important role of dietary and other lifestyle interventions on life-span can be emphasised by analysing the North Karelia Project. Internationally, Finnish males, especially those in the province of North Karelia, had the highest rate of CHD in the late 1960s, as a result of a diet high in salt and saturated fat, and low in vegetables, in addition to high rates of smoking and physical inactivity (Puska, 2008). In order to combat this burden, a low-resource, community-based intervention study titled the North Karelia Project was implemented in 1972 (Puska, 1973). The North Karelia Project aimed to reduce CHD morbidity and mortality rates by reducing LDL-C concentrations and blood pressure by improving diet and exercise patterns; and reducing smoking rates. The project resulted in the most rapid decline in CHD mortality in the world. Within 5 years, a 4.1 and 1.2% reduction in serum cholesterol was exhibited in men and women, respectively (Puska et al., 1979). These figures increased further to a 21% and 23% decline in TC under re-examination in 2007 (Vartiainen et al., 2010). The initial five year study resulted in a 17.4 and 11.5% reduction in CHD risk

in males and females, respectively. Following a further 25 years of implementation, this decline was amplified to a 60% reduction (Puska et al., 1979; Vartiainen et al., 2010). This 30 year project reflected an 85% decrease in CHD-related mortality (Puska, 2008). The impact of lifestyle on cholesterol metabolism, and consequently CVD risk is therefore significant. The role diet and lifestyle plays in reducing risk of age related diseases and in extending life-span is also apparent in those who consume a Mediterranean diet. This dietary pattern has been studied extensively, particularly, the role it plays in optimising lipoprotein profile and reducing CVD risk

1.1.8.1 Mediterranean diet

The Mediterranean diet is characterised by a high intake of vegetables, fruits, legumes, nuts, cereals and olive oil, and a low intake of dairy, and red and processed meats (Trichopoulou and Lagiou, 1997). Richard et al. (2012) demonstrated a five week Mediterranean diet decreased LDL-C by 9.9%, even in the absence of weight loss in men with metabolic syndrome. It was suggested this dietary pattern was able to effect LDL-C levels by increasing LDL-C clearance as well as reducing cholesterol absorption. This was thought to be due to an increase of dietary phytosterols, nutrients, monounsaturated fatty acids (MUFA), polyunsaturated fatty acids (PUFA), fish oils and fibre (Richard et al., 2012; Woodside et al., 2015). The Mediterranean diet affects cholesterol metabolism as follows. Firstly, it is postulated PUFA increases LDLr expression (Fernandez and West, 2005). Furthermore, studies have indicated plant sterols can reduce cholesterol absorption by 30-50% (Law, 2000), although the expression of ABCG5/G8 and NPC1L1 are thought to be unaffected by sterol ingestion (Field et al., 2004). Consumption of a Mediterranean diet has also been associated with a reduction in the incident rate of the age related diseases, T2DM, CVD, and cancer, by 52, 30, and 12%, respectively (Benetou et al., 2008; Estruch et al., 2013; Salas-Salvadó et al., 2011). Furthermore, individuals, from Spain or Italy for example, born in 2000, are expected to live on average 2 years longer than individuals from the UK or USA. In addition, the healthy life expectancy of these individuals is also 2 years more (WHO, 2015).

Thus, the Mediterranean diet is believed to play a role in prolonging both health-span and life-span. It is important to consider health-span in addition to life-span, as an increase in life-span is not necessary associated with an increase in health. With a score of 0 for a state comparable to death, and a score of 1 to describe one year in a state of ideal health, the use of the quality adjusted life year (QALY) can be used to describe disease burden (De Smedt et al., 2012). Dalziel et al. (2006) outlined that a 10 year Mediterranean diet resulted in a 0.31 year increase in life span and 0.4 year QALY year increase in patients who had suffered an acute myocardial infarction (Dalziel et al., 2006).

In another example of the Mediterranean diet being utilised as a strategy to treat age-related disease onset, de Lorgeril et al. (1999) reported a 9.11% reduction in the rate of secondary cardiovascular events in patients who adhered to a Mediterranean diet compared to those that followed a standard diet. It was determined that each 1mmol/L increase in TC resulted in a 20-30% increase in the risk of recurrence (de Lorgeril et al., 1999). Therefore, a Mediterranean diet that results in decreased cholesterol levels is not only protective against primary cardiovascular events but also secondary events. The substantial evidence demonstrating the potential benefit of a Mediterranean diet on prolonging health-span as well as life-span has resulted in large-scale studies, such as the NU-AGE project arising (Santoro et al., 2014). The NU-AGE project aims to utilise the Mediterranean diet as a treatment strategy to slow the rate of inflammaging, in addition to establishing the molecular mechanisms underpinning the anti-inflammaging effect of this dietary approach (Santoro et al., 2014).

1.1.9 The recent emergence of the gut microbiome

The gut microbiome has a range of metabolic roles which maintain host heath, including; facilitating the digestion of starch, fibre, and sugars (Szilagyi et al., 2010); producing short-chain fatty acids (den Besten et al., 2013; Yu et al., 2010); vitamin absorption (Beulens et al., 2013); enhancing host immunity; preventing allergies (Shen and Clemente, 2015) and facilitating enterohepatic circulation of bile acids (Joyce et al., 2014). Alterations to the microbiome can impact host health and this has

increasingly been investigated as a contributor to disease. The close relationship between the microbiome and its human host has resulted in humans being described as metaorganisms (Biagi et al., 2012). The impact of the microbiome on overall health was recently illustrated by a female subject that underwent a faecal transplant from her overweight, but otherwise healthy daughter for the treatment of recurrent *Clostridium difficile* infection. Post-transplant, the recipient experienced substantial weight gain, resulting in a weight gain of 41 pounds and an increase in BMI from 26 to 34.5 at 36 months observation (Alang and Kelly, 2015). This suggests 'obesity promoting' microbiota can be transmitted from human to human, as previously observed in rodents (Ridaura et al., 2013). Understanding the role of the microbiome in health is challenging, due to complex bidirectional interactions with many biological systems. For example, it has been implicated in enhancing alveolar macrophage function in lung infections (Schuijt et al., 2015) and is thought to influence brain morphology and function (Fernandez-Real et al., 2015). A decrease in Actinobacteria with age is associated with amygdala disruption and thalmic microstructure, reduced motor speed and attention, in addition to increased intra-abdominal fat (Fernandez-Real et al., 2015). Conversely, in a classic study, Killian et al. (1998) showed mice exposed to stress exhibited altered intestinal function (Kiliaan et al., 1998). Moreover, administration of probiotic strains impact behaviour by improving mood and decreasing anxiety symptoms in both rodent and humans (Messaoudi et al., 2011; Savignac et al., 2015; Steenbergen et al., 2015). Thus, a bidirectional relationship exists between the gut and brain and it is likely that a similar relationship exists for other organ systems.

1.1.9.1 The gut microbiome and CVD

There is an association between the microbiota and CVD risk. This could be mediated via its effects on bile acid metabolism, or by its contribution to choline diet-induced trimethylamine N-oxide production (Joyce et al., 2014; Koeth et al., 2013). Susceptibility to atherosclerosis has also been demonstrated to be transferable by microbiota transplantation in murine models (Gregory et al., 2015). Moreover, gut

microbiota dysbiosis has been associated with increased low-grade inflammation, which is linked with the development of atherosclerosis (Chistiakov et al., 2015). To examine the role of the gut microbiome on CVD risk, Fu et al. (2015) explored the potential relationships between operational taxonomic units (OTUs) with BMI, and blood lipids. High bacterial diversity was associated with a decreased BMI, and triglyceride levels, whilst a positive correlation was observed with HDL-C levels. A total of 66 OTUs were associated with BMI, while 114 were associated with triglycerides, and 34 OTUs with HDL. In particular *Clostridiaceae/Lachnospiracease* was able to modulate LDL-C levels. Fu et al. (2015) estimated that the gut microbiota is independently responsible for ≤6% of blood lipid level variation (Fu et al., 2015).

1.1.9.2 The gut microbiome and ageing

Due to inter-individual variation, there is conflicting evidence on microbiome changes during ageing. In an elderly Irish cohort (65-96 years), the proportion of Bacteriodetes ranged from 3-92%, while Firmicutes ranged from 7-94% (Claesson et al., 2011). Further differences in the gut microbiome have also been observed in other population groups. For example, *Clostridium* cluster XIVa has been observed to decrease with age in Japanese, Finnish, and Austrian cohorts (Hayashi et al., 2003; Hippe et al., 2011; Makivuokko et al., 2010), whereas an increase has been observed in German and Italian cohorts (Mueller et al., 2006). Biagi et al. (2010) reported higher levels of the Clostridium cluster XIVa in elderly Italians (49%), when compared to younger individuals (44%), although the levels did reduce slightly in centenarians (34%) (Biagi et al., 2010). These conflicting results make it difficult to establish an overall picture of how ageing effects the microbiome. However, it is likely that diet, lifestyle, antibiotic usage, and host health status accounts for much of this variation (Candela et al., 2014; Claesson et al., 2012; O'Sullivan et al., 2013). For example, the reduction in species diversity witnessed with age in humans (Biagi et al., 2010), is amplified in those housed in long-term residential care (Claesson et al., 2012). Furthermore, a carnivorous or herbivorous diet can induce changes to the

microbiome composition to favour metabolism of protein or carbohydrates (David et al., 2014). Moreover, Everard et al. (2014) demonstrated that a high fat diet decreased the expression of regenerating islet-derived 3 gamma (Reg3g), an antimicrobial lectin with activity against Gram-positive species. This reduction of Reg3g increases colonisation of the intestinal epithelium, causing alterations in the microbiome, including a decrease in the Firmicutes/Bacteroides ratio. However, prebiotic administration is able to counteract this decrease in Reg3g (Everard et al., 2014).

Bacteria from the plyla Bacteroidetes and Fimicutes contribute to 95% of faecal microbiota across ages, however a slight decline has been observed in centenarians (93%) (Biagi et al., 2010), while the Firmicutes/Bacteroidetes ratio also lowers with age (Park et al., 2015). In addition, Claesson et al. (2011) demonstrated Firmicutes increased from 40% to 51%, and Bacteriodetes decreased from 57% to 41%, when comparing a young cohort (28-46 years old) to an elderly cohort (≥65 years old) (Claesson et al., 2011). In contrast, Biagi et al. (2010) found that the Firmicutes/Bacteroidetes ratio increased from 3.9 in young individuals to 5.1 in elderly individuals, before decreasing to 3.6 in centenarians (Biagi et al., 2010). Furthermore, species diversity and number of *Bifidobacterium* and *Lactobacillus* species commonly declines with age (Hopkins and Macfarlane, 2002). Hopkins and Macfarlane (2002) found that species diversity of *Bifidobacterium* and *Lactobacillus* decreased by 57.1 and 45.5% respectively between healthy young adults aged 21-34, and healthy elderly individuals, aged 67-73 years old. The number of *Bifidobacterium* and *Lactobacillus* species, measured as $\log_{10}$ CFU/g wet weight of faeces, decreased by 53.2 and 52.2% respectively with age (Hopkins and Macfarlane, 2002). In addition, with age, there is an increase of potentially pathogenic facultative anaerobes. For example, Proteobacteria increased from 1.2% to 2.6% in human centenarians, whilst bacilli increased from 5% to 12% (Biagi et al., 2010).

Evidence suggests centenarians have further altered gut microbiota than elderly cohorts (Biagi et al., 2010). For example, when comparing the gut microbiota of cohorts exhibiting 'normal life-spans' (urbanised town communities, UTC) with those exhibiting exceptional longevity (longevity village

communities, LVC) in South Korea, LVC individuals displayed significantly higher numbers of *Bacteroides*, *Prevotella*, and *Lachnospira*, while levels of *Dialister*, *Subdoligranulum*, *Megamonas*, EF401882_g, and AM275436_g were greater in UTC individuals. The content of pro-inflammatory LPS was also significantly lower in the faecal samples of the LVC cohort. Higher LPS levels were associated with increased meat intake, decreased vegetable intake, and the presence of several bacterial species found only in the UTC cohort (Park et al., 2015). These factors could influence the progression of low-grade inflammation. This view is consolidated as bacteria associated with anti-inflammatory effects were significantly higher in the LVC cohort, making it possible that factors such as diet, influence microbiome composition, and result in a drop in pro-inflammatory LPS and a concomitant reduction in inflammaging. Additionally, Biagi et al. (2010) found that an age-related increase in potentially pathogenic Proteobacteria was correlated with the upregulation of pro-inflammatory IL-6 or IL-8 (Biagi et al., 2010). This further consolidates the belief, that reducing proinflammatory mediators such as LPS/cytokines could reduce inflammaging and promote healthy ageing (Biagi et al., 2010; Park et al., 2015).

The microbiome also affects metabolism. By investigating the bacterial genetic material in human faecal samples, Rampelli et al. (2013) revealed an increase in the bacterial genes involved in tryptophan metabolism with age. It is plausible that this age-dependent increase in bacterial tryptophan metabolism, decreases host bioavailability, a phenomenon which is implicated in a variety of inflammatory related conditions (Capuron et al., 2011; Murr et al., 2015). Furthermore, the abundance of genes involved in SCFA production reduced with age. Moreover there was a decrease in bacterial saccharolytic potential, while an increase in proteolytic potential, diverted metabolism towards putrefaction. In addition, increasing age corresponded with the enrichment of genes relating to pathobionts such as *Escherichia* (Rampelli et al., 2013). Future investigations will no doubt explore further bidirectional relationships between the regulation of lipid metabolism, the gut microbiome and intrinsic ageing.

1.1.10 Current and future therapeutic strategies

The emerging bi-directional relationship between the gut microbiome and human host promotes this as a potential therapeutic target for the regulation of many host systems. Probiotic administration has been highlighted as an effective immunomodulator, which can have potential benefits on many diseases (Patel et al., 2015). For example, Makino et al. (2010) demonstrated that a daily probiotic intake for 8-12 weeks resulted in a 2.6 times lower risk of becoming infected with the influenza virus in individuals ≥40 years old (Makino et al., 2010). Furthermore, it has been demonstrated that administration of probiotics for several weeks prior to a flu vaccination, increases initial antibody titres in addition to maintaining these enhanced levels for increased lengths of time in elderly cohorts (Boge et al., 2009; Nagafuchi et al., 2015). As well as this, probiotics have been found to influence cholesterol metabolism. Al-Sheraji et al. (2012) demonstrated an 8 week probiotic supplementation in an elderly murine model significantly reduced plasma TC, triglycerides, LDL-C, and VLDL-C, in addition to increasing HDL-C levels. Moreover, probiotic supplementation significantly reduced the atherosclerotic index of these animals (Al-Sheraji et al., 2012). These alterations in plasma cholesterol levels could be due to a number of factors, including, the generation of SCFAs which may reduce the rate of hepatic cholesterol synthesis, the increase in bile acid deconjugation resulting in reduced cholesterol solubility and absorption, and the increase in bile acid excretion (Al-Sheraji et al., 2012; Begley et al., 2006; Hara et al., 1999). However, it is important to note, evidence suggests that the byproducts of unconjugated bile acids have been associated with the dysregulation of mucosal functioning (Ajouz et al., 2014; Baptissart et al., 2013).

Furthermore, dietary interventions such as the Dietary Approaches to Stop Hypertension (DASH) and portfolio diets, which target the risk factors for CVD, hypertension and hypercholesterolaemia respectively, can be utilised (Jenkins et al., 2015; Keith et al., 2015; Rifai and Silver, 2015). For example, a recent meta-analysis determined the DASH diet lowered systolic pressure by 6.74mmHg, and diastolic blood pressure by 3.54mmHg (Saneei et al., 2014). Although the portfolio diet is less

successful in lowering blood pressure, it is effective at modifying the lipoprotein profile. Jenkins et al. (2011) observed a 13.1 and 13.8% reduction in LDL-C in individuals undertaking the routine and intensive portfolio diets over a 6 month period. Adherence to the routine or intensive portfolio diet resulted in a respective calculated 10 year CHD risk reduction of 10.8 and 11.3% respectively (Jenkins et al., 2011). As there is a significant risk reduction for CHD, and few adverse reactions associated with these diets, wide-scale utilisation in elderly individuals may play a role in maintaining good health in later years. Further to this, dependence on pharmaceutical intervention may be reduced. Moreover, many of the food items associated with these diets contain phytochemicals that can positively modulate infection and/or inflammaging and its related diseases (London and Beezhold, 2015; McCarthy and O'Gara, 2015; Shayganni et al., 2015).

Another viable therapeutic avenue could be to inhibit PSCK9. Recently inhibition of this enzyme has proven to be effective at lowering LDL-C in patients with hypercholesterolaemia. By inhibiting PCSK9, the rate of LDLr degradation is reduced, and the rate of LDL-C clearance can be maintained. A systematic review and meta-analysis of phase 2 or 3 randomised controlled trials revealed treatment with monoclonal antibodies targeting PCSK9 lowered LDL-C levels by 47.49%, and reduced all-cause mortality and myocardial infarction risk (Navarese et al., 2015).

1.1.11 The role of mathematical modelling in identifying future therapeutic strategies

The term systems biology describes the holistic approach employed to study the interactions of multiple components of a biological system, which, by using techniques from the fields of biology, mathematics and computer science, is highly interdisciplinary in nature (Breitling, 2010; Bruggeman and Westerhoff, 2007; Ideker et al., 2001). In recent years, research in this area has benefitted from adopting a systems biology paradigm to study the inherent complexities associated with ageing and

metabolism (Breitling, 2010; Ideker et al., 2001; Kirkwood, 2011; Mc Auley et al., 2009; Mc Auley and Mooney, 2015b; Mc Auley et al., 2013). It is clear from the biological mechanisms and complex interactions outlined in this review that studying their dynamics is challenging (Borgqvist et al., 2017). The systems biology approach provides a framework for dealing with this intrinsic complexity (Bruggeman and Westerhoff, 2007; Hoffman et al., 2017). Central to this approach is the use of mathematical models, which work in tandem with experimental work by integrating experimental data and enabling dynamic behaviour to be modelled in a holistic manner (Enrique Salcedo-Sora and Mc Auley, 2016; Ideker et al., 2001; Kilner et al., 2016; Kitano, 2002; Mooney et al., 2016). This contrasts with the often reductionist approach that is commonly used in experimental biology, which generally focuses on a small number of processes operating in isolation. The utility of mathematical modelling lies in its inherent ability to facilitate hypothesis exploration, and to make predictions about the behaviour of the biological systems in question, and can often lead to a deeper understanding of the biology. Recently, there has been three excellent reviews of mathematical models in this area (Mc Auley and Mooney, 2015b; Paalvast et al., 2015; Parton et al., 2015). Therefore, the aim here is not to review each of the models already outlined by Mc Auley and Mooney (2015b), Paalvast et al. (2015), and Parton et al. (2015), but to provide a synopsis of how mathematical models of cholesterol metabolism, and its associated processes can be used to enhance our understanding of how ageing impacts this core biological system. Recently a whole body model of cholesterol metabolism and its age associated dysregulation was constructed (Mc Auley et al., 2005; Mc Auley et al., 2012). Within this framework several key mechanisms were included, including LDLr turnover, intestinal cholesterol absorption, and endogenous cholesterol synthesis. Using the model, a number of mechanisms were explored. Firstly, using an *in silico* simulation the efficiency of cholesterol absorption was investigated. Interestingly, by increasing cholesterol absorption from 50% to 80% by 65 years, it was shown that LDL-C increased by 34mg/dL (0.88mmol/L) from its baseline value of 100mg/dL (2.59mmol/L) at 20 years of age in a healthy adult male. However, the key finding of the model centred on hepatic LDLr. It was observed that by decreasing the activity of the LDLr to 50% by age 65 years, this produced a rise

in LDL-C of 116 mg/dL (3.0mmol/L) from a base line value of 100mg/dL (2.59mmol/L) at age 20 years in a healthy male. This model is coded in the Systems Biology Markup Language, SBML (Hucka et al., 2003), and is archived in the BioModels database (Le Novere et al., 2006)(http://www.ebi.ac.uk/biomodels-main/BIOMD0000000434). This makes the model straightforward to adapt and update.
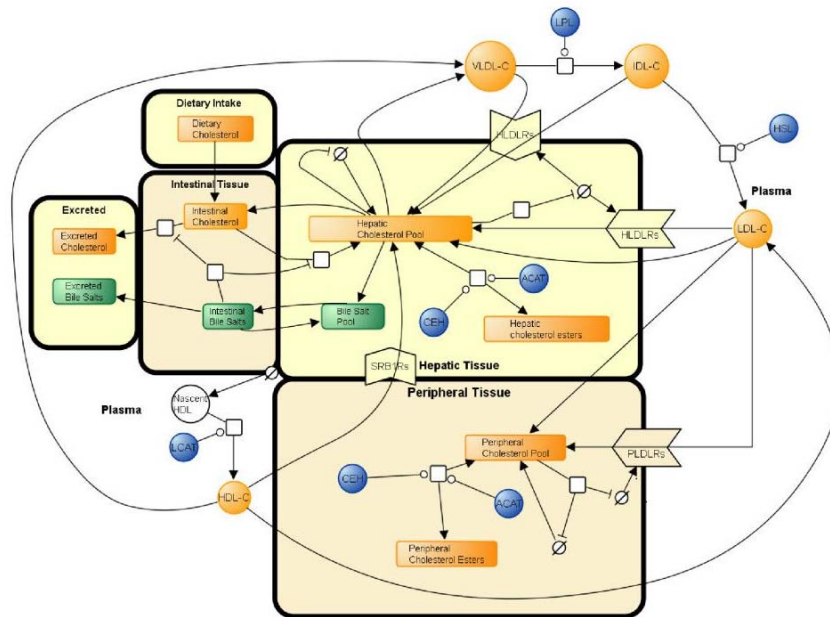
Figure 1.12 SBGN of the original whole-body model of cholesterol metabolism.
Taken from Mc Auley et al. (2012).
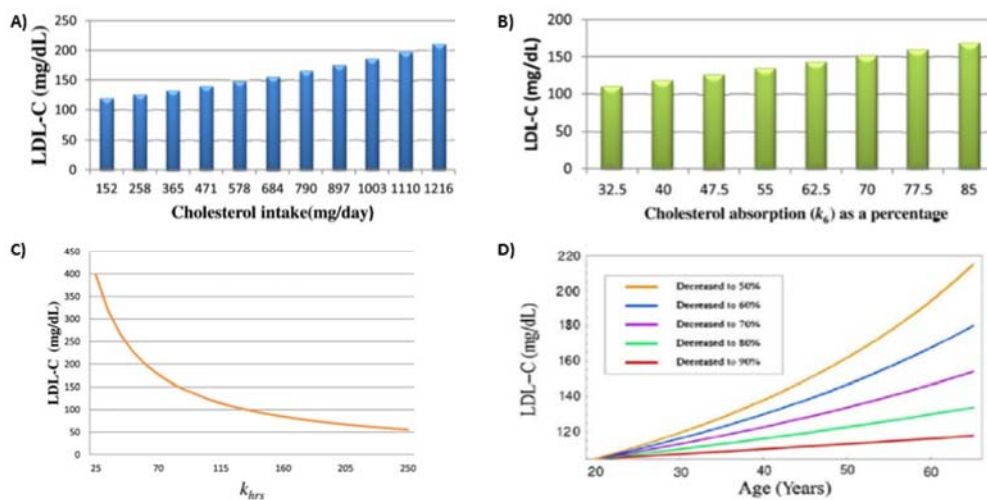
Figure 1.13 Example findings from the original model of whole-body cholesterol metabolism.
Figures show the effect of A) cholesterol intake, B) cholesterol absorption, C) rate of LDLr synthesis, D) ageing in the presence of reduced hepatic LDLr receptor synthesis, on LDL-C. Taken from Mc Auley et al. (2012).

Recently other groups have adapted the model, for example, Mishra et al. (2014) included the variables body weight and physical activity and explored cholesterol absorption in depth (Mishra et al., 2014). Moreover, Paalvast and colleagues (2015) used the model to conduct an *in silico* experiment utilizing the statin, simvastatin (Paalvast et al., 2015). To simulate this effect, the authors reduced hepatic cholesterol synthesis by 75%. This resulted in a reduction in LDL-C of 14% and 33% in six weeks and one year respectively. In recent years a number of other models have mathematically represented various aspects of cholesterol metabolism. Briefly, these include models of cholesterol biosynthesis (Bhattacharya et al., 2014; Kervizic and Corcos, 2008; Mazein et al., 2013; Watterson et al., 2013), lipoprotein dynamics (Chapman et al., 2010; Hubner et al., 2008; Shorten and Upreti, 2005; Sips et al., 2014), LDLr regulation (Shankaran et al., 2007), hepatic LDL-C endocytosis (Wattis et al., 2008), and RCT (Lu et al., 2014). Most of these models do not focus on the ageing process as such, but it is possible they could be adapted and merged to explore in depth some of the changes that occur within cholesterol metabolism during ageing, in particular the interaction of the gut microbiome with cholesterol metabolism.

1.1.12 Summary

Developed populations are living longer, resulting in an increase in the diseases associated with ageing (Prince et al., 2015). Of the diseases whose prevalence increases with age, CVD related mortality is by far the most common in over 85 year olds (Townsend et al., 2015). The risk factors for CVD are many, however together with classic factors such as chronological age, smoking, sex, blood pressure and diabetes; lipid biomarkers have become the cornerstone in determining CVD risk (Appelman et al., 2015). It is generally accepted that the relationship between CVD risk and the dysregulation of lipid metabolism is in part due to the strong association that exists between elevated TC/LDL-C and atherosclerotic plaque formation (Gould et al., 2007). Conversely, due to its role in RCT, HDL-C is widely regarded as being anti-atherogenic; evidenced by the inverse correlation between HDL-C levels

and CVD (Cooney et al., 2009). Fundamentally, cholesterol metabolism is maintained by a subtle balancing act between dietary ingestion, intestinal absorption, whole-body synthesis and excretion. These processes work in a coordinated fashion over a diverse range of spatial and temporal scales to help maintain whole body cholesterol balance. Changes to any of these processes can have a direct impact on the levels of LDL-C and HDL-C, thus indirectly influencing CVD risk, a finding of paramount importance, when considering the complex interactions that exist between cholesterol metabolism and the ageing process.

This section has highlighted the ageing process does not affect cholesterol metabolism at solely one, or even a number of sites, but rather each regulatory component of cholesterol metabolism is affected by the ageing process. There is a currently paucity of studies detailing the mechanistic changes to this system that occur with the ageing process. Furthermore, of those that exist, the majority tend to focus on murine models and were completed several decades ago. Despite this, the review uncovered a number of important findings about how cholesterol metabolism is affected by ageing. It was revealed that NPC1L1 expression significantly increases in the duodenum and jejunum with age, while ABCG5/G8 expression is suppressed (Duan et al., 2006). Moreover, in humans it has been found that the rate of bile acid synthesis declines with age, which occurs with a concomitant reduction in the hepatic expression of the rate limiting enzyme of bile acid synthesis, CYP7AI (Bertolotti et al., 2007). Also, from an intestinal perspective it has been suggested that the rise in LDL-C that accompanies ageing is due to a decline in BSH[+] species, such as *Lactobacillus* and *Bifidobacterium* (Hopkins and Macfarlane, 2002; Joyce et al., 2014). Additionally, when the impact of ageing on lipoprotein dynamics was examined, it was suggested that the mechanistic explanation for the rise in LDL-C during ageing, is due to a reduction in the rate of LDL-C clearance from the circulation (Millar et al., 1995). This assertion is certainly in line with the central finding from the recent mechanistic model of whole body cholesterol metabolism, which revealed that a reduction in the hepatic clearance rate of LDL-C is the central driver in dysregulating cholesterol metabolism (Mc Auley et al., 2012).

For the purposes of abstraction, this model did not incorporate many of the mechanisms outlined in this review. The dysregulation of cholesterol metabolism is the cumulative effect of ageing on many components of cholesterol metabolism and it is naïve to single out any one aspect in particular. This view is supported by findings from this section which revealed how other important aspects of cholesterol metabolism are affected by ageing. For instance, oxidative stress was shown not only to be involved in the progression of atherosclerosis, but to also be involved in the oxidation of HDL particles (Wang et al., 2014). Moreover, various molecular mechanisms involving intracellular cholesterol homeostasis and biosynthesis have been shown to be affected by the metabolic regulators mTOR and sirtuins. These cellular metabolic hubs are widely regarded as having a key role to play in intrinsic ageing and health-span. For instance, mTORC1 regulates SREBP levels, which in turn results in altered LDLr expression (Liu et al., 2015). In addition, Sirt6 has been identified as being involved in Srebp2 gene regulation (Tao et al., 2013). Collectively these findings emphasize that it not the dysregulation of one, or even a few, biological mechanisms; rather, age related dyslipidaemia is likely to be the result of a combination of several factors, and future therapeutic interventions should be underpinned by this.

This section also revealed diet has a key role to play in modulating cholesterol metabolism and could be a key therapeutic avenue to mitigate the effects ageing has on lipid metabolism. The central dietary paradigm of ageing research has been CR. This regime has been shown to have a positive cardioprotective effect in humans, part of which is brought about by an improvement in blood lipid profile in subjects undertaking this diet (Fontana et al., 2004). More conventional diets also affect cholesterol metabolism. The high levels of dietary phytosterols, MUFA, and PUFA typically found in the Mediterranean diet for instance, have been shown to modulate cholesterol metabolism, by increasing hepatic expression of LDLr, in addition to reducing cholesterol absorption (Richard et al., 2012). Thus, experimental evidence suggests employment of healthy diets such as the Mediterranean diet, and supplementation with probiotics for example (Al-Sheraji et al., 2012), could be utilised to slow the rate of LDL-C accumulation, associated with the ageing process.

One way in which the relationship between diet, ageing and cholesterol metabolism could be explored further would be to use mechanistic mathematical models. Recently, mathematical models have been used to explore the dynamics of cholesterol metabolism and the effect that both ageing and dietary changes have on it. One area that a mathematical model could be used to explore in greater depth, is the bi-directional relationship between the gut microbiome and cholesterol metabolism. Thus, modelling could help to identify alternative therapeutic targets, which could reduce the dependence on pharmaceutical intervention in older people to improve blood lipid profile.

1.1.13 Conclusion

It is evident, the breakdown of cholesterol metabolism associated with ageing results in increased LDL-C and has important implications for health-span. Dietary intervention offers a potential non-pharmacological avenue that could be invaluable for mitigating the insidious effects ageing has on this system. In recent years, there has been an increase in the use of mechanistic mathematical models to explore complex systems such as cholesterol metabolism in a more integrated and non-reductionist fashion. Such models should be increasingly used to determine new targets for therapeutic intervention.

1.2 PART 2: Ageing and DNA methylation

1.2.1 Introduction

The epigenetic mechanism of DNA methylation controls gene expression and repression (Lim and Maher, 2010). DNA methylation refers to the covalent addition of methyl (CH_3) groups to the carbon 5 position of the pyrimidine ring of cytosines, typically in a CpG dinucleotide, of which there are approximately 28 million in the haploid genome of a human (Stevens et al., 2013). Regions of DNA with a high CpG content are referred to as CpG islands (CGIs). There are approximately 45,000 CGIs per human haploid genome (Antequera and Bird, 1993), which are typically between 200 and 1400bp in length (Larsen et al., 1992) and generally located around transcription start sites (Saxonov et al., 2006). Saxonov, Berg and Brutlag (2006) determined that 72% of promoters are rich in predominantly unmethylated CpG (Saxonov et al., 2006). DNA methylation can be greatly varied due to a number of factors including age and disease status, as discussed in sections 1.2.2 and 1.2.3. Interestingly, hypermethylation of CpG sites in promoters or enhancers typically leads to transcriptional silencing, whereas hypomethylation of CpG sites in a gene body frequently results in an increase in gene expression (Mendizabal and Yi, 2016; Yang et al., 2014).

As outlined in Figure 1.14, the production of 5-methylcytosine is regulated by DNA methyltransferases (DNMTs) DNMT1, DNMT3A and DNMT3B, which transfer methyl groups from S-adenosyl-L-methionine (SAM). DNMT1 primarily acts as a maintenance methyltransferase, targeting hemimethylated DNA, formed after DNA replication, thus ensuring the re-establishment of the parental DNA methylation pattern in daughter DNA (Goyal et al., 2006); while DNMT3A and DNMT3B act as *de novo* DNA methyltransferases (Okano et al., 1999). Additionally, there is another member of the DNMT3 family, DNMT3L. Although catalytically inactive, DNMT3L has been observed to markedly stimulate the *de novo* methylation of DNA by DNMT3A when coexpressed (Chédin et al., 2002).

Demethylation can be either passive, through incorrect DNA replication, or be an active process regulated by TET enzymes. TET catalyse the oxidation of 5-methylcytosine to 5-carboxylcytosine via the intermediates 5-hydroxymethlcytosine and 5-formylcytosine. Thymine DNA glycosylase (TDG) then removes 5-carboxylcytosine and 5-formylcytosine from the DNA strand allowing the insertion of an unmethylated cytosine into the deleted base site through base excision repair (BER) (Rasmussen and Helin, 2016).
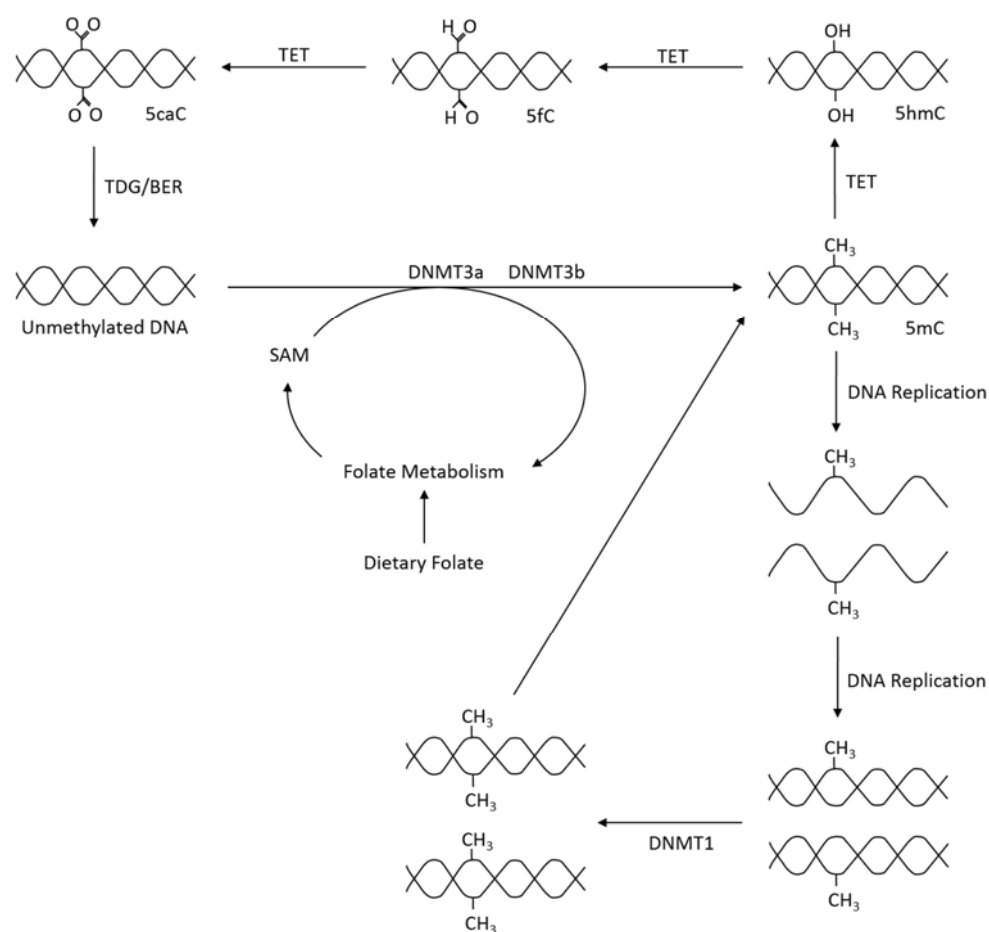
Figure 1.14 Overview of DNA Methylation.
De novo methylation is regulated by DNMT3a and DNMT3b and uses SAM as a methyl donor. The new methylation pattern is passed on to daughter cells through DNMT1, which acts on hemi-methylated DNA. DNA can become demethylated through the TET and TDG enzymes and BER. DNMT, DNA methyltransferase; TET, ten-eleven translocation; BER base excision repair, SAM, S-adenosylmethionine; 5mC, 5-methylcytosine; 5hmC, 5-hydroxymethlcytosine; 5fC, 5-formylcytosine; 5caC, 5-carboxylcytosine.

1.2.2 Impact of ageing on DNA methylation

During ageing, epigenetic drift can be used to describe the increase in methylation in CGI sites which are unmethylated in the young, and the decrease in methylation globally. These findings have been reported across species (Maegawa et al., 2017). Maegawa et al. (2017) showed that average methylation increased from 2±0.1% to 18±5%, 2±0.3% to 22±3%, and 3±0.5% to 20±4 with age in sites observed to be unmethylated in young mice, rhesus monkeys and human subjects respectively. When analysing highly methylated non-CGI sites, ageing resulted in a reduction in methylation from 94±0.4% to 78±4%, 94±0.3% to 73±4%, and 93±1% to 74±2% in the same three mammalian species. These data indicate that methylation drift associated with ageing is evolutionarily conserved. Interestingly, drift rates were calculated as 4.1±1.2%, 0.34±0.14% and 0.1±0.02% per year for mice, rhesus monkeys and human respectively, and an inverse relationship between the rate of methylation drift and longevity in these mammalian species was established (Maegawa et al., 2017). A similar finding was described by Wilson et al. (1987). In this work, ageing resulted in a global decrease in 5-methyldeoxycytidine in multiple tissues from two murine models and human bronchial epithelial cells obtained from autopsy donors, and an inverse relationship between lifespan and rate of loss of 5-methyldeoxycytidine was reported. An estimated loss of 5.6-8.9 $x10^5$ and 2.3-2.8 $x10^5$ 5-methyldeoxycytidine per year was observed for *Mus musculus* and *Peromyscus leucopus* species which have lifespans of 3.5 and 8.0 years respectively, while a loss of $1.6x10^4$/year was observed in human cells (Wilson et al., 1987). Their conclusion corroborates the findings of Drinkwater et al. (1989), where it was determined that lymphocytes obtained from 20-30 year old volunteer donors contained 54.6±1.6% methylated CmCGG sites, while a statistically significant 7.1% reduction (47.5±2.6%) was observed in 65-80 year olds (Drinkwater et al., 1989).

Maegawa et al. (2017) further examined if methylation drift is ubiquitous in differing tissue types. By analysing 12 genes which were associated with hypermethylation and three associated with hypomethylation with age, it was determined that tissue from kidney and liver generally exhibited

lower levels of age related hypermethylation. In contrast, tissue from the intestines (small and large) and bone marrow showed reduced age associated hypomethylation. In further investigations by Maegawa et al. (2017) it was reported that there was a significant inverse relationship between methylation drift and the level of change in gene expression. It was noted that when looking at the methylation pattern of genes which had increased expression, a significant reduction in DNA methylation was observed, while conversely, silenced genes had a concomitant increase in methylation.

Altered expression of the enzymes responsible for DNA methylation and demethylation have been repeatedly reported to be a contributing factor for the changes observed in DNA methylation patterns with age. For instance, Sun et al. (2014) observed the expression of genes encoding for the DNA methyltransferases *dnmt1*, *dnmt3a*, and *dnmt3b*, considerably declined between the ages of 4 months and 24 months in C57BL/6 male mice. Interestingly, the expression of demethylation enzymes *Tet1* and *Tet3* were also reduced with age (Sun et al., 2014). In humans, a reduction in TET1 and TET3 expression was observed with age, and a correlation between TET1 and DNMT1, DNMT3B and TDG was determined in peripheral blood mononuclear cells obtained from 188 volunteers, aged 34-74, from eight European countries. Interestingly, while a global reduction in 5-hydroxymethylcytosine (5hmC) was also detected with age, a statistically significant increase in the methylation of the CpG islands within the TET1 gene was found in 69-74 year olds when compared to 34-41 year olds (Valentini et al., 2016). These findings are consistent with the observation that hypermethylation within certain gene regions is often associated with gene silencing.

In contrast to the findings of Sun et al. (2014), Lopatina et al. (2001) showed that although DNMT1 declined with age in WI-38 fibroblast cells, the activity of *de novo* methylation enzymes decreased in middle age, compared with young cells, and rose slightly with senescence. This resulted in the ratio of *de novo* to maintenance methylation enzymes increasing with age. The authors postulate that the decline in DNMT1 could lead to the global hypomethylation, and the rise in the ratio of *de novo* to

maintenance methylation enzymes with age could be responsible for the regional hypermethylation associated with gene silencing (Lopatina et al., 2002). Similarly, Casillas Jr et al. (2003) observed that DNMT1 expression declined significantly with age in foetal human WI-38 fibroblasts, with old aged cells having 75.44% of the expression exhibited by young cells. Furthermore, the activity of this maintenance methyltransferase declined from 83.2cpm/µg protein in young cells to 52.1cpm/µg protein in middle aged cells, and to 28.1cpm/µg protein in old lung WI-38 fibroblast cells. Conversely, the activity of the *de novo* methyltransferases increased from 21.4cpm/µg protein in young cells to 59.0 and 75.0cpm/µg protein in middle aged and old cells respectively. Interestingly, ageing appeared to have an opposing effect on the expression of the *de novo* methyltransferases, with DNMT3a declining to 60.61% that of young cells in old age, while expression of DNMT3b in young cells was 75.21% of that expressed by old cells. Thus again, the change in the ratio between maintenance methyltransferases and *de novo* methyltransferases could be a key factor in the aberrant DNA methylation associated with ageing.

1.2.3 DNA methylation and cancer

Germline cells have specific DNA patterns to enable suitable gene regulation during embryonic development. Importantly, within a small proportion of genes, one parental allele is exclusively expressed, due to a DNA methylation regulated gene imprinting (Barlow and Bartolomei, 2014). Inappropriate methylation during development can result in imprinting failures and diseases including Beckwith-Wiedemann, Prader-Willi, Silver-Russell and Angelmans's syndromes (Bartolomei and Ferguson-Smith, 2011). Epigenetic modifications are also frequently seen in diseases with later onsets; including cancer (Kulis and Esteller, 2010), neurodegeneration (Sanchez-Mut et al., 2016), and autoimmune disease (Richardson, 2003). With a focus on the effect of epigenetic modification on cancer pathogenesis, both gene silencing, due to hypermethylation in gene promoters (Merlo et al.,

1995), and oncogene activation or chromosomal instability due to global hypomethylation (Gaudet et al., 2003; Rosty et al., 2002) will be discussed.

In one study of promoter hypermethylation, it was reported that in 7/9 non-small cell lung cancers, the tumour suppressor gene *p16* was fully methylated, while the CpG islands in samples of healthy lung, kidney, and blood lymphocytes were found to be unmethylated (Merlo et al., 1995). Interestingly, Christensen et al. (2010) discovered through locus-by-locus analysis, a trend between loci methylation and cancer characteristics including tumour grade and size, oestrogen and progesterone status and triple negative status in invasive breast cancer specimens from 162 women from Northern California. At all 74 CpG loci which were associated with tumour size, there was a positive correlation between the level of methylation and tumour size. Moreover, increased methylation was observed in all five CpG loci associated with lymph node infiltration, when disease-positive lymph nodes were reported. Array validation revealed CpGs within the promoters of P2RX7, a gene encoding for a receptor which mediates apoptosis, and HSD17B12, a gene coding for an enzyme involved in oestrogen metabolism and fatty acid elongation, had statistically elevated methylation levels as tumour size increased. Additionally, methylation of CpGs within the promoter of GSTM2, which reduces mRNA expression of the detoxifying enzyme GSTM2, was correlated with tumour grade (Christensen et al., 2010).

Similarly to the aberrant DNA methylation associated with ageing, disease associated changes to the methylome could be due to changes in DNMT expression. For instance, in a study of 76 women with primary cervical cancer, DNMT1 was observed using immunostaining, in 77.5% of cancer cells. In comparison, this enzyme was observed in only 16% of normal cells. In addition, the intensity score of staining (0 for no staining, 4+ for intense staining), was reported as 1.0 for cancerous cells compared with a reduced figure of 0.2 for normal cells. Interestingly, individuals with >77.5% DNMT1 positive cells were 4.3 times more likely to die prematurely compared with individuals who exhibited <77.5% DNMT1 positive cells, while those with an intensity score >0.9625 were 4.9 times more likely to die

earlier than those <0.9625 (Piyathilake et al., 2017). Furthermore, Mizuno et al. (2001) determined that in 33 patients with acute myeloid leukaemia (AML), DNMT1, DNMT3A and DNMT3B exhibited an average 5.3, 4.4 and 11.7 fold increase in comparison to levels observed in control bone marrow cells. Interestingly, p15^{INA4B}, a tumour suppressor gene commonly silenced by methylation in AML, was methylated in 72% of AML patients, and in these 24 cases, DNMT1 was statistically higher than those without p15^{INA4B} methylation. Further examination of chronic myeloid leukaemia cells revealed that DNMT expression was phase dependent. During the chronic phase, expression of these three methyltransferases was comparable to normal bone marrow cells, however, with advancement to the acute phase, DNMT1, DNMT3A and DNMT3B expression was raised with an average 3.2, 4.5 and 3.4 fold increase respectively (Mizuno et al., 2001). Conversely, Gaudet et al. (2003) reported that mice exhibiting 10% of DNMT1 compared with wild type mice, exhibited a 30% reduction in birth weight, and 80% developed aggressive T cell lymphoma within 8 months. While examining hypomethylated tumours, it was determined that 10/12 exhibited chromosomal instability (gain of chromosome 15), in comparison to only 2/12 Moloney murine leukaemia virus induced tumours, thus indicating that global hypomethylation can also play a role in the pathogenesis of cancer through chromosomal instability (Gaudet et al., 2003).

1.2.3.1 EN1 gene and disease

The EN1 gene encodes for the protein homeobox protein engrailed-1. First characterised in drosophila, EN1 mutation results in abnormal development including posterior-anterior duplications and malformation of the wings (Garcia-Bellido and Santamaria, 1972). Within humans, the EN1 gene has been associated with pattern formation within the central nervous system during development (Zec et al., 1997). Wilson et al. detail that expression of EN1 is observed within multiple neuronal cell types within the cerebellum, and that great changes to its distribution occurs during gestation, with expression remaining until >21 days (Wilson et al., 2011).

Hypermethylation of this gene has been observed in multiple cancer types including colorectal (Mayor et al., 2009), prostate (Devaney et al., 2011), and breast cancer (Carrascosa et al., 2014). For instance, Bell et al. (2011) reported that the EN1 gene transcriptional start site exhibited significant hypermethylation in human salivary gland adenoid cystic carcinoma when compared with normal tissue, with a 59% difference in methylation across the EN1 promoter. Furthermore, the extent of hypermethylation was correlated with tumour grading, location and patient outcome. Significantly, it was observed that out of 32 loci, the EN1 gene displayed the greatest difference in methylation between normal and diseased tissue, and little variation in hypermethylation across nine CpG islands, thus emphasising its possible use as a biomarker for cancer detection (Bell et al., 2011). Similarly for prostate cancer, differential methylation between normal and cancerous cells was greatest in the EN1 gene (Devaney et al., 2011). In addition, the EN1 gene was most frequently methylated in colorectal cancer when compared to the SCTR and INHBB genes. Interestingly, EN1 was more likely to be methylated in colorectal carcinoma compared to colorectal adenoma, with 73% (66/90) colorectal carcinomas and 40% (4/10) adenomas showing hypermethylation, and result in gene silencing (Mayor et al., 2009). Similarly, Frigola determined that the EN1 gene was hypermethylated in 70% of colorectal tumours, and found hypermethylation resulted in suppression of the EN1 gene (Frigola et al., 2006). Importantly Mayor et al. (2009) outlined that only 1.12% (1/89) of EN1 genes in normal samples exhibited hypermethylation, an important factor when searching for a cancer biomarker. Interestingly, EN1 methylation resulted in approximately a 30% reduced survival rate after 5 years compared to patients without hypermethylation of the EN1 gene (Mayor et al., 2009).

1.2.4 Effect of poor diet on DNA methylation and disease

There is a strong association between poor diet, obesity, and cancer (Dobbins et al., 2013). For instance, Zhang et al. (2017) examined the effect of DNA methylation in rats fed a high fat diet for 14 weeks, and reported that within 1000bp of transcriptional start sites of known genes, seven genes

exhibited differentially methylated CpGs. These differences ranged from 5-22%, and resulted in altered gene expression, in animals which gained approximately 90% body mass from the high fat diet, in comparison to rats fed a standard chow diet. When expanding to CpGs within 10,000bp of transcriptional start sites, 147 genes were differentially methylated and expressed. One of the genes of note, *Phlda1*, became hypermethylated with a high fat diet, which was associated with reduced expression, and in turn steatosis, a contributor to the pathophysiology of obesity (Zhang et al., 2017). Furthermore, Vucetic, Kimmel, and Reyes (2011) outlined that mice fed a high fat diet (60% fat) from weaning at 3 weeks, until 18-20 weeks, showed significant hypermethylation in the μ-opioid receptor (MOR) promoter in reward-related brain regions, and repression of the MOR gene, which was related to an increase in binding of the transcriptional repressor methyl CpG binding protein 2 (MeCP2). It was suggested that repression of the MOR gene was responsible for a significantly reduced preference for sucrose; thus indicating that animals on a high fat diet exhibit reward hypofunctioning, which may contribute to difficulties reversing obesity after long term exposure to highly palatable foods (Vucetic et al., 2011). As mentioned, obesity is strongly linked with cancer (Han et al., 2014). For instance, it has been found that many of the 31 differentially methylated CpGs in obese children, and 151 differentially methylated CpGs in severely obese children discussed by Fradin et al. (2017) are also associated with cancer, thus warranting concern regarding the risk for cancer pathogenesis in later life (Fradin et al., 2017). Similar results were observed by Xu et al. (2013) who examined differentially methylated CpG sites in 48 obese African American participants aged 14-20 years old compared to their non-obese counterparts (Xu et al., 2013). It is important to note that the type of ingested fat may differentially methylate DNA. Garcia-Escobar et al. (2017) examined the effect of different fats on TNFα promoter methylation, and reported reduced methylation in animal who were fed coconut oil (high saturated fat, SFA), which was inversely correlated with the pro-inflammatory cytokine TNFα in adipocytes (García-Escobar et al., 2017).

1.2.5 Aberrant DNA methylation therapy

Lifestyle factors including diet, physical activity, weight, and smoking status, have a significant impact on the methylome and age related disease (Lim and Song, 2012). As lifestyle factors such as these can influence DNA methylation, targeting the methylome with a more potent modulator, such as chemotherapy, could provide a promising avenue to treat diseases such as cancer.

1.2.5.1 Diet

The role of diet in modulating metabolic health throughout lifespan has long been known. For instance, a significant amount of insight has been gained from analysing the impact of being born during the Dutch Hunger Winter, which took place in the Netherlands during World War 2. It is now emerging that changes to DNA methylation could be a central player in directing how the deleterious effects of the Dutch Hunger Winter unfold. A recent genome-scale analysis of differential DNA methylation in whole blood after periconceptional exposure to famine during the Dutch Hunger Winter emphasises this phenomenon (Tobi et al., 2014). Following a thorough assessment of prenatal malnutrition-associated differentially methylated regions (P-DMRs), it was found that P-DMRs which preferentially occur at regulatory regions, are characterized by intermediate levels of DNA methylation, and map to genes enriched for differential expression during early development. Moreover, it was revealed differential methylation of P-DMRs was associated with 256 pathways which are defined by growth and metabolism. P-DMRs found in the insulin receptor precursor gene and the carnitine palmitoyltransferase 1A gene (involved in fat metabolism) were found to have enhancer activity *in vitro* and differential methylation was interconnected with birth weight and serum LDL-C levels. In addition to the findings from studying those exposed to the Dutch Hunger Winter, it has also been recognised by Barker since the mid-1990s that exposure to a suboptimal intrauterine environment has deleterious metabolic consequences for later life (Barker, 1995). Similar to the Dutch Hunger Winter, recent studies have revealed that this phenomenon is underpinned by epigenetic

regulation. For instance, it has been shown that placental leptin DNA methylation levels were correlated with glucose levels (2-hours post-oral glucose tolerance test) in women with impaired glucose tolerance and with decreased leptin gene expression in the whole cohort (Bouchard et al., 2010). The methylome is not simply a nutrient sensor during the intrauterine period. Strikingly, in a recent study DNA methylation changes were correlated with body composition in pre-school children as part of the epigenome-wide-analysis in the European Childhood Obesity Project (CHOP). It was found DNA methylation variants were identified to be associated with BMI, fat-mass, fat-free-mass, fat-mass-index and fat-free-mass-index (Rzehak et al., 2017). Specific aspects of diet have also been associated with DNA methylation changes. As discussed, the effect of poor diet on aberrant DNA methylation and disease pathogenesis can be significant, therefore it is conceivable that a healthy diet regime may play a role in the prevention of aberrant DNA methylation. For instance, plant polyphenols, originating in fruit and beverages, and often associated with healthy diets, have been associated with reduced oxidative stress, inflammation and risk of cancer (Zhang and Tsao, 2016), which may be mediated through modulation of DNA methylation (Mileo and Miccadei, 2016). In one example, polyphenols associated with the Mediterranean Annuraca apple, reportedly increased p53, and reduced methylation in the promoters of hMLH1, p14ARF, and p16INK4a, restoring normal expression of silenced tumour suppressor genes in colorectal cancers (Fini et al., 2007). In another example, it was observed that 2 weeks of 6g/day of cocoa, a rich source of polyphenols, lead to a reduction in global DNA methylation in participants with pre-hypertension, type 1 hypertension, or hypercholesterolaemia. In this randomised control trial, global DNA methylation was reported as 3.909 ±0.380% in control subjects, compared with 2.991 ±0.366% in subjects who consumed cocoa (Crescenti et al., 2013). Furthermore, *in vitro* treatment of subject peripheral blood mononuclear cells, revealed cocoa significantly lowered DNMT1, 3a and 3b mRNA expression in addition to methylenetetrahydrofolate reductase (MTHFR) and 5-methyltetrahydrofolate-homocysteine methyltransferase reductase (MTRR) gene expression (Crescenti et al., 2013). Similar results were observed by Nandakumar et al. (2011) who reported that green tea polyphenols epicatechin-gallate

and epigallocatechin-3-galate significantly lowered DNMT1, 3A and 3B activity and expression in a dose dependent manner, reduced global methylation, and reactivated the silenced tumour suppressor genes p16[INK4a] and Cip1/p21 in human skill cancer A431 cells (Nandakumar et al., 2011).

1.2.5.2 Folate feeding studies

One of the most studied supplements in regards to DNA methylation is folate. This is because, folate plays a key role in one carbon metabolism through its conversion to N-5-methyltetrahydrofolate which in turn is converted to SAM, the global methyl donor in DNA methylation (Crider et al., 2012). Methyl group deprivation can lead to changes in one carbon folate metabolism, metabolites, which can irreversibly perturb DNA methylation and interestingly, induce lesions associated with the pathogenesis of cancer. For instance, Pogribny et al. (2006) reported that male F344 rats fed a diet deficient in methyl groups (low methionine and choline, and folic acid negative) for 9 weeks, exhibited a 70% reduction in SAM when compared to mice on a control diet, while S-adenosylhomocysteine (SAH) was unaffected. Thus a significant decrease in the SAM/SAH ratio, an important predictor of methylation capacity, was observed. The methyl-deficient diet also lead to a 60% increase in unmethylated CCGG sites obtained from liver tissue. Interestingly, the reintroduction of a methyl-sufficient diet resulted in normalised DNA methylation in rats who were fed a methyl-deficient diet for 9 weeks. However, in rats fed a methyl-deficient diet for 18, 24 or 36 weeks, the reintroduction of a methyl-sufficient diet could not reverse the hypomethylation induced. Significantly, the appearance of glutathione-S-transferase π (GSTπ), a characteristic of hepatocarcinogenesis was observed despite the reintroduction of the methyl-sufficient diet, even after 9 weeks of exposure to a methyl-deficient diet (Pogribny et al., 2006). Additionally, Jung et al. (2011) reported that 800μg/day for 3 years of folic acids did not influence DNA methylation in moderately hyperhomocysteinemic Dutch males and females aged 50-70 years (Jung et al., 2011).

In contrast, results from Pufulete et al. (2005) suggest DNA hypomethylation brought about by low dietary folate could be reversed by folate supplementation. It was reported that a 400µg/day for 10 weeks supplement of folic acid, in patients with colorectal adenoma, increased serum folate from 7.4 to 13.4µg/l, and plasma homocysteine decreased 12%, while DNA methylation increased by 31 and 25% in leucocytes and colonic mucosa respectively (Pufulete et al., 2005). Interestingly, Park et al. (2017) found folate supplementation produced distinct differences in DNA methylation patterns dependent on body weight. In this study, supplementation of 800µg/day for 8 weeks in normal weight and obese females aged 18-35 increased serum folate by 86.2 and 109.6% respectively. Before supplementation, 10.7% of CpG sites differed between the different weight categories; this rose to 15.2% after supplementation. Higher levels of methylation were observed in 52.9% and 55.0% of obese women before and after treatment respectively. After treatment, CpG sites were more likely to have reduced levels of methylation; 67.9 and 75.8% for normal weight and obese females respectively. Interestingly, while the supplementation induced methylation changes in genes associated with neural tube closures in women of normal weight, overweight women exhibited changes in methylation in genes associated with folate metabolism, methylation and vitamin B metabolism (Park et al., 2017).

Conversely, a 3 month 100µg/day, 400µg/day, and a 4000µg/day supplement of folate resulted in an 11.5, 11.7 and 18.9% reduction in % 5 methyl-deoxycytidine respectively in coagulated blood samples from Chinese women of reproductive age, who showed an average % methyl-deoxycytidine level of 4.42±0.12% at enrolment. Interestingly, it was observed that genotype can influence the DNA methylation response to dietary folate. When analysing the effect of a 3 month 4000µg/day folate supplement in the presence of the MTHFR 677C→T variant, it was found that there was an 11.6, 18.8 and 19.5% reduction in % 5 methyl-deoxycytidine for the CC, CT and TT genotypes respectively compared to baseline results (Crider et al., 2011).

1.2.5.3 Caloric restriction

Recent evidence has suggested that CR, a dietary regime defined by a 20-40% reduction of calories, that does not induce malnutrition even in the short term, could potentially ameliorate aberrant methylation in disease associated genes, as observed in age related methylation drift (Kim et al., 2016). Maegawa et al. (2017) detailed that CR was able to counteract hypermethylation associated with ageing without producing novel methylation patterns. In both DNA from whole blood of mice and Rhesus monkeys, a significant inverse relationship was observed between CR and the rate of methylation drift. Specifically, there was an average DNA methylation, across 24 genes, of 26±2% and 27±0.7% for aged mice and Rhesus monkeys fed *ad libitum*, compared to 17±0.7 and 24±0.9% in aged mice and Rhesus monkeys respectively who underwent CR (Maegawa et al., 2017). Similarly, dietary restriction (DR) has also been shown to have a beneficial effect on DNA methylation. DR can be used to describe a broader range of dietary interventions than CR, and can include short term starvation, fasting, and diets which contain a normal amount of calories, but contain nutrient deficiencies, such as protein or carbohydrates (Lee and Longo, 2016). Hahn et al. (2017) showed that mice which underwent 40% dietary restriction, which was applied by measuring the food intake of *ad libatum* fed mice, and feeding the test group 40% less food, exhibited a reduced number of differentially methylated regions in DNA extracted from the liver. In aged mice fed *ad libitum*, age differentially methylated 3176 regions, of which 1945 became hypermethylated and 1231 became hypomethylated, whereas aged mice who underwent 40% DR exhibited only 2250 differentially methylated regions, of which 1512 became hypermethylated and 738 became hypomethylated (Hahn et al., 2017). To further this, Wang et al. (2017) reported that 40% CR resulted in a predicted 9.4 month reduction in epigenetic age within the livers of 22 month old mice compared with age-matched controls (Wang et al., 2017), therefore it appears that CR may provide a promising treatment strategy for aberrant DNA methylation.

1.2.5.4 Drug therapy

Due to the association of hypermethylation of promoters and tumour suppressor gene silencing in cancer, the use of drugs which ameliorate this change may provide a successful method for reducing DNA methylation in these regions and enable the re-expression of these genes. Hypomethylating agents 5-azacytidine (azacytidine) or 5-Aza-2'-deoxycytidine (decitabine) are two such examples, which were approved for use throughout the European Union, by the European Medicines Agency (EMA) in 2008 and 2012 respectively, for patients with myelodysplastic syndromes (MDS) (European Medicines Agency, 2017a, b).

Following cellular uptake of decitabine, it is phosphorylated to 5-aza-2'-deoxycytidine-triphosphate, and becomes incorporated into DNA strands in place of cytosines within CpG sites. The substitute nucleotide binds DNA methyltransferases similarly to cytosine, however due to the substitution of carbon-5 in the cytosine ring for nitrogen, β-elimination is inhibited and thus covalent bonding is irreversible. This results in enzyme inhibition and eventual degradation of the bound enzyme, and therefore a reduction in DNA methylation. Azacytidine acts in a similar way, however acts upon RNA. Interestingly, during phosphorylation, approximately 10-20% is converted to a 5-aza-2'-deoxycytidine-triphosphate precursor and thus acts upon DNA (Stresemann and Lyko, 2008).

While meta-analysis data suggest that both Azacitadine and Decitabine are superior to best supportive care in patients with MDS (Almasri et al., 2015), there is conflicting evidence on the superiority of these drugs. For instance, Lee et al. (2013) conducted a comparative analysis of Azacytidine, given for 7 days in a 28 day cycle, and Decitabine, given for five consecutive days in a 28 day cycle, in patients with myelodysplastic syndromes, and response rates of 46 and 52%, a median peak response observed at 4.2 and 4.0 months, and median survival time of 23.3 and 22.9 months were reported respectively. While these parameters were not statistically different from one another, it was established that the survival rate was significantly improved in patients >65 taking Azacitidine, and patients showed reduced vulnerability to infection, in addition to a lower incidence of grade 3/4 of cytopenia (Lee et

al., 2013). Xie, Jiang and Xie (2015) conducted a meta-analysis of 11 trials, containing 1392 MDS patients and similarly found that while there was no significant difference between the rate of complete response in patients undertaking Decitabine or Azacytidine treatment (13 vs. 12%), Azacitidine treatment resulted in a significantly higher overall response rate compared with Decitibine (73 vs. 42%). Moreover, a statistically significant improvement in overall survival was observed for Azacytidine treatment when compared to best supportive care, while no statistical difference was observed for Decitabine treatment (Xie et al., 2015).

In contrast, results from a randomised phase II trial in patients with low/intermediate-risk MDS or chronic myelomonocytic leukemia indicated an overall response rate of 70 and 49% for patients who received intravenous Decitabine or Azacytidine for three consecutive days, on a 28 day cycle, respectively. Furthermore, the one year event-free survival rate was significantly greater in patients who received Decitabine (74 vs. 55%). In addition, haematological improvements were observed in 24% of patients treated with Decitabine compared with 8% of Azacytidine patients, and of the patients who were transfusion dependent at the start of the trial, 32 and 16% became transfusion independent following Decitabine or Azacytidine treatment (Jabbour et al., 2017).

However, it is important to note that the use of such hypomethylating agents should be used with caution due to selectivity concerns. For instance, in one study which used Azacytidine to treat the non-invasive breast cancer cell lines MCF-7 and ZR-75-1, the drug lowered DNMT1 and DNMT3b and methylation within the promoters of several pro-metastatic genes, including uPA and MMP2, leading to gene expression. Furthermore, it was shown that treatment increased the invasiveness of both cell lines (Chik and Szyf, 2011).

1.2.6 The use of electrochemical techniques in ageing

In recent years a systems orientated approach has become increasingly popular in bioscience research (Breitling, 2010; Bruggeman and Westerhoff, 2007; Mc Auley et al., 2015a; Mc Auley et al., 2017). The essence of this methodology is to utilise novel approaches to study molecules, cells, or entire organisms. Nutrition research is no different, and is beginning to benefit from this new paradigm (Mc Auley et al., 2013; Morgan et al., 2016c; Salcedo-Sora and Mc Auley, 2016). It can be argued electrochemical techniques, which describe analytical methods that use potential, charge, or current, to determine the concentration, or chemical reactivity, of an analyte (Harvey, 2002), come under this umbrella of systems techniques.

There is great demand for new strategies to detect biomarkers associated with age-related disease, especially those which are available at the point of care, and electrochemical techniques are of great value to this field (Campuzano et al., 2017). There are several examples of the use of electrochemical techniques in ageing. For instance, Fagan-Murphy et al. (2016) developed a sensor for ROS, a chemical implicated in the ageing process. Using the CNS homogenates from young and old common pond snails, it was found that the current was greater at all four potentials examined, indicating there were significantly greater levels of H_2O_2 in the older animals (Fagan-Murphy et al., 2016). In another example, Esteves-Villanueva et al. (2014) used EIS for the electrochemical detection of tau protein misfolding, a protein associated with neurodegeneration. It was reported that a decrease in R_{ct} was observed when binding occurs; this was explained by conformational changes upon binding. The authors postulated this approach could be used to screen for the early onset of neurodegeneration (Esteves-Villanueva et al., 2014).

There are also numerous examples of electrochemical techniques being used to detect cancer. These techniques utilise a broad range of methodologies and biological targets. For instance, Damiati et al. (2017) used anti-CD133 antibodies bound to a Au-SPE to detect liver cancer cells. Results showed that as the number of HepG2 cells captured increased, the peak current decreased (Damiati et al., 2017).

Conversely, Benvidi et al. (2015) used EIS, CV and DPV to detect the tumour suppressor gene *BRCA1* gene in an immobilised probe on a gold working electrode. Using a Ag/AgCl reference electrode and platinum counter electrode, it was shown that the gene could be detected, thus the technique could be implemented in the diagnosis of breast cancer. It is important to note the findings indicated that EIS was the superior electrochemical test for detecting the gene (Benvidi et al., 2015). In another example, Ahmed et al. (2017) used DPV to detect phosphorylation of the EGFR protein, as often cancerous cells exhibit aberrant protein phosphorylation. By adsorbing the purified protein directly onto a gold working electrode, the method required as little as 50ng of protein. The technique was also used to determine the effect of the tyrosine kinase inhibitor Gefinitib, a drug which restores the function of aberrantly phosphorylated proteins. It was observed that cells grown in the presence of this commonly used chemotherapeutic for lung cancer, showed reduced adsorption, resulting in a lower peak current. Thus this work showed that not only can phosphorylated proteins associated with cancer be detected, but drug treatment could also be successfully monitored (Ahmed et al., 2017).

Recently, there has been heightened interest in using electrochemical techniques to detect DNA methylation as a sensor for cancer. This is because they can be rapid, easy to use and cost effective solution to many of the challenges posed by more conventional methods, and enable the quantitative analysis of complex biochemical systems (Hossain et al., 2017).

1.2.7 Detecting DNA methylation

There are several techniques that can be employed to analyse DNA methylation, many of which require prior bisulphite conversion, which converts unmethylated cytosines to uracil, while methylated cytosines remain unchanged. These techniques include bisulphite sequencing (Li and Tollefsbol, 2011), methylation specific PCR (Herman et al., 1996), pyrosequencing (Tost and Gut, 2007), and immuno-based recognition (Rauch and Pfeifer, 2005). Methods which do not require prior bisulphite conversion include high performance liquid chromatography (Armstrong et al., 2011), mass

spectrometry (Lin et al., 2016), microarray analysis (Schumacher et al., 2006), surface plasmon resonance (Sina et al., 2014), and surface enhanced Raman spectroscopy (Hu and Zhang, 2012). Many of these methods have several drawbacks including the need for expensive laboratory equipment and/or biological molecules coupled with long analysis times and the requirement for highly skilled operators. Electrochemical techniques have been investigated as a possible method of detecting DNA methylation due to the sensitive and specific results they are able to produce, in addition to the relatively simple, cost effective and rapid procedure. A significant factor to also consider is that electrochemical detectors can often be miniaturised or multiplexed; important for *in situ* testing (Hossain et al., 2017). An example of an elegant electrochemical DNA-methylation sensor, is the eMethylsorb method of Koo et al. (2014). The method consists of two steps. First, a gold electrode is exposed to a solution of bisulfite modified and asymmetrically amplified DNA. This exploits the findings of Kimura-Suda et al. (2003), who demonstrated that single stranded homo-oligonucleotides adsorbed onto gold with the following affinity A > C ≥ G > T (Kimura-Suda et al., 2003). The DNA adsorption essentially blocks (or passivates) the gold surface, decreasing its reactivity. The lower the methylation level of the original DNA, the higher the number of adenines present in the bisulfite treated sample. Consequently, unmethylated DNA results in a more passivated and less reactive surface than methylated DNA. In the second step of the eMethylsorb method, the reactivity of the gold electrode surface is measured in an electrochemical reaction. Initially, Koo et al. (2014) developed the eMethylsorb method using disposable gold screen printed electrodes (consisting of a 4mm diameter gold working electrode, gold counter electrode, and silver reference electrode). These were exposed to solutions of synthetic oligonucleotides diluted in 5X SSC buffer, designed to represent bisulphite modified and asymmetrically amplified methylated and unmethylated versions of a 53 base section, containing eight CpG sites, of the EN1 gene promoter. After the adsorption step, the reactivity of the modified gold surface was measured by performing differential pulse voltammetry (DPV) in an electrolyte containing 2.5mM ferrocyanide, 2.5mM ferricyanide and 100mM KCl, where the peak current for the reduction of Fe^{3+} to Fe^{2+} inversely correlated with the level of DNA adsorption on the

gold electrode. Optimisation of the adsorption step revealed the greatest current response difference (between methylated and unmethylated samples) was observed when 50nM of synthetic oligonucleotides was adsorbed for 10 minutes (in quiescent solution) at pH 7.0. The method was used to successfully detect 10% methylation in heterogeneous samples of synthetic oligonucleotides. Furthermore, the technique was able to detect 10% methylation in heterogeneous samples containing various combinations of MCF-7 and whole genome amplified (WGA) DNA. Interestingly, the sensitivity of the method was significantly greater for these 140 base DNA samples in comparison to the 53 base synthetic oligonucleotides (Koo et al., 2014). In a related study, the same research group used a 2mm gold disk working electrode (Pt counter electrode and Ag/AgCl reference electrode) to detect methylation levels in the same synthetic oligonucleotides (in 5X SSC buffer). The electrochemical reactivity of the modified gold surface was measured via DPV in a solution of 2.5 mM ferrocyanide, 2.5 mM ferricyanide and 10 mM PBS. Using the two-step eMethylsorb procedure, the greatest relative current difference was observed between methylated and unmethylated DNA, when 200nM DNA was adsorbed for 10 minutes (in quiescent solution) at pH 7.0. Again a negative linear relationship between % methylation in heterogeneous samples of synthetic methylated and unmethylated oligonucleotides and relative current response was observed (R^2 = 0.99398). Sina et al. (2014) also investigated the effect of the number of methylated CpG sites within the 53 base synthetic oligonucleotide (0, 1, 4, and 8). A negative linear relationship was observed between the number of methylated CpG sites and relative DPV current response (R^2 = 0.971411). Finally it was determined that only 20μl of secondary PCR product (from real DNA samples) in 200μl buffer was required to produce a considerable difference in relative current. Once again, the sensitivity of the method greatly improved on moving from synthetic to real DNA samples (Sina et al., 2014). This project set out to improve the repeatability and sensitivity of the eMethylsorb method via a new approach to the adsorption step and the electrochemical technique. The new procedure was optimised using 30 base synthetic oligonucleotides, containing six CpG sites, designed to represent bisulphite modified and

asymmetrically amplified methylated and unmethylated versions of a region downstream of the transcription site of the EN1 gene promoter (Thompson et al., 2016).

It was also imperative to test if % methylation could be determined using these optimised electrochemical procedures in a heterogeneous sample. This was to reflect biopsy samples gained in a clinical setting, as tumours are often found to contain cells exhibiting diverse phenotypic features; including methylation status. This phenomenon, termed intra tumour heterogeneity, has been observed in multiple cancers including breast (Moelans et al., 2014), lung (Quek et al., 2017), endometrial (Varley et al., 2009) and prostate cancer (Litovkin et al., 2015). To test the applicability of the procedure in detecting methylation in DNA derived from humans, the procedure was repeated using bisulphite modified and asymmetrically amplified 140 base ssDNA from the EN1 region of DNA extracted from the non-aggressive breast cancer cell line MCF-7 (methylated). This cell line, which was used by both Koo et al. (2014) and Sina et al. (2014), was derived in 1970 from the pleural effusion of a 69 year old female breast cancer patient, at the Michigan Cancer Foundation, where it gained its name. It is an ideal candidate for studying, as it is positive for the oestrogen and progesterone receptors, and it is therefore commonly used in cancer research (Comsa et al., 2015; Soule et al., 1973). WGA DNA was used as an unmethylated control as in the work conducted by both Koo et al. (2014) and Sina et al. (2014).

1.2.8 Conclusion

DNA methylation is a key regulatory process which is modulated by numerous extrinsic factors. However, it is important to recognise the paramount role diet plays in shaping our methylation profile both during the intrauterine period and throughout lifespan. This review has highlighted that a wide variety of dietary components can influence DNA methylation and it can be argued in many instances aberrant methylation is the direct result of diet. Nowhere is this more apparent than cancer, because the methylation changes which are a hallmark of many cancers are influenced by variations in diet

such as folate levels, calorie intake, and plant polyphenols. It is possible that the early detection of methylation changes could be an effective means of predicting cancer risk. This section has also revealed that in recent years, electrochemical techniques are coming to the fore as an inexpensive means of detecting changes in DNA methylation within specific gene sites associated with disease. Moreover, based on recent work it has been outlined that using electrochemical impedance is an extremely effective means of detecting DNA methylation levels in human DNA derived from MCF-7 cells. There is little doubt that techniques such as this will prove to be an invaluable tool which can supplement and complement existing methods which are currently used to detect cancer.

1.3 Aims

Ageing is a complex process that affects many biological systems and mechanisms. To investigate the vast scope of this field, two different techniques were used to analyse two systems affected by ageing. The aims of this thesis are three-fold:

- To expand an existing mathematical model of cholesterol metabolism and investigate the effects of diet, genotype, and ageing on the lipoprotein profile.

- To use synthetic ssDNA, designed to represent methylated and unmethylated variants of a section of the EN1 gene, to optimise electrochemical detection procedures.

- To use the optimised electrochemical procedures to determine if DNA methylation, in the breast cancer cell line MCF-7, can be detected.

Chapter 2 Methodology

2.1 PART 1: Mathematical modelling

2.1.1 Introduction

Traditionally, when biologists and nutritionists have investigated complex metabolic pathways, such as cholesterol metabolism, they have utilised conventional wet laboratory techniques. However, studying cholesterol metabolism and its interaction with both diet and ageing using conventional approaches is challenging, due to the integrated nature of this system, and the time scales involved in studying the effects of the ageing process. Traditional *in vivo* or *in vitro* techniques can also be limited when testing a hypothesis, as such approaches can be resource-intensive, expensive, impractical and potentially unethical (Mc Auley et al., 2013). Thus, utilisation of the systems biology approach is becoming an increasingly important tool in nutrition based research, as systems biology overcomes a number of the challenges outlined above, but more importantly, facilitates the integration of data generated from a diverse range of sources (Mc Auley et al., 2013), leading to an improved understanding of how cellular dynamics influence the behaviour of tissues and ultimately the health of whole organ systems (Auffray and Hood, 2012). Thus, the systems biology approach seeks to understand complex biological systems by studying them in a more holistic manner, in contrast to the reductionist approach regularly adopted in human nutrition. At the core of the systems biology approach is computational modelling. Computational modelling is an abstract process that is used to represent the dynamics of a biological system in a precise manner using mathematics. Computational models are now used to model a diverse range of complex nutrient centred pathways including cholesterol metabolism (Figure 2.1). Firstly, computational models are capable of providing quantitative data on the interaction of molecular components (Kitano, 2002). Secondly, nutrient-based interactions are inherently complex and often non-linear in nature (de Luca and Olefsky, 2008; Gianchandani et al., 2006; Patti and Kahn, 2004), and can involve complex feedback and feed-forward loops (Huang et al., 2010; Lamb, 2012; Pappu et al., 2002). Thus, it is challenging and even unfeasible to reason about these by human intuition alone. Computational modelling offers an alternative means

of handling this complexity, thus utilisation of computational modelling alongside experimental work provides a means of representing the dynamics of complex biological systems. Models can be used to simulate intrinsic perturbations, such as those associated with ageing and extrinsic perturbations, such as diet. Output from the model provides an overview of how these changes impact the dynamics of the system, and the implications this has for health-span.

2.1.2 Building a mathematical model
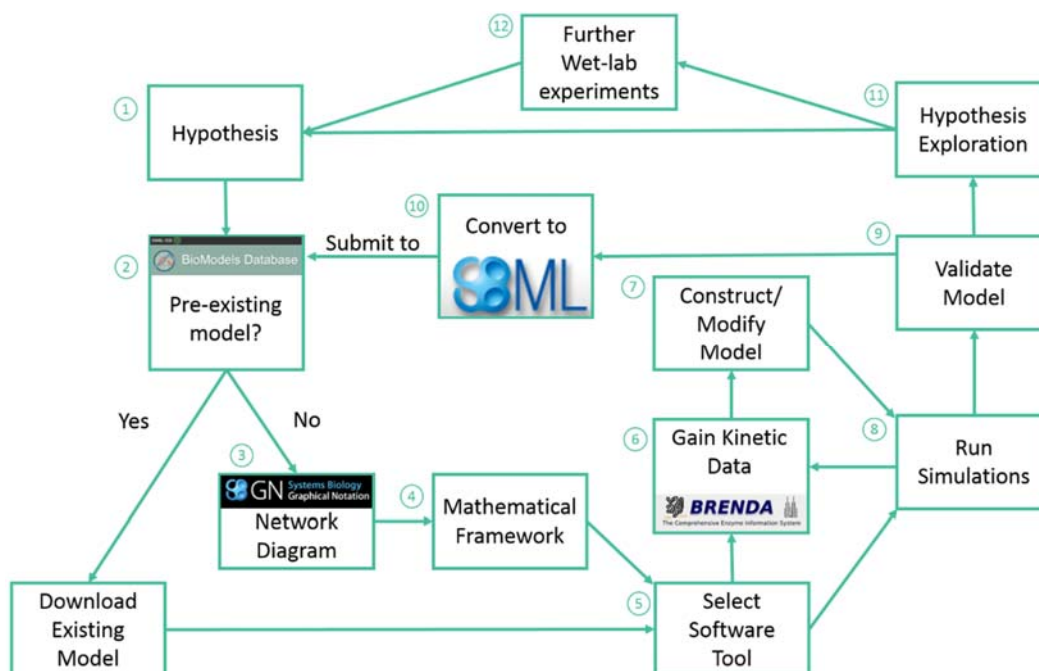
Figure 2.1 Modelling Overview.
(1) Identify the system to model and hypothesis formation. (2) Identify pre-existing models; using the BioModels Database, a repository for peer reviewed models encased in the leading exchange framework. (3) If no model of the system of interest exists: produce a network diagram. If a model does exist: download model and move to step 5, then step 8. (4) Establish mathematical framework. (5) Identify a suitable modelling tool; several are available including COPASI, CellDesigner, Mathematica and MATLAB. (6) Obtain initial concentrations of species, rate laws and kinetic data. The online resources BRENDA and SABIO-RK provide a substantial volume of kinetic data. (7) Construct the model and (8) run simulations. (9) Validate the model. (10) Code the model in the exchange format, Systems Biology Markup Language (SBML) and deposit in the BioModels Database. (11) Explore the hypotheses, and determine if the model accurately represents the biological system, and can be used to make predictions, or if the model needs refining. (12) Conduct further wet laboratory experiments if required. Adapted from Mc Auley and Mooney (2015) (Mc Auley and Mooney, 2015a).

2.1.2.1 Stage 1 and 2: Determining the system to model and searching for pre-existing models

Once a system of interest was selected, in this case cholesterol metabolism, the first step was to search for pre-existing models that could be used exclusively, adapted or combined with another model. This search was conducted using BioModels (Le Novere et al., 2006), an online repository for models encoded in the exchangeable format SBML (Hucka et al., 2004; Hucka et al., 2003).

2.1.2.2 Stage 3: Producing a network diagram

If no pre-existing models are found, or a model requires adaptation or combining, it is necessary to construct a network diagram of the species and their interactions. In this case, the pre-existing model by Mc Auley et al. (2012) was adapted; therefore a network diagram was constructed to clearly outline the system of interest, with the additional mechanisms. To further remove ambiguity, the network diagram was created using the universal language, systems biology graphical notation (SBGN), which standardises the notation used in figures. This uniformity means diagrams are consistent, easily readable and user friendly (Le Novere et al., 2009). SBGN is divided into three languages, the entity relationship (ER), activity flow (AF) and process description (PD), which was used for this work, as this language best characterised processes such as metabolism due to the representation of conversion of species states or location. There are various software packages that SBGN diagrams can be created in, including Celldesigner (Funahashi et al., 2006), PathVisio (Kutmon et al., 2015), LibSBGN (van Iersel et al., 2012) and Edinburgh Pathway Editor (Sorokin et al., 2006). The SBGN diagrams in this work were created using the free software Visualisation and Analysis of Networks containing Experimental Data (VANTED) Version 2.2.1, as it is readily accessible and provides a large range of functions (Rohn et al., 2012). The SBGN figures from Chapter 3 utilise only a small proportion of the glyphs available. Compartments were represented as rectangles with rounded edges, similar to macromolecules, although with a broader outline. Simple chemicals were represented by circles. For this work, cholesterol is represented by an orange circle, while bile acids are represented by green circles. Pools of these substances were designated the macromolecule glyph again in either orange or green.

Enzymes were represented by a blue macromolecule glyph. Receptors were represented by chevrons that crossed the compartment edge. The mathematical symbol for 'empty set' was used to represent the source or sink of a species. Small open squares were used to represent a basic process, such as the conversion of one species to another, while squares with hatchings represent an omitted process. Arrows were used to represent production, while round arrow heads represented catalysis and bar-headed lines represent inhibition (Moodie et al., 2012).

	Compartment
	Simple Chemical
	Pool
	Enzyme
	Receptor
	Source and Sink
	Process
	Omitted Process
	Submap
	Production
	Catalysis
	Inhibition
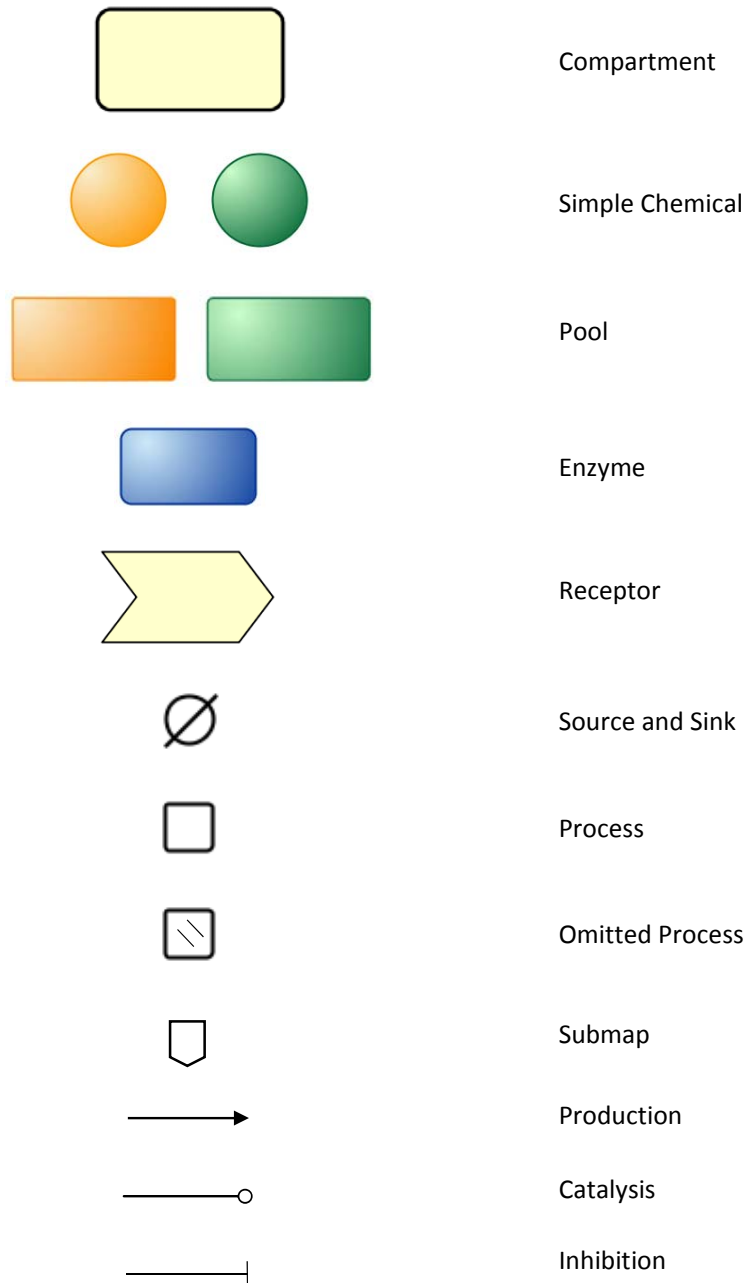
2.1.2.3 Stage 4: Deciding on a mathematical framework

Once the system was outlined in SBGN, a mathematical framework was then decided upon. In the system outlined, it was important to produce results which were clinically significant and comparable to experimental findings. Therefore, cholesterol was represented as several discrete pools of its various forms. As cholesterol was not treated as an individual molecule, there was negligible stochasticity; something which arises when the rate individual species bind, react, or undergo transportation is unpredictable. As it is not relevant or practical to model the individual molecules of cholesterol and their statistical mechanical fluctuations through the mechanisms outlined, a deterministic model was created. This was done by producing a series of ordinary differential equations (ODEs), and was in line with the original model (Mc Auley et al., 2012). ODEs describe the rate of change of a species in a chemical reaction, with the solution expressed as the concentration as a function of time, and incorporate a variety of deterministic rate laws including:

2.1.2.3.1 Constant flux

Constant flux is used when only a product (A) is present (Drager et al., 2015).

$$\emptyset \longrightarrow A$$
$$v = k \tag{1}$$

Only two reactions within the updated whole-body model of cholesterol metabolism were underpinned by constant flux kinetics. These were reactions number two and four, which are the counter reactions for the ingestion of dietary free and esterified cholesterol, respectively. These were assigned the constant flux function as they acted as time counters for the ingestion events, as described in section 2.1.2.5.1.

counter1 -> counter2

counter3 -> counter4

2.1.2.3.2 Mass action

Proposed by Guldberg and Waage, the law of mass action is used to describe elementary chemical reactions, and is the most common rate law used within the systems biology and mathematical modelling community (Voit et al., 2015). First order kinetics can be used to describe reactions where one substrate is converted to one product, for instance:

$$A \longrightarrow B$$

In this case the rate of the reaction is dependent on [A], and is proportional to the frequency the substrate molecules react. Therefore this can be expressed as equation 2 and equation 3:

$$v = k[A] \tag{2}$$

$$v = \frac{d[B]}{dt} = -\frac{d[A]}{dt} \tag{3}$$

Mass action kinetics were used to describe 37 reactions in the updated model of whole-body cholesterol metabolism. This function was commonly used to describe uptake reactions as well as receptor degradation reactions, to simplify often highly complex receptor recycling systems. The example reactions below show receptor independent hepatic uptake of LDL-C, and the degradation of the receptors responsible for the intestinal uptake of cholesterol and bile acids. To model these reactions, [A] was replaced with the substrate of each reaction and a value for K_1 defined.

LDLC -> HCE

NPC1L1 -> NPC1L1D

ASBT -> ASBTD
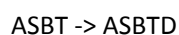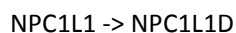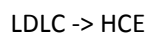
Mass action kinetics can also be used to describe reactions with two substrates. For instance:

$$A + B \longrightarrow C$$

In this example, the rate of the reaction, v, or rate of product (C) formation, is proportional to the concentration of the substrates A and B. The rate constant k is used to describe the reaction speed (Voit et al., 2015), which can be described by equation 4 and 5:

$$v = k[A][B] \tag{4}$$

$$v = -\frac{d[A]}{dt} = -\frac{d[B]}{dt} \tag{5}$$

Equation 4 can be referred to as a second order reaction, termed because of the number of substrates. This is also true for reactions where two of the same substrates react, for instance:

$$2A \longrightarrow B$$

A reaction such as this gives rise to equation 6. This can also be displayed in the form outlined in equation 7:

$$v = k[A]^2 \tag{6}$$

$$v = k[A][A] \tag{7}$$

2.1.2.3.3 Michaelis Menten (non-reversible)

Leonor Michaelis and Maud Menten built on the work of Victor Henri, and in 1913 proposed a model for the observed relationship between the concentration of substrate and rate of catalysis, when enzyme concentration is fixed, as seen in Figure 2.2 (Johnson and Goody, 2011). Used for one-substrate reactions, Michaelis Menten kinetics, are underpinned by the pathway below, where E, ES, and P represent the enzyme, enzyme-substrate complex, and product respectively. The rate constant,

k_1 represents the formation of the enzyme-substrate complex, while k_{-1} characterises the reverse reaction. The rate constant k_2 signifies the formation of a product and dissociation from the enzyme.

$$E + S \underset{k_{-1}}{\overset{k_1}{\rightleftharpoons}} ES \overset{k_2}{\longrightarrow} P + E$$
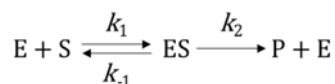
The Michaelis Menten equation calculates the initial velocity of a single substrate reaction (equation 8). The Michaelis Menten constant, K_M, is substrate concentration at half of the maximum velocity of the reaction, V_{max} (equation 9), which can be defined when the substrate is in excess, and enzyme saturation has been reached, thus all enzymes are bound in enzyme-substrate complexes (Johnson and Goody, 2011). This can be calculated as the rate constant k_2 multiplied by the total enzyme concentration, $[E]_T$ (equation 10), which is defined as [E] plus [ES] (equation 11). The enzyme turnover number, k_{cat}, which describes the number of reactions (turnovers) at each active site in a given time, can also be a useful measure in enzyme kinetics, and is calculated by the division of V_{max} by $[E]_T$ (equation 12). Indicative of a high enzyme efficiency, a high k_{cat}/K_M ratio is observed when turnover is rapid (high k_{cat}) and the enzyme has a high affinity for the substrate (low K_M).

$$v_o = \frac{V_{max}[S]}{K_M + [S]} \tag{8}$$

$$K_M = \frac{k_{-1} + k_2}{k_1} \tag{9}$$

$$V_{max} = k_2[E]_T \tag{10}$$

$$[E]_T = [E] + [ES] \tag{11}$$

$$k_{cat} = \frac{V_{max}}{[E]_T} \tag{12}$$
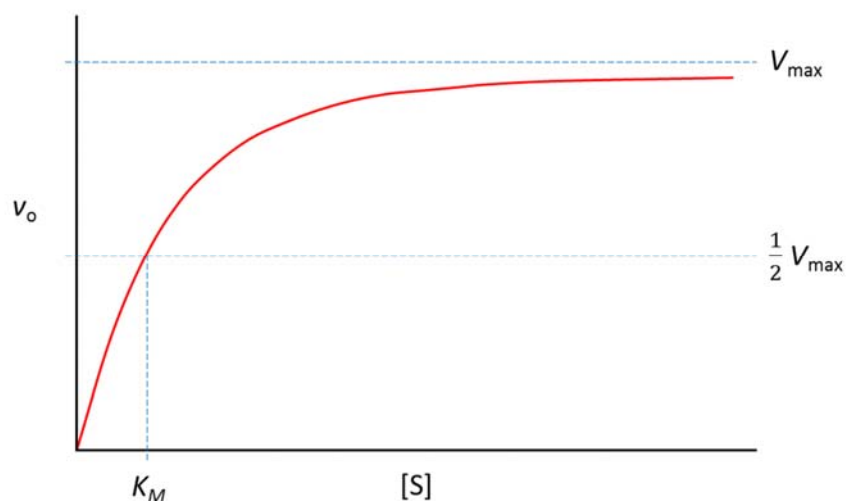
Figure 2.2 Michaelis Menten plot of the relationship between [S] and v_o when [enzyme] is fixed.

The non-reversible Michaelis Menten function was used to describe 58 reactions within the updated model of whole-body cholesterol metabolism. These reactions were mainly those which were enzymatically regulated and well characterised experimentally. This included many of the kinetically well characterised cholesterol biosynthesis reactions, such as the formation of mevalonate from HMG CoA, and the formation of mevalonate-5P from mevalonate (Polo et al., 1999; Potter and Miziorko, 1997).

HMGCoA -> MV

MV -> MV5P
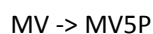
2.1.2.3.4 Michaelis Menten (reversible)

The Michaelis Menten model can be modified to include the reverse reaction. A reversible complex is formed between both the enzyme and substrate, and enzyme and product, therefore an additional intermediate, EP, is required (Keleti, 1986).

$$E + S \underset{k_{-1}}{\overset{k_1}{\rightleftharpoons}} ES \underset{k_{-2}}{\overset{k_2}{\rightleftharpoons}} EP \underset{k_{-3}}{\overset{k_3}{\rightleftharpoons}} P + E$$
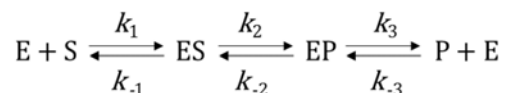
The net rate of the reaction can be calculated using equation 13, where the velocities of the forward and reverse reactions are calculated using equations 14, and 15 respectively, and K_M^S and K_M^P are calculated using reactions 16 and 17 respectively. To determine V_f and V_r, $[E]_0$ is calculated as the sum of free enzyme and enzyme bound in enzyme-substrate and enzyme-product complexes, as seen in equation 18 (Chaplin and Bucke, 1990).

$$v = \frac{\dfrac{V_f[S]}{K_M^S} - \dfrac{V_r[P]}{K_M^P}}{1 + \dfrac{[S]}{K_M^S} + \dfrac{[P]}{K_M^P}} \tag{13}$$

$$V_f = \frac{k_{+2}k_{+3}[E]_0}{k_{+2} + k_{-2} + k_{+3}} \tag{14}$$

$$V_r = \frac{k_{-2}k_{-1}[E]_0}{k_{-2} + k_{+2} + k_{-1}} \tag{15}$$

$$K_M^S = \frac{k_{-1}k_{-2} + k_{-1}k_{+3} + k_{+2}k_{+3}}{k_{+1}(k_{+2} + k_{-2} + k_{+3})} \tag{16}$$

$$K_M^P = \frac{k_{+3}k_{+2} + k_{+3}k_{-1} + k_{-2}k_{-1}}{k_{-3}(k_{-2} + k_{+2} + k_{-1})} \tag{17}$$

$$[E]_0 = [E] + [ES] + [EP] \tag{18}$$

Reversible Michealis Menten kinetics were used to underpin six reactions within the updated model of whole-body cholesterol metabolism. These were the reactions for mevalonate5PP formation and DMAPP formation within the peripheral, hepatic and intestinal compartments (Herdendorf and Miziorko, 2007; Hou et al., 2017). In each case, the species was assigned the prefix P, H or J to denote the peripheral, hepatic, or jejunocyte compartments, which results in the a total of six reactions.

MV5P = MV5PP

IPP = DMAPP
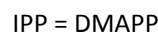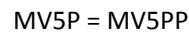
2.1.2.3.5 Bi

To account for reactions where two substrates form one product, the bi reaction was utilised (equation 19), where [A] and [B] represent the concentration of substrates A and B, while K_M^A and K_M^B represent the Michaelis-Menten constants for these substrates. This is similar to the rate law used to generally describe substrate sequential reactions, where the initial K_M^A is replaced with the dissociation constant K_{ia} (Moritz et al., 2000).

$$V = \frac{V_{max}[A][B]}{K_M^A K_M^B + K_M^B[A] + K_M^A[B] + [A][B]} \tag{19}$$

Utilised on nine occasions, the bi rate law was used to describe the formation of HMG CoA, geranyl-PP, and farnesyl-PP within the updated model of whole-body cholesterol metabolism. This rate law was selected as the reaction outlined that two substrates were utilised in the creation of one product. These reactions occurred in the peripheral, hepatic and intestinal compartments, thus in each case, the species were assigned the prefix P, H or J to denote the peripheral, hepatic, or jejunocyte compartments, resulting in nine reactions.

ACoA + AACoA -> HMGCoA

DMAPP + IPP -> GPP

GPP + IPP -> FPP

2.1.2.3.6 Ping pong bi bi

The ping pong bi bi mechanism can be used to describe a reaction where an enzyme converts between forms E and E'. In this instance, substrate A binds with the enzyme, causing the formation of product P, and concomitant conformational change in the enzyme. This change allows substrate B to bind for conversion to product Q, simultaneously converting the enzyme to its original form.
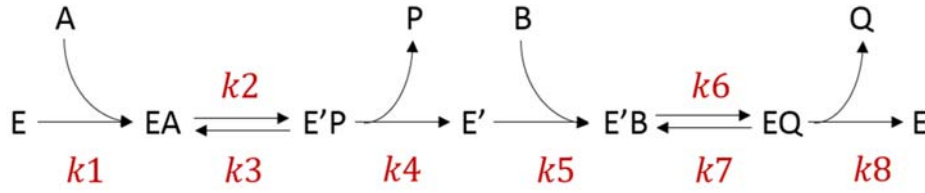
The ping pong rate law can be derived from equation 20, where A and B represent the first and second substrate, and P and Q represent the first and second product respectively, in a two substrate, and two product reaction. V_f and V_r denote the maximum velocities of the forward and reverse reactions respectively. K_M^A represents the concentration of substrate A at $\frac{1}{2}V_f$ at zero P and Q, while K_M^B represents the concentration of substrate B at $\frac{1}{2}V_f$ at high A and zero P. K_M^P signifies the concentration of P at $-\frac{1}{2}V_r$ at zero A and B, while K_M^Q signifies the concentration of P at $-\frac{1}{2}V_r$ at zero A and high P. K_{ia} and K_{iq} denote the inhibition constants of A and Q acting on the reverse and forward reactions respectively. K_{eq} represents the equilibrium constant (EMBL EBI, 2010; Finney et al., 2000).

$$v = \frac{V_f \left([A][B] - \frac{[P][Q]}{K_{eq}}\right)}{[A][B] + K_M^B [A] + K_M^A[B]\left(1 + \frac{[Q]}{K_{iq}}\right) + \frac{Vf}{V_r K_{eq}}\left(K_M^Q[P]\left(1 + \frac{[A]}{K_{ia}}\right) + [Q](K_M^P + [P])\right)} \quad (20)$$

The rate of P and Q formation from substrates A and B can be calculated using equations 21 and 22 respectively. The formation of P requires four rate constants: the rate constant $k1$ which signifies the rate of EA formation from substrate A and enzyme E, the rate constant $k2$ which refers to the formation of E'P from EA, the rate constant $k3$ which denotes the formation of EA from E'P, and the rate constant $k4$ which represents the formation of E' and P from E'P. Similarly, for the formation of Q from B there are 4 rate constants. $k5$ signifies the rate constant for the formation of E'B from the substrate B and modified enzyme E'. The rate constant $k6$ refers to the formation of EQ from E'B,

while the rate constant $k7$ denotes the reverse of this. The rate constant $k8$ refers to the formation of the product Q and original enzyme E from EQ.

$$v = k1[A][E] + k2[EA] - k3[E'P] + k4[E'P] \tag{21}$$

$$v = k5[B][E'] + k6[E'B] - k7[EQ] + k8[EQ] \tag{22}$$

Within the updated model of whole-body cholesterol metabolism, three reactions were underpinned by ping pong bi bi kinetics. These were the interconversion of acetyl CoA and acetoacetyl CoA within the hepatic, peripheral and intestinal compartments (Schomburg et al., 2006). In each case, the species were assigned the prefix P, H or J to denote the peripheral, hepatic, or jejunocyte compartments, thus creating three separate reactions.

2 * ACoA = AACoA + CoASH

2.1.2.4 Stage 5 and 6: Selecting a modelling tool and gaining kinetic data

Once the system was outlined, and the mathematical framework determined, a modelling tool was selected. Deciding upon a tool can be difficult as there are over 280 SBML-compatible software packages available, with a range of capabilities, including creating models, performing simulations, analysing models by sensitivity analyses or flux balance analysis for example, and provision of a database of models. To aid in this decision, it is helpful to consult the online SBML software matrix (http://sbml.org/SBML_Software_Guide/SBML_Software_Matrix). Here the capabilities are outlined and the supported mathematical framework elucidated. Some software tools can support multiple mathematical frameworks, while others are only capable of supporting one. For example, LibSBML (Bornstein et al., 2008), SBMLeditor (Rodriguez et al., 2007), and semanticsSBML (Krause et al., 2009), support ODEs, differential-algebraic equations (DAEs), partial differential equations (PDEs) and stochastic modelling, while RANGE (Long and Roth, 2007), and PRISM (Kwiatkowska et al., 2011), only support models underpinned by stochastic frameworks. The software tool COPASI was chosen for this

work due to its capabilities in creating, simulating and analysing models, and its ability to support ODE and event frameworks. COPASI is also easily accessible, is free for both academic and commercial use, and runs on Linux, Mac OS X and Windows operating systems (Hoops et al., 2006). Following this decision, kinetic data was gained from comprehensive literature searches of the research article depositories Google Scholar, PubMed, and Science Direct, and comprehensive enzyme information system, BRENDA.

2.1.2.5 Stage 7: Model assembly

After obtaining the kinetic data to accompany the mathematics which underpin the reactions, and selecting the modelling tool COPASI, the model was then assembled. Reactions were added by naming and representing the reaction, and defining the rate law and kinetic parameters as demonstrated in Figure 2.3. The initial concentration of species were assigned as shown in Figure 2.4. The calculations for the values used in the updated whole-body cholesterol metabolism model can be found in section 3.2.2.
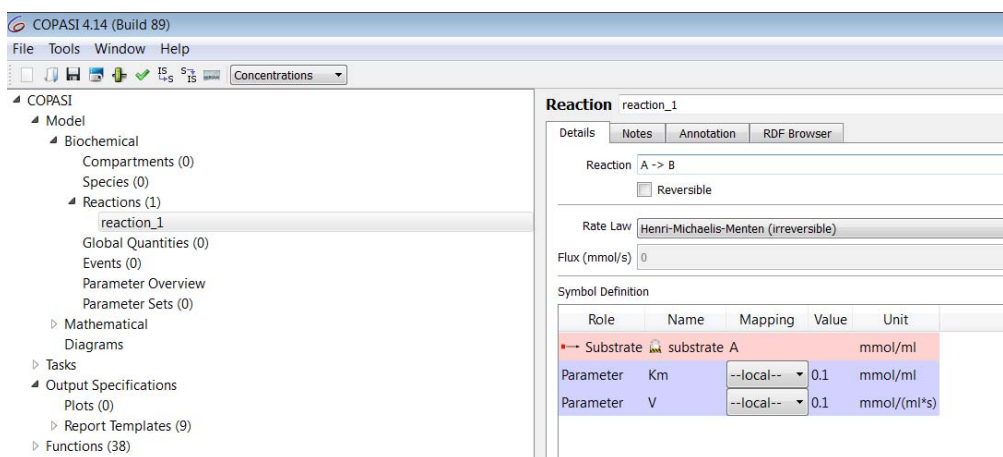
Figure 2.3 Example of Michaelis Menten reaction input in COPASI.
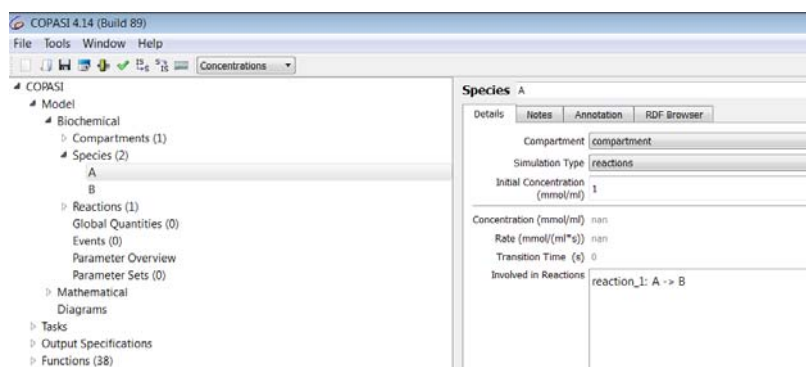
Figure 2.4 Example of species initial concentration input in COPASI.

2.1.2.5.1 Adding events

Events can be added to a model to allow a discrete action to occur, and can represent an action such as the intake of food or the administration of a drug. To create an event, two reactions are required. Firstly, a counter reaction underpinned with constant flux kinetics is needed. This reaction enables time to be monitored, so that an action time can be defined. A second reaction, outlining the input or conversion of a species is also required. This ensures that species are available to be expressed in the event. The event can then be added as shown in Figure 2.5A. To do this, it is necessary that a trigger and assignment are determined. The trigger determines what time the event will occur, while the assignment determines the amount a species is to be modified. To stop an event, an additional event is required to reset the counter reaction, as outlined in Figure 2.5B.
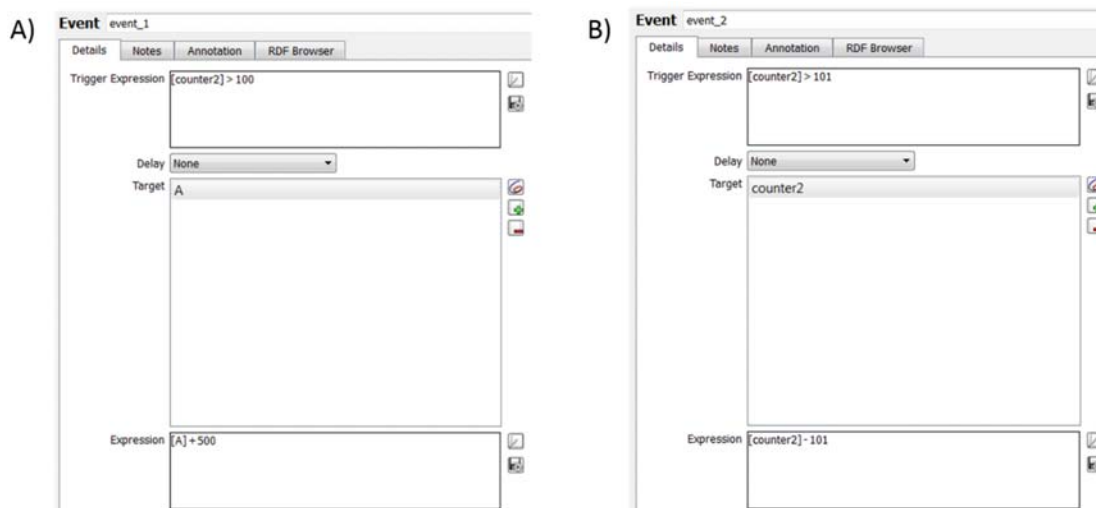
Figure 2.5 Example of the addition of an A) start and B) stop event.

In this example, the reaction of A -> B is under reversible Michaelis Menten kinetics, with a K_M value of 0.1 and V_{max} value of 10. The event reaction counter1 -> counter2 is under constant flux, where parameter v is 1, and counter1 is fixed. The above event resulted in species fluctuation as outlined in Figure 2.6. In this case, it is clear [A] increases to 500mmol/ml before it is converted to [B], which is also visibly affected by the influx of [A] every 100s. Therefore, the use of events can be invaluable when simulating a biological system, as they can more accurately represent a process, such as eating. Cholesterol feeding was simulated in this way, as outlined in Chapter 3. The events specified that at 480 minutes, 12.667mg of esterified cholesterol would be ingested, and at 482 minutes, 88.667mg of free cholesterol would be ingested. This was used to represent the average UK male intake of 304mg per day of cholesterol (Henderson et al., 2003), spread equally over 3 meals.
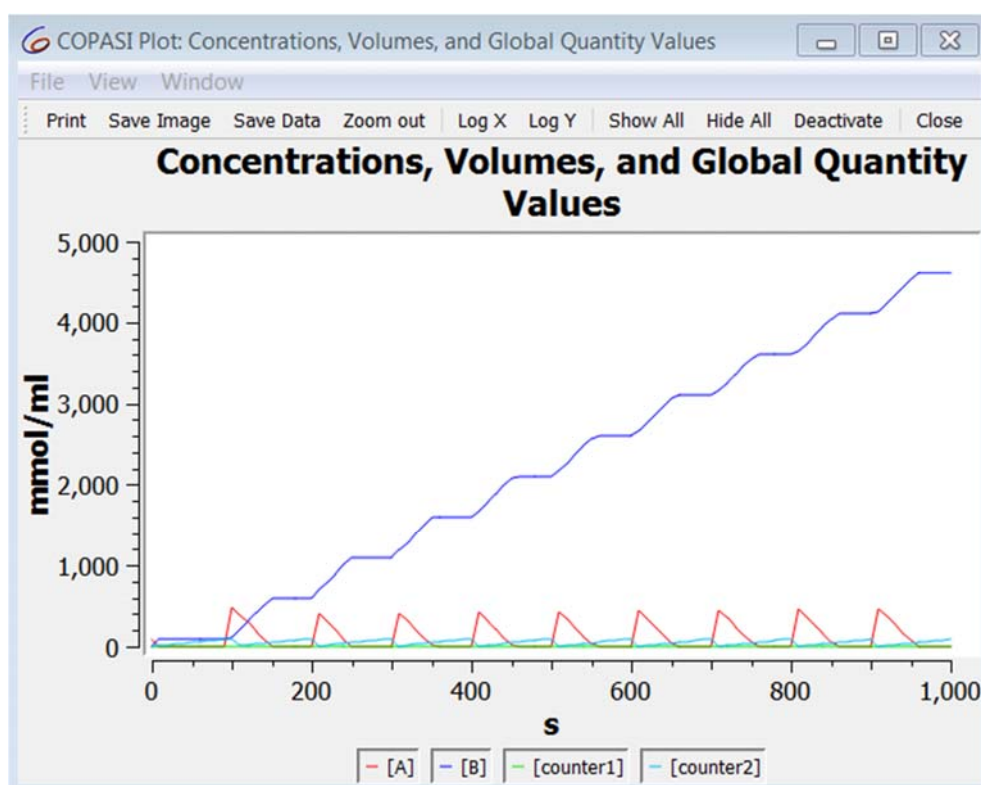
Figure 2.6 Effect of events on species concentration.

2.1.2.6 Stage 8 & 9: Run simulations and validate the model

In the above example, a time course simulation was run. To do this, firstly a plot was defined. In this example, where the events are removed, the transient concentration of the variables [A] and [B] was assigned to the Y axis, while time was assigned to the X axis. The time course simulation variables were adjusted so the simulation was conducted over a specified time, and a suitable number of data points produced. In this example, 100 equidistant time points were recorded over 100 seconds. Following completion of the simulation, a plot is produced with the variables pre-assigned to the X and Y axes, over the time and number of intervals outlined (Figure 2.7). This plot demonstrates that in the reaction A -> B, [A] declines with time, while [B] increases; [A] is transformed to [B] until [A] reaches 0, causing [B] to plateau. To validate the model, the time course data can then be compared with published data or laboratory results. Within the model outlined in Chapter 3, often the lipoproteins, specifically LDL-C, and pools of cholesterol were studied over specified periods of time. In the case of cholesterol feeding, 1000 hours was selected, as biologically this would be sufficient time for a difference in these species to be observed (Lin and Connor, 1980).
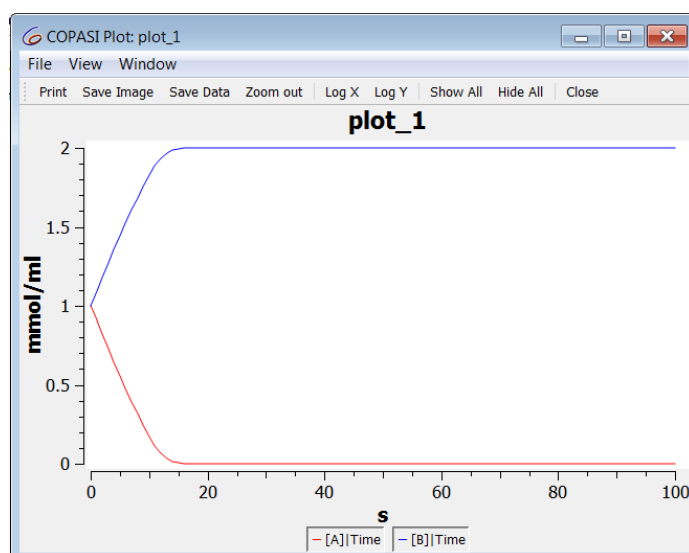
Figure 2.7 Example time course data, demonstrating the change in [A] and [B] with time.

Once the model is in a steady state, it is useful to investigate the relative importance of each parameter in the model, in addition to model robustness, by way of a sensitivity analysis (SA), which can be conducted locally or globally. A local analysis examines the percentage change in a species with a single perturbation to one parameter, and generates only one sensitivity coefficient (S_i) (Bernardo et al., 2013). The sensitivity coefficient, or percentage change in the concentration of a single species can then be compared to results generated from scans of other parameters, by comparing the percentage change in a species concentration. This can be executed by selecting Model > Tasks > Sensitivities, and entering "steady state" in the "subtask" drop down menu, to reflect that the sensitivities gained as a result of a steady state calculation are required. Next, "non-constant concentrations of species" should be selected from the "effect" drop down menu, to indicate that it is these values which the sensitivities are to be derived from. Following this, "local parameter values" should be selected from the "cause" drop down menu, to reflect that only the parameter values specified are to be included in the analysis. Finally "not set" from the "secondary cause" drop down menu should be selected. For the updated model of whole-body cholesterol metabolism outlined in Chapter 3, a sensitivity coefficient, which reflected the percentage change in LDL-C for a 1% change in each of the 266 model parameters was produced.

However, it is important to recognise that parameter values may have some level of uncertainty surrounding them. This can be due to variability surrounding the experimental gaining of data, such as: experimental error, variation between *in vivo* and *in vitro* settings, environmental interaction, and natural variation. Furthermore, uncertainty can arise during the collection of published parameters values, due to; large variation in the source of data (e.g. across species), inconsistencies between protocols used, and absent data. In a biological system it is likely that every parameter has at least a small degree of variability, therefore, the results produced by a local SA should be viewed with caution. To alleviate these difficulties, a global SA can be employed, as it attempts to account for the variation of all parameters, by producing multiple sensitivity coefficients from within the range of parameter value combinations, or parameter space. Random parameter values are selected from between 2

specified limits, usually a 2-fold increase and decrease of the standard value, of multiple parameters, although this can be altered dependent on factors such as confidence in the accuracy of a parameter value (Kent, 2012).

To sample from the parameter space of a global SA, firstly a plot must be defined. In this example, the parameter V_{max} for reaction one was assigned to the X axis while the transient concentrations of species A and B were assigned to the Y axis. V_{max} was scanned between 5 x 10^{-5} and 2, while the K_M for reaction 1 was scanned between the values 5 x 10^{-5} and 100. Random samples were taken between these values 500 times, as outlined in Figure 2.8. The time course menu was set to a duration of 100 seconds with one interval. An interval size of one resulted in the production of 2 results, one at 0 seconds, and one at 100 seconds. Figure 2.9A demonstrates the resulting plot, which shows the effect of divergence from the standard V_{max} value. By exporting the data, and removing the results produced at time 0 (baseline), a more appropriate scatter graph can be produced, in this case in Microsoft Excel 2013, to view the effect of variation in the parameter values as seen in Figure 2.9B.
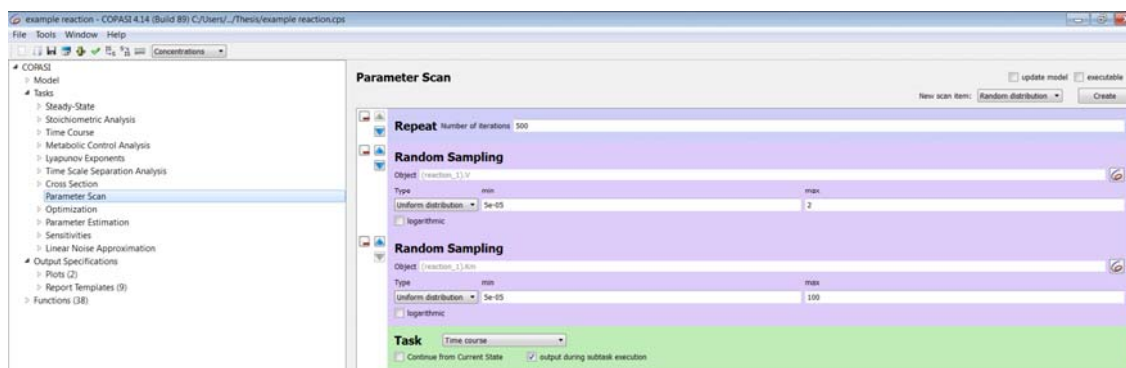
Figure 2.8 Example of specifications to sample from the parameter space of global sensitivity analysis simulation in COPASI.
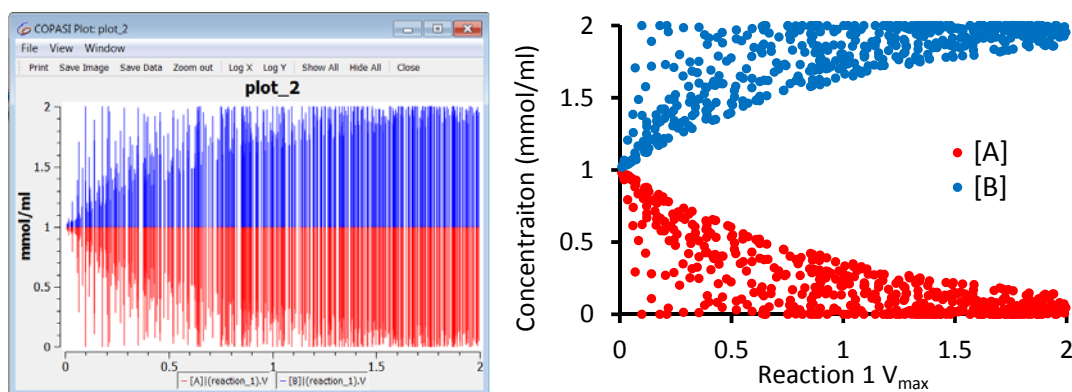
Figure 2.9 Sample from the parameter space of a global sensitivity analysis plot in A) COPASI, and B) in Microsoft Excel 2013.

To analyse the model of cholesterol metabolism described in Chapter 3, the rate constant for hepatic LDLr degradation (reaction 60 in Table A.2) was selected as the parameter of interest, and assigned to the X axis, as the experimental literature suggests this is an important parameter for maintaining cholesterol homeostasis, and the reduction in hepatic LDLr numbers and/or activity has been associated with intrinsic ageing (Field and Gibbons, 2000). Furthermore, of the mechanisms associated with ageing, this parameter was most sensitive (Table A.4). As no *a priori* data was available on this parameter, it was determined that an appropriate sampling choice would be based on a uniform probability density function (Marino et al., 2008). To sample from the parameter space of a global SA, 500 random samples (n=500) were taken between a 2 fold increase and decrease in the default value for this rate constant. Three variations of this were conducted. Firstly, with all "known" parameters scanned and unknown parameters fixed; secondly, with all unknown parameters scanned and "known" parameters fixed, and thirdly, with all parameters scanned simultaneously, at 250 hours. Each scanned parameter also had random samples taken between a 2 fold increase and decrease of its default value.

2.1.2.7 Stage 10, 11, and 12: Coding in SBML and future work

If the model suitably matches the experimental data, the model can be used to make predictions for the user, drive future research, and compliment experimental work in publication. The model can then easily be saved in the exchange format SBML by selecting File > Export SBML, and saving the model in the default file type. It can then be uploaded to the BioModels Database (https://www.ebi.ac.uk/biomodels-main/) by following the onscreen instructions (Figure 2.10) for others to download and utilise (Le Novere et al., 2006; Li et al., 2010). A BioModels ID is issued for the model which can be included into any accompanying published work. For example the original whole body model of cholesterol metabolism was given the ID BIOMD0000000434 (Mc Auley et al., 2012), while the updated model was associated with the BioModels ID MODEL1508170000. However, if the model is behaving unexpectedly, further work may be required to more accurately represent the biological system, including editing rate laws or parameter values. Results may also provide insight into unexpected areas which may warrant further exploration and a change in investigative direction, which may include expanding the model, investigating other related concepts or conducting further laboratory work. It is essential to note that this process is cyclic in nature, and it is important to remember that a model should continually evolve as our knowledge of the biological system grows.
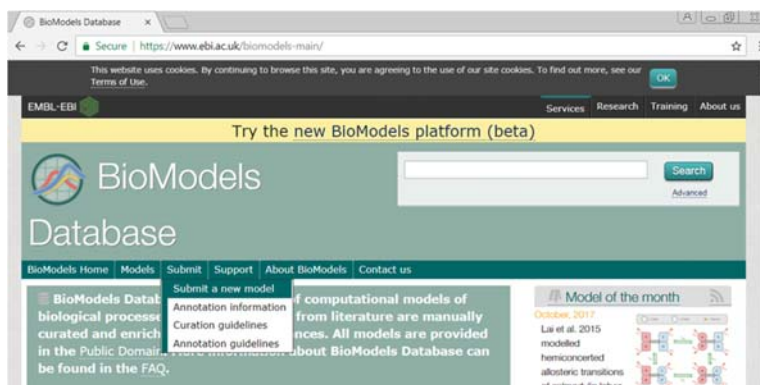
Figure 2.10 Uploading SBML to the BioModels Database.

2.2 PART 2: Electrochemical detection of DNA methylation

There are numerous techniques for detecting DNA methylation, such as bisulphite sequencing (Li and Tollefsbol, 2011), pyrosequencing (Tost and Gut, 2007) and methylation specific PCR (Herman et al., 1996), as discussed in section 1.2.6. In this work, DNA extracted from the human breast adenocarcinoma cell line, MCF-7, was modified through bisulphite treatment (sections 2.2.1), before undergoing asymmetric PCR to amplify a 140 base section of the EN1 gene (section 2.2.2). MCF-7 DNA was used to represent methylated DNA, while WGA DNA was used to represent the unmethylated control (Koo et al., 2014). Following amplification, DNA methylation was detecting using the electrochemical techniques of cyclic voltammetry (section 2.2.4.1), differential pulse voltammetry (2.2.4.2), and impedance (section 2.2.4.3) as described in Chapter 5. The electrochemical procedure was optimised using synthetic DNA designed to represent asymmetrically amplified bisulphite treated ssDNA, as outlined in Chapter 4.

2.2.1 Bisulphite modification

Bisulphite modification of DNA is often required to pre-treat DNA to produce measurable results indicative of DNA methylation. Bisulphite treatment of DNA results in the conversion of unmethylated cytosines to uracil while methylated cytosines remain unchanged (Hayatsu et al., 2008). The mechanism by which this occurs is a three stage process, as outlined in Figure 2.11, whereby: 1) bisulphite is bonded to cytosine at the carbon 6 position, 2) cytosine sulfonate undergoes hydrolytic deamination to produce uracil-sulfonate, and 3) the alkalinic removal of the sulphonate group bonded to uracil (Patterson et al., 2011). Hayatsu et al. (2008) describe that for a sample of DNA from salmon testis, bisulphite modification resulted in the reduction of unmethylated cytosine levels from 20.26% to 0.08%, while a concomitant rise in uracil, from 0.04% to 19.89%, was also observed. Importantly little change was seen in the level of methylated cytosine (mC, 1.41 vs. 1.29%). This change in the

nucleotide sequence can then be detected in a number of ways including combining asymmetric PCR with gel electrophoresis or electrochemical techniques (Koo et al., 2014).
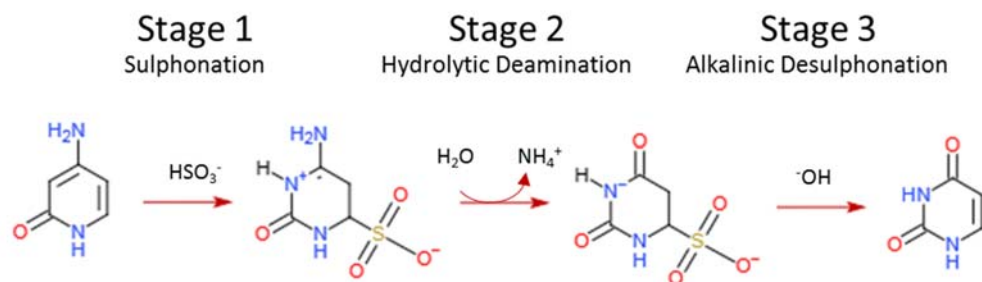
Figure 2.11 Overview of bisulphite treatment.
Adapted from Patterson et al. (2011) using ChemDoodle 2D sketcher.

2.2.2 Asymmetric PCR

The molecular technique of PCR enables the amplification of a gene sequence through a repeated single enzyme reaction, allowing the amplicon to then be analysed or manipulated (Winter, 2005). The process involves the repeated cycling of three stages; 1) denaturation (>90°C), where the dsDNA is destabilised and separated into two ssDNA molecules; 2) annealing (45-65°C), where the primers bind to the ssDNA molecules; and 3) extension (72°C), where DNA polymerase regulates the binding of deoxynucleotide triphosphates (dNTPs) to the template strand, and the DNA sequence is duplicated. The reaction mix requires four key components; template DNA, forward and reverse primers, DNA polymerase, and dNTPs (Winter, 2005). Asymmetric PCR differs from conventional PCR in that it uses unequal concentrations of the forward and reverse primer to generate ssDNA, in contrast to standard PCR which produces dsDNA. However, this modification has led to a reduced efficiency in DNA amplification; conventional PCR has an efficiency of 90% while asymmetric PCR has an efficiency of 60-70% (Citartan et al., 2012). It is therefore important the method uses optimised procedures to enhance PCR efficiency (Heiat et al., 2017). Amplification can be verified with gel

electrophoresis, and the ssDNA generated can be analysed. In this case electrochemical techniques were used to determine the level of DNA methylation. This is because asymmetric amplification of bisulphite treated DNA leads to either an abundance of guanine or adenine for methylated and unmethylated DNA respectively. These nucleotides have different affinities for gold (Kimura-Suda et al., 2003), which is the metal of choice for the working electrode in the electrochemical cell (Koo et al., 2014).

2.2.3 Electrode cells

A three-electrode cell was utilised for the electrochemical detection of DNA methylation. The three-electrode cell consisted of a working electrode, a reference electrode and a counter electrode. The working electrode is where the redox reaction of interest occurs, and relevant electrochemical parameters derived. Therefore, this is where DNA samples or other test solutions are adsorbed, to determine the level of passivation, and methylation status (Koo et al., 2014). Frequently working electrodes are composed of inert materials including silver, platinum, glassy carbon, and in this case gold. Held in close proximity to the working electrode within a three electrode system, the reference electrode has a stable and established electrode potential to which the working electrode potential was referenced against. A commonly used reference electrode is a silver/silver chloride electrode, where the potential is +0.197 relative to a standard hydrogen electrode (Fisher, 1996). The current flows between the working and counter electrode, which is usually made of an inert material such as platinum, gold, graphite or glassy carbon (Figure 2.12A and B). As the counter electrode does not take part in any electrochemical reactions, but is involved in the transport of electrons around the cell, it was vital the surface area of the counter electrode exceeded the working electrode surface area to ensure the counter electrode did not limit the kinetics of the reaction (Elgrishi et al., 2018). The electrodes were submerged in a redox solution, in this case 2.5mM ferrocyanide/2.5mM ferricyanide

(Fe^{2+}/Fe^{3+}/1X PBS), to facilitate the transfer of electrons between the solid electrode and solution, as outlined in the reaction below:

$$Fe^{3+}(aq) + e^-(\text{metal}) \rightleftharpoons Fe^{2+}(aq)$$
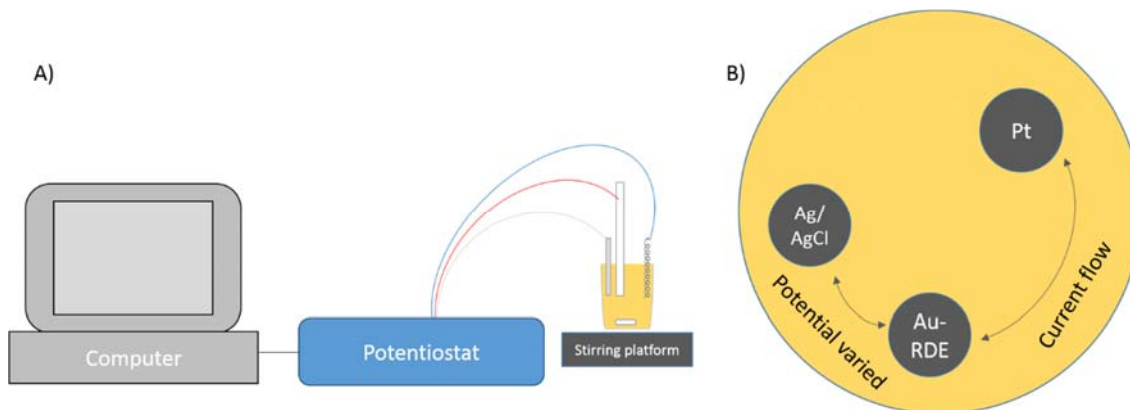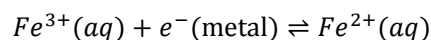
Figure 2.12 Schematic of a three-electrode cell.
A) outlines the attachment of the three electrodes to the potentiostat: working electrode (red), reference electrode (white), and counter electrode (blue). Electrodes are positioned in a 2.5mM Fe^{2+}/Fe^{3+} /1X PBS solution containing a magnetic stirring bar, and the electrochemical cell is placed onto a magnetic stirring plate. B) outlines the positioning of the electrodes within the electrochemical cell, with the Ag/AgCl reference electrode and Au-RDE working electrode positioned in close proximity to one another, while the Pt counter electrode is placed on the opposing side of the beaker.

2.2.4 Electrochemical measurement

There are many electrochemical techniques that could be utilised to detect the adsorption of DNA onto the working electrode. In this study, three were examined; these are cyclic voltammetry (CV), differential pulse voltammetry (DPV) and electrochemical impedance spectroscopy (EIS), which are outlined in sections 2.2.4.1, 2.2.4.2, and 2.2.4.3.

2.2.4.1 Cyclic voltammetry

Cyclic voltammetry is an extension of linear-sweep voltammetry. In linear-sweep voltammetry, when a Fe^{2+}/Fe^{3+} redox solution is utilised, Fe^{3+} is reduced to Fe^{2+}, as the electrode potential is increased, causing an increase in current. Electrode potential, E, is defined as the potential difference between energy levels of the species within the electrode and bulk solution, and is measured in volts (Trasatti, 1986). Current, i, refers to the rate of flow of charged particles and is measured in amps (Vetter, 2013). In this example, the peak current is achieved as the surface concentration of Fe^{3+} diminishes, initiating a reduction in current as the potential continues to increase. In the case of cyclic voltammetry, a reverse sweep of potentials is also conducted, conferring the oxidation of Fe^{2+} to Fe^{3+} (Figure 2.13). In this instance, as the potential is changed, a peak oxidation current is observed, before the Fe^{2+} within the diffusion layer is reconverted to Fe^{3+} and the current reduces (Fisher, 1996). As the redox solution contains both Fe^{2+} and Fe^{3+}, the peak current in the first cycle is significantly lower than that which would be observed if no Fe^{2+} was present. On the second cycle however, peak current is increased as Fe^{2+} was converted to Fe^{3+} in the reverse sweep of cycle 1, therefore all of the solution surrounding the electrode is readily reduced to Fe^{2+}. Peak to peak separation, ΔE_p (equation 23), describes the difference in the potentials required to reach peak oxidation and reduction currents and is calculated as:

$$\Delta E_p = E_p^{red} - E_p^{ox} \qquad (23)$$
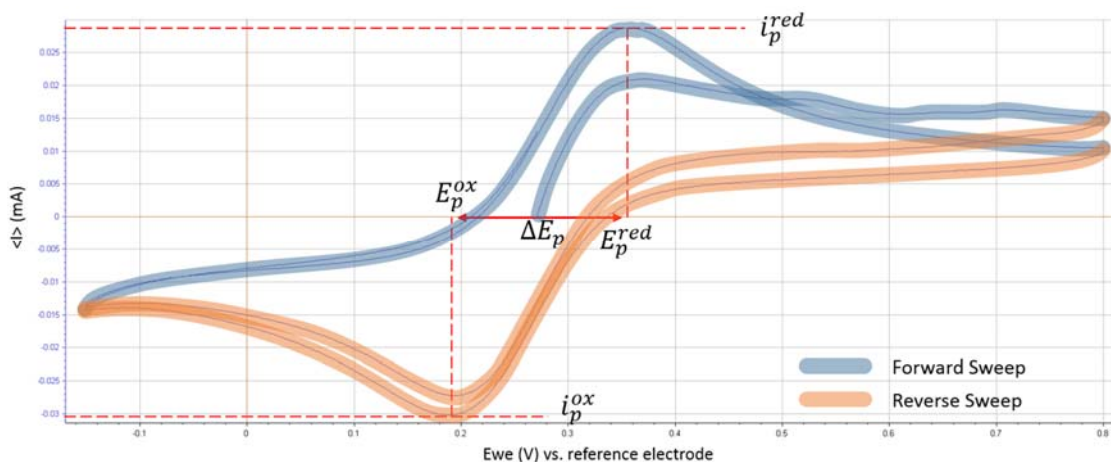
Figure 2.13 Example cyclic voltammogram and peak to peak separation (ΔE_p) derivation.

In a reversible system, where the electron transfer rate is greater than the rate of diffusion from the bulk solution to the electrode surface, equilibrium is reached. In this diffusion controlled system, where reactant and product concentrations are maintained, an increase in scan speed proportionally increases i_p^{red} and lowers i_p^{ox} without influencing E_p^{red}, E_p^{ox}, and ΔE_p, which is maintained at 59mV. i_p^{red} and i_p^{ox} are influenced in this way as the decrease in time taken to record the data is associated with a smaller diffuse layer, and thus increased electron flux. Moreover, in a reversible system, i_p^{red} and i_p^{red} are equivalent, thus $\frac{i_p^{ox}}{i_p^{red}} = 1$ (Honeychurch and Rechnitz, 1998). In an irreversible system, the rate of diffusion from the bulk solution to the electrode surface is greater than the electron transfer rate, causing equilibrium to be disturbed. In this case, ΔE_p is significantly greater than 59mV and often only a single peak is observed as the increase in potential required to reach i_p^{ox} lies outside of the range of potentials scanned (Mabbott, 1983). Electrochemical behaviour between these two forms of reversibility is referred to as a quasi-reversible system. In this case, ΔE_p is greater than 59mV, and is influenced by the scan speed. Additionally, i_p^{red} and i_p^{ox} increase non-proportionally to faster scan speeds (Brownson and Banks, 2014).

2.2.4.2 DPV

DPV is a sensitive technique for detecting small amounts of chemicals. In this technique, the potential is pulsed with time. This is reliant on the pulse height (P_H), pulse width (P_W), step height (S_H) and step time (S_T) being defined (Figure 2.14A). A flat baseline and sharp peak is achieved when the change in current is plotted against potential (Aoki et al., 1984). This is because the difference in current before, i_{bp}, and at the end of the pulse, i_p is utilised (equation 24), enabling the unambiguous recording of peak anodic current (i_{pa}, Figure 2.14B). Δi is calculated by:

$$\Delta i = i_p - i_{bp} \tag{24}$$
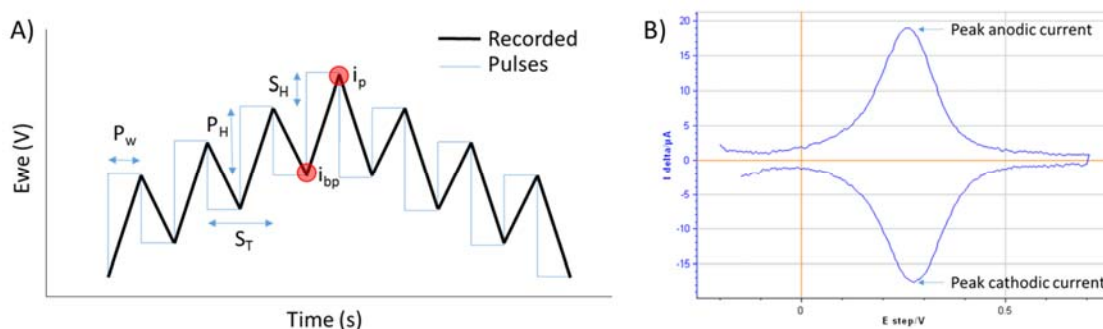
Figure 2.14 DPV A) derivation and B) plot.

2.2.4.3 Impedance

As with electrical resistance, impedance is a measure of circuit resistance to the flow of current. However, it overcomes several simplified properties of electrical resistance and extends to alternating current (AC) circuits (Chang and Park, 2010). When likening impedance to Ohm's Law, Impedance (Z) is defined as:

$$Z(f) = \frac{E(t)}{i(t)} \tag{25}$$

where the impedance at a particular frequency is dependent on the potential and current at a given time (equation 25). $E(t)$ and $i(t)$ are defined as:

$$E(t) = E_m \sin(2\pi f t) \tag{26}$$

$$i(t) = i_m \sin(2\pi f t + \emptyset) \tag{27}$$

Equation 26 and Figure 2.15 describe the oscillating sinusoidal potential, $E(t)$, where the potential at any given time is dependent on the frequency, f, in Hertz (s^{-1}) and E_m, the maximum amplitude (Gamry, 2018). Equation 27 outlines how this oscillating potential impacts on the current at any given time. In this instance, i_m represents the maximum current amplitude and $\emptyset$ relates to the phase difference between the applied potential and observed current (Fisher, 1996).
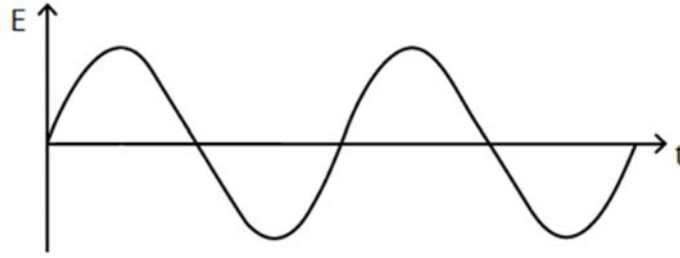
Figure 2.15 Oscillating sinusoidal potential applied in EIS.
Adapted from Gamry (2018).

The efficient but more complex Fourier domain impedance is typically used for EIS, where Z' represents the real component, Z'' represents the imaginary component, j refers to $\sqrt{-1}$, and ω is the radial frequency (equation 28) (Macdonald, 2006). This equation can be viewed in its alternative form, as outlined in equation 29, where $\emptyset$ refers to the phase angle, and $|Z|$ is impedance magnitude (equation 30).

$$Z(j\omega) = Z' - jZ'' \tag{28}$$

$$Z(j\omega) = |Z|e^{j\emptyset} \tag{29}$$

$$|Z| = \sqrt{(Z')^2 + (Z'')^2} \tag{30}$$

The data gained from EIS can be viewed as a Nyquist plot (Figure 2.16). Nyquist plots contain a semi-circular and linear portion. The radius of the semi-circle portion, observed at high frequencies, corresponds to the charge transfer resistance (R_{ct}). R_{ct} is the resistance associated with transferring an electron from one phase to another, for example, electrode to solution (Retter and Lohse, 2010). In this work, R_{ct} is the main parameter of interest as it relates to the level of passivation of the working electrode by adsorbed ssDNA.
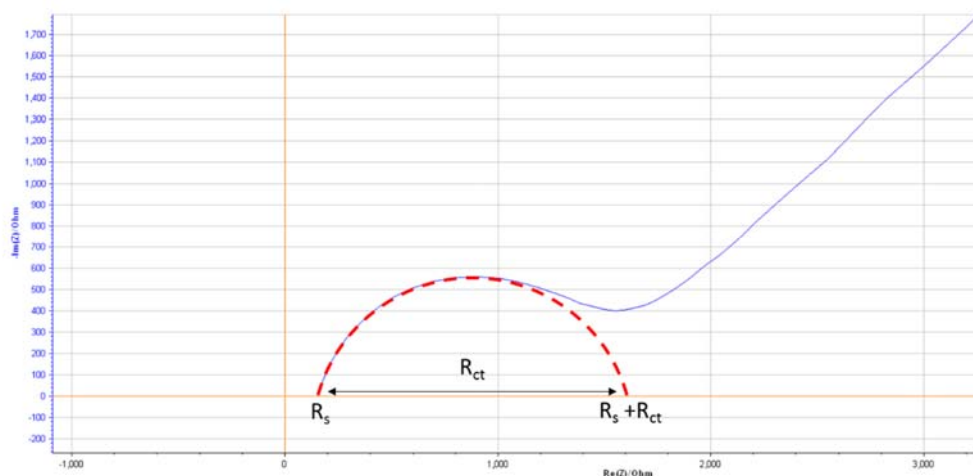
Figure 2.16 Example Nyquist plot with R_{ct} derivation.

2.2.5 EC-Lab

The commercially available software EC-Lab controls potentiostats though multiple electrochemical techniques and allows the post-processing of collected data (http://www.bio-logic.net/softwares/ec-lab-software/). The program can enable the user to conduct voltamperometric techniques including cyclic voltammetry, linear sweep voltammetry and staircase voltammetry; pulsed techniques including differential pulse voltammetry, square wave voltammetry, and normal pulse voltammetry;

and several forms of impedance spectroscopy including potentio EIS, and Galvano EIS. In this work three electrochemical techniques were utilised; EIS, CV (at 200 and 50mV/s) and DPV, as outlined in sections 2.2.5.1, 2.2.5.2 and 2.2.5.3.

2.2.5.1 Impedance

To create the framework to run EIS, firstly a new setting was created. This was done by selecting Experiment > New > Impedance Spectroscopy > Potentio Electrochemical Impedance Spectroscopy and selecting OK. The parameters were then defined; an open circuit potential with a scanning frequency of between 200 kHz to 100mHz, 10 points per decade, sinus amplitude of 20mV, and E range of -2.5 to 2.5V, as shown in Figure 2.17 (BioLogic, 2017b).

Figure 2.17 Parameters for EIS in EC-Lab.

Once the parameters were defined, EIS was conducted by selecting Experiment > Run, as shown in Figure 2.18. The file was saved under an appropriate name and the data was generated. For subsequent measurements the settings for the initial experiment were reloaded.
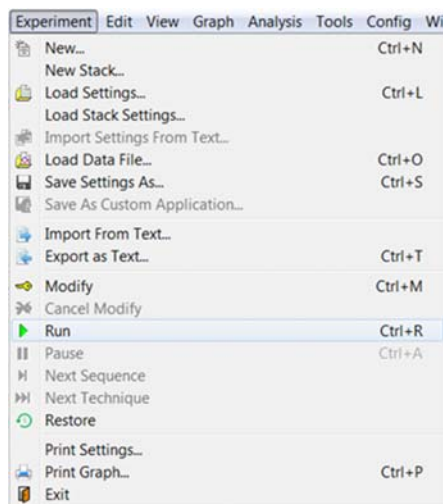
Figure 2.18 Running an experiment in EC-Lab.

Generally, analyses were conducted following the completion of multiple measurements. To reopen a spectra, Experiment > Load Data file were selected and the appropriate spectra opened. A Nyquist plot was selected as the desirable output view; this was done by selecting Re(Z)/Ohm and –Im(Z)/Ohm for the X and Y axes respectively, and selecting OK (Figure 2.19). To gain parameter values from the Nyquist plot, a Z-fit analysis was completed by selecting Analysis > Electrical Impedance Spectroscopy > Z fit (Figure 2.20).
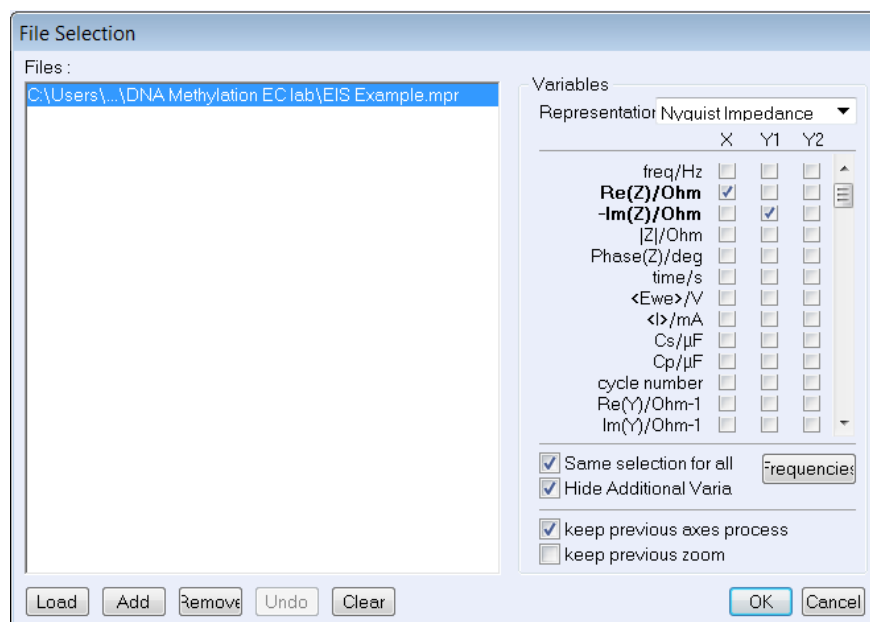
Figure 2.19 Selecting plot axes for EIS data in EC-Lab.

The opening of the Z-fit dialogue box, initiates a default secondary line (red) to appear over the experimental data, representing the fitting of the selected equivalent circuit (Figure 2.21). In this case the equivalent circuit selected was R1+Q2/(R2+W2). This is because it reflected the standard electrochemical cell laid out in the Randals circuit, R1+C2/(R2+W2), but accounted for the fact that the electrode-electrolyte interface does not behave like a perfect capacitor. In this instance, R1 represented R_s, which symbolised ohmic resistance of the cell, which is dominated by solution resistance, while R2 referred to R_{ct}, the charge transfer resistance, which is a function of the electrode kinetics of gold – $Fe^{2+/3+}$, whereby slower kinetics result in a higher R_{ct} value. Q2 represented the constant phase element, and W2 characterised the Warburg element for semi-infinite diffusion (Figure 2.22A and B). There are >130 pre-existing equivalent circuits, and it is possible to construct a circuit if a suitable one does not pre-exist in the EC Lab archive, using a selection of 13 inbuilt components of electrical circuits. Once the R1+Q2/(R2+W2) circuit was selected, the equivalent circuit plot was fitted to the experimental data by selecting minimise. The starting point for the fitting was moved to remove the initial anomalous results to more accurately represent the EIS data (Figure 2.23A

and B), before reselecting minimise to recalibrate the curve (BioLogic, 2017a). Values for the parameter R2 were recorded from experiments conducted in triplicate, and subsequently referred to as R$_{ct}$. Results were recorded as mean ± 1 standard deviation (SD). Relative standard deviation (RSD) was also calculated, by dividing the mean by the standard deviation, and multiplying by 100.
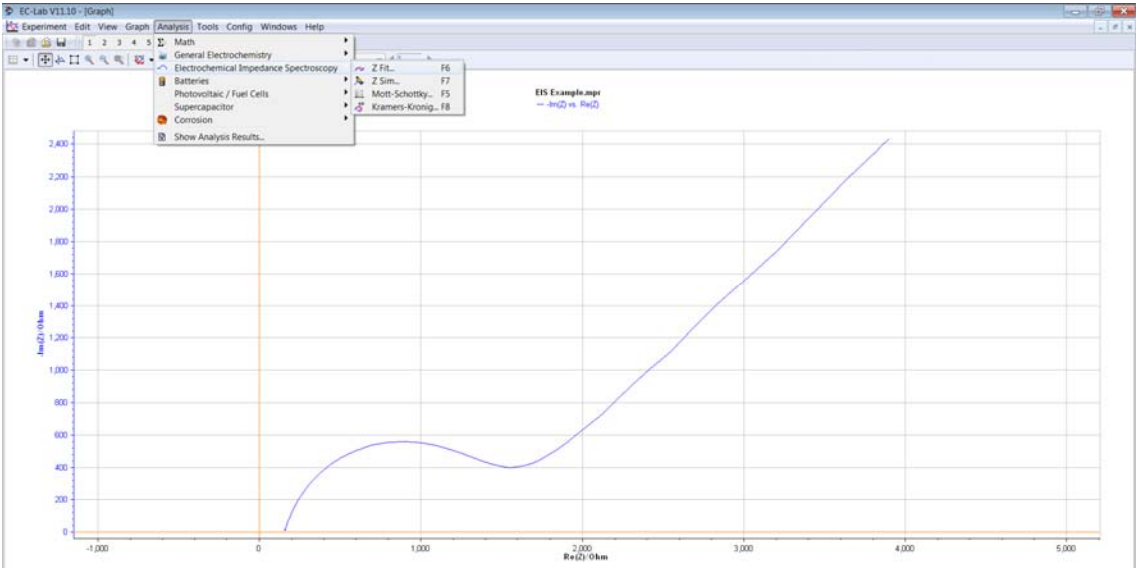
Figure 2.20 Z-Fit analysis of EIS data in EC-Lab.
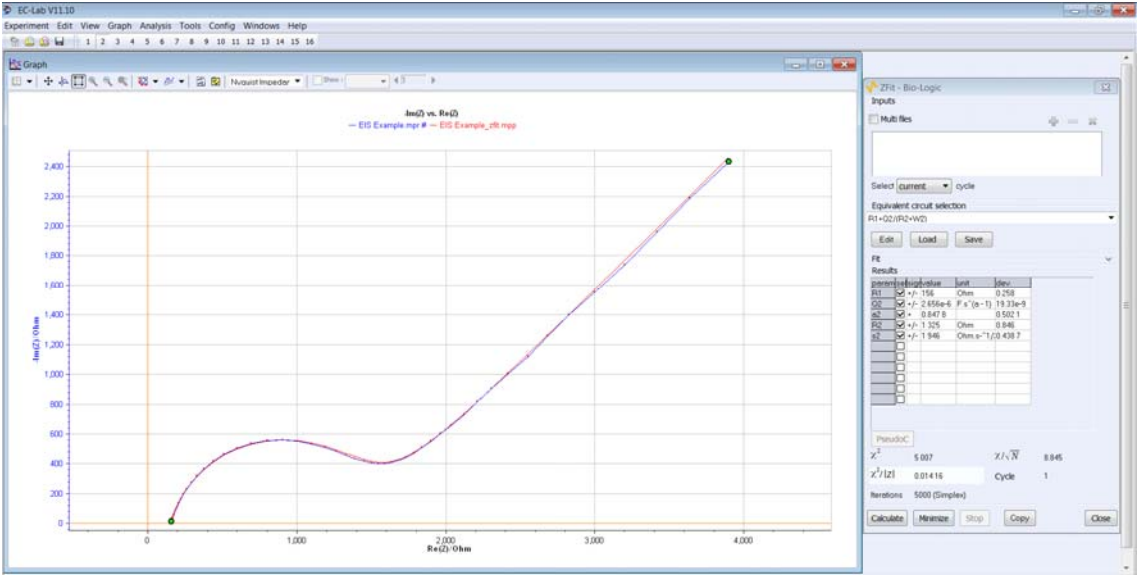
Figure 2.21 Z-Fit analysis in EC-Lab.
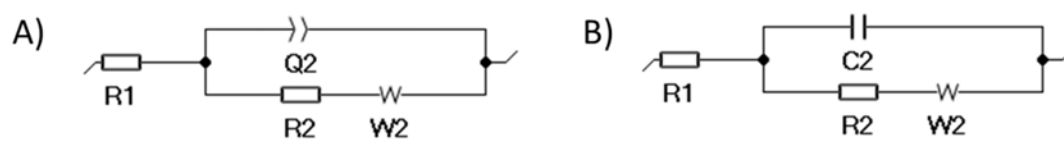
Figure 2.22 Equivalent circuit diagrams of A) R1+Q2/(R2+W2) and B) R1+C2/(R2+W2).
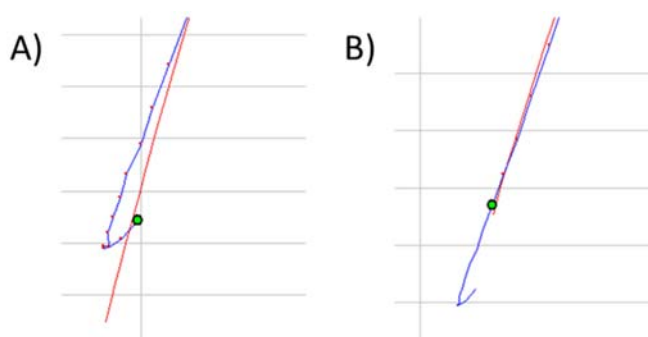
Figure 2.23 A) Before and B) after fitting the equivalent circuit line to the experimental data.

2.2.5.2 Cyclic voltammetry

To create the framework required for CV, the following was selected: Experiment > New > Voltamperometric Techniques > Cyclic Voltammetry (Figure 2.24). The default settings were modified to include a scan speed of 50 or 200mV/s, up to a vertex potential of 0.8V to -0.15V vs. Ag/AgCl with a potential step of 1mV (Figure 2.25). Similar to the EIS experiment, the measurement was commenced by clicking Experiment > Run, and the file was saved before measurement began (BioLogic, 2017b).
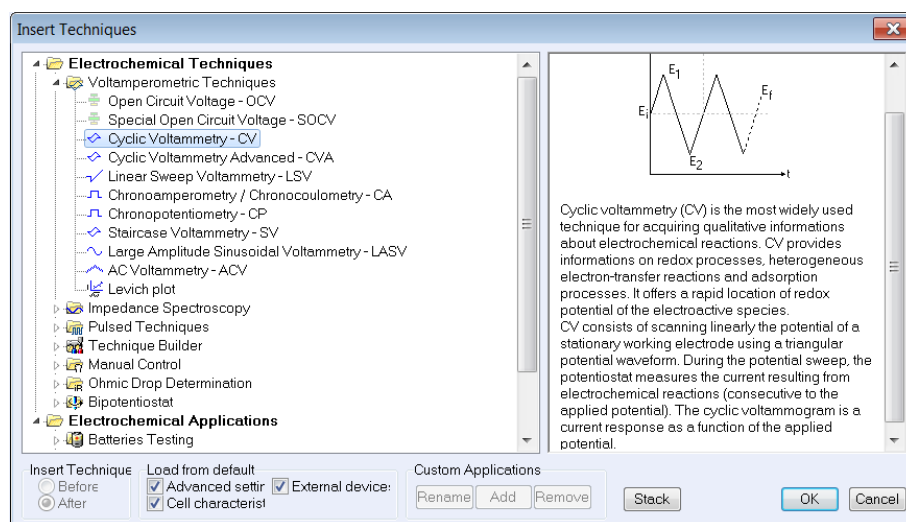
Figure 2.24 Selecting CV in EC-Lab.
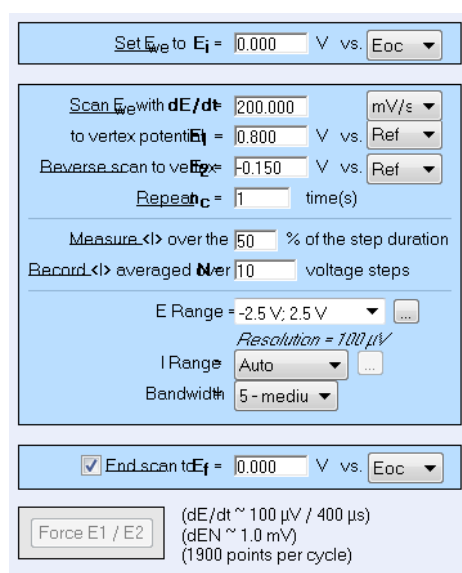
Figure 2.25 Parameters for CV in EC-Lab.

To reopen the saved file for analysis, for either CV200 or CV50, Experiment > Load Data file was selected and the appropriate file opened. The axes were defined as the potential of the working electrode, Ewe/V (x), and <I>/mA (y), as outlined in Figure 2.26. To calculate ΔE_p, the cursor on the task bar was selected and i_p^{red} and i_p^{ox} from the second cycle were selected, as outlined in Figure 2.27 (BioLogic, 2017c). The difference between the corresponding voltages (E_p^{red} and E_p^{ox}) was calculated and recorded as mean ± 1SD (n=3). RSD was also calculated.
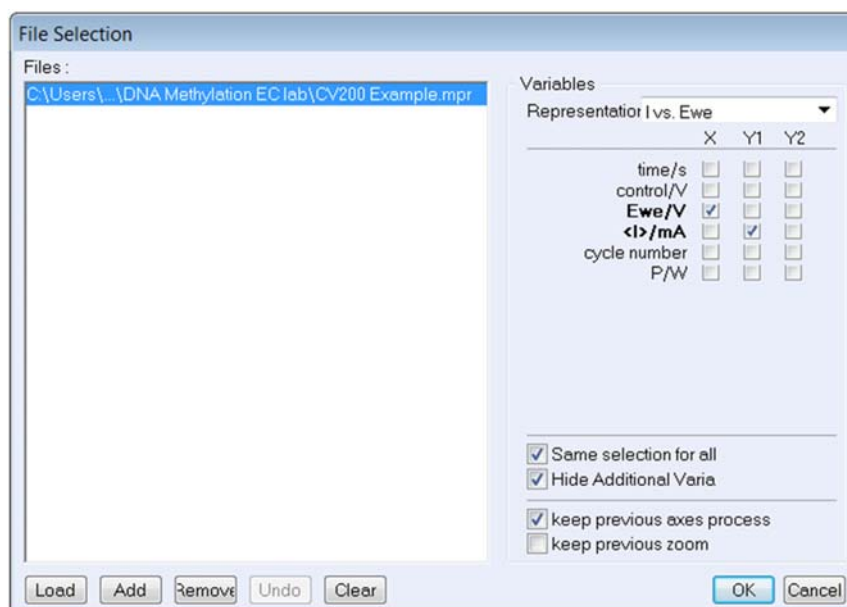
Figure 2.26 Axes determination for CVs in EC-Lab.
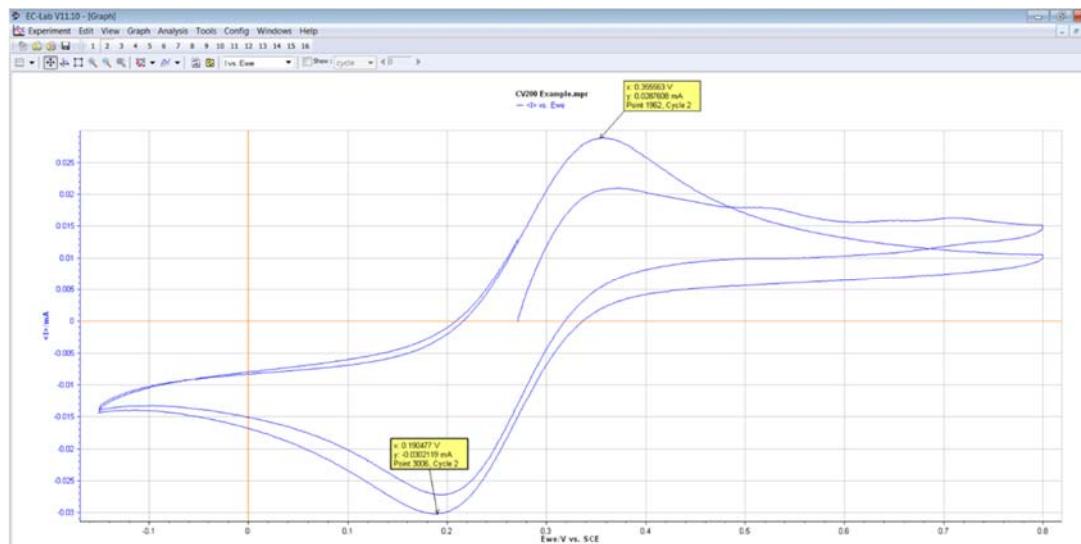
Figure 2.27 CV and deriving peak to peak separation in EC-Lab.

2.2.5.3 DPV

To create a new framework for DPV, the following were selected: Experiment > New > Pulsed Techniques > Differential Pulse Voltammetry (Figure 2.28). As demonstrated in Figure 2.29, the default settings were modified to include a potential scanning range of -0.2 to 0.7V vs. Ag/AgCl, with a potential step of 5mV, a pulse amplitude of 50mV, a pulse width of 50ms, and a pulse period of 100ms (Sina et al. 2014). Once the parameter values were outlined, the measurement could commence by selecting Experiment > Run and saving the new measurement under an appropriate name.
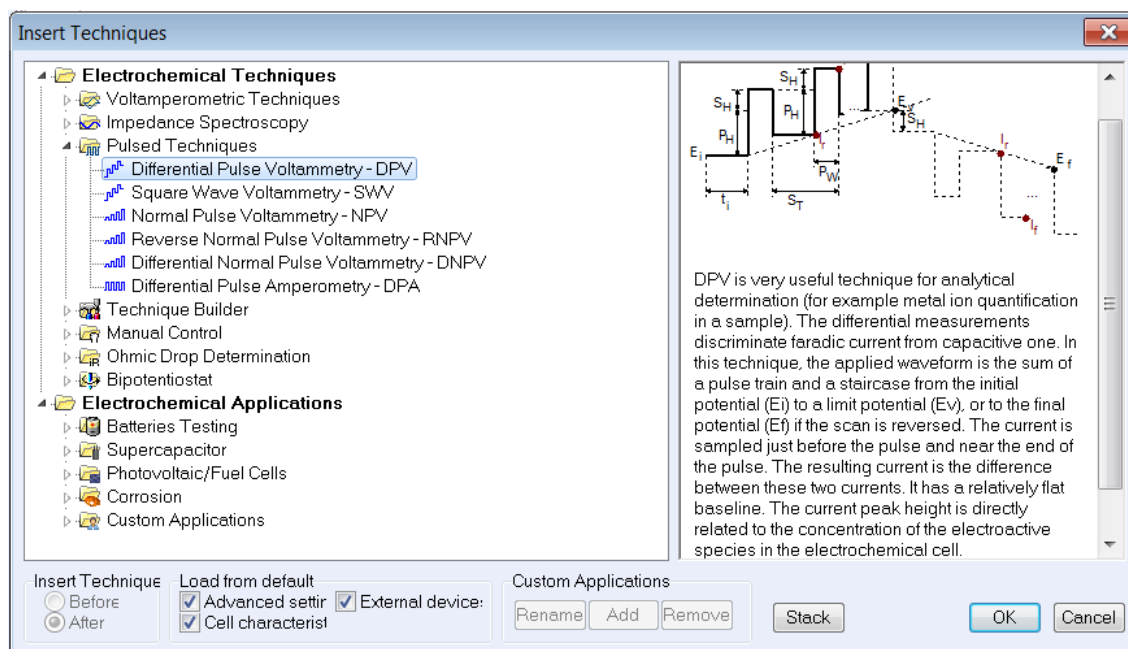
Figure 2.28 Selecting DPV in EC-Lab.

To review the measurement, following experimentation, the file was opened by selecting Experiment > Load Data File, and selecting the appropriate file. The axes were defined as I delta/µA (x) and E step/V (y), as outlined in Figure 2.30.

Figure 2.29 Parameters for DPV in EC-Lab.

Figure 2.30 Determination of Axes for DPV in EC-Lab.

To calculate i_{pa} the cursor tool was used to select the uppermost point (Figure 2.31). This value was recorded from experiments conducted in triplicate and results were displayed as mean ±1SD. RSD was also calculated.
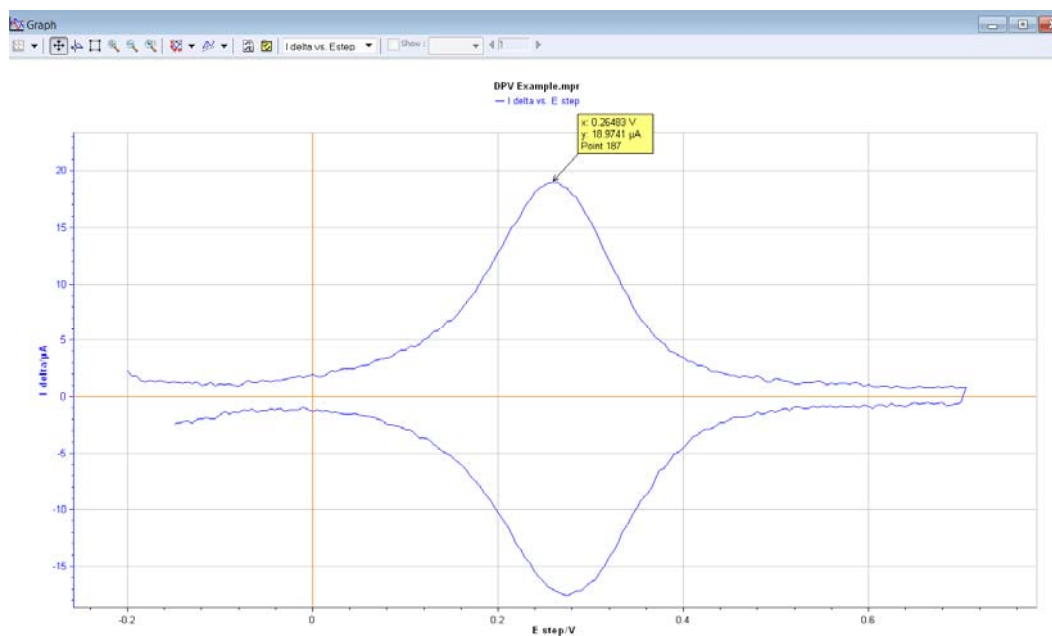
Figure 2.31 DPV and derivation of peak anodic current.

Chapter 3 Mathematically modelling the dynamics of cholesterol metabolism and ageing

3.1. Introduction

The multifaceted nature of cholesterol metabolism, the complexities of its dynamics, and the long term impact of the ageing process on its behaviour makes studying this system a challenge (Mc Auley and Mooney, 2014). In recent years however, several groups have adopted a systems level approach to investigating lipid metabolism (Mc Auley and Mooney, 2015b). The majority of these models have centred on specific metabolic processes, including those directed at lipoprotein metabolism (Hubner et al., 2008; Shorten and Upreti, 2005; Sips et al., 2014), cholesterol biosynthesis (Bhattacharya et al., 2014; Kervizic and Corcos, 2008; Mazein et al., 2013; Watterson et al., 2013), reverse cholesterol transport (Lu et al., 2014), adipocyte metabolism (Micheloni et al., 2015), hepatocyte metabolism (Jerby et al., 2010), cholesterol regulatory enzymes (Chapman et al., 2010), whole body plasma cholesterol metabolism (van de Pas et al., 2012) and enterohepatic circulation of bile acids (Mishra et al., 2014). These models all have noteworthy features and have added to our understanding of lipid metabolism. Among the computational systems biology models, the model by Mc Auley et al (2012) provides an integrated template for investigating ageing and whole-body cholesterol metabolism (Mc Auley et al., 2012). This model is encoded in SBML (Hucka et al., 2004; Hucka et al., 2003), and is part of the curated section in the BioModels web site (Le Novere et al., 2006; Li et al., 2010). This makes the model straightforward to adapt and update. The adaptable nature of this model was emphasized recently by Mishra, Somvanshi & Venkatesh (2014), who used this model in tandem with another model (Demirezen and Barlas, 2008). Their combined model included the variables body weight, diet and exercise and they analysed the feedback mechanisms of enterohepatic circulation of bile acids; specifically, bile acid synthesis, interactions with dietary lipids, and excretion. Despite its integrated nature and its focus on ageing, the model by Mc Auley et al. (2012) is lacking several key mechanisms that are fundamental to cholesterol metabolism. These key mechanisms include the cholesterol biosynthesis pathway, bile acid circulation, and a variety of *in vivo* and intestinal microfloral enzymes. It is imperative that these factors are included in any holistic representation of cholesterol

metabolism. Thus, the aims of this work were threefold. 1) To mechanistically update the whole body mathematical model of cholesterol metabolism by Mc Auley et al. (2012). 2) To use the updated model to explore the role of cholesterol and SFA feeding on lipoprotein profile. 3) To examine the role of age-related alterations to cholesterol metabolism on the lipoprotein profile, specifically, cholesterol absorption, LDL-C clearance, and bile acid synthesis and subsequent deconjugation.

3.2. Methods

3.2.1. Diagrammatic representations of whole body cholesterol metabolism

The updated model consists of eight compartments which are: 1) dietary intake, 2) intestinal lumen, 3) jejunocytes, 4) ileocytes, 5) hepatic tissue, 6) blood, 7) peripheral tissue and 8) excreted (Figure 3.1). Figures 3.1 – 3.3, were created using SBGN (Le Novere et al., 2009). Figure 3.1 is an adaptation of the previous SBGN diagram generated by Mc Auley et al. (2012). The SBGN diagrams were developed with VANTED (Version 2.2.1, http://vanted.ipk-gatersleben.de/, http://www.sbgn.org/Main_Page) (Rohn et al., 2012). To incorporate the additional information into the SBGN diagram, the compartment previously referred to as 'intestine' was divided into three sub-compartments, 'intestinal lumen', 'jejunocytes' and 'ileocytes'. This was so that cholesterol and bile acid absorption could be more accurately represented and mechanistically investigated. This allowed several key processes, receptors and enzymes to then be incorporated. These included the differentiation of dietary free and esterified cholesterol, which often is not delineated in experimental work, and bile acid micelle formation, which is a vital process in cholesterol absorption through the NPC1L1 receptor. The NPC1L1 receptor has gained attention in the last 20 years because of the vast differences in absorption efficacy between individuals (Cohen et al., 2006), and its use as a target for the treatment of hypercholesterolaemia (Dujovne et al., 2002). Additionally, cholesterol esterification in the jejunum, chylomicron transport, and bile acid reabsorption were added. Bile acid reabsorption

was expanded, as bile acid excretion is a key mechanism for cholesterol excretion, and is affected by the ageing process (Hopkins and Macfarlane, 2002; Joyce et al., 2014). Therefore, it is a potential target for the reduction of cholesterol levels in hypercholesterolaemic patients (Al-Sheraji et al., 2012). The mechanisms underpinning RCT were also expanded from those represented in the Mc Auley et al. model as it is a central player in cardiovascular health (Groen et al., 2004). The enzymes phospholipid transfer protein (PLTP), HL, LCAT and CETP and their roles in HDL subtype composition and cholesterol transport were included. Following this, additional receptors were incorporated into the peripheral tissue, hepatic tissue, and the newly formed ileocytes compartment, to further elucidate the transport mechanisms of cholesterol, lipoproteins and bile acids. Next, cholesterol biosynthesis was converted from a one step process in the Mc Auley et al. (2012) model to an 18 step process. Overall, cholesterol biosynthesis has significantly more steps than this. However, the rationale for abstracting to an 18 step reaction system is as follows. The first 13 steps of cholesterol biosynthesis are well characterised (Liscum, 2008). The latter reactions in this process remain poorly characterised. Therefore, the reactions that were included are those that are central to the pathway and are well delineated. Due to the size and complexity of this reaction network, a separate SBGN diagram was developed to illustrate this component of the model (Figure 3.2). In the overall diagrammatic representation of the model (Figure 3.1) these reactions are simplified to three source and sink glyphs labelled *a, in the jejunocytes, hepatic and peripheral tissue compartments. Finally, the *de novo* synthesis of bile acids from hepatic cholesterol was converted from a one step process to a 15 step process, and similar to the cholesterol synthesis pathway, was too detailed to be represented fully in Figure 3.1. Bile acid synthesis is therefore represented by the source and sink glyph labelled *b in Figure 3.1, and is fully illustrated in Figure 3.3. The reactions outlined in Figure 3.3 are derived from various sources (Björkhem et al., 2002; Russell, 2003; Thomas et al., 2008). In essence they are a summary of the initial and end processes that are well characterised. Some well characterised steps are excluded from the summary to reduce the process diagram size, and for clarity. For example, following the chain shortening of 4-cholesten-7α, 12α- diol-3-one by CYP27AI further modification by SLC27A5 (EC

6.2.1.7), ACOX2 (EC 1.17.99.3), HSD1724 (EC 1.1.135) and SCP2 (EC 2.3.1.176), occurs before cholic acid formation. There is ambiguity surrounding the re-entry of compounds involved in the alternative pathways to the final steps before the formation of cholic or deoxycholic acid, which resulted in gaps of knowledge. While it is possible that modelling could be used to help elucidate some of the ambiguous mechanisms in this pathway, this is beyond the scope of this work. For this reason, process glyphs that represent a series of uncertain steps are included.

Figure 3.1 SBGN diagram of mathematical model of whole-body cholesterol metabolism.

The diagram details the transport of cholesterol, bile acids and lipoproteins through cholesterol absorption, lipoprotein metabolism, RCT and enterohepatic circulation. For abbreviations see section 1 of the appendix. Round arrow head represent the target of a catalytic enzyme, represented as blue rounded rectangles. Arrows represent flux. Hatched process nodes represent omitted processes. Bar-headed lines represent inhibition. The mathematical symbol for 'empty set' represents synthesis/degradation. Submap A is for cholesterol synthesis (see Figure 3.2), submap C is for bile acid synthesis (see Figure 3.3).

Figure 3.2 Cholesterol biosynthesis.

Submap A: Synthesis of cholesterol from acetyl CoA via intermediates HMG CoA, mevalonate, squalene and lanosterol. See section 1 of the appendix for abbreviations. Round arrow heads represent the target of a catalytic enzyme, represented as blue rounded rectangles. Arrows represent flux. Hatched process nodes represent omitted processes. Acetoacetyl CoA thiolase catalyses the interconversion of acetyl CoA and acetoacetyl CoA. Acetyl CoA and acetoacetyl CoA undergo a condensation reaction to form HMG CoA. HMG CoA is then converted by HMG CoA reductase to mevalonate. Phosphorylation of mevalonate forms mevalonate-5P, which is further phosphorylated to mevalonate-5PP. Decarboxylation and dehydration of mevalonate-5PP forms IPP, which converts to its isoform DMAPP. DMAPP reacts with IPP to create geranyl-PP. Further condensation and the addition of another IPP creates farnesyl-PP. Condensation of 2 farnesyl-PP molecules forms squalene, which is converted to squalene epoxide before undergoing cyclisation to form lanosterol. A series of reactions, including the branching of 7-dehydrodesmosterol to either desmosterol or 7-dehydrocholesterol, both of which can then be converted to the end product cholesterol via the enzymes DHCR24 and DHCR7, concludes the *de novo* synthesis of cholesterol.
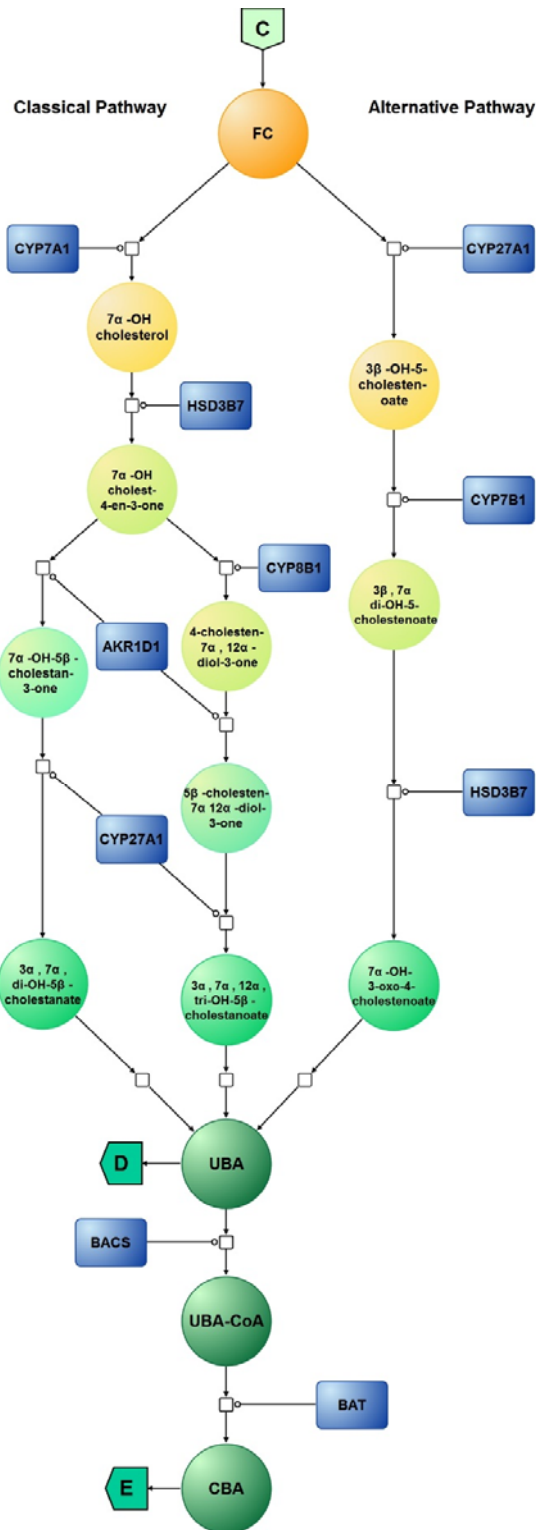
Figure 3.3 Bile Acid Synthesis.
Submap C: Classical Pathway: Hydroxylation of cholesterol creates 7α- hydroxycholesterol. Subsequent modification of the sterol ring forms 7α-hydroxy-5β-cholesten-3-one before the classical pathway splits, to enable the formation of either cholic acid (CA) or chenodeoxycholic acid (CDCA). For the formation of cholic acid, modification of the sterol ring by 12α-hydroxylase (CYP7B1) must occur before further alteration. The side chain of 5β-cholesten-7α, 12α- diol-3-one is then acted upon by a series of oxidation steps leading to its shortening. Further modification by several enzymes then takes place to form CA. The same steps, although in the absence of CYP8B1, are undergone in the other route of the classical pathway, to form CDCA. Alternative Pathway: Side chain shortening occurs first in the alternative pathway creating 27α- hydroxycholesterol, before hydroxylation creates 3β-7α-dihydroxy-5-cholestenoate. HSD3B7, CYP8B1 and AKR1D1 modification of the sterol ring can then occur, and upon further alteration, CA and CDCA can then be formed. This is followed by conjugation of 98% of these bile acids. They are they effluxed from the hepatocyte primarily by BSEP in the rate limiting step of bile acid circulation. See section 1 of the the appendix for abbreviations. Round arrow head represent the target of catalytic enzyme, represented as blue rounded rectangles. Arrows represent flux. Hatched process nodes represent omitted processes.

3.2.2. Model assembly and parameterisation

The SBML for the Mc Auley et al. model was downloaded from the BioModels database (https://www.ebi.ac.uk/biomodels-main/, BIOMD0000000434). It was then imported into Version 4.14.89 of COPASI (Hoops et al., 2006). Within COPASI the model was then reassembled. The original model contained 48 species (Mc Auley et al., 2012). The updated version now contains 144 species including the four species used as counters for the event reactions (Table A.1). The first processes to be added were the ingestion of free cholesterol and cholesterol esters. To represent these reactions, a number of new species and parameters were defined, and two SBML events for each species were then introduced. An event in SBML is a discontinuous change in a variable such as species concentration, compartment size, or parameter, which is activated at a particular point in time. In this case, the rationale for including events was to represent the ingestion of cholesterol every 8 hours. This was more biologically realistic than the single reaction which represented this process previously, as it accounted for the intake of three meals per day. The average UK male ingests 304mg of cholesterol per day (Henderson et al., 2003). Literature suggests that 85-90% of this is in the free form, while 10-15% is esterified (Iqbal and Hussain, 2009). The events stimulated the intake of both free cholesterol and cholesterol esters, by taking the average percentage values of 87.5 and 12.5%. Using these values it can be estimated that a UK male ingests 266mg of free cholesterol and 38mg of esterified cholesterol daily. Assuming that a person eats three equivalent meals each day, it can then be calculated that each meal contains $88.\dot{6}$mg and $12.\dot{6}$mg of free and esterified cholesterol respectively. The events were defined using the syntax outlined in Table 3.1. Separate events could not be triggered simultaneously within the software, therefore, to allow for the two events, the intake of free cholesterol was 2 minutes later than the intake of esterified cholesterol.

Table 3.1 Overview of events included to represent the ingestion of dietary free and esterified cholesterol.
DFC, dietary free cholesterol; DCE, dietary cholesterol esters.

Event	Event_1 DFC	Event_2 DFC	Event_1 DCE	Event_2 DCE
Delay	None	None	None	None
Trigger Expression	[counter2]>482	[counter2]>483	[counter4]>480	[counter4]>481
Target	DFC	counter2	DCE	counter4
Expression	[DFC]+88.667	[counter2]-483	[DCE]+12.667	[counter4]-481

Following the assembly of the events, the entry of dietary esterified cholesterol into the intestinal lumen three times a day was deterministically simulated (Figure 3.4A). Once in the intestinal lumen, esterified cholesterol is converted to free cholesterol for entry into the jejunocytes. Figure 3.4B illustrates how the level of free cholesterol in the jejunocyte was affected by the entry of this converted free cholesterol. This is in addition to the 88.6́mg of free cholesterol that is also ingested three times a day, and biliary cholesterol effluxed back into the lumen from the liver. Within the model, free cholesterol contained in the jejunum fluctuated. Initial concentrations for intestinal cholesterol were stated as 1575mg for both free and esterified cholesterol. This was calculated by taking the intestinal cholesterol value of 3150mg, as stated by Mc Auley et al. (2012), and assuming an equal distribution between forms.

3150mg intestinal cholesterol/2 = 1575mg esterified cholesterol and 1575mg free cholesterol

Initial steady state values for free and esterified cholesterol in the hepatic or peripheral tissues were calculated based on the experimental data in Table 3.2 (Figure 3.4C). Briefly, hepatic values were calculated by taking the estimated concentrations of 67.1nmol/mg and 18.5nmol/mg of free and esterified cholesterol (Mc Auley et al., 2012), and multiplying them by their molecular masses of 386.66 and 349.08 respectively. Then these masses were scaled to represent the total mass in a 1.5kg liver (Mc Auley et al., 2012).

67.1nmol free cholesterol/mg liver

67.1nmol x 10^{-6} x 386.66 x 1,500,000mg =38,917mg free cholesterol/liver

18.5nmol esterified cholesterol/mg liver

18.5nmol x10^{-6} x 649.08 x 1,500,000mg = 18,012mg esterified cholesterol/liver

Van de Pas et al. (2012) outline the peripheral mass totals 64.8kg, and that 465mg of cholesterol is present per kg of tissue. Using the assumption that 14% of this cholesterol is esterified (Mc Auley et al., 2012), it can be calculated that there is 4,218.48mg of esterified cholesterol and 25,913.52mg of free cholesterol in the peripheral tissue:

14% of 465mg = 65.1mg esterified cholesterol/kg

65.1mg x 64.8kg = 4,218mg/peripheral tissue

86% of 465mg = 399.9mg free cholesterol/kg

399.9mg x 64.8kg = 25,914mg/peripheral tissue

Table 3.2 Data used to calculate initial values of cholesterol in each compartment.
See section 1 of the appendix for abbreviations. Data taken from Mc Auley et al. (2012) & van de Pas et al. (2012)

Species	Concentration	Reference	Molecular mass	Location Mass (kg)	Reference	Calculated mass (mg)
HFC	67.1nmol/mg	Mc Auley et al. (2012)	386.66	1.5	Mc Auley et al. (2012)	38,917
HCE	18.5nmol/mg		649.08			18,012
PFC	399.9mg/kg	Mc Auley et al. (2012) & van de Pas et al. (2012)	-	64.8	Van de Pas et al. (2012)	25,914
PCE	65.1mg/kg		-			4,218

Other species were calculated in a similar way, utilising tissue mass and molecular mass. For instance, experimentally it has been shown that apoA1 is 2.97mg/ml in individuals with no cognitive impairment

with an average age of 78 years (Song et al., 2012). This value was scaled up to encompass the full plasma volume of 2.79L (van de Pas et al., 2012).

$$2.97mg/ml \times 2790ml = 8286.3\ apoA1/plasma$$

Values of 303, 210 and 21mg were selected for species involved in hepatic, intestinal and peripheral species involved in cholesterol biosynthesis. This was calculated by taking the synthesis rates (441, 49 and 210mg/day) for each compartment defined by Mc Auley et al. (2012) and calculating the rate relative to the cholesterol pool used in the Mc Auley et al. (2012) work. Following this, the relative percentage was applied to the cholesterol pools utilised in this study. It was calculated that 303, 210 and 21mg/day was present in the hepatic, intestinal and peripheral compartments and thus each species was assigned the value of 303, 210 and 21mg, as this pathway consists of consecutive reactions.

Utilising a plasma volume of 2.79L (van de Pas et al., 2012), the initial steady state values of VLDL-C, LDL-C and HDL-C (Sharma et al., 2010), could be converted to mg/plasma (Table 3.3). Lipoprotein values were converted to mg/dL for analysis, by diving each value by 27.9dL. When the model was simulated, VLDL-C, LDL-C and mean HDL-C values were consistent with these literature values (Figure 3.4D). Mean HDL-C was calculated from HDL_2 and HDL_3 and nascent HDL-C (ndHDL-C) subfractions. Cholesterol and unconjugated bile acids were steadily excreted at a rate of 0.1 and 0.05mg/hour respectively (Figure 3.4E). The initial steady state values for bile acids were assumed. For bile acids contained in the hepatic tissue, a value of 220mg was utilised for those conjugated (HCBA). A value of 180mg was assigned to represent the unconjugated proportion (HUBA), and a value of 200mg was chosen to represent HUBA-CoA. Within the ileocytes, a value of 50mg was utilised for both the conjugated and unconjugated forms (ICBA and IUBA). Within the intestinal lumen a steady state value of 200mg was assumed to represent conjugated bile acids, while a value of 50mg represented the steady state level of unconjugated bile acids (LCBA and LUBA). Levels remained constant over time (Figure 3.4F).

Table 3.3 Data used to calculate the initial values of lipoproteins.

See section 1 of the appendix for abbreviations. Lipoprotein concentrations gained from Sharma et al. (2010), and plasma volume gained from Van de Par et al. (2012)

Lipoprotein	Concentration (mg/dL)	Reference	Plasma Volume (L)	Reference	Calculated mass (mg)
VLDL-C	34				34 x 10 x 2.79 = 949
LDL-C	115	Sharma et al. (2010)	2.79	Van de Pas et al. (2012)	115 x 10 x 2.79 = 3,209
HDL-C	44				115 x 10 x 2.79 = 1,227
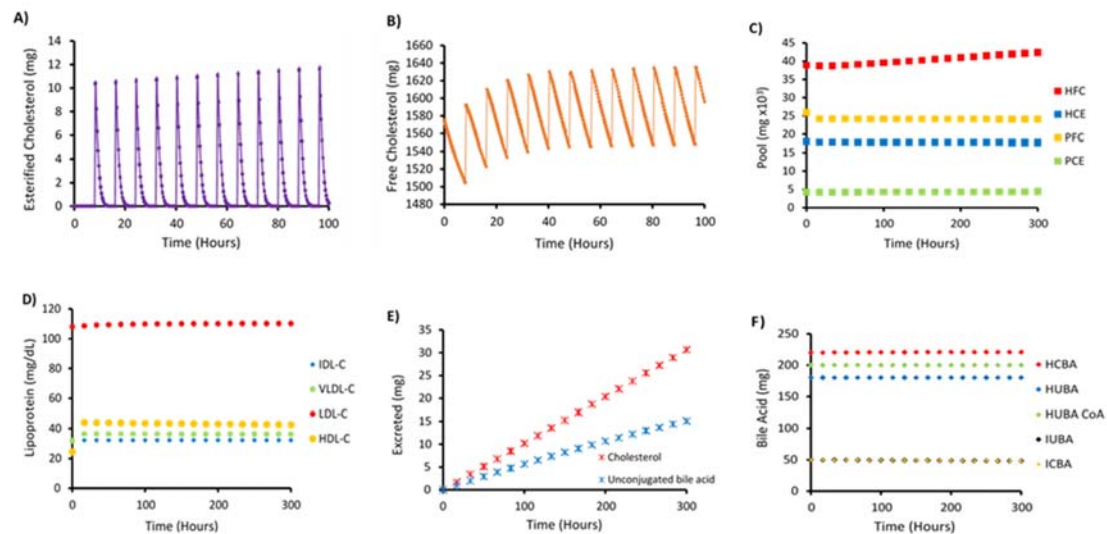
Figure 3.4 Model outputs.

Model Outputs of A) ingestion of esterified cholesterol, B) jejunocyte pool of free cholesterol C) hepatic and peripheral pools of free and esterified cholesterol, D) lipoprotein profile E) excreted cholesterol and unconjugated bile acids and F) hepatic, ileocyte and intestinal lumen pools of conjugated and unconjugated bile acids. For D) mean HDL-C calculated from HDL$_2$, HDL$_3$ and ndHDL-C.

The initial steady state levels of many other intermediate species were assumed. Each value is in mg/compartment. Table A.1 provides the details of the species and their abbreviations, while Table A.2 provides details of over 144 kinetic based reactions which in total make up the new version of the model. To summarise the kinetics, the model includes 37 reactions which are derived using the law of mass action, 58 reactions informed by Michaelis-Menten kinetics, six reversible reactions informed by Michaelis-Menten kinetics, nine bi, three ping pong bi-bi kinetic reactions, and 31 rate laws that were either part of the old model or developed during its adaptation. Each functional form is underpinned by the experimental literature, and examples of all the functional forms are provided within the list of ordinary differential equations found in section 2 of the appendix. Often, enzymes weren't included in the rate equation, as a species, despite the vital role they play. This is because kinetic data for parameters such as V_{max} and K_M were utilised. These parameters represent the maximum velocity of the reaction, and the substrate concentration required to reach $\frac{1}{2} V_{max}$ respectively, and when applied to a rate law such as Michaelis Menten, sufficiently represent the kinetics of enzymatically regulated reactions, when combined with substrate concentration (Johnson and Goody, 2011). In order to parameterise the kinetic reactions summarised in Table A.3, firstly a comprehensive search of the enzyme functional data repository, BRENDA was conducted (http://www.brenda-enzymes.org/) (Chang et al., 2015). Many of the enzymes identified within BRENDA had a wide range of values. Suitable values were selected based on considering the biological source of the kinetic information. Some of the model parameters could not be located within BRENDA, therefore to obtain these parameters, literature searches were conducted using Pubmed, Science Direct and Google Scholar. The source of each parameter is indicated in column four of Table A.3. For a number of parameters, no kinetic information could be obtained, therefore several assumptions were made; the details of these are also given in Table A.3. To obtain suitable parameter values, as each parameter was added to the model, a time course simulation was conducted, using COPASI. This was undertaken to compare the model output to the Mc Auley et al. (2012) model, and to known biological behaviour. The parameters were gradually adjusted until a steady state output was achieved, which was an accurate

biological representation of the system. This process was completed over several months, and it would be impossible to include the details of every time course from this process. To illustrate this point, the tuning of BSH is discussed. For the reaction of deconjugated of lumen conjugated bile acids (LCBA), an average K_M and V_{max} value was calculated as 2.37 and 27.06 respectively, from several sources (Gopal-Srivastava and Hylemon, 1988; Kumar et al., 2006; Lundeen and Savage, 1990, 1992; Nair et al., 1967; Patel et al., 2010; Stellwag and Hylemon, 1976). Using these values, LCBA was utilised before 10 minutes, and lumen unconjugated bile acids (LUBA) reached a ceiling value, as shown in Figure 3.5A. Therefore, K_M and V_{max} were slowly adjusted to values of 1×10^{-4} and 5×10^{-6} respectively, until species concentrations remained steady, as outlined in Figure 3.5B.
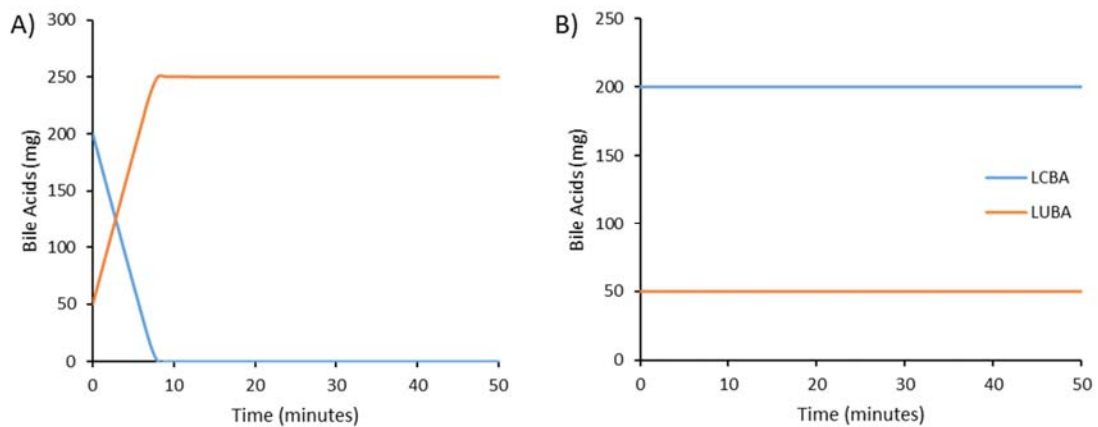
Figure 3.5 Parameter optimisation for the reaction deconjugation of bile acid.
LUBA and LCBA A) before and B) after parameter optimisation.

3.3. Results

3.3.1. Initial examination of the model

Initial simulations were performed to compare model output with the previous model. Figure 3.6 illustrates how several key variables compare to the Mc Auley et al. model. Over a 15 day period it was found that the average concentration of LDL-C, mean HDL-C and TC reduced by 11%, 20% and 0.6% respectively, when compared to the Mc Auley et al. model. Mean HDL-C was calculated from HDL_2, HDL_3 and ndHDL-C. In contrast, IDL-C and VLDL-C increased by 33% and 67% respectively in the updated model. The LDL-C:HDL-C ratio increased slightly from 2.52:1 in the Mc Auley et al. model to 2.77:1 in the updated model. Both of these ratios however are in line with current guidelines, as a ratio <3.0:1 for males is recommended to reduce the risk of CVD onset (Millan et al., 2009).
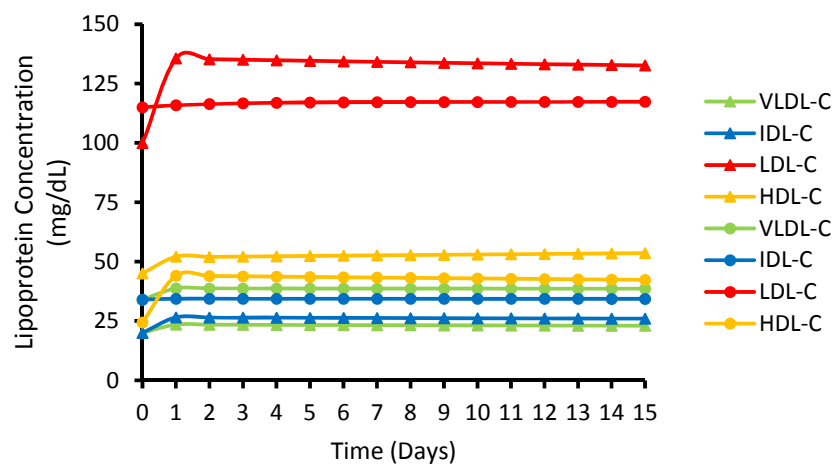
Figure 3.6 Comparison of the lipoprotein profile from the Mc Auley et al. and updated model.
Model run for 15 days or equivalent (21,600 minutes). Circle markers represent the model output from the updated model. Triangle markers represent the lipoprotein profile from the Mc Auley et al. (2012) model. HDL-C from the updated model is the mean average of HDL_2, HDL_3 and ndHDL-C.

3.3.2. Dietary cholesterol ingestion

Differences exist in cholesterol metabolism from one individual to the next (Herron et al., 2003). This is emphasised by dietary cholesterol (DC) feeding studies which demonstrate notable differences in the response to DC from individual to individual. Herron et al. (2003) demonstrated that hypo-responders could ingest ~640mg/day of cholesterol for 30 days with no effect on LDL-C or HDL-C levels. In contrast, hyper-responders exhibited a 30% increase in LDL-C and an 8% increase in HDL-C (Herron et al., 2003). To determine if the model behaves as a hypo- or hyper-responder, fold increases of 0.5, 1, 2, and 3 were applied to both ingested free and esterified DC, and results analysed after 1000 hours. This time, of just under 6 weeks, was chosen because experimentally it has been shown that cholesterol feeding can produce observable differences in the lipoproteins in timescales shorter than this (Herron et al., 2003; Lin and Connor, 1980). For instance Lin and Connor (1980) reported that the response to increased dietary cholesterol was rapid; one week and two weeks for the normal and hypercholesterolaemic patients respectively. Additionally, it was observed that the increase in plasma levels of cholesterol reached a plateau in the normal patient after two weeks, and six weeks in the hypercholesterolaemic patient. Therefore, analysis after 1000 hours would be appropriate experimentally as it would be long enough to produce significant changes to the lipoprotein profile, and thus was employed for the model. To model a change in dietary intake, the events for DC ingestion were modified. For the 0.5-fold analysis, the standard intake values were divided by two, leading to the simulated ingestion of 44.3mg of free cholesterol and 6.3mg of esterified cholesterol three times a day. Whereas an increase to 266mg of free cholesterol and 38mg of esterified cholesterol was ingested three times a day for a 3-fold dietary increase, which was calculated by multiplying the standard values by three (Table 3.4). A positive correlation between LDL-C and cholesterol intake was observed at 1000 hours. A 2-fold increase in DC resulted in a small increase of 0.0012% (0.0014mg/dL) in LDL-C, after 1000 hours. This rose to a 0.0021% increase for the 3-fold analysis (0.003mg/dL). A 50% reduction in DC resulted in a negligible 0.0003% reduction in LDL-C. No change to mean HDL-C level

was observed (data not shown). A 2-fold increase in DC resulted in a 23.72% increase in HFC, and a negligible increase of 0.0002% in PCE; this increased to 47.43 and 0.0004% for HFC and PCE respectively when compared to the normal intake values. Significantly, a 50% reduction in DC resulted in an 11.86% reduction in HFC after 1000 hours. No difference in PFC or HCE was observed (Figure 3.7A).

Table 3.4 Summary of dietary FC and CE values for fold analysis of dietary cholesterol intake.

Species	Fold Change			
	0.5	1	2	3
FC	44.3	88.7	177.3	266.0
CE	6.3	12.7	25.3	38.0

3.3.3. Comparison with clinical data

Both the Mc Auley et al. and updated models were compared to clinical data from a DC feeding study (Figure 3.7B). After a comprehensive literature search in this area, the most suitable time course data that could be obtained was from a healthy 31 year old normocholesterolaemic male that underwent an 11 week high cholesterol diet (1000mg/day) (Lin and Connor, 1980). The purpose of using this data, which clearly shows a hyper-response to DC, was to provide a comparison between this and the models. To compare the model to the clinical data, the intake of cholesterol was raised to 1000mg per day, and baseline LDL-C was reduced to 66.32mg/dL (1.72mmol/L). To recreate a 1000mg/day cholesterol intake, the events were altered to reflect an intake of $291.\dot{6}$mg FC and $41.\dot{6}$mg CE three times a day. These values were calculated as:

$$(291.\dot{6}\text{mg x 3}) + (41.\dot{6}\text{mg x 3}) = 1000\text{mg}$$

Lin and Connor (1980) did not report LDL-C or HDL-C values, therefore LDL-C was calculated from TC and triglyceride values using equation 31 below, in which LDL-C can be calculated in the absence of HDL-C data (Anandaraja et al., 2005).

$$Calculated\ LDL\!-\!C\ =\ (0.9\ x\ Total\ Cholesterol) - \frac{0.9\ x\ triglycerides}{5} - 28 \qquad (31)$$

The Mc Auley et al. (2012) model was then run over 77 days with interval sizes of 7 days. This was to represent a weekly LDL-C level for 11 weeks similarly to the Lin and Connor (1980) study. For the updated model, which was configured in minutes, rather than days, a time course simulation was the run over 110,880 minutes, with interval sizes of 10,080 minutes. This is because 10,080 minutes is equivalent to one week, while 110,880 is equivalent to 11 weeks. Thus the results gained were indicative of weekly changes in LDL-C up to 11 weeks, making the results comparable to those from the Lin and Connor (1980) study.
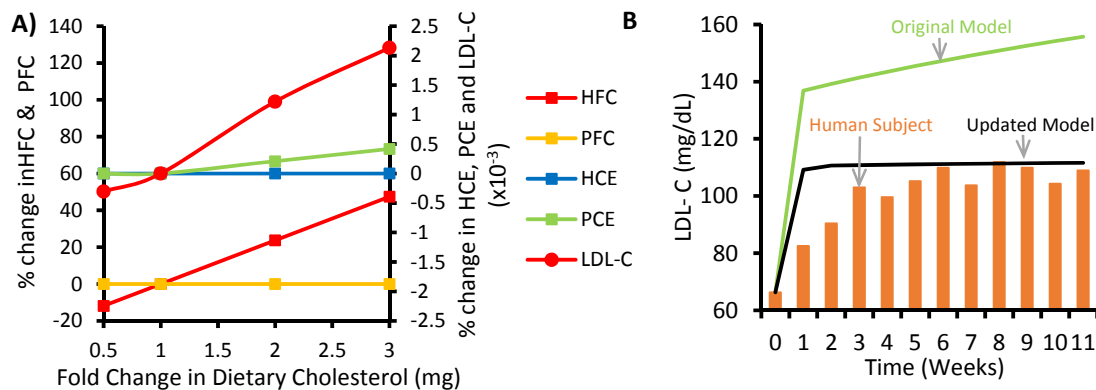
Figure 3.7 Cholesterol ingestion analysis.
A) Response of LDL-C and cholesterol pools in the updated model to fold-change increases in dietary cholesterol after 1000 hours. HFC, hepatic free cholesterol; PFC, peripheral free cholesterol (left axis); HCE, hepatic cholesterol esters; PCE, peripheral cholesterol esters; and LDL-C (right axis). B) Comparison of models to clinical data. Comparison of LDL-C concentration in response to simulated cholesterol feeding in the Mc Auley et al. (2012), and the updated model, with a human cholesterol feeding study. A 1000mg dose of cholesterol was ingested per day by a human subject and induced in both models for an 11 week trial period and the LDL-C monitored. Baseline LDL-C of both models was set at 66.32mg/dL (1.72mmol/L) to match clinical data. Black line represents updated model the green line represents the Mc Auley et al. (2012) model, and the orange bar represents the LDL-C response to cholesterol feeding in a human subject (Lin and Connor, 1980).

When the daily rate of cholesterol ingestion was raised, LDL-C increased from an initial value of 66.32mg/dL (1.72mmol/L), to a steady state value of ~115mg/dL (2.97mmol/L) after one week. It is important to note this is the behaviour of LDL-C regardless of the rate of dietary cholesterol ingestion (data not shown). This finding contrasts with the Mc Auley et al. model's response during this feeding regime, where LDL-C continues to rise after week one. It is feasible the behaviour of the updated model is biologically plausible, as several decades of experimental work in this area have suggested that cholesterol metabolism is tightly regulated in the majority of individuals, with hypo-responders known to exhibit a negligible lipoprotein response (Herron et al., 2003; Jones et al., 1996; Quintao et al., 1971). Consequently, it was important to establish which regulatory mechanisms responded effectively in the model to inhibit a rise in lipoprotein cholesterol.

After examining the simulation data it was found a key regulatory mechanism which adapted to this increase in DC was cholesterol excretion (EFC). EFC increased by 25.1% by the end of the 11 week period (Figure 3.8). In addition to the compensatory effect of excreted cholesterol, intestinal and hepatic cholesterol also increased. It was found high DC resulted in the pool of cholesterol esters in the intestinal lumen (LCE) increasing to 5.97mg after 11 weeks. This contrasted with a value of 0.15mg after a 'normal' cholesterol feeding regime over the same time period. Free cholesterol in the intestinal lumen (LFC) also increased by 4.75% as a result of this simulation. The amount of absorbed free and esterified cholesterol in the jejunocytes (JFC and JCE) also increased; JFC and JCE levels were 24.41 and 0.03% higher respectively after the cholesterol feeding. Furthermore chylomicrons in the jejunum (JCH) increased 25.33%. In addition, hepatic free cholesterol (HFC) increased by 85.25%. Bile acid levels and LDLr activity/number were unaffected during cholesterol feeding, which could account for the substantial cholesterol accumulation within the hepatic tissue, and marginal LDL-C response.
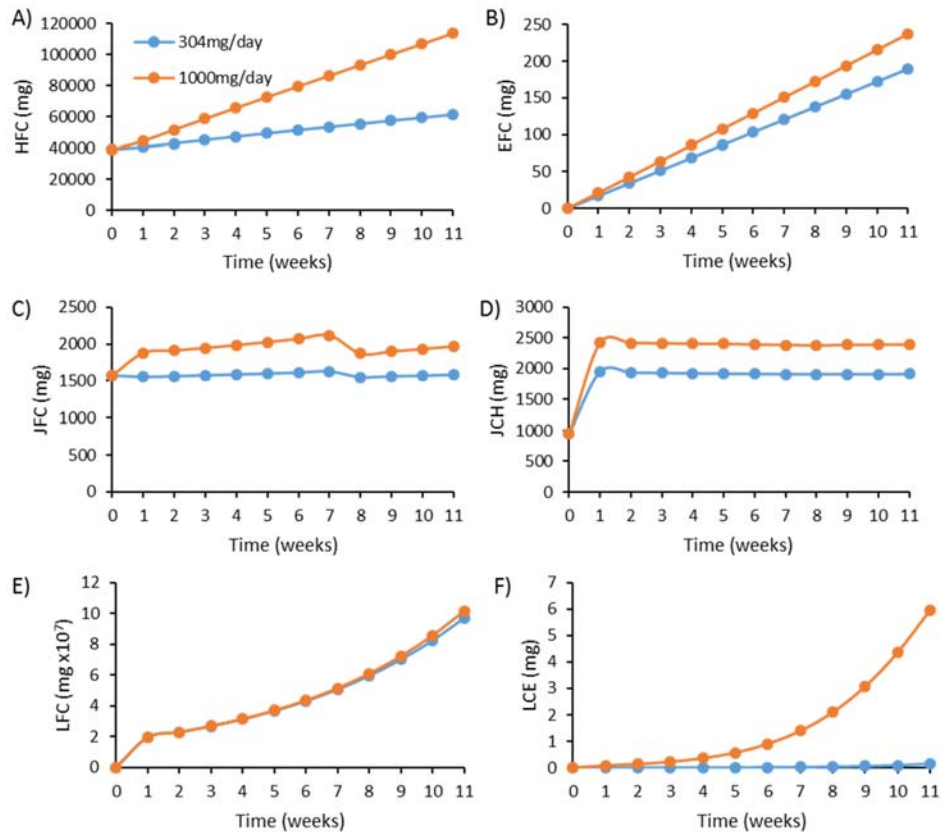
Figure 3.8 Effect of cholesterol feeding.
Response of A) HFC, B) EFC, C) JFC, D) JCH, E) LFC, and F) LCE to 1000mg/day of dietary cholesterol for 11 weeks, in comparison to the UK male average cholesterol intake of 304mg/day.

3.3.4. Acute daily ingestion of saturated fat

Diets high in SFA are associated with raised plasma cholesterol levels (He and Fernandez, 1998). High levels of SFA lead to an increase in LDL-C by three possible mechanisms. 1) A reduced LDL-C clearance rate, as SFA supresses LDLr activity (Woollett et al., 1992). 2) There is an increase in the rate of cholesterol synthesis (Jones et al., 1994). 3) Modulation of RCT occurs (Berard et al., 2004; Jansen et al., 2000). RCT is affected in two ways. Firstly, CETP is upregulated, thus transporting esterified cholesterol from HDL-C to LDL-C and VLDL-C at an increased rate (Jansen et al., 2000). Secondly, LCAT is inhibited which reduces the esterification of cholesterol in HDL-C (Berard et al., 2004). This reduces the concentration gradient for the transfer of cholesterol from the peripheral tissues to HDL. To replicate SFA intake variations, seven parameters were altered simultaneously (Table 3.5). This

156

analysis resulted in a slight increase in LDL-C, HCE and PCE levels, whereas HDL-C decreased (Figure

3.9). LDL-C, HCE, and PCE increased 1.7, 0.4 and 0.5% respectively for the 2 fold-analysis. There was

no effect on hepatic and peripheral free cholesterol (HFC and PFC) after 1000 hours.

Table 3.5 Summary of parameters involved in fold analysis of SFA intake.

Reaction		Parameter	Fold Change			
			0.5	1	2	3
36	LCAT activity	K_{hdl3}	8×10^{-4}	4×10^{-4}	2×10^{-4}	1.33×10^{-4}
39	CETP mediated transfer to VLDL	K_{cetp2}	5×10^{-8}	1×10^{-7}	2×10^{-7}	3×10^{-7}
40	CETP mediated transfer to LDL	K_{cetp1}	5×10^{-8}	1×10^{-7}	2×10^{-7}	3×10^{-7}
63	LDLr degradation	K_1	5×10^{-8}	1×10^{-7}	2×10^{-7}	3×10^{-7}
78	Hepatic acetyl CoA synthesis	K_1	0.5	1	2	3
96	Peripheral acetyl CoA synthesis	K_1	5×10^{-6}	1×10^{-5}	2×10^{-5}	3×10^{-5}
114	Intestinal acetyl CoA synthesis	K_1	0.5	1	2	3
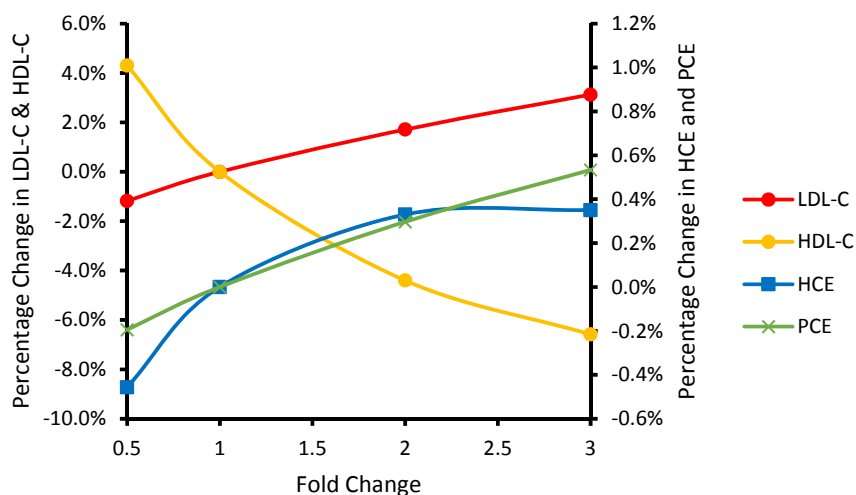
Figure 3.9 Fold change analysis of dietary SFA.
The percentage change in LDL-C, HDL-C (left axis), HCE and PCE (right axis) with fold changes to SFA

intake. A total of seven parameters were modified in the fold change analysis to represent an

equivalent change in dietary SFA. To represent an increase in dietary SFA, increases to the rate of LDLr

degradation, cholesterol synthesis and CETP mediated transport, and decreases to the LCAT mediated

cholesterol esterification were conducted. Measurements recorded at 1000 hours.

3.3.5. Local sensitivity analysis

To gain further insight into the robustness of the model a SA was performed. A robust model is resilient to relatively small perturbations in parameter values. Therefore given the lack of sensitivity of the model during the initial investigations the aim of the SA was to investigate the effect of both local and global parameter changes on model outputs, in particular LDL-C, and to identify critical parameter inputs. Firstly, a local SA was completed and the S_i for each of the parameters were calculated. To do this, the discrete feeding events were removed and replaced with a continuous feed for both DC and DFC. Table A.4 gives the percentage change in LDL-C for a 1% change in each of the 266 model parameters and ranks them by sensitivity. Figure 3.10 presents the 20 most sensitive parameters of this analysis. The most sensitive parameter was the rate constant for LDL-C formation, K_{ldl}. The second most sensitive parameter was K_{hldlu}, the rate constant for receptor dependent hepatic uptake of LDL-C. Third most sensitive was K_{idlu}, the rate constant for IDL-C reuptake. The rate constant K_1, for VLDL-C formation was fourth most sensitive. V_{max} for the conversion of HDL$_3$ to HDL$_2$, was fifth, while V_{max} for the conversion of HDL$_2$ to HDL$_3$ was sixth. K_{idlf} for IDL-C formation, and K_{vldl} for VLDL-C reuptake were seventh and eighth. K_{pldlu} for the receptor dependent peripheral uptake of LDL-C was ninth, and V_{max} for the esterification of hepatic free cholesterol was tenth most sensitive. The 11th most sensitive parameter was K_1 for hepatic LDLr degradation. The rate constants K_{cetp1} and K_{cetp2} for CETP mediated transfer of esterified cholesterol to LDL and VLDL respectively were 12th and 14th most sensitive; 13th was V_{max} for the hepatic conversion of esterified cholesterol to free cholesterol. K_1 for the degradation of peripheral LDLr was 15th. The rate constants for the conversion of HDL$_3$ to HDL$_2$, and the conversion of HDL$_2$ to HDL$_3$, both termed K_M were 16th and 17th most sensitive. K_1 for the receptor independent peripheral uptake of LDL-C was 18th, and K_{pldlrs} for the synthesis of peripheral LDLr was 19th. K_{ch3}, the parameter the reaction chylomicron free cholesterol uptake by hepatic LDLr, was 20th most sensitive.
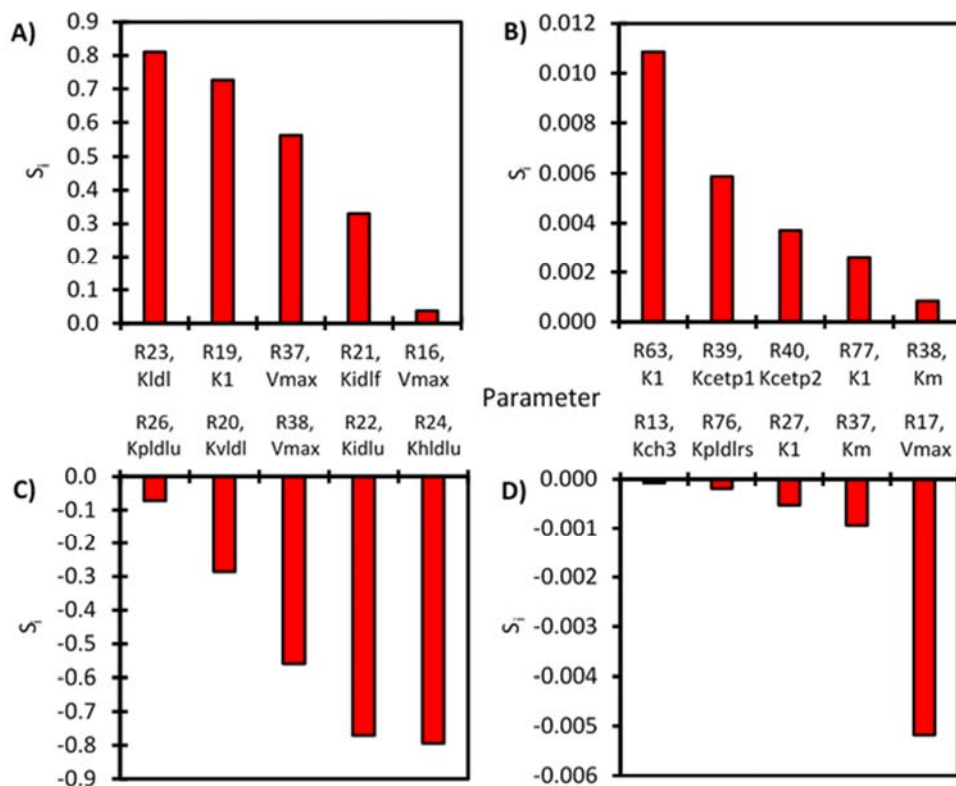
Figure 3.10 The 20 most sensitive parameters.
A) and B) denote the top 10 most sensitive reaction parameters, where LDL-C increases with a 1% change in model parameters. C) and D) denote the top 10 most sensitive reaction parameters where LDL-C decreases with a 1% change in model parameters. Si, sensitivity index, percent change in LDL-C for a 1% change in model parameters; R, reaction. See Table A.2 for reaction details.

3.3.6. Local parameter analysis of CETP dynamics

CETP mediates the transport of cholesterol esters from HDL to LDL and VLDL. Mutation to the CETP gene has been associated with longevity in Ashkenazi Jews (Atzmon et al., 2005; Barzilai et al., 2003). The amino acid substitution of 405 isoleucine to valine (I405V) in the CETP gene results in a lower serum CETP concentration and subsequently significantly larger LDL and HDL. The CETP I405V genotype is associated with a reduced prevalence of CVD, T2DM, and hypertension, possibly contributing to the exceptional longevity observed in these individuals (Atzmon et al., 2005; Barzilai

et al., 2003). The assertion that reduced CETP levels convey a protective phenotype for healthy ageing, has led to investigations into the use of CETP inhibitors as a therapeutic strategy for the treatment of hypercholesterolaemia. For example, it has been recently revealed that in phase II clinical trials the CETP inhibitor TA-8995 decreased LDL-C by 27.4% with a 1mg daily dose, with minimal adverse effects (Hovingh et al., 2015). Therefore, with the updated model, there was a clear emphasis on these aspects of lipid metabolism.

Due to apparent local sensitivity of both K_{cetp1} and K_{cetp2}, these parameters were further investigated, as CETP inhibitors are widely suggested as a potential therapeutic strategy for the treatment of hypercholesterolaemia (Hovingh et al., 2015). To analyse the role of a CETP inhibitor such as TA-8995 on the lipoprotein profile, the parameters K_{cept1} and K_{cept2} were analysed (Reactions 39 and 40, Table A.2). K_{cept1} is the rate constant representing the CETP mediated transfer of cholesterol from HDL_2 to LDL whereas K_{cept2} represents the CETP mediated transfer of cholesterol from HDL_2 to VLDL. A value of 1×10^{-7} was defined for both parameters under "normal conditions". To mimic CETP inhibition, firstly rate constants K_{cept1} and K_{cept2} were analysed separately, between values of 0 and 1×10^{-7}. Decreases to both rate constants resulted in a decline in LDL-C and an increase to HDL subfractions. Alterations to K_{cetp1} led to a greater decrease in LDL-C than K_{cetp2}. The reduction of K_{cetp1} and K_{cept2} to 0 resulted in a 0.50% (0.59mg/dL) and 0.15% (0.18mg/dL) decrease in LDL-C respectively after 250 hours. The increase in HDL_2 and HDL_3 was equivalent for both parameters; a 15% (1.87mg/dL) increase in HDL_2 and a 0.2% (0.024mg/dL) in HDL_3 was observed when K_{cetp1} and K_{cetp2} reached 0. The local parameter analysis suggests that a reduction in K_{cetp1} or K_{cept2} leads to a reduction in LDL-C and an increase in HDL subfractions. As both reactions are catalysed by the same enzyme, the administration of a CETP inhibitor would in theory result in both processes being simultaneously affected. To predict the effect of CETP inhibition *in vivo*, simultaneous parameter scans were conducted. This involved gradually reducing both K_{cept1} and K_{cept2}, where 0 represented full CETP inhibition. This resulted in a 0.72% reduction in LDL-C (Figure 3.11A), and a mean HDL-C increase by 3.1% (Figure 3.11B). Mean HDL-C was calculated from HDL_2, HDL_3 and ndHDL-C, after 250 hours.
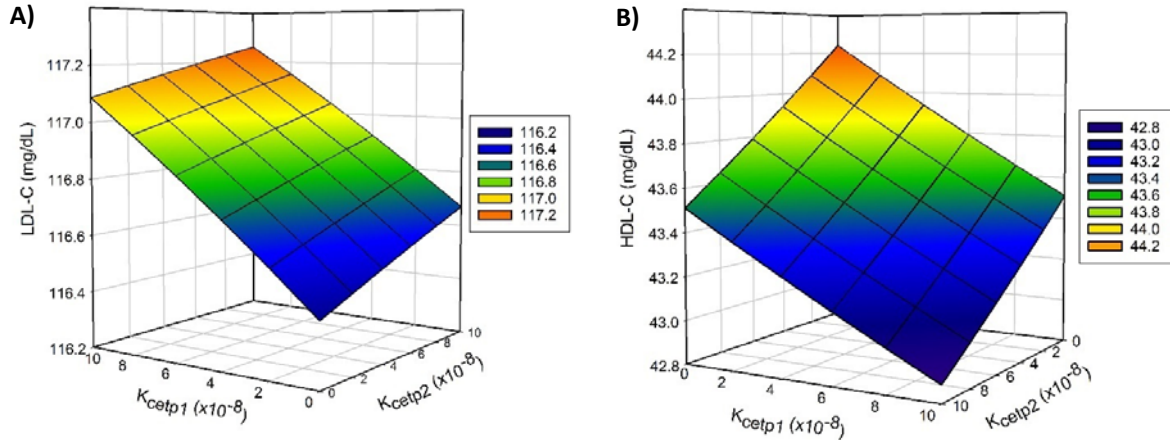
Figure 3.11 Inhibition of CETP by simultaneous inhibition of K$_{cetp1}$ and K$_{cetp2}$ parameters.
K$_{cept1}$ is the rate constant representing the CETP mediated transfer of cholesterol from HDL2 to LDL.

K$_{cept2}$ represents the CETP mediated transfer of cholesterol from HDL2 to VLDL. Effect of manipulation

on A) LDL-C, and B) mean HDL-C. Mean calculated from HDL2, HDL3 and ndHDL-C. LDL-C and mean

HDL-C concentration analysed after 250 hours.

3.3.7. Global sensitivity analysis

Given the uncertainty surrounding a number of the parameter values in the model, especially those

associated with the less well characterised aspects of cholesterol metabolism, it is apparent that any

inferences from the local SA should be interpreted with caution. Therefore, it was deemed that it

would be appropriate to sample from the parameter space of a global SA. This attempts to mitigate

this problem by examining model parameters in broader regions of parameter space. Figure 3.12

presents the results from sampling from the parameter space of a global SA, where 500 random

samples (n=500) were taken over a range of a 2 fold increase and decrease in the default value for the

rate constant K_1 for hepatic LDLr degradation (reaction 60 in Table A.2), with A) all "known"

parameters scanned and unknown parameters fixed, B) all unknown parameters scanned and

"known" parameters fixed, and C) all parameters scanned simultaneously, at 250 hours. Each scanned

parameter had random samples taken between a 2 fold increase and decrease of its default value.

161

The variability of LDL-C was small when 151 "known" parameters were scanned, and 113 unknown parameters remained fixed. The results show that LDL-C varied ~2mg/dL (0.05mmol/L) for any value of the rate constant for hepatic LDLr degradation between a 2 fold increase and decrease from its default value (Figure 3.12A). In contrast, LDL-C varied by ~500mg/dL when the "known" parameters were fixed and the unknown parameters scanned. Consequently the relationship between hepatic LDLr degradation and LDL-C was lost (Figure 3.12B). When all 266 parameters were scanned (including the two parameters used for the counter reactions for DFC and DCE intake), the range of LDL-C values remained similar. A marginal further reduction in R^2 was also observed (Figure 3.12C). The significant difference in LDL-C variation when scanning parameters with well characterised kinetics versus parameters with assumed parameter values suggests the unknown parameters influence the behaviour of the model significantly. Moreover, the large range in LDL-C when unknown parameters were scanned, reinforces the finding from the local sensitivity scan, that parameters with assumed kinetics were most sensitive.
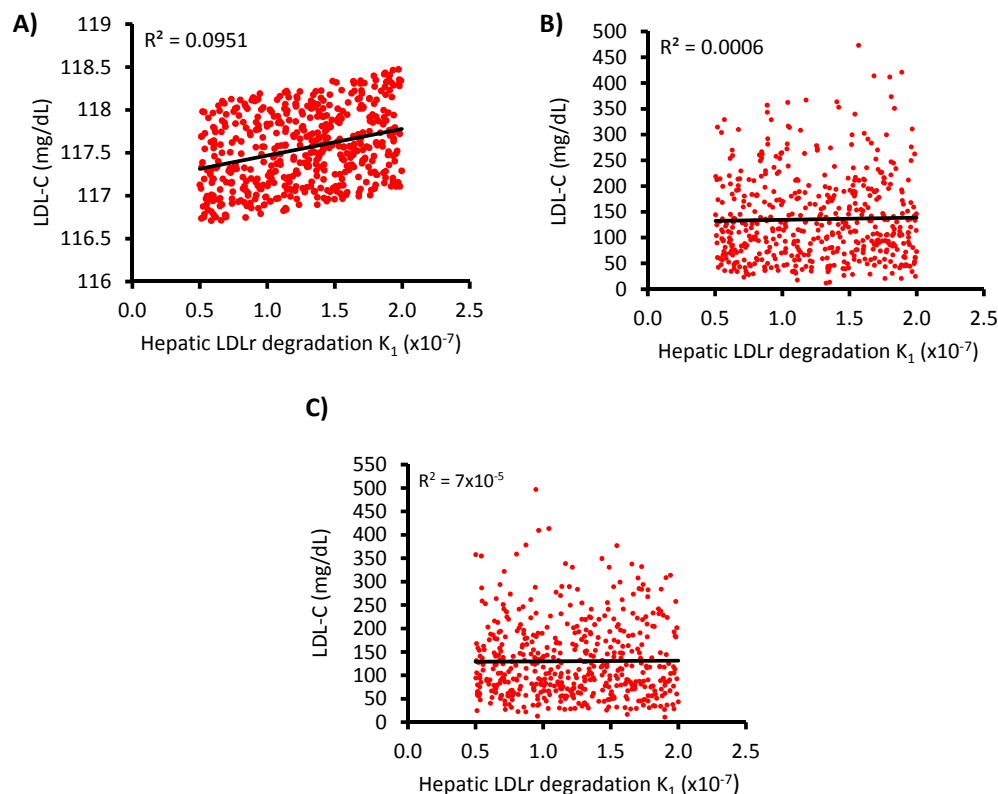
Figure 3.12 Sampling from the parameter space of a global sensitivity analysis of parameter K1, hepatic LDLr degradation.

Role of parameter K_1 for hepatic LDLr degradation (reaction 60) with A) all unknown, assumed, and adapted parameters fixed, B) all "known" parameters fixed, and C) all parameters scanned. Non-fixed parameters were analysed between a 2-fold increase and decrease of that parameter value; calculated at 250 hours, n=500. R^2 = Coefficient of determination.

3.3.8. Ageing

As outlined in Chapter 1, the ageing process affects many of the key mechanisms involved in cholesterol metabolism. Specifically, there is 1) an age-related decline in hepatic LDLr and subsequent reduction in LDL-C clearance (Millar et al., 1995), 2) an increase in cholesterol absorption (Duan et al., 2006), 3) a decline of BSH-positive intestinal microflora, such as *Lactobacillus* and *Bifidobacterium* species (Hopkins and Macfarlane, 2002), and 4) a decline in bile acid synthesis (Bertolotti et al., 2007). To represent the ageing process, four parameters were modified. These modifications were a 2-fold decrease to the rate of NPC1L1 degradation, bacterial deconjugation, and CYP7AI activity. In addition,

the rate of LDLr degradation was increased 2-fold (Table 3.6). The inverse of this analysis, was assumed to represent a young individual. The default age group was built based upon the Mc Auley et al. (2012) model, which represented a healthy 20 year old male. The young and old age groups were arbitrarily defined and thus were not given a numerical definition.

Table 3.6 Summary of parameters involved in the ageing analysis.

Reaction		Parameter	Age group		
			Young	Default	Old
45	Bile acid Deconjugation	V_{max}	1×10^{-5}	5×10^{-6}	2.5×10^{-6}
54	NPC1L1 degradation	K_1	2×10^{-7}	1×10^{-7}	5×10^{-8}
60	LDLr degradation	K_1	5×10^{-8}	1×10^{-7}	2×10^{-7}
132	CYP7AI activity	V_{max}	1.11358×10^{-3}	5.5679×10^{-4}	2.78395×10^{-4}

By simultaneously conducting a 2-fold decrease to the parameters K_{cetp1} and K_{cept2}, a CETP I405V genotype could also be replicated (reactions 40 and 39 respectively, Table A.2). A 2-fold increase in K_{cept1} and K_{cept2} was also conducted to replicate a genotype reflective of a genetic predisposition for atherogenesis. These CETP genotypes were applied to each age category and LDL-C was recorded after 1000 hours, in line with the cholesterol and saturated fat feeding simulations (Figure 3.13). Ageing resulted in an increased LDL-C for all CETP genotypes. The ageing process, in the presence of the genotype representing high CETP activity, resulted in a 1.6% increase in LDL-C. Similarly, the normal CETP genotype also produced a 1.6% increase in LDL-C when comparing results from the young and aged categories. The CETP 1405V genotype however resulted in a less significant rise (0.6%) in LDL-C with the ageing process. By contrasting the genotypes within each age category, the beneficial effects of the CETP I405V genotype were further substantiated. This advantageous genotype was more obvious in the aged category than the youth and normal categories. A 1.63% reduction in LDL-C was observed in the aged category, compared to a 0.64% reduction in both the normal and youth category.

Simulation of a genetic predisposition to atherosclerosis, resulted in a 0.617, 0.617 and 0.616% rise in LDL-C for the youth, normal and aged categories respectively.
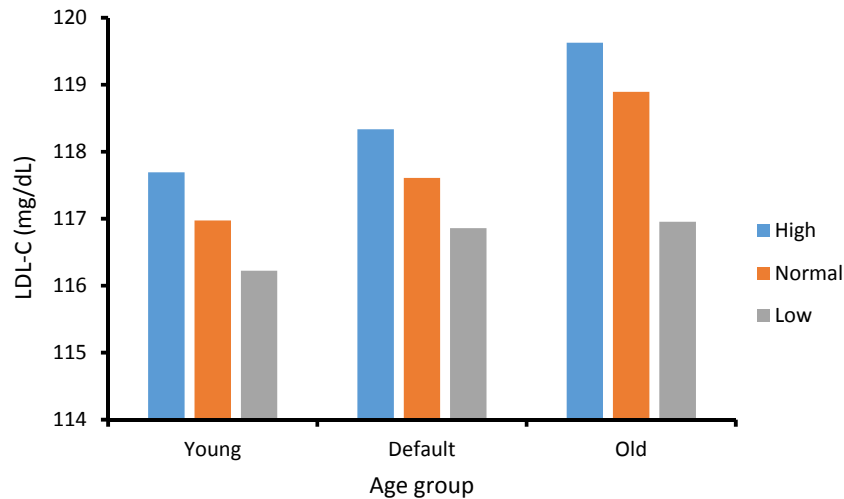
Figure 3.13 Role of CETP genotypes on LDL-C with ageing.
To mimic an aged individual, a 2 fold increase in LDLr degradation, and a 2 fold decrease in NPC1L1 degradation, bile acid deconjugation, and CYP7AI activity was applied. For the youth analysis, the inverse of this protocol was conducted. A 2 fold increase or decrease in CETP activity was then applied to each group. High (blue), normal (orange), and low (grey), CEPT activities. LDL-C measured at 1000 hours.

3.4. Discussion

An updated whole-body mathematical model of cholesterol metabolism was created, which included 96 additional mechanisms. This was deposited in the BioModels database (MODEL1508170000). In contrast to the Mc Auley et al. model, this model is significantly less sensitive to cholesterol feeding, and can be categorised as a hypo- rather than hyper-responder to cholesterol ingestion. This finding is perhaps unsurprising in light of experimental evidence which suggests 62.5% of healthy normocholesterolaemic males exhibit a hypo-response to dietary cholesterol (Herron et al., 2003). Moreover, it is widely regarded that cholesterol metabolism adapts to cholesterol feeding by invoking

two major compensatory regulatory mechanisms; these are an increase in cholesterol excretion, and a decrease in whole-body cholesterol biosynthesis (Quintao et al., 1971). When there is effective feedback control mechanisms this can result in dietary cholesterol failing to illicit a response in lipoprotein metabolism. For instance, McNamara et al. (1987) demonstrated using 12 week studies that both low and high levels of dietary cholesterol did not induce significant increases in mean levels of plasma total, LDL, or HDL cholesterol. Moreover, there was no relationship between baseline plasma cholesterol levels and sensitivity to a dietary cholesterol challenge (McNamara et al., 1987).

In the model, LDL-C did not rise, however both hepatic free cholesterol and intestinal cholesterol increased significantly during high cholesterol feeding. In the seminal work by Quintao et al. (1971) it is postulated that cholesterol feeding in humans is primarily controlled by one compensatory mechanism – an increase in cholesterol excretion, but not bile acid excretion (data not shown); the model helps to substantiate this claim. Intriguingly, the authors also suggest that when there is an accumulation of cholesterol in the body pools, the effects on lipoprotein levels are insignificant, regardless of the quantity of cholesterol absorbed. This appears to be the case in humans, as regulatory processes inhibit an increase in lipoprotein cholesterol when body pools accumulate. Model organisms have also shown that body pools of cholesterol can increase significantly as a result of cholesterol feeding. Ohtani et al. (1990) suggest that, in hamsters, an additional 0.1% dietary cholesterol is enough to induce the accumulation of cholesterol in the liver through the chylomicron remnant pathway (Ohtani et al., 1990). Wang et al. (2010) also reported that concentrations of the hepatic TC increased ~4-fold by with a 1% increase in dietary cholesterol in rats (Wang et al., 2010).

Although it has been reported experimentally that cholesterol can accumulate within the liver and peripheral tissues, this behaviour in the model could also suggest that the regulatory mechanisms may not be sufficiently adequate to deal with the excess cholesterol. One mechanism in this model that may need to be improved is the turnover of LDLr. In the updated model, an increase in dietary cholesterol, did not elicit a decrease in LDLr number. This contrasted with the previous model. This is

an important point that needs to be emphasised. Hennessey et al. (1992) have demonstrated that a high intake of dietary cholesterol suppresses hepatic LDLr mRNA by 29% in cebus monkeys (Hennessy et al., 1992). Conversely, Spady and Cuthbert (1992) observed that rats fed on high levels of dietary cholesterol, did not exhibit suppressed hepatic LDLr activity despite a 350-fold increase in hepatic cholesterol ester levels (Spady and Cuthbert, 1992). More recently, Boone et al. (2011) found that LDLr expression in Sprague-Dawley rats was not altered by dietary cholesterol. There was also a significant increase in mean hepatic cholesterol and paradoxically a decrease in serum cholesterol (Boone et al., 2011). However, studies in humans, such as Lichtenstein et al. (1993), demonstrate that the addition of dietary cholesterol (~1.5 eggs per/day) to a corn oil-diet, can result in a significant increase in concentrations of TC (6%), LDL-C (8%), and HDL-C (7%), when compared to diets with low dietary cholesterol, in 14 middle-aged and older individuals (Lichtenstein et al., 1993). Despite the lack of sensitivity of lipoprotein metabolism to cholesterol feeding, the model was sensitive to increases in dietary SFA. This finding is in line with the experimental literature as dietary SFA has been shown clinically to have a more profound effect on cholesterol metabolism than dietary cholesterol (He and Fernandez, 1998; Herron et al., 2003).

Large inter-individual differences in cholesterol metabolism, can in part be explained by genetic factors. For example, the I405V genotype is associated with longevity and reduced levels of CETP. This results in larger LDL-C and HDL-C particle size, in addition to reduced levels of LDL-C and increased HDL-C. This genotype is related to lower prevalence of hypertension, CVD, T2DM and metabolic syndrome (Atzmon et al., 2005; Barzilai et al., 2003). The role of the I405V CETP genotype, in reducing the risk of age-associated disease, was consolidated with the simulations. It was demonstrated that increased CETP activity resulted in raised LDL-C in all age groups. Conversely, decreased CETP activity, led to a lower LDL-C in all age categories. Furthermore, the age-related increase in LDL-C was reduced with the presence of the I405V genotype (0.6% vs. 1.6%). Although it is important to note that a reduction in CETP levels and subsequent increase in HDL-C, either due to a genetic polymorphism or pharmaceutical intervention, has been associated with an increase in mortality rate (Barter et al.,

2007; Zhong et al., 1996). It is therefore important that the findings from this work, and other studies, are fully evaluated before *in vivo* application.

An important finding from the updated model was that the parameter values associated with the less well characterised aspects of cholesterol metabolism, such as lipoprotein dynamics and RCT, were particularly sensitive to changes in their values. This is supported by the findings of August et al. (2007), who demonstrated that plasma levels of cholesterol could vary widely, in their dynamical model of lipoprotein metabolism (August et al., 2007). Another key finding from our work was that the cholesterol biosynthesis pathway, which has been well characterised, was particularly robust to parameter variation. Similarly, Pool et al. (2018), who created a kinetic model of the mevalonate pathway using ODEs, found that the feedback loops of cholesterol biosynthesis tightly regulated cellular cholesterol levels (Pool et al., 2018). These findings from our local SA were supported by sampling the parameter space of a global sensitive analysis, which demonstrated the increase in variation in LDL-C when unknown parameters were scanned, when compared with known parameters. Therefore, it is important to also consider the fact that the functional forms used to represent the interactions in this model may need further improvements, and that interactions may be due to many components of the model, such as RCT, lipoprotein dynamics and the enterohepatic circulation of bile acids, being poorly understood from a kinetic perspective.

There are a number of aspects of the model that could be developed in the future. For example, when conjugated and unconjugated bile acid levels are in a steady state, the V_{max} value for the deconjugation of bile acids was significantly lower than that reported in the experimental literature (reaction 45 Table A.2). For example, for the intestinal bacteria *Clostridium perfringens*, *Bacteriodes fragilis* and *Lactobacilli*, BSH has suggested V_{max} values of 0.05, 38.4 and 25.4mg/min/mg (Gopal-Srivastava and Hylemon, 1988; Lundeen and Savage, 1992; Stellwag and Hylemon, 1976). However, a far lower V_{max} value of 5 x 10^{-6} was used in the model. Areas such as cholesterol and bile acid synthesis could also be further developed to incorporate less well understood mechanisms that have not be

included in the model. Furthermore, this model could be combined with other pre-existing models, or further developed to include other compartments such as the gallbladder, or other interconnected metabolic pathways such as fatty acid or carbohydrate metabolism, or cortisol homeostasis. For example, cortisol is synthesised from cholesterol and is involved in provoking the breakdown of lipids, and a wide variety of other metabolites. Therefore this model could be connected to a previously developed computational model of whole body cortisol metabolism (Mc Auley et al., 2009; Mc Auley et al., 2013).

3.5. Conclusion

In combination with the previous model, the updated model presented here emphasises the important role of intrinsic ageing in disrupting whole-body cholesterol metabolism. Constructing this model has revealed a number of findings. Firstly, simulations indicated that the model is a hypo-responder to cholesterol feeding, but is sensitive to simulated SFA feeding. Secondly, the model tentatively supports that genotypes such as I405V has a protective role in healthy ageing. The model also highlights the robustness of the cholesterol biosynthesis pathway, and suggests key areas where experimental work needs to focus in the future. This study has highlighted the need for kinetic data in several key areas of cholesterol metabolism, including RCT, lipoprotein dynamics and the enterohepatic circulation of bile acids. As these areas could provide potential therapeutic targets for lowering cholesterol, it is believed that a more in depth understanding of this process could lead to novel interventions in the future. Finally, this work has demonstrated the important role computational systems biology has to play in improving our understanding of lipid metabolism and health-span.

Chapter 4 Detecting the methylation status of synthetic DNA using electrochemistry

4.1 Introduction

DNA methylation is an important epigenetic mechanism required to control gene expression (Lim and Maher, 2010). DNA methylation is regulated by DNA methyltransferases DNMT1, DNMT3a and DNMT3b (Goyal et al., 2006; Okano et al., 1999); concomitantly, demethylation is regulated by a family of TET enzymes and TDG (Rasmussen and Helin, 2016). Ageing and diseases, including cancer, are often accompanied by aberrant expression of these regulatory enzymes and consequently results in genome-wide hypomethylation, and promoter-specific hypermethylation (Kulis and Esteller, 2010; Maegawa et al., 2017; Valentini et al., 2016). Promoter-specific hypermethylation often results in gene silencing, and potentially disease pathogenesis (Mendizabal and Yi, 2016). Hypermethylation of the EN1 gene promoter has been detected in various forms of cancer, thus EN1 promoter methylation has been identified as a possible biomarker (Devaney et al., 2011; Mayor et al., 2009). Several techniques have been utilised for the analysis of DNA methylation, including bisulphite sequencing (Li and Tollefsbol, 2011), and methylation specific PCR (Herman et al., 1996). However, these techniques often require expensive laboratory equipment and reagents, long analysis times, and staff require extensive training. Recently there has been heightened interest in using electrochemical techniques to detect DNA methylation as it can be a rapid and cost effective solution to many of the challenges posed by previous methods (Koo et al., 2014; Sina et al., 2014).

Electrochemical analysis relies on the principle that single stranded homo-oligonucleotides adsorb onto gold with the following affinity A > C ≥ G > T (Kimura-Suda et al., 2003). As methylated samples contain a greater proportion of guanine after bisulphite treatment and asymmetric PCR, and unmethylated samples contain a greater proportion of adenine, unmethylated samples more readily passivate the gold working electrode due to the higher affinity of adenine for gold (Figure 4.1). This can be observed as increased resistance when a current is applied to the redox cell. Based on the work of Koo et al. (2014), 30 base synthetic oligonucleotides, containing six CpG sites, designed to represent bisulphite modified and asymmetrically amplified methylated and unmethylated versions of a region

downstream of the transcription site of the EN1 gene promoter, will be used to explore the electrochemical detection of DNA methylation. In contrast to the static gold screen printed electrodes (Au-SPE) utilised by Koo et al. (2014), the aim of this chapter will be to use a gold rotating disk electrode (Au-RDE) to determine if rotation enhances DNA adsorption. Additionally, DNA methylation will be detected using EIS, and CV (at 200 and 50mV/s, CV200 and CV50), in addition to DPV as employed by Koo et al. (2014).
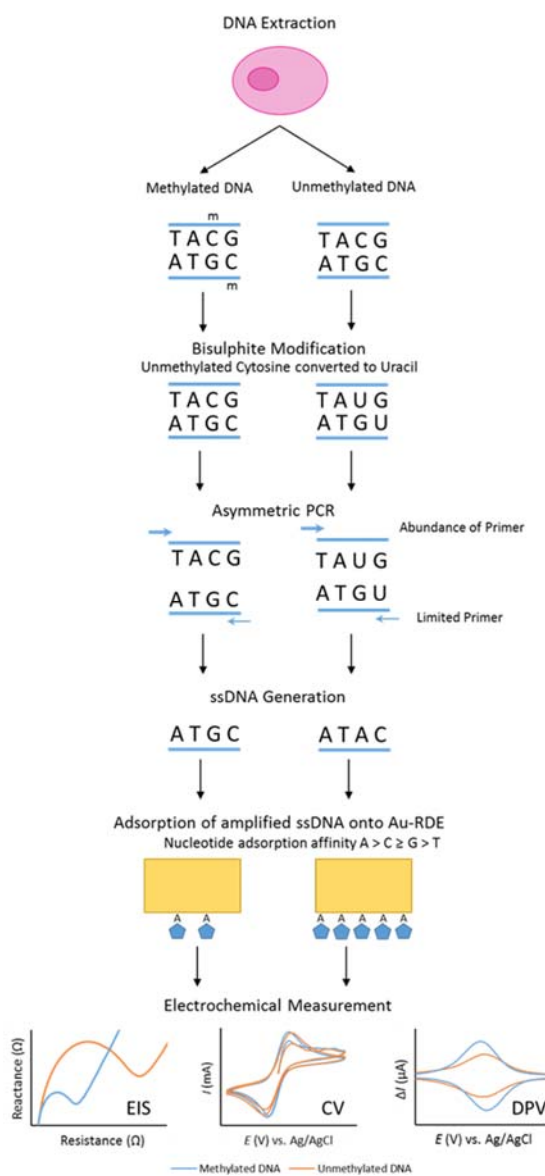
Figure 4.1 Overview of bisulphite treatment, asymmetric PCR and electrochemical measurement.

Using this adapted method, adsorption time, rotation speed, and DNA concentration, will be optimised before the technique is used to detect % methylation in a heterogeneous sample. It is important to determine if % methylation can be established from heterogeneous samples as often biopsy samples from cancerous tumours contain cells with differing levels of methylation, in a phenomenon termed tumour heterogeneity (Litovkin et al., 2015).

4.2 Methods

4.2.1 Preparation of synthetic oligonucleotides

Synthetic oligonucleotides, 30 bases in length, containing six CpG sites, were purchased from Eurofins Genomics, and were used to optimise the electrochemical procedure (Table 4.1), before the sensor was applied to cancer cell DNA (Chapter 5). The single stranded synthetic oligonucleotides were used to represent a bisulphite treated and asymmetrically amplified region, downstream of the transcription start site, of the EN1 gene promoter. Sequences were diluted to 100pmol/µl (100µM) by adding the appropriate volume of 1X PBS solution (amresco, E404-200TABS), as recommended by the manufacturer, and further diluted in PBS to create a 50ml solution of 50nM DNA for the optimisation of adsorption time and rotation speed. Concentrations ranging from 0-400nM were created to study the effect of concentration. Following the optimisation of oligonucleotide concentration, 200nM synthetic oligonucleotide solutions were utilised for % methylation tests. Solutions were stored at 4°C for up to 1 month, and were tested at room temperature.

Table 4.1 Sequences of synthetic methylated and unmethylated oligonucleotides (30 bases).
 CpG sites are underlined

Oligonucleotide	5'-Sequence-3'
Methylated sequence	GATAACGACGACAATAAAAACGACGCGAAA
Unmethylated sequence	AATAACAACAACAATAAAAACAACACAAAA

4.2.2 Optimisation outline

Three variables of the procedure were optimised; 1) adsorption time (0, 1, 2, 5, 10, 15, 20, 25, and 30 minutes), 2) rotation speed (0, 1000, 2000, and 4000rpm) and 3) DNA concentration (0, 1, 10, 25, 50, 100, 200, and 400nM), n=3. Following optimisation, percentage methylation was investigated. For this, 200nM methylated and 200nM unmethylated synthetic oligonucleotides were combined in varying proportions to represent the differing level of methylation (0, 25, 50, 75, and 100%). These tests were conducted by adsorbing DNA onto a polished 2mm Au-RDE and measuring the level of resistance in a three electrode electrochemical cell by EIS, CV at 200mV/s, CV at 50mV/s, and DPV as described in sections 4.2.4.1 and 4.2.4.2 and 4.2.4.3, at room temperature (Figure 4.2).
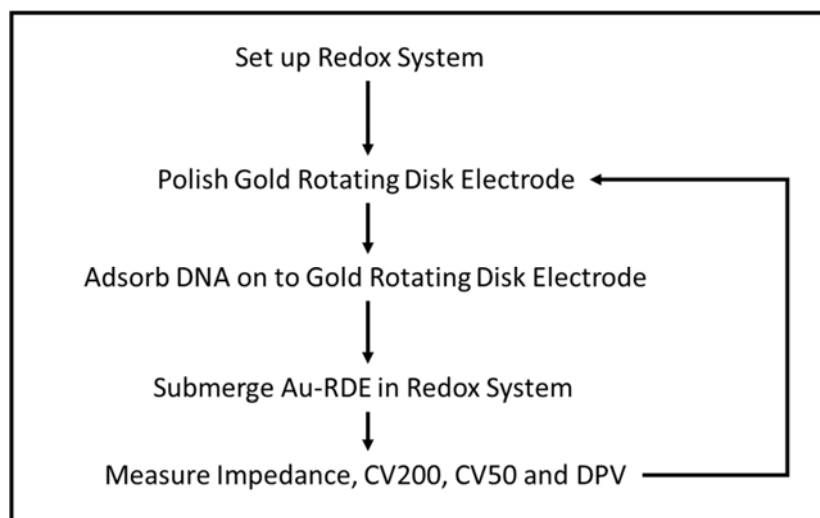
Figure 4.2 Overview of electrochemical analysis procedure.

4.2.3 Redox system

The redox system comprised of a 3-electrode cell in ~70ml of 2.5mM Fe^{2+}/2.5mM Fe^{3+} redox solution in a 100ml glass beaker along with a stir bar, located on a plastic topped stirring platform (HANNA Instruments, HI-190M). The redox solution was created by combining 0.264g potassium hexacyanoferrate (II) trihydrate (AnalaR NORMAPUR, 26816.298) and 0.206g potassium hexacyanoferrate (III) (AnalaR NORMPUR, 26810.232) with 250ml 1X PBS solution (137mM sodium chloride, 2mM potassium chloride, 10mM phosphate buffer, pH 7.4), and was stored at room

temperature in the dark for up to 1 week. 1X PBS solution was made using ultrapure water (ELGA, Purelab Ultra). Electrodes were then processed and attached to the potentiostat (Princeton applied research, BiStat) as described in sections 4.2.3.1, 4.2.3.2 and 4.2.3.3 (Figure 4.3). The redox solution was stirred for 10 seconds before each measurement, and was halted for each test due to noise interference. The solution did not continuously stir for more than 10 seconds to restrict the oxidation of Fe^{2+}.

4.2.3.1 Reference electrode

Stored in a saturated KCl solution, the silver/silver chloride reference electrode (ALS, RE1CP) was washed in ultrapure water before it was fixed into position within the redox cell and attached to the potentiostat (white).

4.2.3.2 Counter electrode

The 0.127mm diameter coiled platinum counter electrode (Alfa Aesar, 00263) was rinsed in ultrapure water before flaming to clean. The counter electrode was then fixed in position opposite the Ag/AgCl reference electrode in the redox cell and attached to the potentiostat (blue).

4.2.3.3 Working electrode

A 2mm Au-RDE was selected as the working electrode (Radiometer analytical, BM-EDI101); the diameter was obtained using optical microscope Leica M125 with the software package LAS V4.5. Before adsorbing DNA onto the electrode, the electrode required polishing. Firstly the electrode was rinsed in ultrapure water before the three step polishing process could take place. Briefly this process consisted of 1) polishing with 6µm diamond spray (Kemet, 116005) on silk (Kemet, 341752); 2) polishing with 3µm diamond spray (Kemet, 116004) on silk; and 3) polishing with a saturated 1µm alumina solution (Kemet, 600253) on felt (Kemet, 341208). For each polishing step the electrode was

placed onto the silk/felt firmly and polished by making figures of eight for 30 seconds (Elgrishi et al., 2018). The electrode was rinsed in ultrapure water between each polishing step. Following the completion of this three step process, the electrode was then sonicated for 30 seconds in ultrapure water to remove any remaining polish (Ultrasonic Cleaner, Branson 200). After drying, the 2mm Au-RDE was placed in 50ml of the relevant synthetic oligonucleotide at room temperature. The electrode was then rotated at a suitable speed (Radiometer analytical, CTV101 speed control unit) for an appropriate time. Following adsorption, the electrode was dried and fixed in close proximately to the reference electrode, and attached to the potentiostat (red). The potentiostat was also attached to the clamp stand as a ground (black).
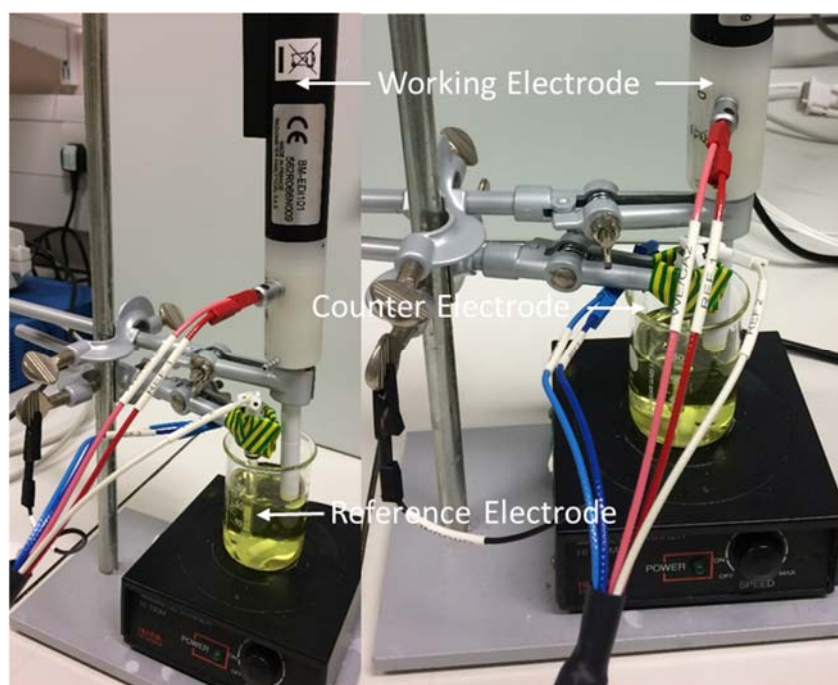
Figure 4.3 Image of redox cell set up.

4.2.4 Electrochemical measurements

For each sample (n=3), four measurements were taken using EC lab V11.10, in the following order; EIS, CV at 200mV/s, CV at 50mV/s and DVP.

4.2.4.1 EIS

Impedance was measured at open circuit potential, and scanning frequency between 200 kHz to 100mHz, with 10 points per decade and a voltage amplitude of 20mV.

4.2.4.2 CV at 200mV/s and 50mV/s

CV was performed at open circuit potential with either a scan speed 200 or 50 mV/s up to a vertex potential of 0.8V and back down to -0.15V vs. Ag/AgCl with a potential step of 1mV.

4.2.4.3 DPV

DPV was performed by scanning the potential between -0.2 and 0.7V vs. Ag/AgCl with a potential step of 5mV, a pulse amplitude of 50mV, a pulse width of 50ms, and a pulse period of 100ms (Sina et al., 2014).

4.2.5 Data extraction

4.2.5.1 EIS

A Z-fit analysis was conducted within EC-Lab V11.10, using the equivalent circuit selection R1+Q2/(R2+W2) to gain parameter values for R2. R2 was subsequently referred to as R_{ct}.

4.2.5.2 CV at 200mV/s and 50mV/s

Peak to peak separation, ΔE_p (mV), was determined for CVs at scan speeds of 200mV/s and 50mV/s.

4.2.5.3 DPV

The uppermost point of the plot was selected, and the ΔI value was recorded as peak anodic current, i_{pa} (μA).

4.2.6 Data analysis

Results were denoted as mean ± 1 standard deviation. RSD, also known as the coefficient of variance, was also reported. RDE denotes the standard deviation relative to the mean, and was calculated by equation 32:

$$RSD = \frac{SD}{\bar{x}} \text{ X } 100 \tag{32}$$

4.2.7 Statistical analysis

To perform multiple comparison statistical testing, all analyses were performed using a one-way ANOVA with a Tukey Post Hoc test on SPSS Version 23.

4.3 Results

4.3.1 DNA adsorption time

4.3.1.1 Effect of DNA adsorption time on impedance

The first variable to be optimised was DNA adsorption time. For this, DNA was adsorbed onto the 2mm Au-RDE for 1, 2, 5, 10, 15, 20, 25 and 30 minutes, and compared to 0 minutes. Nyquist plots revealed that generally, as adsorption time increased the radius of the arc increased, suggesting an increase in R_{ct}. The radius of the arc appeared to be greater for unmethylated DNA samples than methylated samples of equivalent concentration (Figure 4.4A and B), and were significantly reduced for 1X PBS samples (Figure 4.4C and D). Analysis of these Nyquist plots using Z-fit analysis in EC lab V11.10 revealed that R_{ct} generally increased with time for 50nM methylated and unmethylated DNA, in addition to 1X PBS (Table 4.2 and Figure 4.5). For example, at 0 minutes, R_{ct} was 76.41 ±2.59Ω; after 1 minute R_{ct} increased to 263.17 ±12.79Ω and 323.3 ±10.67Ω for 50nM methylated and unmethylated DNA respectively, while after 30 minutes an R_{ct} of 1039.03 ±62.48Ω and 1233.33 ±67.25Ω was observed for 50nM methylated and unmethylated DNA respectively. A DNA adsorption time of 1 minute was sufficient to bring about a statistically significant increase in R_{ct}, when compared to 0 minutes ($p<0.05$). However, it was not until 30 minutes that R_{ct} values showed a statistically significant difference between 50nM methylated and unmethylated samples ($p<0.05$), as shown in Table A.5.
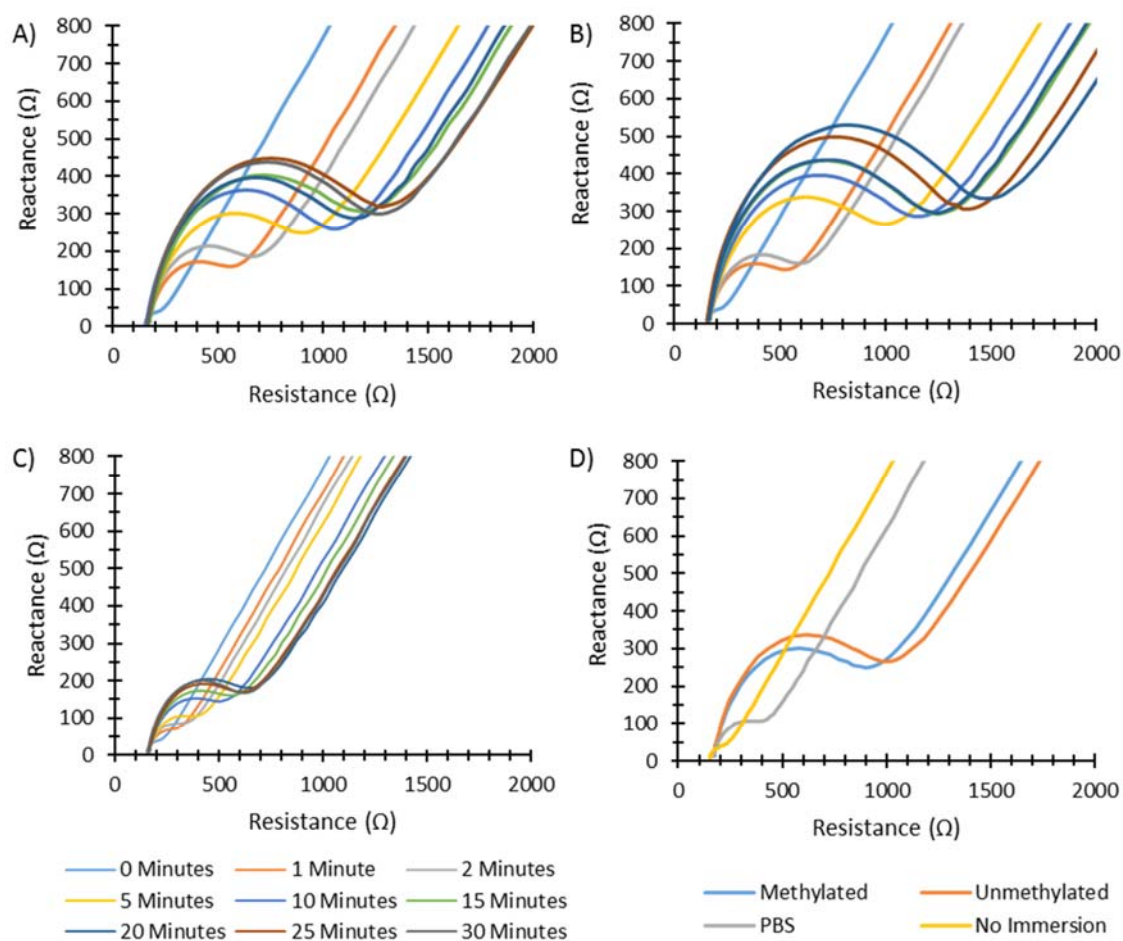
Figure 4.4 Effect of DNA adsorption time on Nyquist plots.
Nyquist plots for a 2mm Au-RDE in 2.5mM ferrocyanide/2.5mM ferricyanide/1X PBS after rotation assisted adsorption at 2000rpm for a range of times in A) 50nM methylated DNA, B) 50nM unmethylated DNA, C) 1X PBS. Plot D) compares the 5 minute adsorption Nyquist plots from A), B) and C) against no immersion. Mean shown (n=3, PBS n=1).

Table 4.2 Effect of DNA adsorption time on R$_{ct}$.

R$_{ct}$ (determined from Z-fit analysis of Nyquist plots) for a 2mm Au-RDE in 2.5mM ferrocyanide/2.5mM ferricyanide/1X PBS after rotation assisted adsorption at 2000rpm for a range of times in 50nM methylated and unmethylated DNA, and 1X PBS. Mean ±SD (n=3, PBS n = 1). *Statistical difference between values for methylated and unmethylated DNA, when tested for using a one-way ANOVA ($p<0.05$).

Time (Mins)	R$_{ct}$ (Ω)									PBS
	No Immersion			Methylated			Unmethylated			
	Mean	SD	RSD (%)	Mean	SD	RSD (%)	Mean	SD	RSD (%)	
0	76.41	2.59	3.39							
1				263.17	12.79	4.86	323.30	10.67	3.30	140.70
2				335.97	24.06	7.16	395.10	17.29	4.38	178.90
5				707.57	10.62	1.50	795.23	11.62	1.46	228.00
10				844.97	18.15	2.15	937.53	10.25	1.09	343.90
15				967.27	82.51	8.53	1019.87	57.02	5.59	391.40
20				927.57	31.41	3.39	1014.27	65.37	6.45	466.00
25				1062.33	37.00	3.48	1145.33	25.15	2.20	436.30
30				1039.03*	62.48	6.01	1233.33*	67.25	5.45	443.60

Figure 4.5 Effect of DNA adsorption time on R$_{ct}$.

R$_{ct}$ (determined from Z-fit analysis of Nyquist plots) for 2mm Au-RDE in 2.5mM ferrocyanide/2.5mM ferricyanide/1X PBS after rotation assisted adsorption at 2000rpm for a range of times in 50nM methylated DNA, 50nM unmethylated DNA and 1X PBS. Mean ±SD (n=3, PBS n=1). *Statistical difference between values for methylated and unmethylated DNA, when tested for using a one-way ANOVA ($p<0.05$).

4.3.1.2 Effect of DNA adsorption time on cyclic voltammetry

Table 4.3 Effect of DNA adsorption time on peak to peak separation.
ΔE_p (mV) for CVs conducted for 2mm Au-RDE in 2.5mM ferrocyanide/2.5mM ferricyanide/1X PBS after rotation assisted adsorption at 2000rpm for a range of times in 50nM methylated DNA, 50nM unmethylated DNA and 1X PBS, at scan speeds of 200 and 50mV/s. Mean ±SD (n=3, PBS n=1). *Statistical difference between values for methylated and unmethylated DNA, when tested for using a one-way ANOVA ($p<0.05$).

| Time (Mins) | ΔE_p (mV) | | | | | | | | | |
| | No immersion | | | Methylated | | | Unmethylated | | | PBS |
	Mean	SD	RSD (%)	Mean	SD	RSD (%)	Mean	SD	RSD (%)	
CV200										
0	87.9	0.5	0.57							
1				100.3	2.6	2.61	101.3	0.60	0.55	94.6
2				110.7	1.7	1.51	110.8	1.60	1.48	94.9
5				126.0*	2.3	1.83	135.2*	2.10	1.57	99.7
10				143.8	2.8	1.97	143.6	2.00	1.38	104.9
15				140.9*	1.7	1.18	155.8*	3.70	2.36	108.8
20				145.8*	5.0	3.44	157.9*	0.80	0.49	112.5
25				155.6*	2.9	1.86	168.4*	2.20	1.29	111.2
30				148.8*	1.7	1.15	167.9*	1.70	1.04	111.6
CV50										
0	78.5	1.7	2.17							
1				85.0	1.7	1.95	89.0	1.1	1.25	82.3
2				90.5	2.5	2.75	93.7	1.0	1.02	82.5
5				104.1	4.3	4.14	109.8	1.4	1.31	81.1
10				117.5	3.8	3.24	118.1	3.9	3.31	85.4
15				115.6*	1.9	1.67	129.8*	0.5	0.39	89.3
20				120.5*	0.6	0.48	133.3*	3.4	2.58	98.4
25				126.7*	1.0	0.80	142.2*	2.1	1.47	96.3
30				125.7*	2.1	1.65	141.4*	2.3	1.62	96.3

For both CV200 and CV50, ΔE_p increased with time for 50nM methylated DNA, unmethylated DNA, and 1X PBS (Table 4.3). For instance, using CV200 data, a ΔE_p of 87.9 ±0.5mV was observed at 0 minutes, whereas at 1 minute ΔE_p increased to 100.3 ±2.6mV and 101.3 ±0.60mV for 50nM methylated and unmethylated DNA respectively. ΔE_p further increased to 148.8 ±1.7mV and 167.9

±1.7mV at 30 minutes for 50nM methylated and unmethylated DNA respectively (Figure 4.6A). The effect of time on ΔE_p was less well defined when CV was conducted at a scan speed of 50mV/s. For instance, at 30 minutes, ΔE_p was 125.7 ±2.1mV and 141.4 ±2.3mV for 50nM methylated and unmethylated DNA respectively, compared to 78.5 ±1.7mV at 0 minutes (Figure 4.6B).

As outlined in Table A.5, a statistically significant difference was observed between the ΔE_p at a scan speed of 200mV/s for 50nM methylated and unmethylated DNA adsorbed onto the Au-RDE for 5, 15, 20, 25, and 30 minutes at a rotation speed of 2000rpm ($p<0.05$). The ΔE_p gained at a scan speed of 50mV/s showed significant differences between 50nM methylated and unmethylated DNA solutions adsorbed onto Au-RDE for 15-30 minutes ($p<0.05$).

Figure 4.6 Effect of DNA adsorption time on peak to peak separation.
ΔE_p (mV) for CVs conducted for 2mm Au-RDE in 2.5mM ferrocyanide/2.5mM ferricyanide/1X PBS after rotation assisted adsorption at 2000rpm for a range of times in 50nM methylated DNA, 50nM unmethylated DNA and 1X PBS, at scan speeds of A) 200mV/s and B) 50mV/s. Mean ±SD (n=3, PBS n=1). *Statistical difference between values for methylated and unmethylated DNA, when tested for using a one-way ANOVA ($p<0.05$).

4.3.1.3 Effect of DNA adsorption time on DPV

i_{pa} decreased as adsorption time increased (Table 4.4). Adsorption of 50nM unmethylated DNA produced a lower i_{pa} than the adsorption of its methylated counterpart, while the adsorption of 1X PBS onto the 2mm Au-RDE led to a substantially greater i_{pa}. Further to this, i_{pa} was greatest when no

immersion occurred (Figure 4.7A, B, C and D). To elucidate this point, at 0 minutes i_{pa} was 50.82±1.02µA, while adsorption of 50nM methylated and unmethylated DNA for 30 minutes produced a i_{pa} of 20.94±0.61µA and 17.72±0.32µA respectively; i_{pa} was 36.13µA when 1X PBS was adsorbed for 30 minutes (Figure 4.8). There was a statistically significant difference between the i_{pa} gained for 50nM methylated and unmethylated DNA adsorbed onto the 2mm Au-RDE for 5, 20 and 30 minutes (p<0.05) as described in Table A.5.
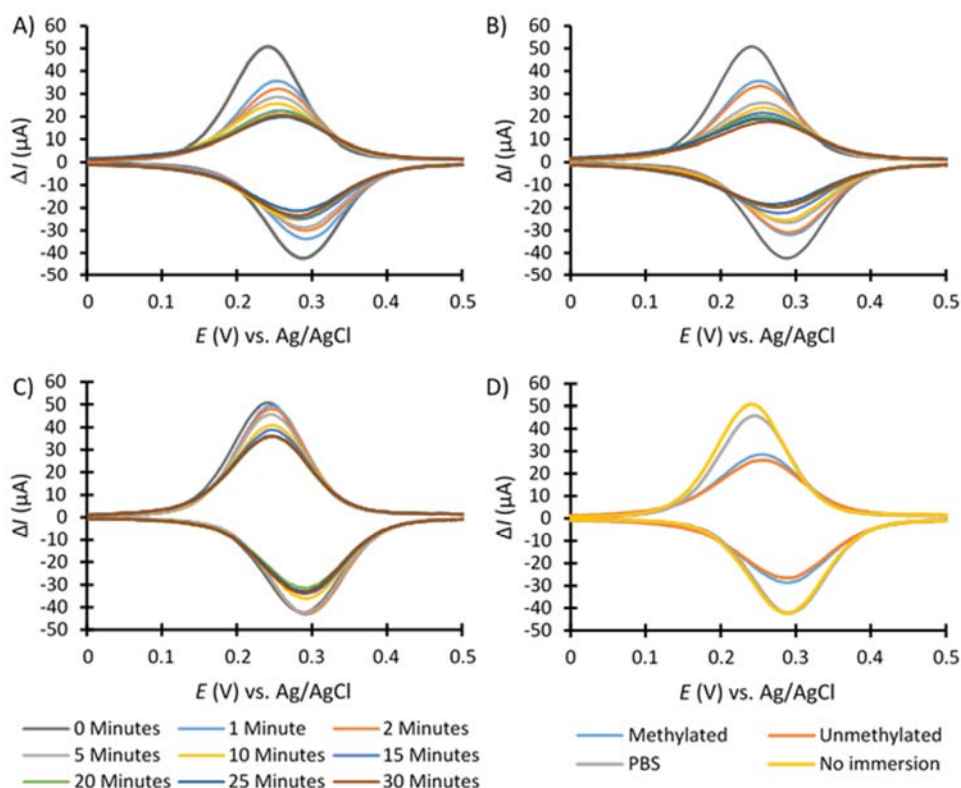
Figure 4.7 Effect of DNA adsorption time on DPV.
DPV signals for 2mm Au-RDE in 2.5mM ferrocyanide/2.5mM ferricyanide/1X PBS after rotation assisted adsorption at 2000rpm for a range of times in A) 50nM methylated DNA, B) 50nM unmethylated DNA and C) 1X PBS. Plot D) compares the 5 minute adsorption DPV signals from A), B) and C) against no immersion. Mean (n=3, PBS n=1).

An adsorption time of 5 minutes was selected to conduct further experimentation at, as it was the minimum time required for a statistical difference to be observed between 50nM methylated and unmethylated DNA samples (ΔE_p for CV200, and i_{pa}).

Table 4.4 Effect of DNA adsorption time on peak current.
i_{pa} (µA) obtained with 2mm Au-RDE in 2.5mM ferrocyanide/2.5mM ferricyanide/1X PBS after rotation assisted adsorption at 2000rpm for a range of times in 50nM methylated DNA, 50nM unmethylated DNA and 1X PBS. Mean ±SD (n=3, PBS n=1). *Statistical difference between values for methylated and unmethylated DNA, when tested for using a one-way ANOVA ($p<0.05$).

| Time (Mins) | i_{pa} (µA) | | | | | | | | | |
| | No immersion | | | Methylated | | | Unmethylated | | | PBS |
	Mean	SD	RSD (%)	Mean	SD	RSD (%)	Mean	SD	RSD (%)	
0	50.82	1.02	2.01							
1				35.66	0.42	1.17	35.67	0.44	1.23	49.55
2				32.18	0.71	2.22	33.40	0.38	1.13	48.15
5				28.65*	0.56	1.95	26.09*	0.34	1.30	45.94
10				25.66	0.42	1.65	23.81	0.12	0.50	40.91
15				22.67	1.01	4.45	21.65	0.29	1.33	38.99
20				22.33*	0.29	1.28	20.18*	1.23	6.09	36.17
25				19.87	0.51	2.56	18.98	0.34	1.78	36.01
30				20.64*	0.61	2.95	17.72*	0.32	1.82	36.13
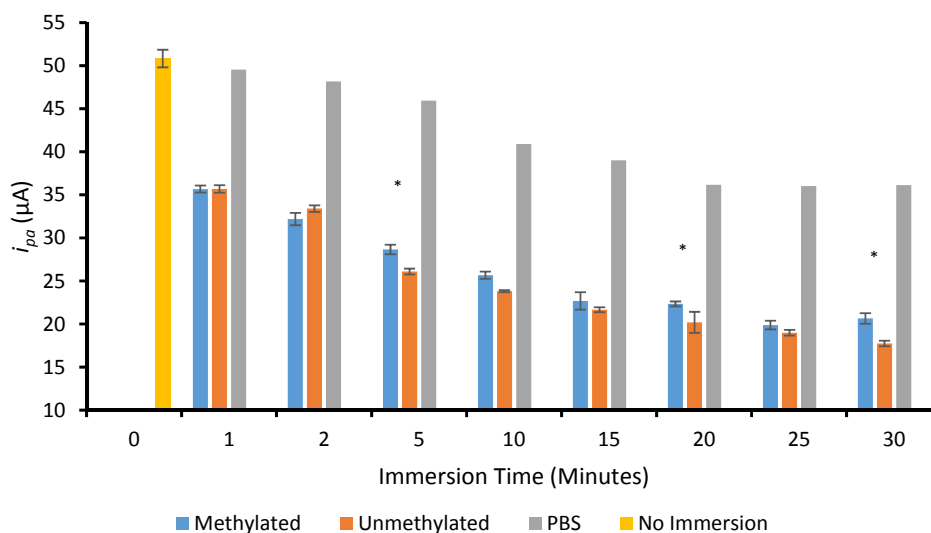
Figure 4.8 Effect of DNA adsorption time on peak anodic current.
i_{pa} (µA) obtained with 2mm Au-RDE in 2.5mM ferrocyanide/2.5mM ferricyanide/1X PBS after rotation assisted adsorption at 2000rpm for a range of times in 50nM methylated DNA, 50nM unmethylated DNA and 1X PBS. Mean ±SD (n=3, PBS n=1). *Statistical difference between values for methylated and unmethylated DNA, when tested for using a one-way ANOVA ($p<0.05$).

4.3.2 Rotation speed

4.3.2.1 Effect of rotation speed on impedance
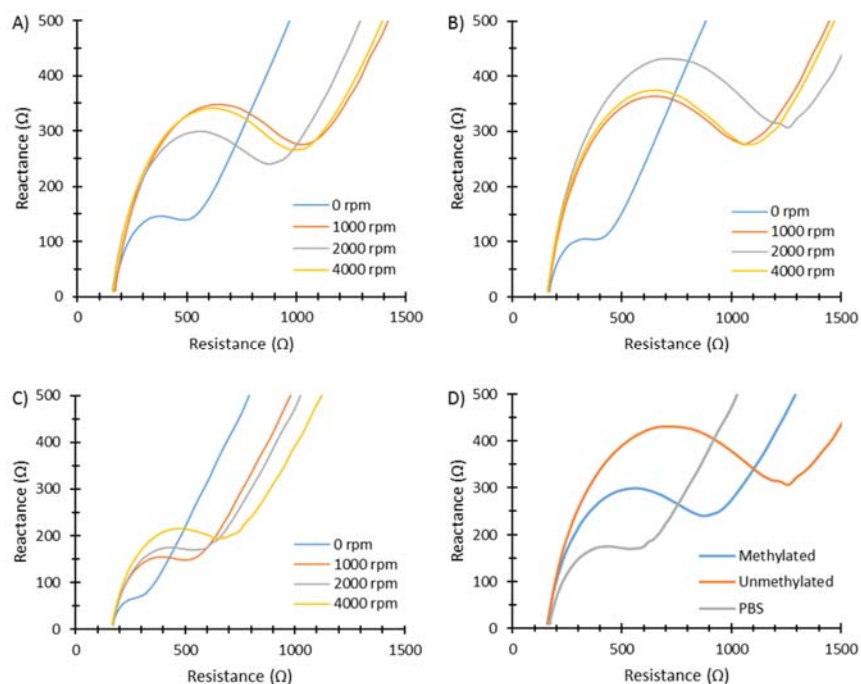
Figure 4.9 Effect of rotation speed on Nyquist plots.
Nyquist plots for a 2mm Au-RDE in 2.5mM ferrocyanide/2.5mM ferricyanide/1X PBS after rotation assisted adsorption at varying rotation speeds for 5 minutes in A) 50nM methylated DNA, B) 50nM unmethylated DNA, and C) 1X PBS. Plot D) compares adsorption at 2000rpm Nyquist plots from A), B) and C). Mean shown (n=3, 1X PBS n=1).

The second variable optimised was rotation speed, and again impedance was measured first. The Nyquist plots showed variation in results between samples. While, the radius of the arc was smallest for all samples, when the 2mm-RDE was not rotated, results for 1000, 2000 and 4000rpm for each sample differed. For example, for 1X PBS, the radius of the arc increased as rotation speed increased; for 50nM unmethylated DNA, a rotation speed 2000rpm gave the biggest arc radius, while at the same rotation speed, the second smallest arc was seen for 50nM methylated DNA (Figure 4.9A, B and C). However, this allowed for the greatest difference between samples to be observed (Figure 4.9D). Further to this, investigation of the Nyquist plots using Z-fit analysis revealed the greatest difference

in R_{ct} between 50nM methylated and unmethylated samples was seen at 2000rpm, with a difference of 321.43Ω between means (Table 4.5 and Figure 4.10). Moreover, the R_{ct} for 50nM methylated and unmethylated DNA samples were exclusively statistically distinguishable at a rotation speed of 2000rpm ($p<0.05$).

Table 4.5 Effect of rotation speed on R_{ct}.
R_{ct} (determined from Z-fit analysis of Nyquist plots) for 2mm Au-RDE in 2.5mM ferrocyanide/2.5mM ferricyanide/1X PBS after rotation assisted adsorption at varying rotation speeds for 5 minutes in 50nM methylated DNA, 50nM unmethylated DNA, and 1X PBS. Mean ±SD (n=3, PBS n=1). *Statistical difference between values for methylated and unmethylated DNA, when tested for using a one-way ANOVA ($p<0.05$).

Rotation Speed (rpm)	R_{ct} (Ω)						PBS
	Methylated			Unmethylated			
	Mean	SD	RSD (%)	Mean	SD	RSD (%)	
0	326.83	4.87	1.49	231.87	14.95	6.45	140.60
1000	817.67	24.93	3.05	846.87	43.67	5.16	345.00
2000	684.00*	53.21	7.78	1005.43*	32.35	3.22	396.90
4000	792.37	6.29	0.79	868.93	49.16	5.66	502.60
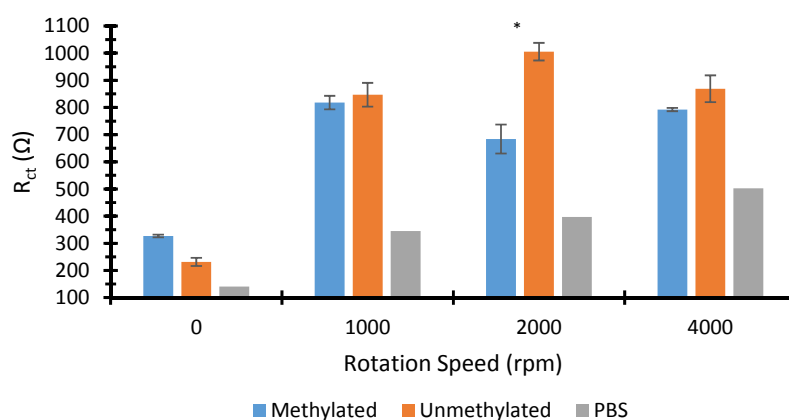
Figure 4.10 Effect of rotation speed on R_{ct}.
R_{ct} (determined from Z-fit analysis of Nyquist plots) for 2mm Au-RDE in 2.5mM ferrocyanide/2.5mM ferricyanide/1X PBS after rotation assisted adsorption at varying rotation speeds for 5 minutes in 50nM methylated DNA, 50nM unmethylated DNA and 1X PBS. Mean ±SD (n=3, PBS n=1). *Statistical difference between values for methylated and unmethylated DNA, when tested for using a one-way ANOVA ($p<0.05$).

4.3.2.2 Effect of rotation speed on cyclic voltammetry

A general increase in ΔE_p was observed as rotation speed increased, for both CV200 and CV50. As with the results from the analysis of R_{ct}, a statistically significant difference was only observed for ΔE_p at 2000rpm when 50nM methylated and unmethylated DNA solutions were adsorbed onto the 2mm Au-RDE for 5 minutes ($p<0.05$). This was true for the ΔE_p calculated from CVs performed at 200 and 50mV/s, as shown in Table A.6. Again, CV50 produced lower ΔE_p values than CVs conducted at 200mV/s (Table 4.6). For instance, at a rotation speed of 2000rpm, ΔE_p for 50nM methylated and unmethylated DNA was 129.3 ±5.4mV and 147.4 ±0.6mV respectively for CV200 (Figure 4.11A), compared with the reduced values of 109.1 ±1.5mV and 121.1 ±3.0mV for CV50 (Figure 4.11B).

Table 4.6 Effect of rotation speed on peak to peak separation.
ΔE_p (mV) for CVs conducted with 2mm Au-RDE in 2.5mM ferrocyanide/2.5mM ferricyanide/1X PBS after rotation assisted adsorption at varying rotation speeds for 5 minutes in 50nM methylated DNA, 50nM unmethylated DNA and 1X PBS, at scan speeds of 200 and 50mV/s. Mean ±SD (n=3, PBS n=1). [*]Statistical difference between values for methylated and unmethylated DNA, when tested for using a one-way ANOVA ($p<0.05$).

Rotation Speed (rpm)	ΔE_p (mV)						
	Methylated			Unmethylated			PBS
	mean	SD	RSD (%)	mean	SD	RSD (%)	
CV200							
0	110.3	0.1	0.06	98.7	3.0	3.03	92.4
1000	138.5	1.7	1.26	139.7	3.3	2.33	102.7
2000	129.3*	5.4	4.17	147.4*	0.6	0.41	108.4
4000	137.0	2.0	1.46	143.7	1.8	1.28	112.6
CV50							
0	95.0	2.0	2.07	86.3	2.8	3.21	78.7
1000	113.6	3.8	3.37	115.4	1.5	1.27	87.1
2000	109.1*	1.5	1.39	121.1*	3.0	2.47	87.2
4000	112.6	2.7	2.39	117.7	4.6	3.92	96.7
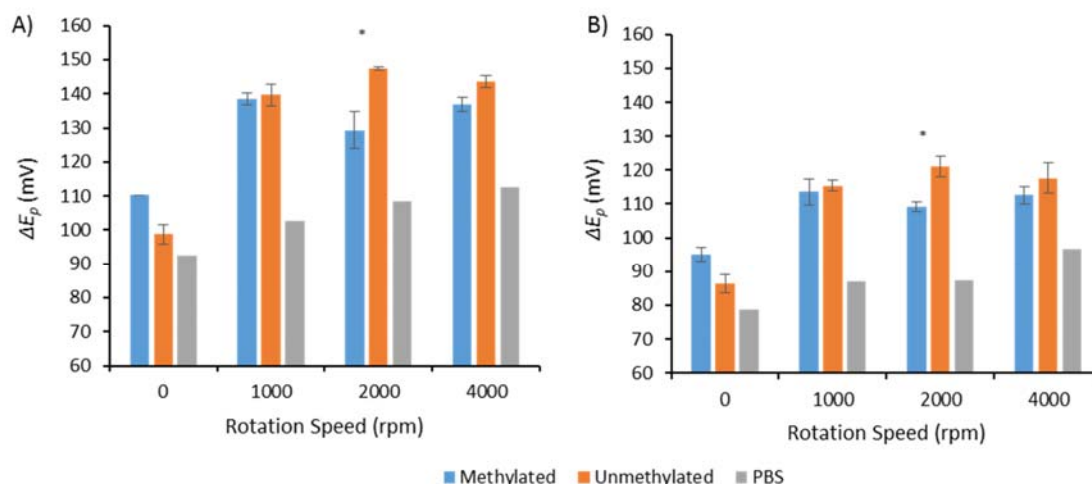
Figure 4.11 Effect of rotation speed on peak to peak separation.
ΔE_p (mV) for CVs conducted with 2mm Au-RDE in 2.5mM ferrocyanide/2.5mM ferricyanide/1X PBS after rotation assisted adsorption at varying rotation speeds for 5 minutes in 50nM methylated DNA, 50nM unmethylated DNA and 1X PBS, at scan speeds of A) 200 and B) 50mV/s. Mean ±SD (n=3, PBS n=1). *Statistical difference between values for methylated and unmethylated DNA, when tested for using a one-way ANOVA (p<0.05).

4.3.2.3 Effect of rotation speed on DPV

i_{pa} decreased as rotation speed increased for 1X PBS adsorbed onto the 2mm Au-RDE for 5 minutes (Figure 4.12 and 4.13, and Table 4.7). i_{pa} appeared to be unaltered for 50nM unmethylated DNA adsorbed onto the Au-RDE for 5 minutes between rotation speeds of 1000-4000rpm, and between these limits, i_{pa} for 50nM methylated DNA was greatest at 2000rpm. At 2000rpm, i_{pa} was 27.32 ±0.75 and 23.50±0.65µA for 50nM methylated and unmethylated DNA respectively. This difference in i_{pa} at 2000rpm reached statistical significance using a one-way ANOVA with Tukey post-hoc test (p<0.05), as shown in Table A.6.
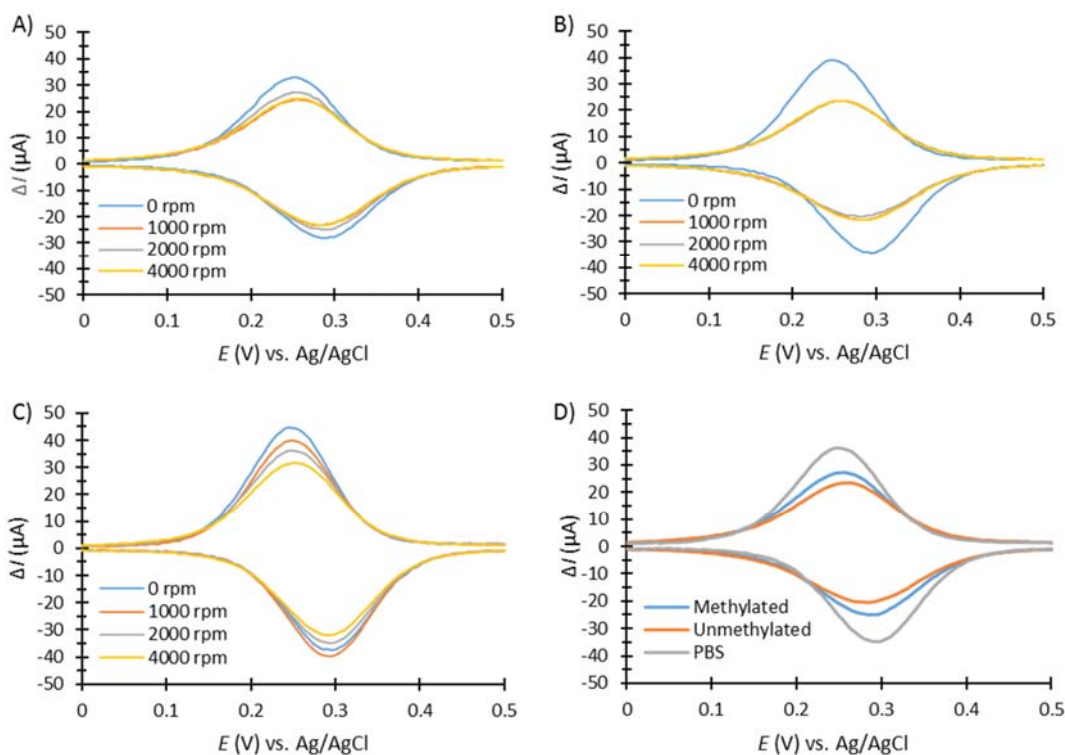
Figure 4.12 Effect of rotation speed on DPV.
DPV signals for 2mm Au-RDE in 2.5mM ferrocyanide/2.5mM ferricyanide/1X PBS after rotation assisted adsorption at varying rotation speeds for 5 minutes in A) 50nM methylated DNA, B) 50nM unmethylated DNA and C) 1X PBS. Plot D) compares adsorption at 2000rpm from plots A), B) and C). Mean (n=3, PBS n=1).

Table 4.7 Effect of rotation speed on peak current.
i_{pa} (μA) obtained with 2mm Au-RDE in 2.5mM ferrocyanide/2.5mM ferricyanide/1X PBS after rotation assisted adsorption at varying rotation speeds for 5 minutes in 50nM methylated DNA, 50nM unmethylated DNA and 1X PBS. Mean (n=3, PBS n=1). *Statistical difference between values for methylated and unmethylated DNA, when tested for using a one-way ANOVA ($p<0.05$).

Rotation Speed (rpm)	i_{pa} (μA)						PBS
	Methylated			Unmethylated			
	Mean	SD	RSD (%)	Mean	SD	RSD (%)	
0	32.88	0.33	1.01	39.20	0.57	1.47	44.72
1000	24.58	1.19	4.83	23.64	0.32	1.37	39.93
2000	27.32*	0.75	2.73	23.50*	0.65	2.77	36.19
4000	25.00	0.25	1.02	23.66	1.03	4.33	31.75
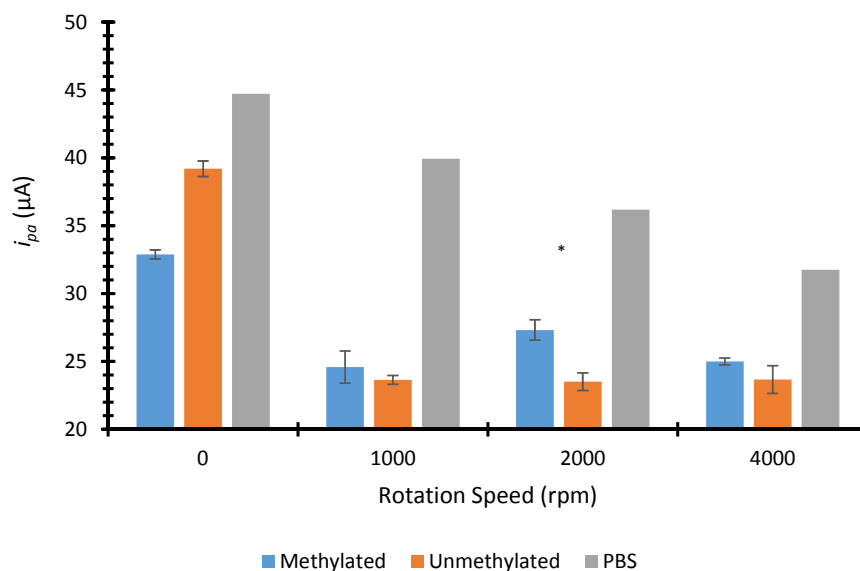
Figure 4.13 Effect of rotation speed on peak current.
i_{pa} (µA) obtained with 2mm Au-RDE in 2.5mM ferrocyanide/2.5mM ferricyanide/1X PBS after rotation assisted adsorption at varying rotation speeds for 5 minutes in 50nM methylated DNA, 50nM unmethylated DNA and 1X PBS. Mean (n=3, 1X PBS n=1). *Statistical difference between values for methylated and unmethylated DNA, when tested for using a one-way ANOVA ($p<0.05$).

4.3.3 DNA concentration

4.3.3.1 Effect of DNA concentration on impedance

The third test parameter to be optimised was DNA concentration. Concentrations between 0-400nM (in 1X PBS) of methylated and unmethylated DNA were adsorbed onto a 2mm Au-RDE before the electrode was submerged in the redox system. Nyquist plots showed that for methylated DNA, the radius of the arc continued to increase as concentration increased, up to 200nM. The arc radius produced for 400nM methylated DNA closely resembled that of the 200nM sample (Figure 4.14A). Similarly, unmethylated DNA arc radii grew in size as concentration increased, however the radius of the arc for 200nM was greatly enlarged (Figure 4.14 B). Thus indicating that 200nM would produce the greatest difference in electrochemical measurements between DNA solutions (Figure 4.14C).

In line with observational changes in the arc radii, R_{ct} generally increased as the concentration of oligonucleotide increased (Table 4.8). Furthermore, the greatest difference between methylated and unmethylated DNA solutions was observed at 200nM. The R_{ct} for 200nM methylated DNA was determined to be 1387.00 ±60.23Ω, while the R_{ct} for 200nM unmethylated DNA was greatly elevated at 1999.67 ±20.53Ω. It is important to note the substantial difference between these values and the value given for 0nM of 346.27 ±31.34Ω (Figure 4.14D). Using a one-ANOVA with a Tukey post-hoc test, the minimal amount of DNA required to produce a significant difference could be determined. The limit of detection of methylated and unmethylated DNA was determined to be 10nM (Table A.7 and A.8). However the methylation status was not distinguishable until >25nM ($p<0.05$), as observed in Table A.9.
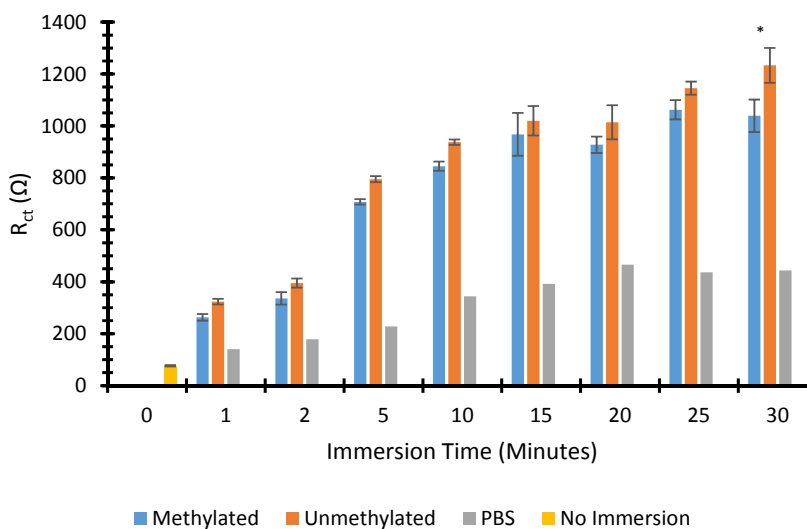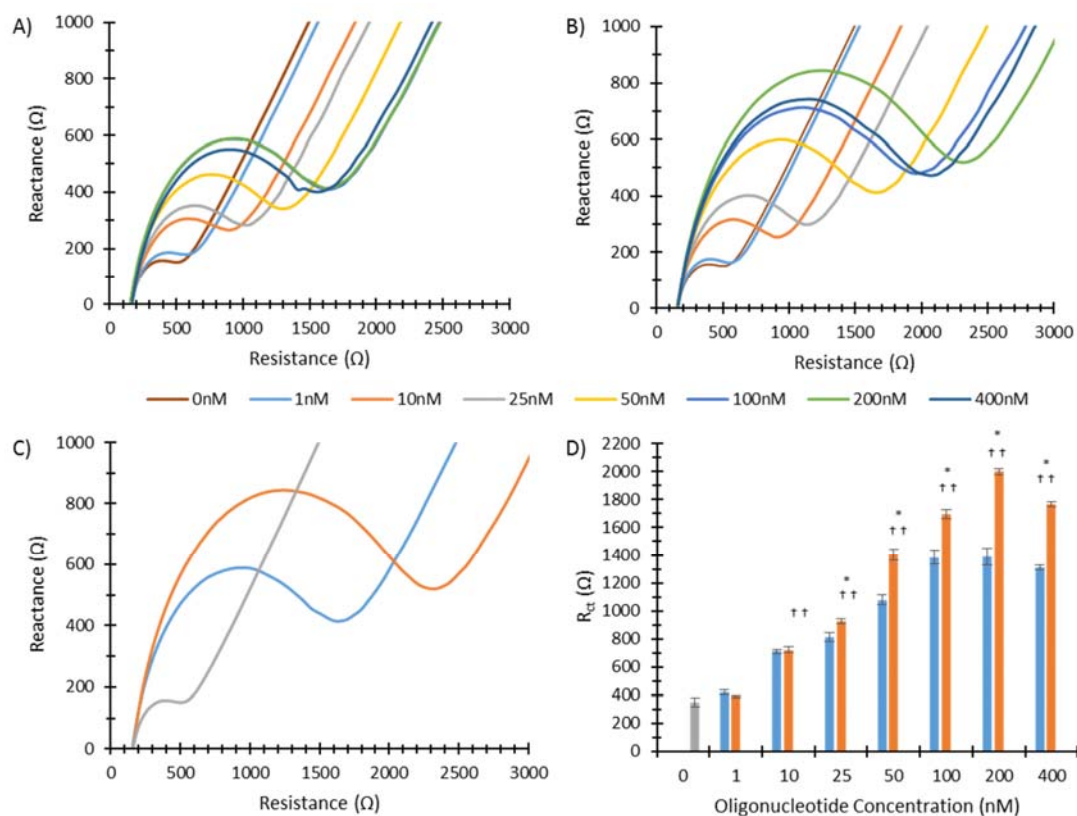
Figure 4.14 Effect of DNA concentration on impedance.

Nyquist plots for a 2mm Au-RDE in 2.5mM ferrocyanide/2.5mM ferricyanide/1X PBS after rotation

assisted adsorption at 2000rpm for 5 minutes in varying concentrations of A) methylated DNA, and B)

unmethylated DNA. Plot C) compares adsorption of 200nM DNA and 1X PBS Nyquist plots from A) and

B). D) R_{ct} (determined from Z-fit analysis of Nyquist plots) for a 2mm Au-RDE in 2.5mM

ferrocyanide/2.5mM ferricyanide/1X PBS after rotation assisted adsorption at 2000rpm for 5 minutes

in varying concentrations of methylated and unmethylated DNA. Mean ±SD (n=3). *Statistical

difference between values for methylated and unmethylated DNA, when tested for using a one-way

ANOVA ($p<0.05$), †statistical difference to value for baseline 1X PBS ($p<0.05$).

Table 4.8 Effect of DNA concentration on R_{ct}.
R_{ct} (determined from Z-fit analysis of Nyquist plots) for a 2mm Au-RDE in 2.5mM ferrocyanide/2.5mM ferricyanide/1X PBS after rotation assisted adsorption at 2000rpm for 5 minutes in varying concentrations of methylated and unmethylated DNA. Mean ±SD (n=3). *Statistical difference between values for methylated and unmethylated DNA, when tested for using a one-way ANOVA ($p<0.05$), †statistical difference to value for baseline 1X PBS ($p<0.05$).

Concentration (nM)	R_{ct} (Ω)								
	PBS			Methylated			Unmethylated		
	Mean	SD	RSD (%)	Mean	SD	RSD (%)	Mean	SD	RSD (%)
0	346.27	31.34	9.05						
1				419.73	16.60	3.95	388.80	9.09	2.34
10				710.73†	15.10	2.12	722.00†	21.20	2.94
25				813.97*†	31.11	3.82	926.17*†	15.51	1.68
50				1078.33*†	35.02	3.25	1403.67*†	38.07	2.71
100				1385.00*†	52.42	3.78	1696.67*†	35.00	2.06
200				1387.00*†	60.23	4.34	1999.67*†	20.53	1.03
400				1309.67*†	16.65	1.27	1770.67*†	17.95	1.01

4.3.3.2 Effect of DNA concentration on cyclic voltammetry

ΔE_p increased as concentrations of methylated and unmethylated DNA increased for both CV200 and CV50 (Table 4.9). For instance, for CV200, ΔE_p increased from 105.8 ±2.0mV at 0nM, to 161.2 ±2.0mV and 192.6 ±1.1mV for 200nM methylated and unmethylated DNA respectively (Figure 4.15A). The greatest difference between DNA samples was observed at 200nM. For CV50, 0nM corresponded to a ΔE_p of 86.7 ±1.1mV which increased to 132.4 ±1.7mV and 149.7 ±4.0mV (Figure 4.15B). The limit of detection was shown statistically to be 10nM for methylated and 25nM for unmethylated DNA when considering ΔE_p for both CV200 and CV50 ($p<0.05$) as observed in Tables A.7 and A.8. However, DNA solutions were not statistically distinguishable from one another until >25nM and >50nM for CV200 and CV50 respectively (Table A.9).
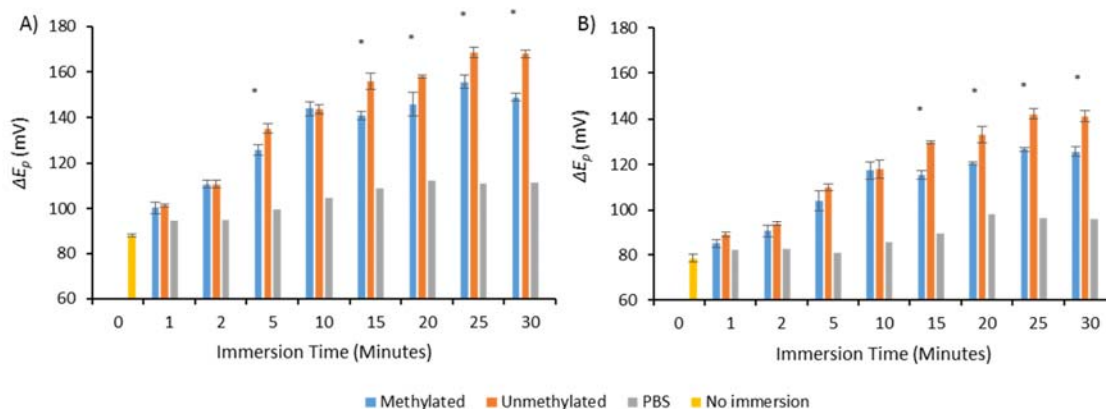
Table 4.9 Effect of DNA concentration on peak to peak separation.

ΔE_p (mV) for a 2mm Au-RDE in 2.5mM ferrocyanide/2.5mM ferricyanide/1X PBS after rotation assisted adsorption at 2000rpm for 5 minutes in varying concentrations of methylated and unmethylated DNA, at scan speeds of 200 and 50mV/s. Mean ±SD (n=3). *Statistical difference between values for methylated and unmethylated DNA, when tested for using a one-way ANOVA ($p<0.05$), †statistical difference to value for baseline 1X PBS ($p<0.05$).

| Concentration (nM)	ΔE_p (mV)								
	PBS			Methylated			Unmethylated		
	Mean	SD	RSD (%)	Mean	SD	RSD (%)	Mean	SD	RSD (%)
CV200									
0	105.8	2.0	1.91						
1				111.1	0.8	0.73	109.7	1.7	1.60
10				121.1†	2.6	2.12	126.4†	1.4	1.07
25				130.0*†	1.7	1.32	140.9*†	3.3	2.33
50				146.3*†	2.4	1.67	162.8*†	5.6	3.44
100				155.4*†	2.0	1.27	173.3*†	0.7	0.38
200				161.2*†	2.0	1.21	192.6*†	1.1	0.55
400				155.7*†	0.3	0.18	183.3*†	1.3	0.70
CV50									
0	86.7	1.1	1.29						
1				89.5	1.7	1.92	90.1	3.1	3.49
10				98.8†	0.5	0.53	105.3†	0.2	0.24
25				106.5†	1.7	1.62	110.2†	0.5	0.43
50				118.4*†	1.1	0.90	128.8*†	5.1	3.99
100				126.2*†	2.8	2.24	142.0*†	1.8	1.26
200				132.4*†	1.7	1.27	149.7*†	4.0	2.67
400				124.0*†	0.3	0.22	145.2*†	2.1	1.43
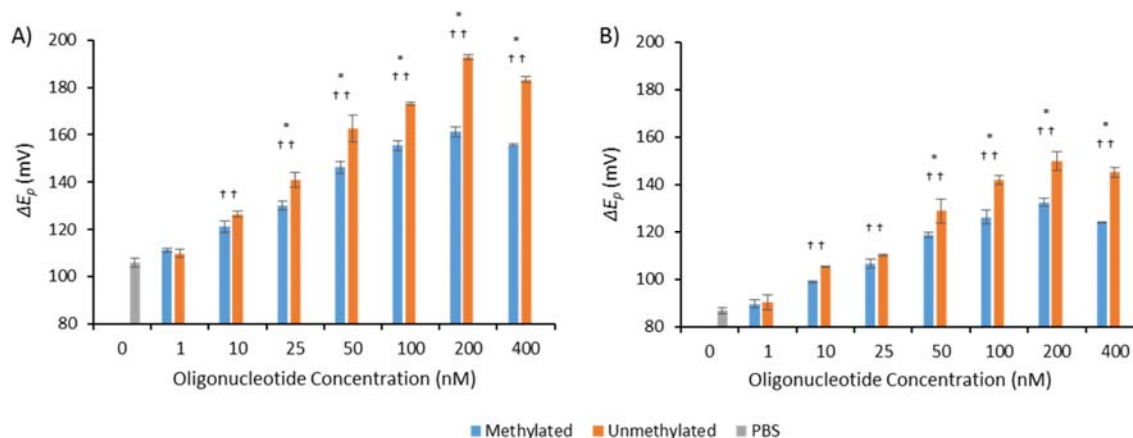
Figure 4.15 Effect of DNA concentration on peak to peak separation.
ΔE_p (mV) for a 2mm Au-RDE in 2.5mM ferrocyanide/2.5mM ferricyanide/1X PBS after rotation assisted adsorption at 2000rpm for 5 minutes in varying concentrations of methylated and unmethylated DNA, at scan speeds of A) 200 and B) 50mV/s. Mean ±SD (n=3). *Statistical difference between values for methylated and unmethylated DNA, when tested for using a one-way ANOVA ($p<0.05$), †statistical difference to value for baseline 1X PBS ($p<0.05$).

4.3.3.3 Effect of DNA concentration on DPV

Increasing the concentration of both methylated and unmethylated DNA resulted in reduced i_{pa} (Figure 4.16A and B). For instance, a i_{pa} of 43.09 ±1.37µA was observed at 0nM, while at 200nM a i_{pa} of 19.92 ±0.17µA and 16.17 ±0.83µA was seen for 200nM methylated and unmethylated DNA respectively (Figure 4.16C and D, and Table 4.10). Interestingly the limit of detection for methylated DNA was 1nM, although 10nM of unmethylated DNA was required to produce a statistically significant difference from 0nM ($p<0.05$), as outlined in Tables A.7 and A.8. However, >50nM was required to allow for the differentiation of methylated and unmethylated DNA solutions by one way ANOVA with a Tukey post hoc test (Table A.9).
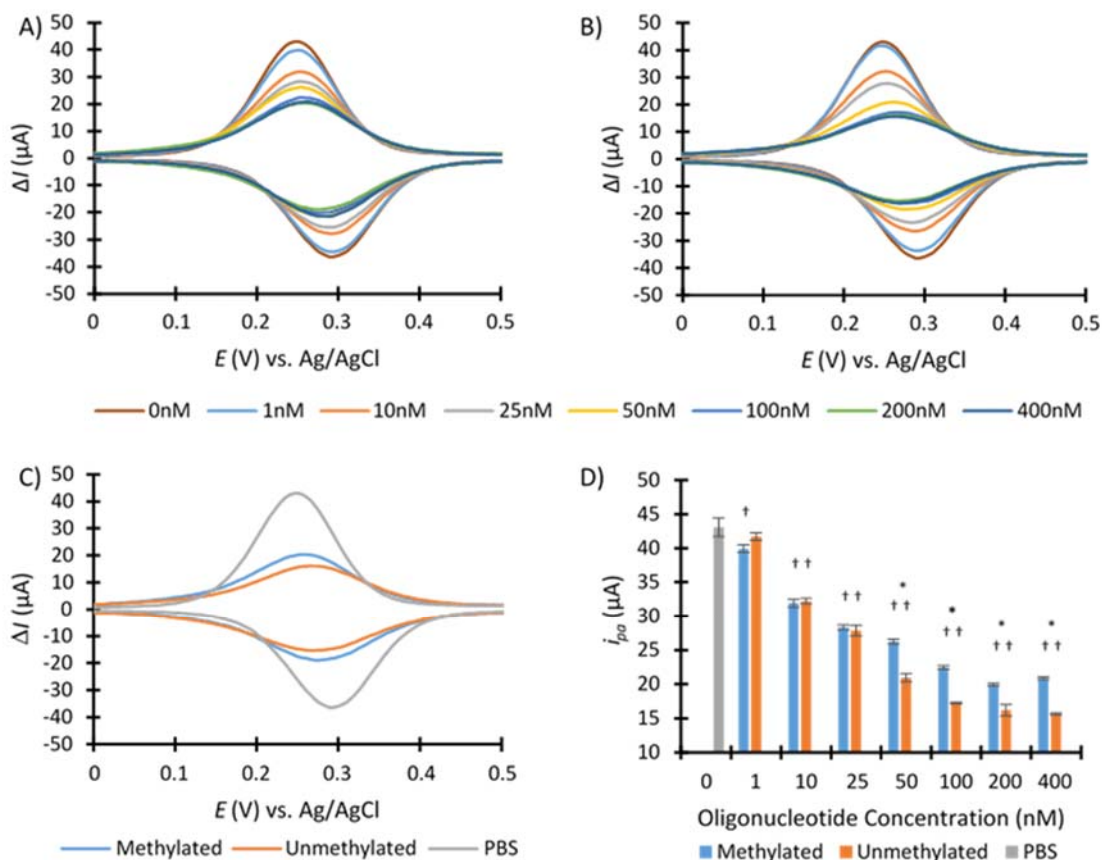
Figure 4.16 Effect of DNA concentration on DPV.
DPV signals for a 2mm Au-RDE in 2.5mM ferrocyanide/2.5mM ferricyanide/1X PBS after rotation assisted adsorption at 2000rpm for 5 minutes in varying concentrations of A) methylated DNA and B) unmethylated DNA. Plot C) compares adsorption of 200nM DNA and 1X PBS DPV signals (mean, n=3). D) i_{pa} (µA) obtained with a 2mm Au-RDE in 2.5mM ferrocyanide/2.5mM ferricyanide/1X PBS after rotation assisted adsorption at 2000rpm for 5 minutes in varying concentrations of methylated and unmethylated DNA. Mean ±SD (n=3). *Statistical difference between values for methylated and unmethylated DNA, when tested for using a one-way ANOVA ($p<0.05$), †statistical difference to value for baseline 1X PBS ($p<0.05$).

Table 4.10 Effect of DNA concentration on peak anodic current.

i_{pa} (µA) obtained with a 2mm Au-RDE in 2.5mM ferrocyanide/2.5mM ferricyanide/1X PBS after rotation assisted adsorption at 2000rpm for 5 minutes in varying concentrations of methylated and unmethylated DNA. Mean ±SD (n=3). *Statistical difference between values for methylated and unmethylated DNA, when tested for using a one-way ANOVA ($p<0.05$), †statistical difference to value for baseline 1X PBS ($p<0.05$).

Concentration (nM)	i_{pa} (µA)								
	PBS			Methylated			Unmethylated		
	mean	SD	RSD (%)	mean	SD	RSD (%)	mean	SD	RSD (%)
0	43.09	1.37	3.17						
1				39.93†	0.56	1.39	41.74	0.53	1.28
10				31.93†	0.56	1.76	32.23†	0.39	1.21
25				28.32†	0.34	1.20	27.85†	0.78	2.81
50				26.23*†	0.35	1.35	20.94*†	0.63	3.01
100				22.43*†	0.28	1.26	17.23*†	0.11	0.65
200				19.92*†	0.17	0.84	16.17*†	0.83	5.13
400				20.86*†	0.16	0.78	15.63*†	0.14	0.89

4.3.4 Percent methylation

4.3.4.1 Effect of percent methylation on impedance
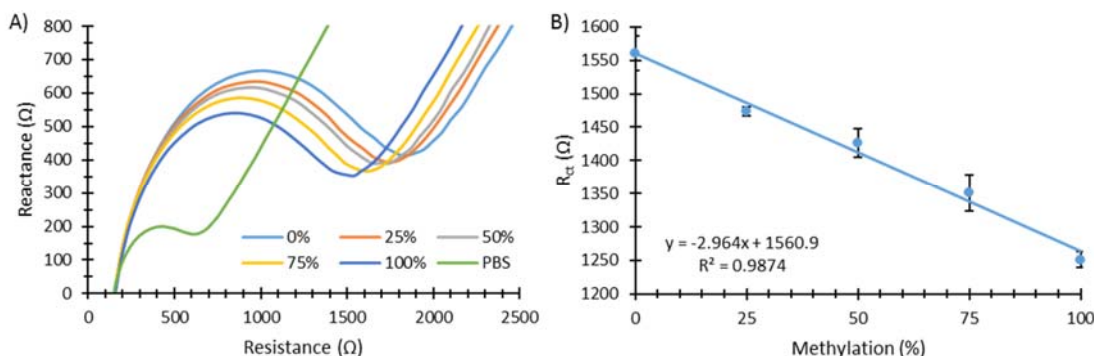
Figure 4.17 Effect of % methylation on impedance.
A) Nyquist plots for a 2mm Au-RDE in 2.5mM ferrocyanide/2.5mM ferricyanide/1X PBS after rotation assisted adsorption at 2000rpm for 5 minutes in varying % methylation solutions (200nM), and 1X PBS (mean, n=3). B) R_{ct} (determined from Z-fit analysis of Nyquist plots) for a 2mm Au-RDE in 2.5mM ferrocyanide/2.5mM ferricyanide/1X PBS after rotation assisted adsorption at 2000rpm for 5 minutes in varying % methylation solutions (200nM) and 1X PBS. Mean ±SD (n=3). 1X PBS R_{ct} 454.17 ±37.08 Ω.

To determine if electrochemical techniques could detect % methylation in a heterogeneous sample, solutions with varying proportions of 200nM DNA were tested. Nyquist plots revealed that all solutions containing varying percentages of methylated and unmethylated DNA produced substantially larger arc radii than those corresponding to 1X PBS. The arc radius decreased in size as % methylation increased. By analysing the Nyquist plots using Z-fit analysis, a negative correlation between % methylation and R_{ct} was observed and described by the equation $y = -2.964x + 1560.9$ (Figure 4.17A and B, and Table 4.11). R_{ct} decreased from 1560.67 ±25.15Ω for the 0% methylated solution to 1251.33 ±12.01Ω for the 100% methylated solution. The linear correlation represented experimental data well with an R^2 value of 0.9874. All solutions tested produced statistically distinguishable R_{ct} values, except for 25 vs. 50% solutions (Table A.10).

Table 4.11 Effect of % methylation on R$_{ct}$.
R$_{ct}$ (determined from Z-fit analysis of Nyquist plots) for a 2mm Au-RDE in 2.5mM ferrocyanide/2.5mM ferricyanide/1X PBS after rotation assisted adsorption at 2000rpm for 5 minutes in varying % methylation solutions (200nM) and 1X PBS. Mean ±SD (n=3).

% methylation	R$_{ct}$ (Ω)		
	Mean	SD	RSD (%)
PBS	454.17	37.08	8.16
0	1560.67	25.15	1.61
25	1473.67	6.66	0.45
50	1426.67	21.59	1.51
75	1351.33	27.32	2.02
100	1251.33	12.01	0.96

4.3.4.2 Effect of percent methylation on cyclic voltammetry

Cyclic voltammetry was a less effective tool for distinguishing % methylation in a heterogeneous sample, although a trend for a decrease in ΔE_p as % methylation increased was observable for results from both CV200 and CV50 (Figure 4.18A and B, and Table 4.12). For example, CV200 data showed ΔE_p decreased from 178.5 ±1.2mV for the 0% methylated solution to 159.9 ±1.7mV for the 100% methylated solution. ΔE_p values were lower for CV50 with ΔE_p decreasing from 144.9 ±5.3mV to 131.7 ±1.4mV for 0% and 100% methylated samples respectively. From CV200, ΔE_p for only 0, 25 and 50% solutions were statistically different against 100% methylation ($p<0.05$); all other results did not reach statistical significance (Table A.10). CV50 was even less effective at differentiating % methylation; only 0 and 50% methylated solutions were significantly different from the 100% methylated solution.

Table 4.12 Effect of % methylation on peak to peak separation.

ΔE_p (mV) for CVs conducted with a 2mm Au-RDE in 2.5mM ferrocyanide/2.5mM ferricyanide/1X PBS after rotation assisted adsorption at 2000rpm for 5 minutes in varying % methylation solutions (200nM) and 1X PBS, at scan speeds of 200 and 50mV/s. Mean ±SD (n=3).

% Methylation	ΔE_p (mV)		
	Mean	SD	RSD (%)
CV200			
PBS	115.3	8.0	6.93
0	178.5	1.2	0.70
25	177.8	6.6	3.70
50	177.7	6.7	3.79
75	169.0	0.5	0.27
100	159.9	1.7	1.07
CV50			
PBS	94.2	2.7	2.88
0	144.9	5.3	3.63
25	140.9	1.3	0.93
50	145.8	6.2	4.23
75	136.2	3.0	2.19
100	131.7	1.4	1.06
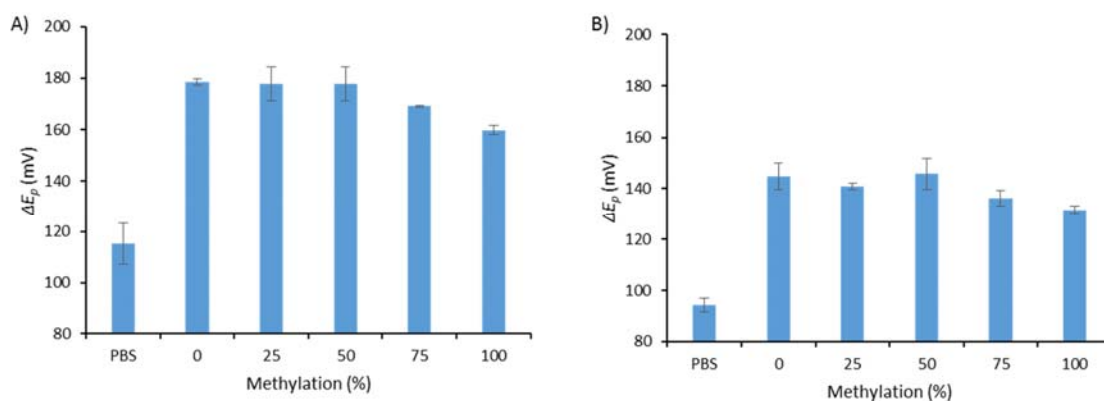
Figure 4.18 Effect of % methylation on peak to peak separation.

ΔE_p (mV) for CVs conducted with a 2mm Au-RDE in 2.5mM ferrocyanide/2.5mM ferricyanide/1X PBS after rotation assisted adsorption at 2000rpm for 5 minutes in varying % methylation solutions (200nM) and 1X PBS, at scan speeds of A) 200 and B) 50mV/s. Mean ±SD (n=3).

4.3.4.3 Effect of percent methylation on DPV

i_{pa} increased from 18.34 ±0.58µA to 20.89 ±0.30µA as methylation increased from 0 to 100%. This positive correlation between % methylation and i_{pa} was described by the equation $y = 0.0254x + 18.0652$ (Figure 4.19A and B, and Table 4.13). The linear relationship described here represents the data well as R^2 = 0.9144. i_{pa} was more effective than cyclic voltammetry in differentiating methylation status. Only 0% vs. 25% and 50% vs. 75% solutions could not be distinguished by statistical analysis, while all other comparisons reached statistical significance (p<0.05), as described in Table A.10.
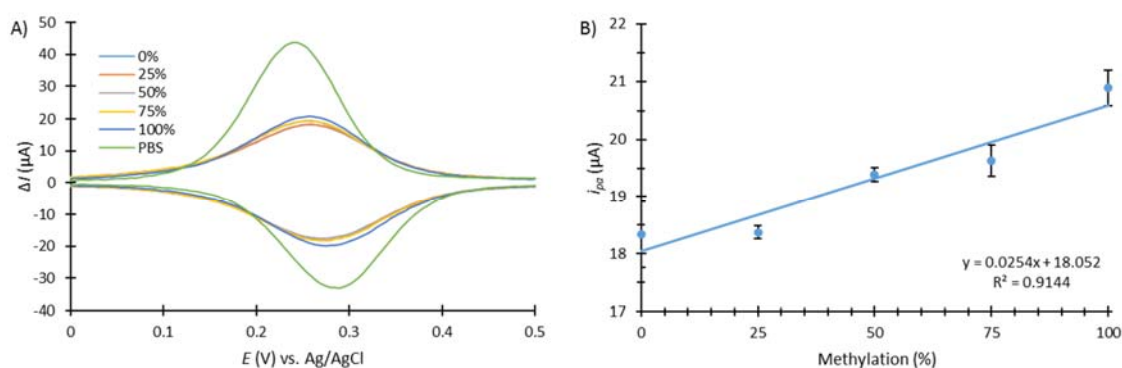
Figure 4.19 Effect of % methylation on DPV.
A) DPV signals and B) i_{pa} (µA) for 2mm Au-RDE in 2.5mM ferrocyanide/2.5mM ferricyanide/1X PBS after rotation assisted adsorption at 2000rpm for 5 minutes in varying % methylation solutions (200nM) and 1X PBS. Mean ±SD (n=3). PBS i_{pa} 43.72±2.82µA.

Table 4.13 Effect of % methylation on peak anodic current.
i_{pa} (µA) for 2mm Au-RDE in 2.5mM ferrocyanide/2.5mM ferricyanide/1X PBS after rotation assisted adsorption at 2000rpm for 5 minutes in varying % methylation solutions (200nM). Mean ±SD (n=3).

% Methylation	i_{pa} (µA)		
	Mean	SD	RSD (%)
PBS	43.72	2.82	6.44
0	18.34	0.58	3.16
25	18.38	0.11	0.61
50	19.38	0.12	0.61
75	19.63	0.27	0.61
100	20.89	0.30	1.42

4.4 Discussion

The work conducted in this chapter was based on the protocol developed by Koo et al. (2014), who used DPV to detect DNA methylation. By expanding on their findings to include EIS and CV, it was determined that ΔE_p derived from both CV200 and CV50, and R$_{ct}$ derived from EIS, were better able to differentiate between methylated and unmethylated samples. The parameter R$_{ct}$, derived from EIS, was most effective at detecting the percentage of methylation in heterogeneous solutions; detecting a statistically significant difference at 25% methylation. Interestingly, DPV was second most effective at detecting percentage of methylation in heterogeneous solutions, while CV was comparably ineffective at detecting % methylation in heterogeneous samples. Furthermore, DPV was most effective at detecting the presence of methylated DNA (vs 0mM). The ability of DPV to be more effective at detecting the presence of low concentration of DNA is not surprising, as DPV is often described as a technique that has higher sensitivity to very low concentrations than other conventional sweep techniques (Radhakrishnan et al., 2014). Therefore, it is important to consider these factors when deciding which electrochemical test to use in the detection of DNA methylation.

CVs at 200 and 50mV/s revealed the electrochemical reactions were quasi-reversible. This was determined for a number of reasons. Firstly, a higher scan speed (200mV/s) increased ΔE_p; ΔE_p values from CV200 analyses were statistically greater than their CV50 counterparts ($p<0.05$); this was true for all values from adsorption time, rotation speed, concentration and percent methylation analyses, when statistically analysed by a one way ANOVA with a Tukey post-hoc test. Secondly, ΔE_p values were significantly greater than 59mV, and were effected by DNA adsorption. For instance, when the Au-RDE was immediately immersed into the redox solution following polishing, ΔE_p was 87.9 and 78.5mV for CV200 and CV50 respectively. Immersion in PBS for 30 minutes elevated ΔE_p to 111.6 and 96.3mV, while immersion in methylated DNA for 30 minutes further elevated ΔE_p to 148.8 and 125.7mV for CV200 and CV50 respectively. The greater affinity of adenine for Au-RDE lead to increased passivation of the electrode for unmethylated samples, with ΔE_p further rising to 167.9 and 141.4mV

respectively for CV200 and CV50. This trend associates passivation with a decline in the reversibility of the system (Connell et al., 2016). Thirdly, a reverse peak was present, eliminating the possibility of an irreversible system (Mabbott, 1983). Thus, enabling the series of reactions to be termed quasi-reversible, with a trend towards irreversibility with increased passivation.

This work has shown that the optimum electrochemical procedure involved adsorbing 200nM DNA for 5 minutes at 2000rpm onto the Au-RDE. Similarly, Sina et al. (2014) reported 200nM was the optimum DNA concentration for creating greatest current difference between samples. Although Koo et al. (2014) reported that a concentration of 50nM was optimum, this may be because a 53 base sequence containing eight CpG sites was used, in comparison to the 30 base sequence containing six CpG sites utilised in this work. Another difference is that the technique outlined in this work resulted in a 50% reduction in adsorption time, compared to that reported by both Sina et al. (2014) and Koo et al. (2014). This could be explained by the use of a rotating gold electrode in comparison to a non-motile electrode. While one-time use Au-SPE, as used by Koo et al. (2014), have benefits such as a low cost, ability to change their design and are disposable, their inability to rotate could lead to reduced adsorption. Additionally, it is important to consider that although the Au-RDE requires polishing between tests, while the Au-SPE does not require cleaning due to its disposable nature, the polishing procedure outlined in this study took approximately 3 minutes to complete. Therefore, this electrode processing time totalled 8 minutes, 20% less time than required for the disposable Au-SPR. It is also important to note the Au-RDE used here was 2mm in diameter, 50% smaller than the SPE-Au used by Koo et al. (2014).

4.5 Conclusion

The work outlined in this chapter provides evidence for the use of electrochemical techniques in the detection of DNA methylation. Results indicated all three electrochemical techniques (EIS, CV and DPV) were able to detect the DNA methylation status of 30 base synthetic DNA, designed to represent a methylated and unmethylated bisulphite modified and asymmetrically amplified section of the EN1 gene promoter. Greater R$_{ct}$ (EIS) and ΔE_p (CV), and lower i_{pa} (DPV) were observed for unmethylated samples, demonstrating its higher affinity for the Au-RDE than its methylated counterpart. R$_{ct}$ (EIS) was the most effective electrochemical parameter (method) for the detection of DNA methylation in heterogeneous solutions of synthetic DNA, when the optimum procedure (200nM DNA for 5 minutes at 2000rpm) was employed; followed by i_{pa} (DPV), and ΔE_p (CV200 then CV50). This work provides insight into the potential of this technology for determining DNA methylation in human derived samples. This is vital as changes to DNA methylation patterns are often observed with age and disease, and identifying these changes may allow for the early detection of diseases such as cancer.

Chapter 5 Detecting the methylation status of MCF-7 cell DNA using electrochemistry

5.1 Introduction

In 2016, cancer was the most common cause of death in both men and women in England and Wales, accounting for 30.8% and 26.2% of deaths respectively (OFNS, 2017). Of the cancer related deaths in females in the UK, 15% were caused by breast cancer, the second most common cancer in females (Cancer Research UK, 2018). Commonly used to investigate breast cancer *in vitro*, the non-aggressive MCF-7 cell line, was derived from the pleural effusion of a 69 year old female breast cancer patient, at the Michigan Cancer Foundation in 1970, where it gained its name. The cell line is oestrogen and progesterone receptor positive, making it an ideal candidate for studying the effects of anticancer drugs that interfere with these hormones or their receptors (Comsa et al., 2015; Soule et al., 1973). This cell line was utilised by Koo et al. (2014) and Sina et al. (2014), to test the applicability of the eMethylsorb method for electrochemically detecting DNA methylation.

The aims of this chapter are to determine if the procedure outlined in Chapter 4 can be used to detect DNA methylation in human derived DNA, and determine if percentage methylation can be detected in heterogeneous samples of human-derived DNA. Following on from the work completed in Chapter 4, and building on the findings of Koo et al. (2014), the optimised procedure will be used to detect DNA methylation in the human cell line MCF-7. Briefly, the procedure involves 1) extracting cellular DNA, and 2) modifying the DNA through bisulphite treatment, before the DNA undergoes 3) asymmetric PCR. The methylation status of bisulphite modified and asymmetrically amplified 140 base ssDNA from the EN1 region of MCF-7 DNA (methylated), and WGA DNA (unmethylated) will then be 4) electrochemically analysed through a) EIS, b) CV at 200mV/s and 50mV/s and c) DPV. Following the determination of the optimum fractional proportion of secondary PCR product in test solution, % methylation in a heterogeneous sample will be tested. Akin to the work conducted in Chapter 4, it is imperative to determine if the procedure is able to detect % methylation in heterogeneous samples comprising of varying proportions of MCF-7 and WGA DNA, as biopsies of various cancerous tumours

have often been observed to exhibit cells with differing levels of methylation (Litovkin et al., 2015; Moelans et al., 2014; Quek et al., 2017).

5.2 Methods

5.2.1 MCF-7 cell culturing

MCF-7 Cells (P10-P50, gifted from, and grown at, The Institute of Medicine, Bache Hall, University of Chester) were cultured in a 75ml tissue culture flask (Fisher, 10364131) in 15ml Eagle's Minimum Essential Medium (EMEM, Lonza, SLS, LZBE12-611F) supplemented with 10% foetal bovine serum (FBS, Invitrogen Gibco, Fisher, 11573397) and 1% non-essential amino acids (NEAA, SLS, M7145). Cells were incubated at 37°C at 5% CO_2. At 70% confluence, cells were trysinised with a Trypsin-Versene mixture (Lonza, SLS, LZBE17-161E), and resuspended in media. Cells were then centrifuged at 500 x g for 5 minutes and the media removed. The cells were next resuspended in an equal volume of PBS, and their number determined by mixing an aliquot of cells and trypan blue (SLS, T8154) in a 1:1 ratio and examining on a haemocytometer (Labtech, DHC-N01 and Fisher EVOS XL Core microscope). It was determined there were 16.5 million cells in 30ml, 5.5×10^5 cells per ml, and 1.1×10^5 cells per 200µl aliquot.

5.2.2 MCF-7 DNA extraction

DNA was extracted from MCF-7 cells using QIAGEN QIAamp® DNA Mini Kit (50) (QIAGEN, 51304) according to the manufacturer's instructions, with few alterations. To 200µl of MCF-7 cells, 20µl of proteinase K, and 200µl buffer AL were added. The sample was then vortexed for 15 seconds, before undergoing a 10 minute incubation at 56°C. Following this, the sample was pulse centrifuged to remove drops from inside the lid, and 200µl of 100% ethanol (VWR, 20821.310) was added. The

sample was then vortexed again for 15 seconds before a second pulse centrifugation. This 620µl sample was then pipetted into a QIAamp Mini spin column (in a 2ml collection tube) and centrifuged at 6,000 x g for 1 minute. The QIAamp Mini spin column was then placed into a clean 2ml collection tube, and 500µl of buffer AW1 supplemented with 100% ethanol was added to the spin column before centrifugation at 6,000 x g for 1 minute. Again the filtrate was discarded and the spin column added to a clean 2ml collection tube. Following this, 500µl of buffer AW2 was added, and the sample was centrifuged at 17,000 x g for 4 minutes. The spin column was then placed into a 1.5ml microcentrifuge tube, and 200µl of buffer AE was added. The sample was then incubated at room temperature for 5 minutes before centrifugation at 6,000 x g for 1 minute. Extracted DNA was stored at -20°C.

5.2.3 MCF-7 DNA concentration, purity and yield calculation

The concentration and purity of MCF-7 DNA was calculated by diluting 50µl in 200µl of nuclease free water (USB Corporation, 71786) and measuring the absorbance at 260, 280 and 320nm in triplicate (Table 5.1), using the Varioskann Lux fluorescent plate reader (Thermo scientific, 3020219). These wavelengths were utilised as nucleic acids are maximally absorbed at a wavelength of 260nm, while proteins have an absorbance maxima of 280nm. The ratio of absorbance values at these wavelengths were therefore employed in the determination of sample purity. Additionally, 320nm was utilised as neither nucleic acids or proteins absorb at this wavelength, therefore it is commonly used to provide a background correction value (Teare et al., 1997).

As outlined in the QIAGEN QIAamp® DNA Mini Kit, the concentration of DNA was calculated using equation 33:

$$\text{Concentration (µg/ml)} = (A_{260} - A_{320}) \times \text{dilution factor} \times 50\text{µg/ml} \qquad (33)$$

The purity of DNA was calculated via equation 34:

$$\text{DNA purity} = A_{260}/A_{280} \tag{34}$$

A ratio of 1.7-1.9 indicates pure DNA. A value below this range is indicative of contaminants within the sample, which absorb at 280nm (i.e. protein). A value of 1.763 was calculated using equation 34, thus indicating that the extracted MCF-7 DNA was pure. Purity of DNA can also be calculated using equation 35:

$$\text{DNA purity} = (A_{260} - A_{320}) \div (A_{280} - A_{320}) \tag{35}$$

The Yield of DNA was calculated by equation 36:

$$\text{DNA yield (µg)} = \text{DNA concentration (µg/ml)} \times \text{total sample volume (ml)} \tag{36}$$

Table 5.1 MCF-7 DNA absorbance at 260, 280 and 320nm.
n=3.

Replicate	Absorption		
	260nm	280nm	320nm
1	3.901	2.221	0.204
2	3.904	2.210	0.205
3	3.907	2.214	0.207
Average	3.904	2.215	0.205

DNA concentration

$$\text{Concentration (µg/ml)} = (A_{260} - A_{320}) \times \text{dilution factor} \times 50\text{µg/ml}$$

$$= (3.904\text{-}0.205) \times 4 \times 50\text{µg/ml}$$

= 739.8 µg/ml

DNA purity

$$\text{DNA purity} = A_{260}/A_{280}$$

$$= 3.904/2.215$$

$$= 1.763$$

DNA purity (Equation 2)

$$\text{DNA purity} = (A_{260} - A_{320}) / (A_{280} - A_{320})$$

$$= (3.904 - 0.205) / (2.215 - 0.205)$$

$$= 3.699 / 2.01$$

$$= 1.840$$

DNA yield from 1.1×10^5 cells in 200µl

$$\text{DNA yield (µg)} = \text{DNA concentration (µg/ml)} \times \text{total sample volume (ml)}$$

$$= 739.8\text{µg/ml} \times 0.2\text{ml}$$

$$= 147.96 \text{ µg}$$

5.2.4 Whole genome amplified DNA

Whole genomic DNA (Roche Diagnostics GmbH, 11691112001) was diluted in nuclease free water to a concentration of 50ng/µl and amplified using the whole genome amplification kit - REPLI-g UltraFast Mini kit (QIAGEN, 150033) according to the manufacturer's instructions. Briefly, Buffer DLB was prepared by adding 500µl nuclease free water and mixing thoroughly; 5µl Reconstituted Buffer DLB was combined with 35µl nuclease free water to create Buffer D1. Buffer N1 was prepared by combining 8µl of Stop solution with 72µl of nuclease free water. Next, 1µl of Buffer D1 was added to 1µl of 50ng/µl whole genomic DNA in a microcentrifuge tube, and mixed by vortexing for 5 seconds

and pulse centrifuging. Following incubation at room temperature for 3 minutes, 2µl of Buffer N1 was added and mixed by vortexing for 5 seconds and pulse centrifuging. Next, 16µl of mastermix, which was stored on ice and created by combining 15µl of REPLI-g UltraFast Reaction buffer with 1µl REPLI-g UltraFast DNA polymerase, was added to the 4µl of denatured DNA. The sample was then incubated at 30°C for 90 minutes. The REPLI-g UltraFast DNA Polymerase was then inactivated by heating the sample to 65°C for 3 minutes. The REPLI-g UltraFast Mini kit outlined that 7-10µg of DNA was produced using this procedure. A value of 10µg was assumed to calculate a concentration of 500ng/µl. Excess whole genome amplified (WGA) DNA was stored at -20°C.

5.2.5 Bisulphite modification

The MCF-7 DNA and amplified whole genomic DNA then underwent bisulphite modification using the MethylEasy Xceed kit (Human Genetic Signatures, ME002) according to the manufacturer's instructions. In 1.5µl eppendorf tubes, 2.5µl of 739.8ng/µl extracted MCF-7 DNA, and 2.5µl of 500ng/µl of WGA DNA were separately combined with 17.5µl nuclease free water. Following this, 2.2µl of 3M NaOH (AnalaR NORMAPUR, 28244.295) was added to each DNA solution and mixed well by pipetting, before undergoing a 15 minute incubation at 37°C. Then 220µl of combined reagent 1 and 2 was added. Each sample was then incubated at 80°C for 45 minutes. Following this, the samples were pulse centrifuged to remove condensation, and 240µl of reagent 3 was added and mixed well by pipetting. The samples were transferred to a purification column in a collection tube, and centrifuged for 1 minute at 13,000 x g at room temperature. The flow-through was discarded and 300µl of reagent 4 supplemented with 100% ethanol was added to each column before centrifugation for 1 minute at 13,000 x g. This step was repeated before further centrifugation for 4 minutes at 13,000 x g, to ensure complete drying. The purification columns were transferred to a nuclease free eppendorf tube and 92.48µl of reagent 5, prewarmed to 65°C, was added to the MCF-7 DNA sample, while 62.5µl was added to the WGA DNA to create concentrations of 20ng/µl. Samples were then incubated at room

212

temperature for 1 minute. The samples were next centrifuged for 1 minute at 13,000 x g, and the flow-through incubated for 20 minutes at 95°C. For the modification of methylated control sample 1, 5µl was used initially, and steps repeated similarly to the MCF-7 DNA, although 12µl of reagent 5 was utilised for the final elution. The bisulphite modified DNA was stored at -20°C.

5.2.6 Polymerase chain reaction

Asymmetric PCR was utilised to generate ssDNA of the EN1 gene promoter from MCF-7 and WGA DNA. For the first round of PCR, 2µl of MCF-7 or WGA DNA was combined with 12.5µl 2X PCR master mix (BIO-RAD, 1662119), and 6.5µl nuclease free water. Following this, 3µl of 10µM forward primer, and 1µl of 1µM reverse primer (Eurofins Genomic) were added to the PCR tube to give overall concentrations of 1.2 and 0.04µM (30:1 ratio) of forward and reverse primer respectively (Table 5.2), as shown to be optimum by Heiat et al. (2017). For control samples, a reduced volume of DNA (1µl) was utilised, with an adjusted volume of water (7.5µl).

Table 5.2 Asymmetric PCR forward and reverse primers.
Data taken from Heiat et al. (2017) and Koo et al. (2014).

Primer	5'-Sequence-3'	Concentration in PCR Tube (µM)	
		First Round	Second Round
Forward primer	ATTCAGTCCACAACAAYGTTGGTTGAGTTTATAA GTAGGATAGT	1.2	2
Reverse primer	ACRACCRCAACAACCAAACCCT	0.04	0.04

The cycler (VWR, UNO[96] Thermocycler) was programed for predenaturation at 95°C for 3 minutes, before a 30 cycle program of denaturation at 95°C for 1 minute, annealation at 50°C for 2 minutes, and extension at 72°C for 2 minutes. Final extension followed for 10 minutes at 72°C (Table 5.3).

Table 5.3 Thermocycler programming for first and second round PCR.

Cycle	Step	Function	Temperature (°C)	Time (minutes)
1	Step 1	Pre-denaturation	95	3
	Repeat 1 time			
2	Step 1	Denature	95	1
	Step 2	Anneal	50	2
	Step 3	Extend	72	2
	Repeat 30 times			
3	Step 1	Final Extension	72	10
	Repeat 1 time			

For the second round of PCR, 2µl of PCR product was combined with 12.5µl 2X PCR master mix, 4.5µl nuclease free water, 5µl 10µM forward primer and 1µl 1µM reverse primer. Primer ratio for second round PCR was 50:1, with final concentrations of 2µM and 0.04µM of the forward and reverse primers respectively (Heiat et al., 2017). Thermocycler programming was kept constant for the second round of PCR. This process was repeated using the primers included in the bisulphite modification kit. In this case, for the first round of PCR, 2µl of control primer 3A was utilised in place of the forward and reverse primers used in the Koo et al. (2014) study, and the nuclease free water adjusted to 9.5µl. For second round PCR, 2µl primer 3B was used in place of the Koo et al. (2014) primers and the water adjusted to 8.5µl (Table 5.4). Secondary PCR product was stored for one week at 4°C. To verify amplification, gel electrophoresis was conducted. Before this could be done, 10µl of Orange G loading buffer (BIO-RAD, 1662119) was added to 25µl of each secondary PCR product.

To complete all experiments, approximately 100µl of first round PCR product was required to produce 1000µl of secondary PCR product, as outlined in Table 5.5.

Table 5.4 Overview of PCR reaction mixes.

Tube	Volume in PCR tube (µl)					
	Converted control sample 1	Unconverted control sample 1	Control sample 2	No template negative control	MCF-7 DNA	WGA DNA
Using Koo et al. (2014) Primers						
First Round						
Converted control sample 1	1	-	-	-	-	-
Unconverted control sample 1	-	1	-	-	-	-
Control sample 2	-	-	1	-	-	-
MCF-7 DNA	-	-	-	-	2	-
WGA DNA	-	-	-	-	-	2
2x PCR master mix	12.5	12.5	12.5	12.5	12.5	12.5
Forward Primer	3	3	3	3	3	3
Reverse Primer	1	1	1	1	1	1
Water	7.5	7.5	7.5	1	6.5	6.5
Second Round						
First round PCR product	2	2	2	2	2	2
2x PCR master mix	12.5	12.5	12.5	12.5	12.5	12.5
Forward Primer	5	5	5	5	5	5
Reverse Primer	1	1	1	1	1	1
Water	4.5	4.5	4.5	4.5	4.5	4.5
Using Bisulphite Kit Primers						
First Round						
Converted control sample 1	1	-	-	-	-	-
Unconverted control sample 1	-	1	-	-	-	-
Control sample 2	-	-	1	-	-	-
MCF-7 DNA	-	-	-	-	2	-
WGA DNA	-	-	-	-	-	2
2x PCR master mix	12.5	12.5	12.5	12.5	12.5	12.5
Control primer 3A	2	2	2	2	2	2
Water	9.5	9.5	9.5	1	8.5	8.5
Second Round						
First round PCR product	2	2	2	2	2	2
2x PCR master mix	12.5	12.5	12.5	12.5	12.5	12.5
Control primer 3B	2	2	2	2	2	2
Water	8.5	8.5	8.5	8.5	8.5	8.5

Table 5.5 Overview of reagents required for asymmetric PCR.

First Round PCR Reagent	Volume (µl)	Second Round PCR Reagent	Volume (µl)
MCF-7 or WGA DNA	8	First Round PCR product	80
2X Master Mix	50	2X Master Mix	500
Forward Primer (10µM)	12	Forward Primer (10µM)	200
Reverse Primer (1µM)	4	Reverse Primer (1µM)	40
Nuclease free water	26	Nuclease free water	180
Total	100	Total	1000

It was estimated that 100µl of secondary PCR product contained 3,869ng of ssDNA. This was calculated by using the average fold increase in DNA after asymmetric PCR as reported by Citartan et al. (2012). Fold increases were reported as ranging from 20.0 to 27.5 (Citartan et al., 2012), with the mean calculated as 24.18. The estimated output of 3,869ng ssDNA was calculated by multiplying the mass of input DNA per µl by 24.18. For a sample where 2µl of 20ng/µl DNA was used in a 25µl PCR mix:

$$2µl \times 20ng/µl \ DNA = 40ng \ DNA$$

$$40ng/25µl = 1.6ng/µl$$

$$1.6ng/µl \times 24.18 = \textbf{38.69ng/µl second round PCR product}$$

5.2.7 Gel electrophoresis

Gel electrophoresis was conducted to ensure amplification of MCF-7 and WGA DNA. Amplification was confirmed by the presence of a band, while the absence of a band indicated improper amplication. To prepare 750ml of 1X TAE buffer, 15ml of 50X TAE buffer (BIO-RAD, 166-0742) was combined with 735ml of distilled water. For the 2% agarose gel, 100ml of 1X TAE buffer was combined with 2g agarose (Amresco, 0710) and heated until molten; 10µl of GelRed nucleic acid stain (Biotium, 41003-1) was then added to the molten agarose before gel casting. The remaining 1X TAE buffer was used as chamber buffer, and 10µl of each PCR product containing Orange G, and EZ load precision molecular

mass ruler (BIORAD, 170-8356) were loaded into each well, before running gel electrophoresis at 100V for 90 minutes. Images of the gel were taken using UVP BioDoc-It 220 Imaging system M-20V Transilluminator and Doc-It LS image analysis software (Version 8.6).

5.2.8 Using MCF-7 and WGA DNA in the electrochemical procedure

Bisulphite treated and asymmetrically amplified DNA samples were electrochemically tested similarly to synthetic oligonucleotide samples as outlined in sections 4.2.3 - 4.2.7, with minor modification. Due to the impracticalities of amplifying DNA for dilution in a 50ml volume, it was necessary to reduce the vessel size. By exchanging the vessel for a smaller container, a volume of 1.8ml was sufficient to cover the 2mm Au-RDE. Firstly a 1/3 relationship between secondary PCR product and buffer, as described by Koo et al. (2014), was tested. Following this, it was important to determine the minimal amount of secondary PCR product required to produce differential electrochemical signals (Table 5.6). Volumes of 600µl (1/3), 100µl (1/18), 50µl (1/36) and 10µl (1/180) of secondary PCR product were combined with 1X PBS to make an overall volume of 1.8ml. A volume of 100µl secondary PCR product in 1.8ml (1/18) was determined as optimal, as the greatest difference in signals were observed. Therefore this was used test combinations of MCF-7 and WGA DNA (0, 25, 50, 75 and 100%), similarly to the tests conducted using synthetic oligonucleotides. Statistical analyses were conducted by one-way ANOVA with a Tukey Post Hoc test on SPSS Version 23, as outlined in Chapter 4.

Table 5.6 Overview of fractional proportion of secondary PCR product in test solution.

Fractional proportion of secondary PCR product	Volume of secondary PCR product (µl)	Volume of PBS (µl)	Percentage of secondary PCR product	Estimated DNA (ng)	Estimated DNA Concentration (ng/µl)
1/3	600	1200	33.3%	23,214	12.90
1/18	100	1700	5.56%	3,869	2.15
1/36	50	1750	2.78%	1,934.5	1.07
1/180	10	1790	0.56%	386.9	0.215

5.3 Results

5.3.1 Using gel electrophoresis to detect DNA amplification

Gel electrophoresis was used to verify DNA amplification. The bands corresponding to DNA amplified in the presence of the primers included in the bisulphite kit were measured at 4.0cm while bands corresponding to DNA amplified in the presence of the Koo et al. (2014) primers measured 4.7cm (Figures 5.1 and 5.2). Using the equation $y = -0.3143x + 3.6306$, created by analysis of the ladder, and exchanging x for these migration distances, the calculated DNA fragment lengths were 236.3 and 142.4bp. These calculated fragment lengths are in good agreement to the 240bp length and 140bp length stated in the literature.
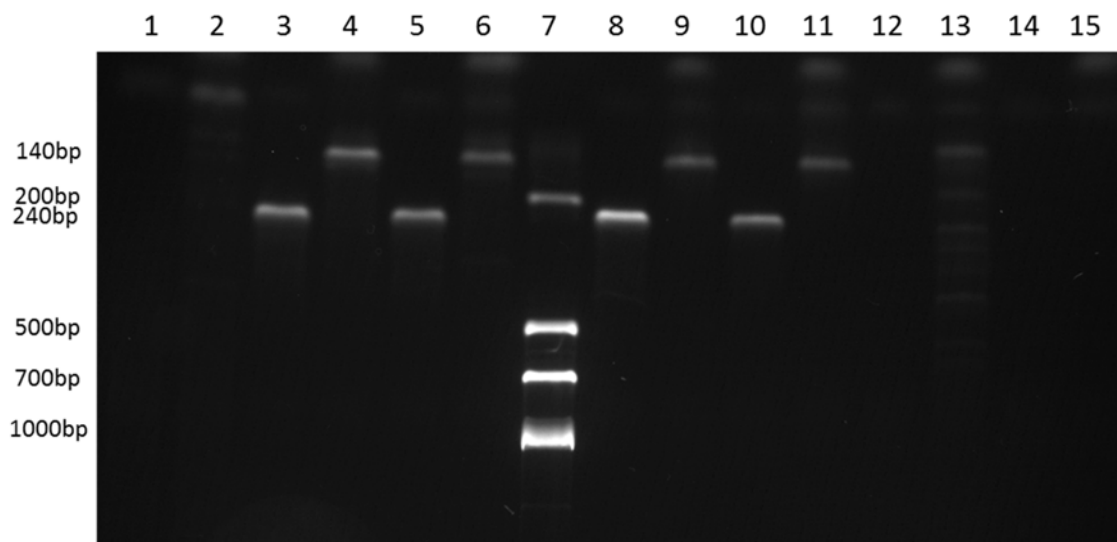
Figure 5.1 Gel electrophoresis analysis.
Electrophoresis run at 100V for 90 minutes on 2% agarose. Each lane contains: WGA DNA with 1) bisulphite kit primers 2) Koo et al. (2014) primers; bisulphite modified WGA DNA with 3) bisulphite kit primers, 4) Koo et al. (2014) primers; bisulphite modified MCF-7 DNA with 5) bisulphite kit primers, 6) Koo et al. (2014) primers; 7) ladder, standard bands 1000, 700, 500 and 200bp; bisulphite modified control sample with 8) bisulphite kit primers, 9) Koo et al. (2014) primers; pre-treated positive control with 10) bisulphite kit primers, 11) Koo et al. (2014) primers; untreated negative control sample with 12) bisulphite kit primers, 13) Koo et al. (2014) primers; DNA negative sample with 14) bisulphite kit primers, 15) Koo et al. (2014) primers.

Base Pairs	Log Base Pairs	Migration Distance (cm)
1000	3.00	1.95
700	2.85	2.55
500	2.70	3.00
200	2.30	4.20
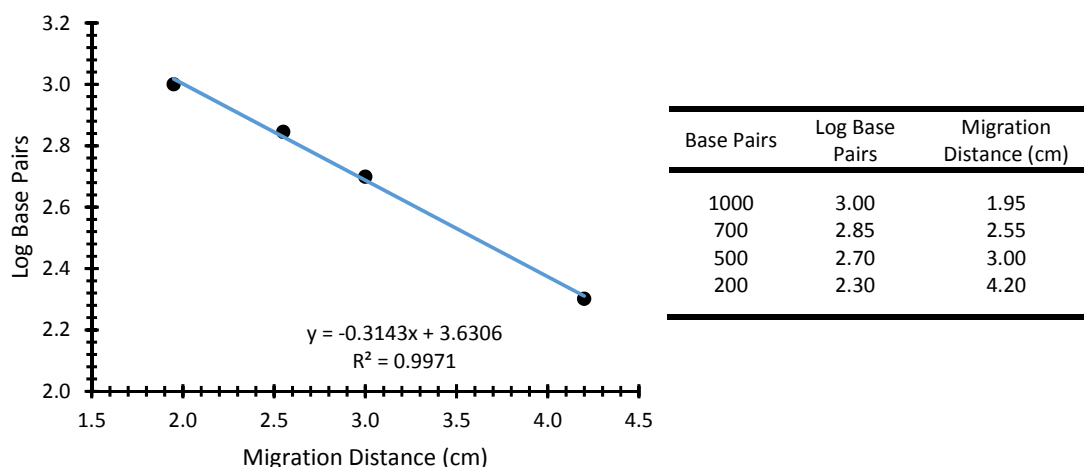
Figure 5.2 Gel electrophoresis ladder analysis.

5.3.2 MCF-7 and WGA DNA concentration

5.3.2.1 Effect of MCF-7 and WGA DNA concentration on impedance

Nyquist plots reveal the largest arc radii for 1/36 MCF-7 DNA, and 1/18 WGA DNA, however due to the reduced arc radius at 1/18 MCF-7, it can be predicted macroscopically that 1/18 secondary PCR product in 1X PBS was optimum for differentiating methylation status (Figure 5.3A and B). By analysing the Nyquist plots using Z-fit analysis to determine R_{ct}, it was established only 10μl of secondary PCR product in 1.8ml PBS (1/180) was required to detect the presence of MCF-7 and WGA DNA statistically ($p<0.05$) as shown in Tables A.11 and A.12. However, it was not possible to statistically distinguish the EN1 gene promoter amplicon from MCF-7 and WGA DNA until 100μl of secondary PCR product was used in 1.8ml 1X PBS (1/18), as outlined in Table A.13. This was also the ratio where the greatest difference in R_{ct} between MCF-7 and WGA DNA was observed (Figure 5.3C and D), where 1/18 MCF-7 solution corresponded to an R_{ct} value of 765.17 ±15.01Ω while 1/18 WGA corresponded to a greatly elevated value of 2073.67 ±28.54Ω (Table 5.7).
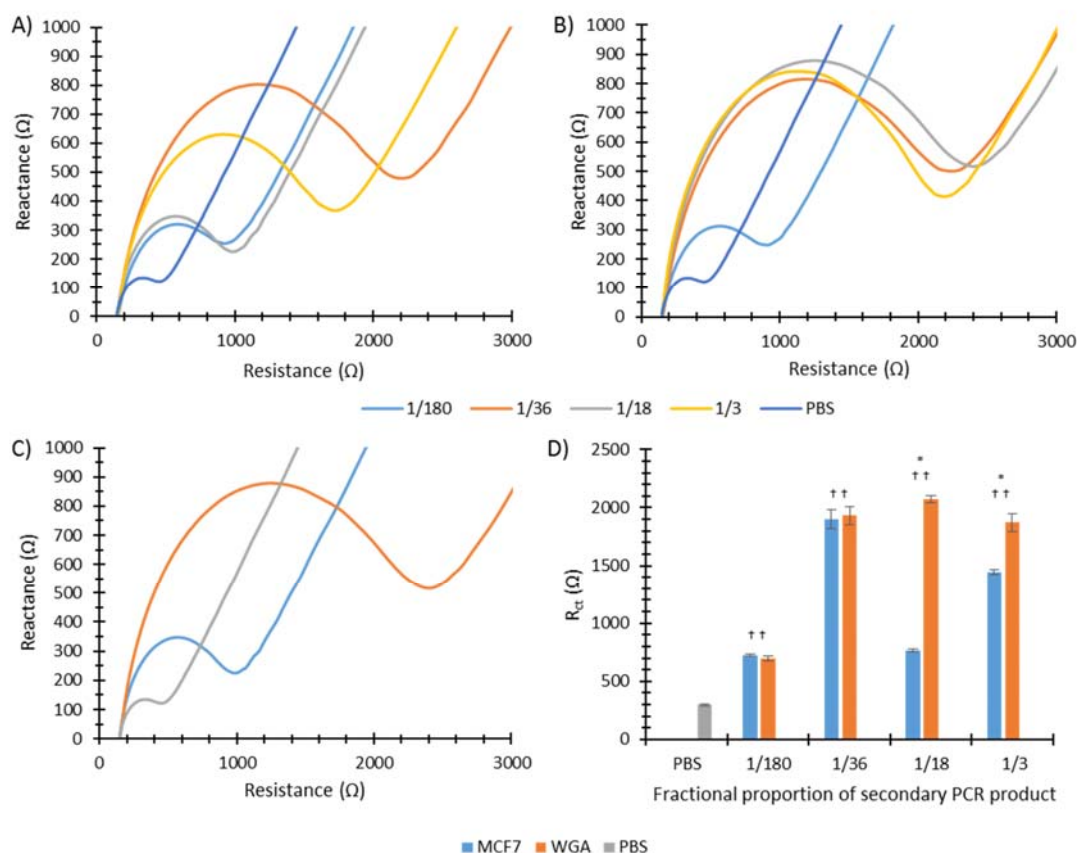
Figure 5.3 Effect fractional proportion of secondary PCR product in test solution on impedance.
Nyquist plots for a 2mm Au-RDE in 2.5mM ferrocyanide/2.5mM ferricyanide/1X PBS after rotation assisted adsorption at 2000rpm for 5 minutes in varying dilutions of amplicons of the EN1 gene promoter from A) MCF-7 DNA and B) WGA DNA. Plot C) compares the adsorption of 1/18 dilution Nyquist plots from A), and B) against 1X PBS (mean, n=3). D) R_{ct} (determined from Z-fit analysis of Nyquist plots) for a 2mm Au-RDE in 2.5mM ferrocyanide/2.5mM ferricyanide/1X PBS after rotation assisted adsorption at 2000rpm for 5 minutes in varying dilutions of amplicons of the EN1 gene promoter from MCF-7 and WGA DNA against 1X PBS. Mean ±SD (n=3). [*]Statistical difference between values for EN1 amplicons from MCF-7 and WGA DNA, when tested for using a one-way ANOVA ($p<0.05$), [†]statistical difference to value for baseline 1X PBS ($p<0.05$).

Table 5.7 Effect of fractional proportion of secondary PCR product in test solution on R_{ct}.
R_{ct} (determined from Z-fit analysis of Nyquist plots) for a 2mm Au-RDE in 2.5mM ferrocyanide/2.5mM ferricyanide/1X PBS after rotation assisted adsorption at 2000rpm for 5 minutes in varying dilutions of amplicons of the EN1 gene promoter from MCF-7 and WGA DNA against 1X PBS. Mean ±SD (n=3). *Statistical difference between values for EN1 amplicons from MCF-7 and WGA DNA, when tested for using a one-way ANOVA ($p<0.05$), †statistical difference to value for baseline 1X PBS ($p<0.05$).

Fraction	R_{ct} (Ω)								
	PBS			MCF-7 DNA			WGA DNA		
	Mean	SD	RSD (%)	Mean	SD	RSD (%)	Mean	SD	RSD (%)
0	296.27	10.30	3.48						
1/180				724.63†	9.58	1.32	698.03†	22.67	3.25
1/36				1901.33†	83.07	4.37	1931.67†	75.08	3.89
1/18				765.17*†	15.01	1.96	2073.67*†	28.54	1.38
1/3				1444.67*†	23.18	1.60	1871.33*†	77.36	4.13

5.3.2.2 Effect of MCF-7 and WGA DNA concentration on cyclic voltammetry

ΔE_p for both CV200 and CV50 generally increased as the amount of secondary PCR product in 1X PBS increased (Table 5.8). For both CV200 and CV50, ΔE_p was statistically different from background 1X PBS when >50µl of the EN1 gene promoter amplicon from MCF-7 or WGA DNA in 1.8ml 1X PBS (1/36) was analysed (Tables A.11 and A.12). Additionally at this level, amplicons from MCF-7 and WGA DNA were statistically distinguishable ($p<0.05$), as shown in Table A.13. However, the difference between ΔE_p values for MCF-7 and WGA DNA was greatest when 100µl secondary PCR product was used in 1X PBS (1/18). For instance, for CV200, ΔE_p was 152.7 ±2.8mV and 243.7 ±8.4mV for MCF-7 and WGA respectively. Again, ΔE_p was reduced for CV50 measurements with values of 133.4 ±2.3mV and 199.1 ±4.3mV for MCF-7 and WGA DNA respectively (Figure 5.4A and B).

Table 5.8 Effect of fractional proportion of secondary PCR product in test solution on peak to peak separation.

ΔE_p (mV) for CVs conducted with a 2mm Au-RDE in 2.5mM ferrocyanide/2.5mM ferricyanide/1X PBS after rotation assisted adsorption at 2000rpm for 5 minutes in varying dilutions of amplicons of the EN1 gene promoter from MCF-7 and WGA DNA, against 1X PBS at scan speeds of 200 and 50mV/s. Mean ±SD (n=3). *Statistical difference between values for EN1 amplicons from MCF-7 and WGA DNA, when tested for using a one-way ANOVA ($p<0.05$), †statistical difference to value for baseline 1X PBS ($p<0.05$).

| Fraction | ΔE_p (mV) | | | | | | | | |
| | PBS | | | MCF-7 DNA | | | WGA DNA | | |
	Mean	SD	RSD (%)	Mean	SD	RSD (%)	Mean	SD	RSD (%)
CV200									
0	108.5	2.5	2.32						
1/180				124.3	3.4	2.71	123.6	0.3	0.28
1/36				200.3*†	8.9	4.46	227.6*†	12.6	5.55
1/18				152.7*†	2.8	1.80	243.7*†	8.4	3.46
1/3				213.7*†	5.1	2.40	264.9*†	5.7	2.15
CV50									
0	91.4	1.9	2.05						
1/180				96.5	1.1	1.10	92.8	1.8	1.92
1/36				155.3*†	5.9	3.78	177.9*†	8.5	4.75
1/18				133.4*†	2.3	1.70	199.1*†	4.3	2.16
1/3				190.5*†	4.6	2.39	234.6*†	11.5	4.92
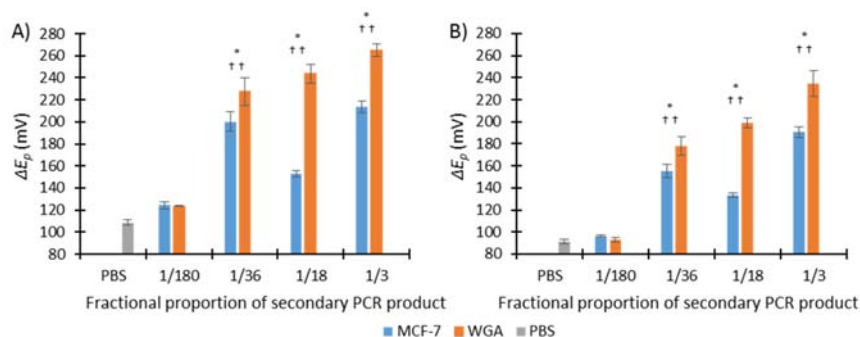
Figure 5.4 Effect of fractional proportion of secondary PCR product in test solution on peak to peak separation.

ΔE_p (mV) for CVs conducted with a 2mm Au-RDE in 2.5mM ferrocyanide/2.5mM ferricyanide/1X PBS after rotation assisted adsorption at 2000rpm for 5 minutes in varying dilutions of amplicons of the EN1 gene promoter from MCF-7 and WGA DNA, against 1X PBS at scan speeds of 200 and 50mV/s. Mean ±SD (n=3). *Statistical difference between values for EN1 amplicons from MCF-7 and WGA DNA, when tested for using a one-way ANOVA ($p<0.05$), †statistical difference to value for baseline 1X PBS ($p<0.05$).

5.3.2.3 Effect of MCF-7 and WGA DNA concentration on DPV
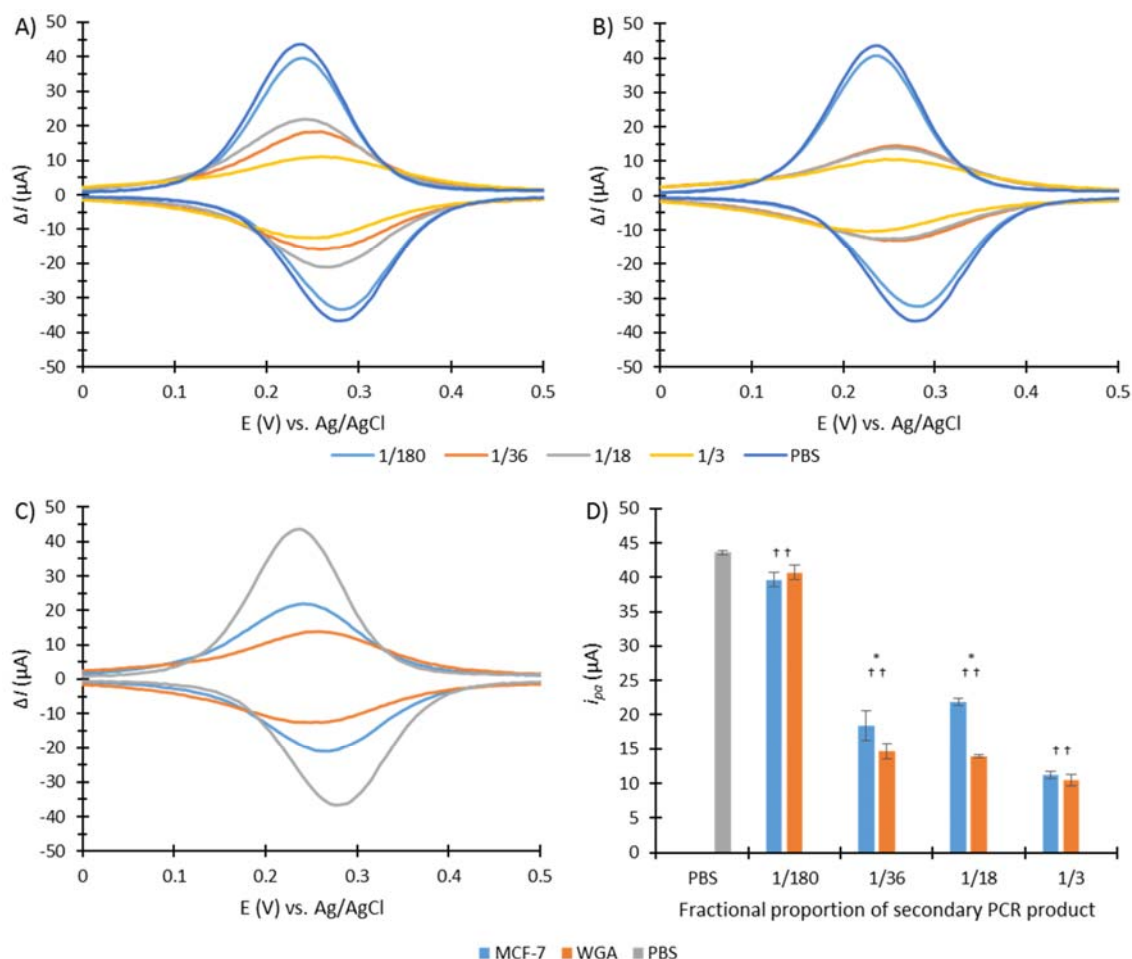
Figure 5.5 Effect of fractional proportion of secondary PCR product in test solution on DPV.
DPV signals for a 2mm Au-RDE in 2.5mM ferrocyanide/2.5mM ferricyanide/1X PBS after rotation assisted adsorption at 2000rpm for 5 minutes in varying dilutions of amplicons of the EN1 gene promoter from A) MCF-7 DNA and B) WGA DNA. Plot C) compares 1/18 dilution of EN1 gene promoter amplicon from MCF-7 and WGA DNA against 1X PBS DPV signals (mean, n=3). D) i_{pa} obtained with 2mm Au-RDE in 2.5mM ferrocyanide/2.5mM ferricyanide/1X PBS after rotation assisted adsorption at 2000rpm for 5 minutes in varying dilutions of amplicons of the EN1 gene promoter from MCF-7 and WGA DNA against 1X PBS. Mean ±SD (n=3). *Statistical difference between values for EN1 amplicons from MCF-7 and WGA DNA, when tested for using a one-way ANOVA ($p<0.05$), †statistical difference to value for baseline 1X PBS ($p<0.05$).

A decrease in i_{pa} was typically observed as the amount of secondary PCR product in 1.8ml 1X PBS increased (Figure 5.5A and B, and Table 5.9). Remarkably >10µl of MCF-7 or WGA DNA in 1.8ml was required to bring about a statistical difference when compared to 1X PBS (Table A.11 and A.12). However 50-100µl of secondary PCR product in 1.8ml 1X PBS was required to differentiate the two amplicons using DPV (p<0.05), as described in Table A.13. The greatest difference was observed for 1/18 solutions, where i_{pa} for MCF-7 DNA was 21.94±0.53µA compared with 13.90 ±0.18µA for WGA DNA (Figure 5.5C and D).

Table 5.9 Effect of fractional proportion of secondary PCR product in test solution on peak current. i_{pa} obtained with 2mm Au-RDE in 2.5mM ferrocyanide/2.5mM ferricyanide/1X PBS after rotation assisted adsorption at 2000rpm for 5 minutes in varying dilutions of amplicons of the EN1 gene promoter from MCF-7 and WGA DNA against 1X PBS. Mean ±SD (n=3). *Statistical difference between values for EN1 amplicons from MCF-7 and WGA DNA, when tested for using a one-way ANOVA (p<0.05), [†]statistical difference to value for baseline 1X PBS (p<0.05).

Fraction	i_{pa} (µA)								
	PBS			MCF-7 DNA			WGA DNA		
	mean	SD	RSD (%)	mean	SD	RSD (%)	mean	SD	RSD (%)
0	43.61	0.25	0.58						
1/180				39.61[†]	1.05	2.65	40.73[†]	1.08	2.65
1/36				18.47[*†]	2.17	11.77	14.66[*†]	1.11	7.55
1/18				21.94[*†]	0.53	2.42	13.90[*†]	0.18	1.32
1/3				11.16[†]	0.53	4.74	10.44[†]	0.81	7.78

5.3.3 Percent methylation

5.3.3.1 Effect of percent methylation on impedance
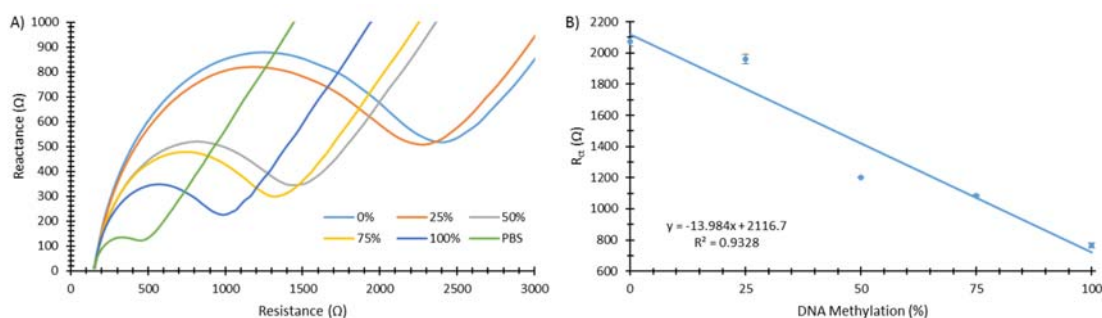
Figure 5.6 Effect of MCF-7/WGA percentage in test solution on impedance.
A) Nyquist plots for a 2mm Au-RDE in 2.5mM ferrocyanide/2.5mM ferricyanide/1X PBS after rotation assisted adsorption at 2000rpm for 5 minutes in varying % methylation solutions (mean, n=3). Methylated and unmethylated DNA derived from amplicons of the EN1 gene promoter from MCF-7 and WGA DNA respectively. Secondary PCR product of amplicons total 1/18 in solution. B) R_{ct} (determined from Z-fit analysis of Nyquist plots) for a 2mm Au-RDE in 2.5mM ferrocyanide/2.5mM ferricyanide/1X PBS after rotation assisted adsorption at 2000rpm for 5 minutes in varying % methylation solutions. Mean ±SD (n=3).

To determine if the experimental procedure was effective at detecting DNA methylation in heterogeneous solutions of MCF-7 or WGA DNA, combinations of DNA were tested, at a total concentration of 1/18 secondary PCR product in 1.8ml 1X PBS. The Nyquist plot revealed increased arc radii as DNA methylation decreased (Figure 5.6A). These arc radii were significantly more spread than the results gained using the synthetic oligonucleotides. Furthermore, as with the synthetic oligonucleotides, a negative correlation was observed between % methylation and R_{ct}, and similarly to the results of the macroscopic inspection, the effect of percentage methylation was more pronounced (Table 5.10). This relationship was described by the equation $y = -13.984x + 2116.7$, and the linear correlation represented the data well, with R^2=0.9328 (Figure 5.6B). Importantly, the R_{ct} values for 0, 25, 50, 75, and 100% methylated solutions adsorbed onto the 2mm Au-RDE for 5

minutes at 2000rpm was were all statistically different from one another ($p<0.05$) as shown in Table A.14.

Table 5.10 Effect of MCF-7/WGA percentage in test solution on R$_{ct}$.
R_{ct} (determined from Z-fit analysis of Nyquist plots) for a 2mm Au-RDE in 2.5mM ferrocyanide/2.5mM ferricyanide/1X PBS after rotation assisted adsorption at 2000rpm for 5 minutes in varying % methylation solutions. Methylated and unmethylated DNA derived from amplicons of the EN1 gene promoter from MCF-7 and WGA DNA respectively. Secondary PCR product of amplicons total 1/18 in solution. Mean ±SD (n=3).

% methylation	R_{ct} (Ω)		
	Mean	SD	RSD (%)
PBS	296.27	10.30	3.48
0	2073.67	28.54	1.38
25	1962.00	31.43	1.60
50	1203.67	1.53	0.13
75	1083.00	7.55	0.70
100	765.17	15.01	1.96

5.3.3.2 Effect of percent methylation on cyclic voltammetry

Similar to the experiments conducted with the synthetic oligonucleotides, a negative trend between % methylation in heterogeneous solutions and ΔE_p was observed when using the 140 base EN1 region from MCF-7 and WGA DNA as the methylated and unmethylated standards (Figure 5.7A and B, and Table 5.11). Again, the effect of using this DNA was more pronounced than the effect seen for the synthetic oligonucleotides. Using ΔE_p data from CV200 and CV50 was less effective at differentiating % methylation than impedance data, as ΔE_p from CV200 for 0% vs. 25% and 50% vs. 75% were not statistically distinguishable as shown in Table A.14. For CV50 only 50% vs. 75% were not statistically distinguishable ($p>0.05$).

Table 5.11 Effect of MCF-7/WGA percentage in test solution on peak to peak separation.
ΔE_p (mV) for CVs conducted with a 2mm Au-RDE in 2.5mM ferrocyanide/2.5mM ferricyanide/1X PBS after rotation assisted adsorption at 2000rpm for 5 minutes in varying % methylation solutions at scan speeds of 200 and 50mV/s. Methylated and unmethylated DNA derived from amplicons of the EN1 gene promoter from MCF-7 and WGA DNA respectively. Secondary PCR product of amplicons total 1/18 in solution. Mean ±SD (n=3).

% Methylation	ΔE_p (mV)		
	Mean	SD	RSD (%)
CV200			
PBS	108.5	2.5	2.32
0	243.7	8.4	3.46
25	234.0	1.5	0.62
50	183.7	4.2	2.30
75	175.3	5.2	2.99
100	152.7	2.8	1.80
CV50			
PBS	91.4	1.9	2.05
0	199.1	4.3	2.16
25	180.8	4.1	2.26
50	159.9	6.6	4.11
75	153.7	1.5	0.95
100	133.4	2.3	1.70
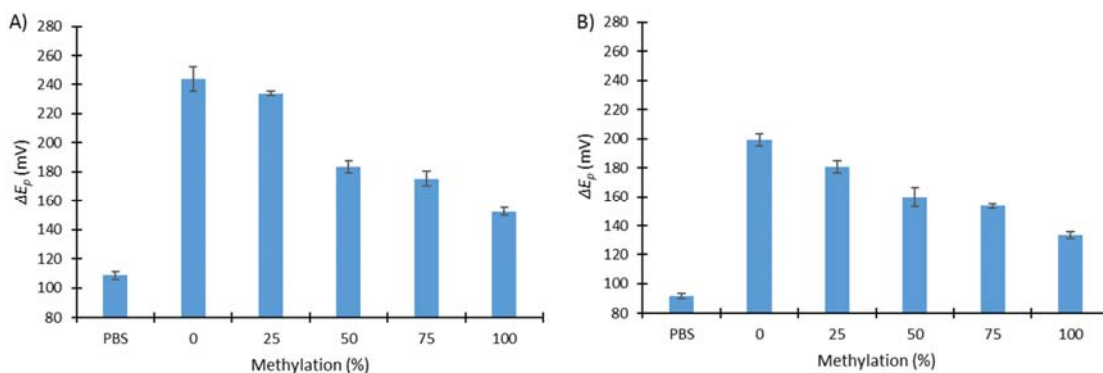
Figure 5.7 Effect of MCF-7/WGA percentage in test solution on peak to peak separation.
ΔE_p (mV) for CVs conducted with a 2mm Au-RDE in 2.5mM ferrocyanide/2.5mM ferricyanide/1X PBS after rotation assisted adsorption at 2000rpm for 5 minutes in varying % methylation solutions at scan speeds of A) 200mV/s and B) 50mV/s. Methylated and unmethylated DNA derived from amplicons of the EN1 gene promoter from MCF-7 and WGA DNA respectively. Secondary PCR product of amplicons total 1/18 in solution. Mean ±SD (n=3).

5.3.3.3 Effect of percent methylation on DPV

i_{pa} increased as % methylation in a heterogeneous solution increased, similarly to results seen when synthetic oligonucleotides were used, and again the effect was more pronounced (Figure 5.8A and B). For instance, when using MCF-7 and WGA DNA, i_{pa} ranged between 13.90 ±0.18 and 21.94 ±0.53 for 0-100% methylation (Table 5.12), whereas using synthetic oligonucleotides produced results ranging from 18.34 ±0.58 to 20.89 ±0.30. Despite this increase in range, 0% vs. 25%, 0% vs. 50%, and 25% vs. 50% were not statistically different when analysed using a one-way ANOVA with a Tukey post-hoc test (p>0.05), as described in Table A.14.
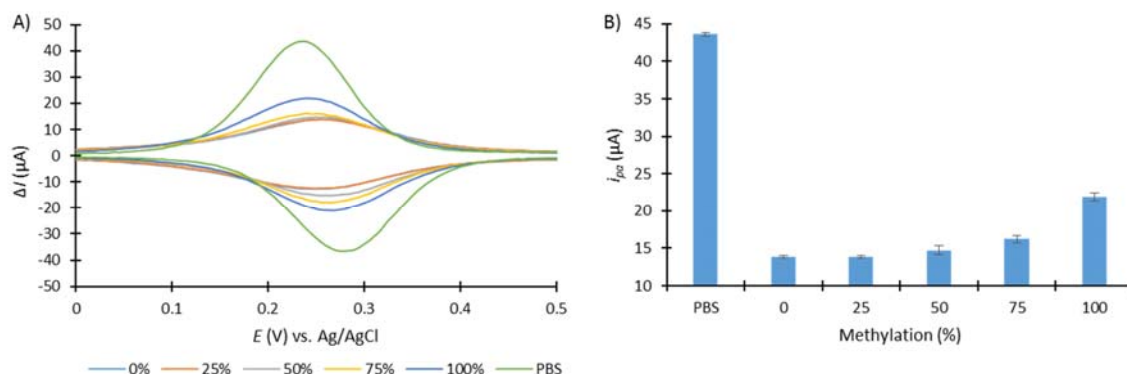
Figure 5.8 Effect of MCF-7/WGA percentage in test solution on DPV.
A) DPV signals and B) i_{pa} (µA) obtained with a 2mm Au-RDE in 2.5mM ferrocyanide/2.5mM ferricyanide/1X PBS after rotation assisted adsorption at 2000rpm for 5 minutes in varying % methylation solutions. Methylated and unmethylated DNA derived from amplicons of the EN1 gene promoter from MCF-7 and WGA DNA respectively. Secondary PCR product of amplicons total 1/18 in solution. Mean ±SD (n=3).

Table 5.12 Effect of MCF-7/WGA percentage in test solution on peak current.
i_{pa} (µA) obtained with a 2mm Au-RDE in 2.5mM ferrocyanide/2.5mM ferricyanide/1X PBS after rotation assisted adsorption at 2000rpm for 5 minutes in varying % methylation solutions. Methylated and unmethylated DNA derived from amplicons of the EN1 gene promoter from MCF-7 and WGA DNA respectively. Secondary PCR product of amplicons total 1/18 in solution. Mean ±SD (n=3).

% Methylation	i_{pa} (µA)		
	Mean	SD	RSD (%)
PBS	43.61	0.25	0.58
0	13.90	0.18	1.32
25	13.87	0.15	1.10
50	14.74	0.57	3.85
75	16.21	0.45	2.75
100	21.94	0.53	2.42

5.4 Discussion

The electrochemical techniques explored in this chapter were capable of detecting DNA methylation in samples derived from the human breast cancer cell line MCF-7, when compared to unmethylated WGA DNA. The optimum ratio of secondary PCR product to PBS was 1/18, which corresponded to 100µl DNA diluted with 170µl 1X PBS. To create 100µl of secondary PCR product, <1µl of bisulphite treated MCF-7 DNA was required. Table 5.13 outlines the reagents required for the amplification 1µl of bisulphite modified DNA to generate 100µl secondary PCR product through asymmetric PCR. Assuming the same cell density, and efficacy of DNA extraction and bisulphite modification when using reduced volumes, only 27nl of cell culture, containing 14.8 cells could be sufficient to extract 49.99ng DNA, and produce 1µl of 20ng/µl bisulphite modified DNA. Thus the low levels of DNA required, as described here, could be a factor in deciding which technology to use to detect DNA methylation. There are several technologies which require larger concentrations of DNA which could limit their applicability in some instances; for example ELISA based kits require >100ng DNA, while the DNA restriction digest based technique LUMA requires 250-500ng DNA (Kurdyukov and Bullock, 2016).

Table 5.13 Minimal quantities of DNA and reagents required for asymmetric PCR for successful electrochemical detection of methylation status.

Reagent	Volume (μl)	Reagent	Volume (μl)
Round 1		Round 2	
MCF-7 or WGA DNA	1	First Round PCR product	8
2X Master Mix	6.25	2X Master Mix	50
Forward Primer (10μM)	1.5	Forward Primer (10μM)	20
Reverse Primer (1μM)	0.5	Reverse Primer (1μM)	4
Nuclease free water	3.25	Nuclease free water	18
Total	12.5	Total	100

Using DPV, Koo et al. (2014) found the methylation detection level in heterogeneous solutions of methylated MCF-7 DNA and unmethylated WGA DNA, was 10%, however it is unclear if statistical testing was used in this determination. Additionally, Koo et al. (2014) state an RSD of 5.8% was calculated for these 10% heterogeneous samples, indicating good reproducibility. Within the work outlined in this chapter, it was shown that all i_{pa} derived from DPV had an RSD <3.85%, thus has increased reproducibility. However, it was found that methylation had to be >75% to statistically be distinguished from unmethylated samples using DPV. R_{ct} and ΔE_p had lower limits of detection; 25% for R_{ct} (RSD <1.96%) and ΔE_p for CV50 (RSD <4.11%), and 50% for CV200 (RSD <3.46%). From this it can be concluded that R_{ct} derived from EIS may be a more appropriate electrochemical technique for detecting methylation status of heterogeneous samples due to its increased sensitivity and reliability. Interestingly, ΔE_p derived from both CV200 and CV50 were most effective at differentiating between methylated and unmethylated homogeneous samples. However R_{ct} derived from EIS, and i_{pa} derived from DPV, were more sensitive at detecting lower concentrations of homogeneous methylated and unmethylated samples.

Signals were significantly greater for human derived DNA compared to the synthetic oligonucleotides. This finding was mirrored by Koo et al. (2014). This could be due to the greater length of the ssDNA derived from humans; 140 bases in comparison to 30 bases. Alternatively the unknown MCF-7 and WGA ssDNA concentration could have played a role in this. However, the significant elevation in R_{ct}

and ΔE_p and decrease in DPV is likely due to increased passivation; whether this be due to ssDNA size or concentration. Further optimisation of this procedure is required before the technique can be applied to patient samples. These steps include purifying and quantifying the amplified ssDNA, optimising the adsorption step for the 140 base MCF-7 ssDNA, and further testing the sensitivity of the assays. Once this has been completed, this proof of concept can be expanded to other cell lines and gene promoters, and applied to patient samples.

This research has indicated that DNA methylation can be detected in heterogeneous samples. It is important this is the case as cancerous masses often exhibit intratumour heterogeneity (Litovkin et al., 2015). However, there may be an additional benefit from this finding. This technology may be useful in the detection and monitoring of tumours through a non-invasive blood test, rather than through the more invasive traditional biopsy. Tumour DNA is often released into circulation as cell free fragments of DNA, and this circulating tumour DNA (ctDNA) has been suggested as a potential biomarker for cancer (Warton and Samimi, 2015). Bettegowda et al. (2014) determined ctDNA was detectable in >75% of patients with metastatic cancers, including, but not limited to, bladder, ovarian, breast, colorectal, and hepatocellular cancer. Additionally, a correlation between the number of cancer patients with detectable levels of ctDNA and cancer stage was reported; ctDNA was detected in 47% of patients with stage 1 cancer, 55% of patients with stage 2 cancer, 69% of patients with stage 3 cancer, and 82% of patients with stage 4 cancer. Furthermore, the amount of detectable ctDNA was positively correlated with grade, and negatively correlated with two year survival rate (Bettegowda et al., 2014). Therefore, this technology could be used to indicate disease severity and prognosis, in addition to determining the presence of the disease.

Importantly, Jahr et al. (2001) report circulating DNA in cancer patients was on average 219ng/ml (range 10-1200ng/ml) while most control individuals exhibited <2ng/ml (Jahr et al., 2001). Therefore, based on the above calculation, the developed sensor should be sensitive enough to detect the presence of cancer given the collection of a standard 5ml blood sample. However, it is important to

recognise the importance of the results of Fujiwara et al. (2005) who used methylation specific PCR to determine ctDNA methylation, as a biosensor for lung cancer. Results show ≥1 out of 5 genes analysed exhibited aberrant methylation in 77% of lung biopsies from patients, whereas the same result was only observed in 49.5% of samples derived from serum (Fujiwara et al., 2005). Similar findings were reported by Jahr et al. (2001), who outlined only 44% of serum samples from cancer patients exhibited hypermethylation of the CDKN2A gene promoter. Therefore, these so called liquid biopsies may have reduced sensitivities than traditional biopsies. However, this could be due to the methodologies employed to detect DNA methylation.

In this work, methylation of the EN1 gene was analysed for the detection of breast cancer, however it is vital to realise that this technology could be applied to alterative gene promoters for the detection of cancer, such as BRCA1 for breast cancer (Zhang and Long, 2015). Furthermore, it is important to recognise the potential of this technology if it were applied to commonly methylated gene promoters from a larger scope of age-related disease; such as the INS gene promoter in T2DM (Yang et al., 2011), the OPRD1 gene promoter in AD (Ji et al., 2017), the SLC6A4 gene promoter in obesity (Zhao et al., 2012), or the ABCA1 gene promoter in CAD (Guay et al., 2014), which have all been shown to be hypermethylated during disease. Moreover, this technology could be used to estimate age itself. This is a logical assumption to make, as Horvaths epigenetic clock describes the methylation trend of 353 CpG sites with age, and has an accuracy of 3.6 years. Within this model, methylation of 193 CpG sites positively correlate with age, and 160 CpG sites negatively correlate with age. Given further optimisation of the electrochemical procedure outlined, it may be possible to use these methods to determine epigenetic age (Horvath, 2013).

5.5 Conclusion

Three electrochemical techniques were analysed to determine their effectiveness at detecting DNA methylation from methylated MCF-7 DNA and unmethylated WGA DNA. R_{ct} derived from EIS was superior at detecting DNA methylation in heterogeneous samples compared with ΔE_p from CV at 200 and 50mV/s, and i_{pa} derived from DPV. While this is important due to the intratumour heterogeneity often observed, this simple and inexpensive electrochemical technique could also be useful in diagnosis of cancer through a non-invasive liquid biopsy i.e. from ctDNA in blood. This work has also potentially provided a foundation for the application of this test for the detection of other age related diseases such as AD, CAD, and T2DM, where aberrant methylation is observed. Moreover the literature indicates testing in this manner could be used to diagnose the stage of disease and survival rate.

Chapter 6 Discussion

6.1 Overview

With an ageing population, there has been a significant increase in age related morbidity, due to the onset of conditions such as CVD, neurodegeneration, cancer, and T2DM (Prince et al., 2015). Due to the complexities of ageing and age related disease, there is a precedence for the development of investigative techniques which enable, the elucidation of disease pathogenesis, and clarification of interactions with factors such as diet and genetics. There is also an urgency to develop inexpensive and rapid diagnostic techniques, which exhibit improved sensitivity, to allow the diagnosis of early stage disease. In this work, two age related diseases and their associated underpinning mechanisms were investigated.

The first aim of this work was to expand an existing mathematical model of cholesterol metabolism and investigate the effect of intrinsic and extrinsic factors which influence cholesterol metabolism and CVD risk. This is because changes to cholesterol metabolism with age have strongly been associated with an increased risk for CVD (Gould et al., 2007), with figures from 2014 indicating it was the leading cause of death in people over 85 years old (Townsend et al., 2015).

The second aim was to use synthetic ssDNA, designed to represent methylated and unmethylated variants of a section of the EN1 gene, to optimise electrochemical procedures. Closely related to this, the third aim was to use the optimised electrochemical procedures to determine if DNA methylation, in the breast cancer cell line MCF-7, could be detected. Aberrations to DNA methylation are often observed in disease including cancer; specifically hypermethylation within the gene promoters, and hypomethylation globally (Mendizabal and Yi, 2016; Yang et al., 2014). In 2016, cancer was the leading cause of death in both males and females in England and Wales (OFNS, 2017). Therefore, the development of a sensor which can detect and monitor DNA methylation aberrations rapidly and simply, may promote an improvement in patient outcome, in addition to lowering costs. In this case, methylation of the EN1 gene was investigated, as hypermethylation of this gene promoter has been

observed in numerous cancers, including breast cancer (Bell et al., 2011; Carrascosa et al., 2014; Devaney et al., 2011; Mayor et al., 2009).

This work has outlined how mathematical modelling can be a useful tool for studying cholesterol metabolism and how diet and genetics play a role in modulating lipoprotein levels and disease risk. This work has also highlighted how electrochemical techniques can be utilised to rapidly detect DNA methylation as a sensor for cancer. In this chapter, these techniques are discussed and research findings critically analysed.

6.2 The mathematical model of cholesterol metabolism and ageing

In recent years mathematical modelling has come to the fore as a useful tool for understanding biological systems, by aiding hypothesis formation, elucidating mechanisms, and identifying drug targets. Due to the complexities of studying ageing experimentally, modelling has been widely applied to the study of numerous biological systems. Ageing has a significant impact on cholesterol metabolism, which in turn perturbs the lipoprotein profile, thus influencing cardiovascular health (Morgan et al., 2016a). Mathematically modelling this system enables the complex interactions to be analysed. The model outlined in Chapter 3 contained eight compartments, 144 species, 144 reactions, and 266 parameters, and encompassed dietary intake, cholesterol absorption, cholesterol biosynthesis, RCT, lipoprotein dynamics, and the enterohepatic circulation of bile acids. The model examined cholesterol metabolism holistically, rather than at the molecular or cellular level, enabling the production of clinically meaningful results. Thus results gained through simulation are comparable blood parameters, such as LDL-C and HDL-C, gained from randomised control trials, population analyses, and individual reports (Lin and Connor, 1980).

The updated model of cholesterol metabolism was used to study the impact of ageing, cholesterol feeding, SFA feeding, and CETP genotype. The model behaved as a hypo-responder to cholesterol feeding, which is biologically relevant as LDL-C is unaffected by dietary cholesterol in 62.5% of the population (Herron et al., 2003). However, by manipulating seven parameters simultaneously, it was shown that the model was sensitive to SFA feeding. This is clinically significant as feeding studies indicate SFA has more of an impact on cholesterol levels than dietary cholesterol (He and Fernandez, 1998; Herron et al., 2003). The model was also able to replicate the ageing process, through the modification of four parameters. These modifications were: an increase in LDLr degradation (K_1), and decreases in bile acid deconjugation (V_{max}), NPC1L1 degradation (K_1), and CYP7A1 activity (V_{max}). These reactions were chosen as an earlier literature review suggested they were key mechanisms affected by the ageing process. It is possible that additional mechanisms, including cholesterol synthesis and cholesterol esterification may also be affected by ageing, however these were not included in this study; this limitation is discussed in section 6.2.2.1. The model showed that ageing resulted in an increase in LDL-C. However, the presence of a genotype conferring low CETP activity (Barzilai et al., 2003), led to a slower increase in LDL-C with age. Additionally, it was shown that the cholesterol biosynthesis pathway was robust to parameter change, something which has been found in other work (Pool et al., 2018). Moreover, this work highlighted the absence of *a priori* data and need for further experimental work, to enable the advancement of ageing research through the use of systems biology. To this end, the model was encoded in SBML and submitted to the BioModels database, to allow the future utilisation and adaption of this work. It is important models are made available in easily accessible formats such as this to ensure the continual development of our knowledge through systems biology.

6.2.1 Model limitations

While the updated model outlined in Chapter 3 included 96 additional mechanisms, elucidating some key aspects of cholesterol metabolism, there were several limitations to the model. Firstly, numerous species initial concentrations and parameter values were assumed due to a lack of experimental kinetic data available. It is clear from Figure 3.12B that slight variation to assumed parameters can have a significant impact on the model, while alterations to the known parameters had little impact. Thus, simulations relating to assumed parameter values may have influenced the results. For instance, the model behaved as a hypo-responder. Although 62.5% of individuals are classified as a hypo-responder to cholesterol feeding (Herron et al., 2003), the mechanisms by which this was regulated, may not be realistic. LDL-C did not significantly rise with an increase in dietary cholesterol up to a three-fold level. However, the hepatic pool of free cholesterol rose by 85.25% over an 11 week period. Although there is some evidence to substantiate this finding; that increased dietary cholesterol induces an increase in hepatic cholesterol, while not influencing the lipoprotein profile (Quintao et al., 1971), there are numerous studies that have opposing findings (Ohtani et al., 1990; Wang et al., 2010). It is possible the use of many assumed parameters was responsible for this significant accumulation of hepatic cholesterol during cholesterol feeding. Furthermore, the model was unresponsive to changes to HMG CoA reductase inhibition (data not shown), when the effect of statins was investigated. While again, this is possible, as experimental work has indicated that 10.8% of people are unresponsive to this drug (Ridker et al., 2016), it is likely the robustness of the cholesterol biosynthesis pathway, due to the availability of experimental kinetic data, and sensitivity of the assumed reactions, is responsible. This is substantiated by Palvast et al. (2015), who investigated the impact of simulated statin use using the original Mc Auley et al. (2012) model, by lowering hepatic cholesterol synthesis by 75%. After 6 weeks, LDL-C was reduced by 14%, and after 12 months, LDL-C had further reduced, by 33% (Paalvast et al., 2015).

Secondly, there were many mechanisms which were described by a condensed series of reactions, while other pathways were fully elucidated. For instance, the lanosterol pathway of cholesterol biosynthesis was fully mechanised, while receptor recycling was only denoted by two reactions; synthesis and degradation. In the case of NPC1L1 recycling, the membrane bound SREBP2 has been implicated as a transcriptional factor, regulated by cellular cholesterol. Low cellular cholesterol levels induce the activation of SREBP2, which in turn migrates to the nucleus, causing increased NPC1L1 gene expression, thus increasing cholesterol absorption (Alrefai et al., 2007). This feedback loop, and important transcription factor, were not incorporated into the model. Furthermore, there have been numerous nuclear receptors implicated in cholesterol absorption such as peroxisome proliferator–activated receptor (PPAR)α, PPARδ, LXR, and retinoid X receptor (RXR), which again were excluded (Jia et al., 2011). Additionally, the aforementioned SREBP2 also plays a role in LDLr recycling. In this instance, low cellular levels of cholesterol cause the cleavage of inactive SREBP2, which in turn leads to the production of LDLr mRNA, and thus increased LDLr and subsequent LDLC uptake alleviate this issue (Attie and Seidah, 2005). In addition, SREBP2 induces the transcription of PCSK9 which causes the lysosomal degradation of LDLr to prevent the unregulated expansion of LDLr numbers (Mousavi et al., 2009). Again this transcription factor, which also plays a role in upregulating cholesterol synthesis, was not included.

Thirdly, many of the kinetic functions were also assumed and thus provided simplistic representations of several mechanisms. For instance, the use of mass action rate laws to describe receptor synthesis and degradation fall short of the mathematics that underpin the complex interactions of receptor recycling. However, it is important to note that these processes were simplified to remove the need to include transcriptional factors and gene expression, thus reducing the issues associated with producing multiscale models. However, quantities and parameters were scaled up to organ/compartment size in a crude manner, assuming equal distribution throughout the tissue, and undisturbed function with increased compartment size.

6.2.2 Model extension and future work

There were many aspects of cholesterol metabolism which were investigated in this work; these include the influence of diet, ageing and genotype. Further investigations such as pharmacological investigations were not conducted for a number of reasons. Firstly, there was overlap in the way these changes were modelled. For instance, CETP inhibitors reduce the rate of conversion of HDL-C to LDL-C and VLDL-C, while some genotypes can lower CETP activity. These two scenarios would be modelled in a similar way and results would be repetitious. Secondly, the model was robust to change in many of the mechanisms as discussed above, therefore in many instances, single perturbations did not impact LDL-C. However, due to the extensive work completed in this area of ageing research, there are several avenues future research could take, using this work as a foundation. Below are three examples of mathematical models which could use the work completed in Chapter 3 as a basis to further investigate the age related disruption of cholesterol metabolism with age.

6.2.2.1 Investigating additional age related changes to cholesterol metabolism

6.2.2.1.1 Investigating the age associated increase of ROS on HMG CoA reductase activity

The accumulation of free radical damage, is a key principle in the mechanistic reasoning for ageing, as suggested by Harman (Harman, 1956; Harman, 1972). Produced mainly in the mitochondria, free radicals induce oxidative damage, including to the mitochondria, which in turn leads to further mitochondrial dysfunction and ROS production. The use of antioxidants can therefore be useful in reducing oxidative damage. This was illustrated in Kirkwood and Kowald's (2012) model which showed increased amounts of antioxidants lowered mitochondrial DNA damage (Kirkwood and Kowald, 2012). Experimentally, it has been shown that antioxidants can improve mitochondrial respiration, reduce oxidative stress and IL-6, and reduce markers for organ dysfunction (Lowes et al., 2013). A recent review outlined that antioxidants may also ameliorate exercise induced oxidative stress, although

there was some conflicting evidence outlined (Yavari et al., 2015). Further to this, antioxidants have been associated with reduced disease risk. For instance the antioxidant vitamins A, C and E, in addition to beta-carotene have been associated with a reduced rate of atherosclerosis pathogenesis, as a result of reduced oxidation of LDL-C (Singh et al., 1995). A reduced risk for strokes has also been observed in people aged >65 years old, who had higher dietary vitamin C and plasma concentrations of ascorbic acid (Gale et al., 1995). Furthermore, antioxidants have been associated with extended life. Mococci et al. (2000) concluded from their work on centenarians, that high levels of the antioxidants vitamin A and E were an important factor in providing extreme longevity (Mecocci et al., 2000). Additionally, CR has been associated with a decline in ROS, a key mediator of oxidative damage (Qiu et al., 2010).

There is significant evidence suggesting ROS impacts cholesterol metabolism. Data gained from murine models indicates that increased ROS induces the dephosphorylation and activation of HMG CoA reductase (Pallottini et al., 2007). Importantly, HMG CoA reductase regulates the rate limiting step of cholesterol biosynthesis. Thus the age associated increase in ROS has been associated with the rise in plasma cholesterol often observed with age (Pallottini et al., 2005). It would therefore be appropriate to incorporate the effects of ROS on the system. However, this was a robust aspect of the model, and the parameters regulating the production of mevalonate were not sensitive to change. As outlined previously, this robustness could be due to the size of the model and sensitivities of reactions with assumed parameters. Solely taking the cholesterol biosynthesis pathway from the model to investigate the influence of ROS may overcome this difficulty and ensure that these assumed reactions do not influence the results significantly.

6.2.2.1.2 Investigating the age associated decrease in ACAT

A further experimental finding to consider is the decrease in ACAT observed with age in Watanabe heritable hyperlipidaemic rabbits (Shiomi et al., 2000). It has been hypothesised that a decline in ACAT, could explain the phenomemon that LDL-C decreases with age. It has been suggested a reduction in

ACAT2 results in reduced VLDL-C secretion, which in turn leads to a reduction in LDL-C. The excess cholesterol accumulates in the liver resulting in a condition akin to non-alcoholic fatty liver disease (Mc Auley and Mooney, 2017). However, in contrast to the findings in Watanabe heritable hyperlipidaemic rabbits, macrosomic and control Wistar rats, had ACAT levels which were observed to increase with age. In this study LCAT also increased with age whilst HMG CoA reductase decreased in both experimental groups (Merzouk et al., 2001). Simulating these additional age associated changes to cholesterol metabolism within the updated model would also be a worthwhile task, as it may provide some clarity to these varied experimental findings.

6.2.2.2 Fatty acid metabolism

To analyse lipid metabolism more holistically, the model of cholesterol metabolism could be expanded to incorporate fatty acid metabolism. There are several aspects of these two pathways which overlap. For instance, both cholesterol and TAG are incorporated into the chylomicron (Jamil et al., 1995), before entry into the blood stream. Here, LPL located on the capillary endothelium, causes the hydrolysis of TAG to glycerol and FFA for either energy production or storage within the tissues (Kersten, 2014). The chylomicron remnant then returns to the liver for degradation (Cooper, 1997). Additionally, during RCT, cholesterol esters from HDL are exchanged for TAG from VLDL and LDL by CETP in a 1:1 ratio (Zhang et al., 2015). In Chapter 3, it was outlined that SFA feeding modulated several mechanisms of cholesterol metabolism. Experimental evidence suggests SFA suppresses LDLr activity (Woollett et al., 1992), increases cholesterol synthesis (Jones et al., 1994), upregulates CETP (Jansen et al., 2000), and inhibits LCAT (Berard et al., 2004). These findings may account for the increase in CVD mortality with elevated TAG, as reported by Liu et al. (2013). Through a meta-analysis of 61 prospective studies, Liu et al. (2013) concluded that for each 1mmol/L plasma TAG, there was a 13% increase in CVD mortality. Additionally, all-cause mortality rose 12% for each 1mmol/L increase in TAG (Liu et al., 2013). Therefore it is important the interactions between these two pathways are fully

elucidated. This could be achieved by incorporating fatty acid metabolism and the whole body model of cholesterol metabolism. There are already several models of fatty acid metabolism which could be incorporated. For instance, the comprehensive ODE model by Pratt et al. (2015), which showed the effect FFA and glucose feeding has on glucose, TAG, NEFA, and insulin, within the liver, adipose tissue, muscle, and plasma. This eloquent model outlines the intake of TAG, its movement to the liver, secretion in VLDL, and deposition in the muscle and adipose (Pratt et al., 2015). In another example, Shorten and Upreti (2005) created a model which outlined the biosynthesis of TAG, phospholipids and cholesterol esters, and their assembly into VLDL. The affinities of the liver enzymes to different fatty acids was also investigated (Shorten and Upreti, 2005). Additionally the comprehensive model, SteatoNet, encompasses glucose metabolism, β-oxidation, lipoprotein metabolism and amino acid metabolism, in order to investigate liver associated pathologies (Naik et al., 2014). Any of examples outlined above could easily be combined with the model of cholesterol metabolism to produce a superior model of whole body lipid metabolism and help delineate these pathway interactions.

6.2.2.3 Combining cholesterol metabolism with vitamin D metabolism

The model could also be adapted to include the vitamin D pathway. A low vitamin D status has been linked with an atherogenic lipid profile (Cutillas-Marco et al., 2013). Conversely, vitamin D supplementation has been shown to raise HDL-C, which may have a positive impact on CVD risk (Tavakoli et al., 2016). However, evidence also suggests vitamin D supplementation could have either no effect on the lipoprotein profile (Andersen et al., 2009), or have a negative impact, through an increase in TC, LDL-C and VLDL-C (Schwetz et al., 2018). In a country such as the UK, where vitamin D deficiency is prevalent, and 12.9 and 19.8% of middle aged UK men and women take vitamin D supplements (Hyppönen and Power, 2007), it is vital these associations are well understood. However, to date, the interactions between these two metabolic pathways remains ambiguous. For instance, vitamin D is synthesised in the presence of sunlight from 7-dehydrocholesterol, an intermediate of the cholesterol biosynthesis pathway, it would therefore be logical to assume that increased cholesterol

synthesis would also lead to an increase in vitamin D. However increased TC has been associated with a reduction in vitamin D (Vitezova et al., 2015). Moreover, statin treatment, which inhibits cholesterol synthesis upstream of 7-dehydrocholesterol production has been shown to increase vitamin D (Yavuz et al., 2009). Additionally, a negative relationship between HDL-C and circulating vitamin D has been observed, and it is suggested this association in bidirectional (Vitezova et al., 2015). The mechanisms underpinning these findings could be elucidated through the use of mathematical modelling using the model outlined here as a basis, and incorporating the vitamin D pathway. Currently there are no existing models linking cholesterol and vitamin D metabolism, thus this could be a novel expansion and application of the model.

6.3 Electrochemical analysis of DNA methylation

To investigate another pathway affected by the ageing process, electrochemistry was employed to detect changes to DNA methylation, as a sensor for cancer. It is clear electrochemical techniques are an excellent method for detecting a range of biological species, and there have been numerous examples in recent years, such as bacteria (Altintas et al., 2018), glucose (Douglas and Teaney, 1988), and dissolved oxygen (Xiao et al., 2003) quantification. The detection of DNA methylation using electrochemistry has seen much interest over the last decade due to the association of aberrant DNA methylation and disease. There are multiple examples of its use in the detection of cancer across a range of genes. For instance Topkaya et al. (2012) used EIS and DPV to detect DNA hypermethylation in the GSTP1 gene promoter, as marker for prostate cancer (Topkaya et al., 2012), while Sahab et al. (2014) also investigated this gene promoter using CV (Saheb et al., 2014). All three electrochemical tests were able to detect hypermethylation, however, is it difficult to determine a superior procedure from the results available. This is compounded by the varied adsorption procedures used. The work outlined in Chapters 4 and 5 overcomes these issues and gives a comprehensive overview of the strengths and weaknesses of each technique, providing new insights into how a sensor for DNA

methylation can be developed. The results gained here indicate EIS is a superior technique for detecting DNA methylation. In a similar study, where CV, DPV and EIS were used to detect the BRCA1 gene, Benvedi et al. (2015) also conclude EIS exhibited a superior analytical performance.

In addition to being a successful procedure for both homogenous and heterogeneous samples, this work has revealed that this procedure could be used to detect cancer from a blood sample, in a so called liquid biopsy. For instance, using square wave voltammetry, Cai et al. (2018) showed that ctDNA could be detected at concentrations as low as 10fM, where cancer patients typically exhibit concentrations greater than 200fM (Cai et al., 2018). Additionally, based on a comprehensive search of the literature, it can be hypothesised this procedure could be applied to numerous age related diseases (Guay et al., 2014; Ji et al., 2016). However, it is important the limitations of this research are discussed to enable the growth of this technology.

6.2.2 Sensor limitations

The work conducted here demonstrates that DNA methylation can be detected in the EN1 gene of both synthetic and MCF-7 DNA using a three electrode redox cell. Additionally the electrochemical procedures were able to detect % DNA methylation in heterogeneous samples. Thus, these findings provide a strong basis for the application of this technology as a sensor for cancer, as often biopsies show heterogeneity. However, there are several limitations that should be discussed.

The first limitation is the significant difference in the number of nucleotides between the synthetic and MCF-7 ssDNA. MCF-7 DNA and the unmethylated control WGA DNA induced a significant increase in R_{ct} and ΔE_p, and a decrease in i_{pa} when compared to their synthetic counterparts. The synthetic oligonucleotides were 30 bases in length while the MCF-7 DNA was 140 bases long. This procedure was replicated based on the work of Koo et al. (2014), who utilised a 53 base synthetic oligonucleotide and a 140 base section of the EN1 gene from MCF-7. This work reported similar findings of increased electrode passivation. Ideally, the synthetic DNA would contain the same number of nucleotides as

the MCF-7 amplicon, to ensure the optimisation procedure could be appropriately applied to the MCF-7 DNA. Alternatively, complete optimisation for the MCF-7 DNA could be conducted, as the increased passivation of Au-RDE by the 140 base ssDNA could substantially alter the parameter values gained during the optimisation procedure completed with 30 base synthetic ssDNA.

Another issue is that the amplified ssDNA from MCF-7/WGA was not purified or quantified, similarly to Koo et al. (2014). Although the MCF-7 DNA was quantified (equation 33) and the samples were determined to be pure (equation 34 and 35) following DNA extraction, it is important to consider that unused PCR reagents such as dNTPs could interfere with the signals produced. Although often it took several attempts to get three consistent results, it does not appear this occurred, or that it occurred an insignificant amount, as this also occurred for the synthetic DNA. To support this, Kimura-Suda et al. (2003) report smaller sections of DNA produce a thinner film on gold, which may be difficult to detect (Kimura-Suda et al., 2003). Additionally, although MCF-7/WGA ssDNA was not quantified, various ratios of the amplicons in PBS were analysed. This is an improvement from the Koo et al. (2014) study, which only used one measurement of 10µl secondary PCR product diluted with 20µl 5 X SSC buffer. By conducting tests with a range of different dilutions, the optimum fractional proportion of secondary PCR product was established as 1/18, where 100µl secondary PCR product was diluted with 1700µl 1 X PBS. Although the volume of secondary PCR product was ten times greater than that used in Koo et al. (2014), the dilution was significantly greater; 1/18 compared to 1/3. This indicates that the redox system containing the Au-RDE and/or procedure was significantly more sensitive than that employed by Koo et al. (2014). Additionally, the test samples were applied in excess when adsorbed to the Au-RDE, and therefore this volume could be reduced from 1.8ml. Moreover, it is important to consider that using an electrode such as the Au-SPE, could enable the use of substantially smaller volumes. Koo et al. (2014) reported 30µl of diluted sample was sufficient to coat the working electrode surface. Therefore, to create a 1/18 dilution, only 1.7µl of secondary PCR product would be required. However this would depend on an Au-SPE exhibiting a similar sensitivity to the Au-RDE. While this is

unlikely, it is worth investigating as the use of this type of electrode may be more appropriate as a single use electrode for patient samples in a clinical setting.

Furthermore, as the electrochemical procedures were the key area of interest, the PCR procedure was taken from the MethylEasy Xceed kit, and the primer concentration and ratio was derived from Heiat et al. (2017) without adaption. Although the method was successful, it is important to consider that small changes to the procedure could impact the concentration of the amplicon (Heiat et al., 2017), thus investigating the PCR method could further enhance the overall technique.

6.2.3 Future work

The work conducted in Chapters 4 and 5 clearly show that DNA methylation is measurable in the EN1 gene of both synthetic and cancer derived DNA by electrochemical techniques. There are several further tests and applications that this sensor could be applied to; these are outlined below.

6.2.3.1 EN1 gene methylation and cancer

This work outlines the use of this electrochemical sensor for detecting DNA methylation in the EN1 gene of the breast cancer cell line MCF-7. However, methylation of the EN1 gene has been observed in multiple cancers. Therefore, this sensor could be applied to not only the detection and monitoring of breast cancer, but numerous other cancers. For instance, hypermethylation of the EN1 gene was observed in 80% of high grade serous ovarian carcinoma samples (Montavon et al., 2012), 70% of colorectal tumours (Frigola et al., 2006), and 65% of prostate tumours (Devaney et al., 2011). It is important to note, the form of cancer can have a significant impact, for instance, while EN1 hypermethylation was observed in 80% of high grade serous ovarian carcinoma, it was only observed in 8.3% of epithelial ovarian cancers (Montavon et al., 2012). Furthermore, Mayor et al. (2009) showed that while EN1 methylation was observed in 73% of colorectal carcinomas, only 40% of colorectal

adenomas exhibited EN1 hypermethylation (Mayor et al., 2009). To overcome the possibility of false

negative results, it may be beneficial to select two or more genes for analysis of patient samples. For

instance, in the work conducted by Montavon et al. (2012), it was shown that the combination of the

HOXA9 and EN1 gene discriminated high grade serous ovarian carcinoma from controls with a

sensitivity of 98.8% and specificity of 91.7%, while detecting DNA methylation in HOXA9 singularly

reduced the sensitivity to 95%. Selecting for 3 genes, and including the CA125 gene with HOXA9 and

EN1, further increased the sensitivity to 100% without affecting specificity (Montavon et al., 2012).

Therefore, from this evidence it is clear that combining genes for analysis could produce a superior

test for detecting DNA methylation as a sensor for cancer.

6.2.3.2 Alternative genes and other age related disease

Following on from the above work, a further expansion for this technology is the investigation of other

age related disease. In these instances, EN1 may not be an appropriate gene promoter to analyse.

However hypermethylation in alternative gene promoters associated with age related disease has

been observed. These could easily be selected for, through the use of alternative primers during

asymmetric PCR. For instance, the ABCA1 gene promoter could be investigated to determine CAD.

Guay et al. (2014) showed that in males >61 years of age, there was a 4.7% increase in DNA

methylation in those with CAD compared with those without CAD. Additionally, treatment with

acetylsalicylic acid resulted in a 3.6% reduction ($p<0.05$) in mean ABCA1 methylation compared with

participants not under this treatment (Guay et al., 2014). Therefore, it is possible that monitoring DNA

methylation during clinical intervention could help determine treatment effectiveness. In another

example, Ji et al. (2016) found that methylation across four CpG sites in the DRD4 gene promoter, was

significantly raised in men with AD. The mean methylation was 15.22±3.72% in male patients with AD

while methylation levels were 11.40±3.47% in matched controls (Ji et al., 2016). Conversely in females,

no statistical difference between groups was observed (14.13±4.51 vs. 11.56±4.40%). Therefore, it may be important to consider sex differences during future investigations.

6.2.3.3 Number and order of methylated CpG sites

The work conducted in Chapters 4 and 5 analysed sections of fully methylated or unmethylated DNA. It also examined heterogeneous combinations of these two samples to detect % methylation. However, it was not investigated if % methylation could be determined in a homogenous sample; i.e. could this method determine the number of methylated CpG sites. Furthermore, it was not investigated if the positioning of methylated CpG sites could be differentiated using this sensor. A sensible next step in this work would be to use synthetic oligonucleotides to test this. This is because differential CpG site methylation has been associated with different health factors. For instance, within a series of eight CpG of the XAF1 tumour suppressor gene promoter, the -1st CpG site was methylated in 96.8% of carcinoma, in comparison to 73.3% of adenoma tissues. Conversely at the -2nd CpG site, only 19% and 3.3% were methylated in carcinoma and adenoma respectively. These results suggest that some CpG sites may have unequal importance in the progression of human colon cancer (Zou et al., 2006).

Similar findings have been observed in alternative diseases and related gene promoters. For example, Ji et al. (2017) investigated 3 CpG sites within a CpG island of 105 CpG dinucleotides. In this analysis it was found that percent methylation of CpG3 was significantly higher (77.96±4.08 vs. 74.41±3.98%) in patients with AD compared with the control group. Conversely, no significant difference in methylation levels between groups was observed for CpG1 or CpG2 (Ji et al., 2017). In another example, there were statistically significant increases of 7.8, 7.1, 4.4 and 9.3% in the level of DNA methylation of CpG sites 235, 180, and 102bp upstream and 63bp downstream of the TSS of the INS gene promoter respectively, in patients with T2DM compared with non-diabetic controls (Yang et al., 2011). Furthermore, in this study of diabetic patients, Yang et al. (2011) showed through analysis of

25 CpG sites of the insulin promoter from human pancreatic islets, the methylation of 7 CpG sites were correlated with HbA1c, while the methylation of 11 CpG sites were associated with BMI, with only four CpG sites related to both these health factors. Additionally, methylation of nine CpG sites were associated with insulin mRNA expression; five and seven of which were also correlated with HbA1c, and BMI respectively (Yang et al., 2011). Based on these examples, it may therefore be important for diagnosis to determine which CpG sites are methylated. For this reason, determining if this technology is capable of detecting the number and positioning of methylated CpG sites could be of significant benefit. The prospect of this is promising as outlined by Sina et al. (2014). Although Sina et al. (2014) did not investigate if the order of CpG methylation impacted the DPV current response, the number of methylated CpG sites was analysed. This was achieved by using oligonucleotides containing 53 bases designed to represent bisulphite treated and asymmetrically amplified regions of the EN1 gene, containing 0, 1, 4 and 8 methylated CpG sites. A negative correlation between the number of methylated sites and current was observed, with an R^2 of 0.97411. Therefore the authors outline that the eMethylsorb technique is able to successfully detect DNA methylation at a single CpG site.

6.2.3.4 Non-invasive and point of care testing

It is important to explore the possibility that the detection of cancer through this method, could be conducted using a blood sample, rather than a tissue sample obtained through biopsy. This less invasive test could have the potential to save time, money and resources. The rationale behind this is that recent evidence suggests that tumour DNA is released into circulation. It has therefore been suggested that ctNDA from a blood sample could be used as a biomarker for cancer (Warton and Samimi, 2015). Bettegowda et al. (2014) investigated if ctDNA could be detected in 640 patients diagnosed with various cancers. Using digital PCR based technologies, it was determined that ctDNA could be detected in >75% of patients with advanced pancreatic, ovarian, colorectal, bladder, gastroesophageal, breast, melanoma, hepatocellular, and head and neck cancers. Additionally this study outlined, that ctDNA was correlated with cancer grade, and there was a negative correlation

with 2 year survival rate (Bettegowda et al., 2014). However, there is evidence to suggest that sensors are less able to detect aberrant methylation from ctDNA than samples from traditional biopsies. For instance, Fujiwara et al. (2005) showed that aberrant methylation could only be detected in 49.5% of serum samples from patients with lung cancer, while 77% of lung biopsies exhibited aberrant DNA methylation. Therefore, it is possible that using liquid biopsies such as this may produce a higher number of false negatives than traditional biopsies. However, it is important to consider that this could be a limitation of the methodologies employed, and that electrochemical techniques appear to have increased sensitivities which may overcome this (Cai et al., 2018). It is also important to consider the benefits the miniaturisation of such technology, to a low cost hand held portable device, can have. Although this may require the use of a replaceable single use working electrode, instead of a reusable Au-RDE as utilised in this work, the use of such sensors has been beneficial for monitoring other biological components such as; dissolved oxygen (Xiao et al., 2003), glucose (Douglas and Teaney, 1988), and cholesterol (Rodriguez-Silva et al., 2016).

6.2.3.5 Financial benefits

By applying these suggestions to a clinical setting, there are potential significant savings for the NHS. For instance, the cost of treatment for a patient with stage 1 colon cancer is £3,373 in comparison to £12,519 for a patient with stage 4 colon cancer (Birtwistle and Earnshaw, 2014). In a collaborative report conducted by Incisive health and Cancer research UK in 2014, it was estimated that early diagnosis could benefit 52,000 people, and could reduce the cost of treatment for all cancers by just under £210 million. Additionally, the cost of diagnosis (excluding blood tests) for stage 1 colon cancer is 31.4% less than the diagnosis of a stage 4 colon cancer. For these reasons, the report outlines the need for technologies to offer early diagnosis (Birtwistle and Earnshaw, 2014). With the preliminary findings outlined in this work and evidence suggesting that tumour grading, location and outcome are correlated with the extent of EN1 hypermethylation (Bell et al., 2011), the sensor developed here could provide a suitable means of achieving this goal, especially as the test is inexpensive and rapid.

Furthermore, it is important to note that additional patient benefits and NHS savings could be made if the technology were to be applied to other age related conditions such as CVD.

6.3 Conclusion

To summarise, this work outlines the use of novel investigatory techniques for two age related diseases; namely CVD and cancer. In the first instance, cholesterol metabolism, a key regulator of CVD, was investigated using mathematical modelling. The updated model created behaved as a hypo-responder to cholesterol metabolism, and outlined the impact saturated fat, ageing and CETP can have on cholesterol metabolism. The model also showed the robustness of the cholesterol biosynthesis pathway, and highlighted the absence of *a priori* kinetic data, and the sensitivity of the sections of the model represented by assumed kinetics. Secondly, electrochemical techniques were used to determine DNA methylation within the EN1 gene promoter as a sensor for cancer. These electrochemical techniques were able to detect DNA methylation in synthetic DNA designed to represent a bisulphite modified and asymmetrically amplified section of the EN1 gene promoter, and DNA derived from the breast cancer cell line MCF-7. It was established that EIS was the superior electrochemical technique at detecting DNA methylation when compared to CV at 50 and 200mV/s, and DPV, with a limit of detection for the 30 base synthetic DNA of 10nM. A concentration of 25nM was required to differentiate methylated DNA from unmethylated synthetic DNA. It was also found that the techniques could determine % DNA methylation from heterogeneous solutions of methylated/unmethylated synthetic oligonucleotides and MCF-7/WGA DNA. Additionally, it was hypothesised that this technology could be applied to the diagnosis and monitoring of multiple age related diseases, which may lead to better patient care. Therefore, this work has shown the value of using non-traditional techniques to investigate age related disease. Furthermore, due to the complex nature of ageing, there is no doubt these techniques will prove invaluable to the future study of this multifaceted phenomenon and the diseases associated with it.

6.4 Summary of key research findings

- The updated mathematical model behaved as a hypo-responder to cholesterol feeding but was sensitive to SFA feeding.

- Cholesterol biosynthesis was a robust section of the model, while pathways described by assumed kinetics were sensitive to parameter variation.

- CETP genotype can influence the extent to which LDL-C rises with age.

- DNA methylation can be detected in both homogeneous and heterogeneous samples, using the electrochemical techniques; EIS, CV, and DPV.

- EIS is a superior technique for detecting DNA methylation, as a sensor for cancer.

References

Abbott, R.D., Garrison, R.J., Wilson, P.W., Epstein, F.H., Castelli, W.P., Feinleib, M., LaRue, C., 1983. Joint distribution of lipoprotein cholesterol classes. The Framingham study. Arteriosclerosis, Thrombosis, and Vascular Biology 3, 260-272.

Agerholm-Larsen, B., Tybjærg-Hansen, A., Schnohr, P., Steffensen, R., Nordestgaard, B.G., 2000. Common Cholesteryl Ester Transfer Protein Mutations, Decreased HDL Cholesterol, and Possible Decreased Risk of Ischemic Heart Disease: The Copenhagen City Heart Study. Circulation 102, 2197-2203.

Ahmed, M., Carrascosa, L.G., Ibn Sina, A.A., Zarate, E.M., Korbie, D., Ru, K.-l., Shiddiky, M.J.A., Mainwaring, P., Trau, M., 2017. Detection of aberrant protein phosphorylation in cancer using direct gold-protein affinity interactions. Biosensors and Bioelectronics 91, 8-14.

Ajouz, H., Mukherji, D., Shamseddine, A., 2014. Secondary bile acids: an underrecognized cause of colon cancer. World Journal of Surgical Oncology 12, 164-164.

Al-Sheraji, S.H., Ismail, A., Manap, M.Y., Mustafa, S., Yusof, R.M., Hassan, F.A., 2012. Hypocholesterolaemic effect of yoghurt containing Bifidobacterium pseudocatenulatum G4 or Bifidobacterium longum BB536. Food Chem 135, 356-361.

Alang, N., Kelly, C.R., 2015. Weight Gain After Fecal Microbiota Transplantation. Open Forum Infectious Diseases 2.

Aldini, R., Montagnani, M., Roda, A., Hrelia, S., Biagi, P.L., Roda, E., 1996. Intestinal absorption of bile acids in the rabbit: Different transport rates in jejunum and ileum. Gastroenterology 110, 459-468.

Almasri, J., Alkhateeb, H.B., Damlaj, M., Wang, Z., Murad, M.H., Al-Kali, A., 2015. Comparative Analysis of Azacitidine and Decitabine in Myelodysplastic Syndromes: A Systematic Review and Network Meta-Analysis. Blood 126, 1692-1692.

Alrefai, W.A., Annaba, F., Sarwar, Z., Dwivedi, A., Saksena, S., Singla, A., Dudeja, P.K., Gill, R.K., 2007. Modulation of human Niemann-Pick C1-like 1 gene expression by sterol: role of sterol regulatory element binding protein 2. American Journal of Physiology-Gastrointestinal and Liver Physiology 292, G369-G376.

Altintas, Z., Akgun, M., Kokturk, G., Uludag, Y., 2018. A fully automated microfluidic-based electrochemical sensor for real-time bacteria detection. Biosensors and Bioelectronics 100, 541-548.

Ambrose, J.A., Barua, R.S., 2004. The pathophysiology of cigarette smoking and cardiovascular disease: An update. Journal of the American College of Cardiology 43, 1731-1737.

Anandaraja, S., Narang, R., Godeswar, R., Laksmy, R., Talwar, K.K., 2005. Low-density lipoprotein cholesterol estimation by a new formula in Indian population. International Journal of Cardiology 102, 117-120.

Andersen, R., Brot, C., Mejborn, H., Mølgaard, C., Skovgaard, L.T., Trolle, E., Ovesen, L., 2009. Vitamin D supplementation does not affect serum lipids and lipoproteins in Pakistani immigrants. European Journal Of Clinical Nutrition 63, 1150.

Andrew Skaff, D., Miziorko, H.M., 2010. A visible wavelength spectrophotometric assay suitable for high-throughput screening of 3-hydroxy-3-methylglutaryl-CoA synthase. Analytical Biochemistry 396, 96-102.

Antequera, F., Bird, A., 1993. Number of CpG islands and genes in human and mouse. Proceedings of the National Academy of Sciences of the United States of America 90, 11995-11999.

Aoki, K., Tokuda, K., Matsuda, H., 1984. Theory of differential pulse voltammetry at stationary planar electrodes. Journal of Electroanalytical Chemistry and Interfacial Electrochemistry 175, 1-13.

Appelman, Y., van Rijn, B.B., ten Haaf, M.E., Boersma, E., Peters, S.A.E., 2015. Sex differences in cardiovascular risk factors and disease prevention. Atherosclerosis 241, 211-218.

Arashiro, R., Katsuren, K., Maung, K.K., Fukuyama, S., Ohta, T., 2001. Effect of a Common Mutation (D442G) of the Cholesteryl Ester Transfer Protein Gene on Lipids and Lipoproteins in Children. Pediatric Research 50, 455.

Armstrong, K.M., Bermingham, E.N., Bassett, S.A., Treloar, B.P., Roy, N.C., Barnett, M.P., 2011. Global DNA methylation measurement by HPLC using low amounts of DNA. Biotechnol J 6, 113-117.

Asselbergs, Folkert W., Guo, Y., van Iperen, Erik P., Sivapalaratnam, S., Tragante, V., Lanktree, Matthew B., Lange, Leslie A., Almoguera, B., Appelman, Yolande E., Barnard, J., Baumert, J., Beitelshees, Amber L., Bhangale, Tushar R., Chen, Y.-Der I., Gaunt, Tom R., Gong, Y., Hopewell, Jemma C., Johnson, T., Kleber, Marcus E., Langaee, Taimour Y., Li, M., Li, Yun R., Liu, K., McDonough, Caitrin W., Meijs, Matthijs F., Middelberg, Rita P., Musunuru, K., Nelson, Christopher P., O'Connell, Jeffery R., Padmanabhan, S., Pankow, James S., Pankratz, N., Rafelt, S., Rajagopalan, R., Romaine, Simon P., Schork, Nicholas J., Shaffer, J., Shen, H., Smith, Erin N., Tischfield, Sam E., van der Most, Peter J., van Vliet-Ostaptchouk, Jana V., Verweij, N., Volcik, Kelly A., Zhang, L., Bailey, Kent R., Bailey, Kristian M., Bauer, F., Boer, Jolanda M., Braund, Peter S., Burt, A., Burton, Paul R., Buxbaum, Sarah G., Chen, W., Cooper-DeHoff, Rhonda M., Cupples, L A., deJong, Jonas S., Delles, C., Duggan, D., Fornage, M., Furlong, Clement E., Glazer, N., Gums, John G., Hastie, C., Holmes, Michael V., Illig, T., Kirkland, Susan A., Kivimaki, M., Klein, R., Klein, Barbara E., Kooperberg, C., Kottke-Marchant, K., Kumari, M., LaCroix, Andrea Z., Mallela, L., Murugesan, G., Ordovas, J., Ouwehand, Willem H., Post, Wendy S., Saxena, R., Scharnagl, H., Schreiner, Pamela J., Shah, T., Shields, Denis C., Shimbo, D., Srinivasan, Sathanur R., Stolk, Ronald P., Swerdlow, Daniel I., Taylor, Herman A., Topol, Eric J., Toskala, E., van Pelt, Joost L., van Setten, J., Yusuf, S., Whittaker, John C., Zwinderman, A.H., LifeLines Cohort, S., Anand, Sonia S., Balmforth, Anthony J., Berenson, Gerald S., Bezzina, Connie R., Boehm, Bernhard O., Boerwinkle, E., Casas, Juan P., Caulfield, Mark J., Clarke, R., Connell, John M., Cruickshanks, Karen J., Davidson, Karina W., Day, Ian N., de Bakker, Paul I., Doevendans, Pieter A., Dominiczak, Anna F., Hall, Alistair S., Hartman, Catharina A., Hengstenberg, C., Hillege, Hans L., Hofker, Marten H., Humphries, Steve E., Jarvik, Gail P., Johnson, Julie A., Kaess, Bernhard M., Kathiresan, S., Koenig, W., Lawlor, Debbie A., März, W., Melander, O., Mitchell, Braxton D., Montgomery, Grant W., Munroe, Patricia B., Murray, Sarah S., Newhouse, Stephen J., Onland-Moret, N C., Poulter, N., Psaty, B., Redline, S., Rich, Stephen S., Rotter, Jerome I., Schunkert, H., Sever, P., Shuldiner, Alan R., Silverstein, Roy L., Stanton, A., Thorand, B., Trip, Mieke D., Tsai, Michael Y., van der Harst, P., van der Schoot, E., van der Schouw, Yvonne T., Verschuren, WM M., Watkins, H., Wilde, Arthur A., Wolffenbuttel, Bruce H., Whitfield, John B., Hovingh, G K., Ballantyne, Christie M., Wijmenga, C., Reilly, Muredach P., Martin, Nicholas G., Wilson, James G., Rader, Daniel J., Samani, Nilesh J., Reiner, Alex P., Hegele, Robert A., Kastelein, John J., Hingorani, Aroon D., Talmud, Philippa J., Hakonarson, H., Elbers, Clara C., Keating, Brendan J., Drenos, F., 2012. Large-Scale Gene-Centric Meta-analysis across 32 Studies Identifies Multiple Lipid Loci. American Journal of Human Genetics 91, 823-838.

Atsuta, Y., Okuda, K., 1982. Partial purification and characterization of 5 beta-cholestane-3 alpha, 7 alpha, 12 alpha-triol and 5 beta-cholestane-3 alpha, 7 alpha-diol 27-monooxygenase. J Lipid Res 23, 345-351.

Attie, A.D., Seidah, N.G., 2005. Dual regulation of the LDL receptor—Some clarity and new questions. Cell Metabolism 1, 290-292.

Atzmon, G., Rincon, M., Rabizadeh, P., Barzilai, N., 2005. Biological evidence for inheritance of exceptional longevity. Mech Ageing Dev 126, 341-345.

Auffray, C., Hood, L., 2012. Editorial: Systems biology and personalized medicine - the future is now. Biotechnol J 7, 938-939.

August, E., Parker, K.H., Barahona, M., 2007. A Dynamical Model of Lipoprotein Metabolism. Bulletin of Mathematical Biology 69, 1233-1254.

Austin, M.A., Breslow, J.L., Hennekens, C.H., Buring, J.E., Willett, W.C., Krauss, R.M., 1988. Low-density lipoprotein subclass patterns and risk of myocardial infarction. Jama 260, 1917-1921.

Bae, S.H., Paik, Y.K., 1997. Cholesterol biosynthesis from lanosterol: development of a novel assay method and characterization of rat liver microsomal lanosterol delta 24-reductase. The Biochemical journal 326 (Pt 2), 609-616.

Baidya, S., Zeng, Q., 2005. Helper T cells and atherosclerosis: the cytokine web. Postgraduate Medical Journal 81, 746-752.

Baigent, C., Blackwell, L., Emberson, J., Holland, L.E., Reith, C., Bhala, N., Peto, R., Barnes, E.H., Keech, A., Simes, J., Collins, R., 2010. Efficacy and safety of more intensive lowering of LDL cholesterol: a meta-analysis of data from 170,000 participants in 26 randomised trials. Lancet 376, 1670-1681.

Ballatori, N., Christian, W.V., Lee, J.Y., Dawson, P.A., Soroka, C.J., Boyer, J.L., Madejczyk, M.S., Li, N., 2005. OSTalpha-OSTbeta: a major basolateral bile acid and steroid transporter in human intestinal, renal, and biliary epithelia. Hepatology (Baltimore, Md.) 42, 1270-1279.

Barber, M.J., Mangravite, L.M., Hyde, C.L., Chasman, D.I., Smith, J.D., McCarty, C.A., Li, X., Wilke, R.A., Rieder, M.J., Williams, P.T., Ridker, P.M., Chatterjee, A., Rotter, J.I., Nickerson, D.A., Stephens, M., Krauss, R.M., 2010. Genome-Wide Association of Lipid-Lowering Response to Statins in Combined Study Populations. PLoS ONE 5, e9763.

Barker, D.J., 1995. Intrauterine programming of adult disease. Mol Med Today 1, 418-423.

Barlow, D.P., Bartolomei, M.S., 2014. Genomic Imprinting in Mammals. Cold Spring Harbor Perspectives in Biology 6.

Barter, P.J., Caulfield, M., Eriksson, M., Grundy, S.M., Kastelein, J.J.P., Komajda, M., Lopez-Sendon, J., Mosca, L., Tardif, J.-C., Waters, D.D., Shear, C.L., Revkin, J.H., Buhr, K.A., Fisher, M.R., Tall, A.R., Brewer, B., 2007. Effects of Torcetrapib in Patients at High Risk for Coronary Events. New England Journal of Medicine 357, 2109-2122.

Bartolomei, M.S., Ferguson-Smith, A.C., 2011. Mammalian Genomic Imprinting. Cold Spring Harbor Perspectives in Biology 3, a002592.

Barzilai, N., Atzmon, G., Derby, C.A., Bauman, J.M., Lipton, R.B., 2006. A genotype of exceptional longevity is associated with preservation of cognitive function. Neurology 67, 2170-2175.

Barzilai, N., Atzmon, G., Schechter, C., Schaefer, E.J., Cupples, A.L., Lipton, R., Cheng, S., Shuldiner, A.R., 2003. Unique lipoprotein phenotype and genotype associated with exceptional longevity. JAMA 290, 2030-2040.

Barzilai, N., Gabriely, I., Gabriely, M., Iankowitz, N., Sorkin, J.D., 2001. Offspring of centenarians have a favorable lipid profile. J Am Geriatr Soc 49, 76-79.

Barzilai, N., Huffman, D.M., Muzumdar, R.H., Bartke, A., 2012. The critical role of metabolic pathways in aging. Diabetes 61, 1315-1322.

Batta, A.K., Salen, G., Rapole, K.R., Batta, M., Batta, P., Alberts, D., Earnest, D., 1999. Highly simplified method for gas-liquid chromatographic quantitation of bile acids and sterols in human stool. J Lipid Res 40, 1148-1154.

Begley, M., Hill, C., Gahan, C.G.M., 2006. Bile Salt Hydrolase Activity in Probiotics. Applied and environmental microbiology 72, 1729-1738.

Bell, A., Bell, D., Weber, R.S., El-Naggar, A.K., 2011. CpG island methylation profiling in human salivary gland adenoid cystic carcinoma. Cancer 117, 2898-2909.

Benetou, V., Trichopoulou, A., Orfanos, P., Naska, A., Lagiou, P., Boffetta, P., Trichopoulos, D., 2008. Conformity to traditional Mediterranean diet and cancer incidence: the Greek EPIC cohort. Br J Cancer 99, 191-195.

Bennet, A.M., Di Angelantonio, E., Ye, Z., Wensley, F., Dahlin, A., Ahlbom, A., Keavney, B., Collins, R., Wiman, B., de Faire, U., Danesh, J., 2007. Association of apolipoprotein E genotypes with lipid levels and coronary risk. JAMA 298, 1300-1311.

Bentzon, J.F., Otsuka, F., Virmani, R., Falk, E., 2014. Mechanisms of Plaque Formation and Rupture. Circulation Research 114, 1852-1866.

Benvidi, A., Dehghani Firouzabadi, A., Dehghan Tezerjani, M., Moshtaghiun, S.M., Mazloum-Ardakani, M., Ansarin, A., 2015. A highly sensitive and selective electrochemical DNA biosensor to diagnose breast cancer. Journal of Electroanalytical Chemistry 750, 57-64.

Berard, A.M., Dabadie, H., Palos-Pinto, A., Dumon, M.F., Darmon, M., 2004. Reduction of dietary saturated fatty acids correlates with increased plasma lecithin cholesterol acyltransferase activity in humans. Eur J Clin Nutr 58, 881-887.

Bernardo, M., de Vink, E., Di Pierro, A., Wiklicky, H., 2013. Formal Methods for Dynamical Systems. Lecture Notes in Computer Science 7938.

Berthiaume, J.M., Wallace, K.B., 2007. Adriamycin-induced oxidative mitochondrial cardiotoxicity. Cell Biology and Toxicology 23, 15-25.

Bertolotti, M., Abate, N., Bertolotti, S., Loria, P., Concari, M., Messora, R., Carubbi, F., Pinetti, A., Carulli, N., 1993. Effect of aging on cholesterol 7 alpha-hydroxylation in humans. J Lipid Res 34, 1001-1007.

Bertolotti, M., Gabbi, C., Anzivino, C., Crestani, M., Mitro, N., Del Puppo, M., Godio, C., De Fabiani, E., Macchioni, D., Carulli, L., Rossi, A., Ricchi, M., Loria, P., Carulli, N., 2007. Age-related changes in bile acid synthesis and hepatic nuclear receptor expression. Eur J Clin Invest 37, 501-508.

Bettegowda, C., Sausen, M., Leary, R.J., Kinde, I., Wang, Y., Agrawal, N., Bartlett, B.R., Wang, H., Luber, B., Alani, R.M., Antonarakis, E.S., Azad, N.S., Bardelli, A., Brem, H., Cameron, J.L., Lee, C.C., Fecher, L.A., Gallia, G.L., Gibbs, P., Le, D., Giuntoli, R.L., Goggins, M., Hogarty, M.D., Holdhoff, M., Hong, S.-M., Jiao, Y., Juhl, H.H., Kim, J.J., Siravegna, G., Laheru, D.A., Lauricella, C., Lim, M., Lipson, E.J., Marie, S.K.N., Netto, G.J., Oliner, K.S., Olivi, A., Olsson, L., Riggins, G.J., Sartore-Bianchi, A., Schmidt, K., Shih, l.-M., Oba-Shinjo, S.M., Siena, S., Theodorescu, D., Tie, J., Harkins, T.T., Veronese, S., Wang, T.-L., Weingart, J.D., Wolfgang, C.L., Wood, L.D., Xing, D., Hruban, R.H., Wu, J., Allen, P.J., Schmidt, C.M., Choti, M.A., Velculescu, V.E., Kinzler, K.W., Vogelstein, B., Papadopoulos, N., Diaz, L.A., 2014. Detection of Circulating Tumor DNA in Early- and Late-Stage Human Malignancies. Science translational medicine 6, 224ra224-224ra224.

Betters, J.L., Yu, L., 2010. NPC1L1 and cholesterol transport. FEBS letters 584, 2740-2747.

Bhattacharya, B.S., Sweby, P.K., Minihane, A.M., Jackson, K.G., Tindall, M.J., 2014. A mathematical model of the sterol regulatory element binding protein 2 cholesterol biosynthesis pathway. J Theor Biol 349, 150-162.

Biagi, E., Candela, M., Fairweather-Tait, S., Franceschi, C., Brigidi, P., 2012. Ageing of the human metaorganism: the microbial counterpart. Age 34, 247-267.

Biagi, E., Nylund, L., Candela, M., Ostan, R., Bucci, L., Pini, E., Nikkïla, J., Monti, D., Satokari, R., Franceschi, C., Brigidi, P., De Vos, W., 2010. Through Ageing, and Beyond: Gut Microbiota and Inflammatory Status in Seniors and Centenarians. PLoS ONE 5, e10667.

BioLogic, 2017a. BT-Lab & EC-Lab Software Analysis and Data Process. 1-113.

BioLogic, 2017b. EC-Lab & BT-Lab Software: Techniques and Applications. 1-260.

BioLogic, 2017c. EC-Lab/BT-Lab Software User's Manual. 1-113.

Birru, W.A., Warren, D.B., Ibrahim, A., Williams, H.D., Benameur, H., Porter, C.J., Chalmers, D.K., Pouton, C.W., 2014. Digestion of phospholipids after secretion of bile into the duodenum changes the phase behavior of bile components. Molecular pharmaceutics 11, 2825-2834.

Birtwistle, M., Earnshaw, A., 2014. Saving lives, averting costs: An analysis of the financial implications of achieving earlier diagnosis of colorectal, lung and ovarian cancer.

Biswas, H.H., Gordon, A., Nunez, A., Perez, M.A., Balmaseda, A., Harris, E., 2015. Lower Low-Density Lipoprotein Cholesterol Levels Are Associated with Severe Dengue Outcome. PLoS Negl Trop Dis 9, e0003904.

Björkhem, I., Araya, Z., Rudling, M., Angelin, B., Einarsson, C., Wikvall, K., 2002. Differences in the Regulation of the Classical and the Alternative Pathway for Bile Acid Synthesis in Human Liver: No Coordinate Regulation of CYP7A1 and CYP27A1. Journal of Biological Chemistry 277, 26804-26807.

Bjorksten, J., 1968. The Crosslinkage Theory of Aging. Journal of the American Geriatrics Society 16, 408-427.

Bloch, K., 1965. The Biological Synthesis of Cholesterol. Science 150, 19-28.

Boge, T., Remigy, M., Vaudaine, S., Tanguy, J., Bourdet-Sicard, R., van der Werf, S., 2009. A probiotic fermented dairy drink improves antibody response to influenza vaccination in the elderly in two randomised controlled trials. Vaccine 27, 5677-5684.

Boone, L.R., Brooks, P.A., Niesen, M.I., Ness, G.C., 2011. Mechanism of Resistance to Dietary Cholesterol. Journal of Lipids 2011, 9.

Borgqvist, J., Dainese, R., Cvijovic, M., , 2017. Systems Biology of Aging, Systems biology.

Bornstein, B.J., Keating, S.M., Jouraku, A., Hucka, M., 2008. LibSBML: an API library for SBML. Bioinformatics 24, 880-881.

Bosner, M.S., Lange, L.G., Stenson, W.F., Ostlund, R.E., 1999. Percent cholesterol absorption in normal women and men quantified with dual stable isotopic tracers and negative ion mass spectrometry. Journal of Lipid Research 40, 302-308.

Bouchard, L., Thibault, S., Guay, S.P., Santure, M., Monpetit, A., St-Pierre, J., Perron, P., Brisson, D., 2010. Leptin gene epigenetic adaptation to impaired glucose metabolism during pregnancy. Diabetes Care 33, 2436-2441.

Breitling, R., 2010. What is systems biology? Frontiers in physiology 1, 9-9.

Brown, M.S., Goldstein, J.L., 1984. How LDL receptors influence cholesterol and atherosclerosis. Sci Am 251, 58-66.

Brownson, D.A.C., Banks, C.E., 2014. Interpreting Electrochemistry, The Handbook of Graphene Electrochemistry. Springer London, London, pp. 23-77.

Bruggeman, F.J., Westerhoff, H.V., 2007. The nature of systems biology. Trends in Microbiology 15, 45-50.

Buijsse, B., Feskens, E.J., Kwape, L., Kok, F.J., Kromhout, D., 2008. Both alpha- and beta-carotene, but not tocopherols and vitamin C, are inversely related to 15-year cardiovascular mortality in Dutch elderly men. The Journal of nutrition 138, 344-350.

Cai, C., Guo, Z., Cao, Y., Zhang, W., Chen, Y., 2018. A dual biomarker detection platform for quantitating circulating tumor DNA (ctDNA). Nanotheranostics 2, 12-20.

Callegari, E., Norata, G.D., Inoue, H., Catapano, A.L., 2006. Oxidized-HDL3 modulates the expression of Cox-2 in human endothelial cells. Int J Mol Med 18, 209-213.

Campuzano, S., Yáñez-Sedeño, P., Pingarrón, J.M., 2017. Electrochemical Genosensing of Circulating Biomarkers. Sensors (Basel, Switzerland) 17, 866.

Cancer Research UK, 2018. Cancer mortality for common cancers.

Candela, M., Biagi, E., Brigidi, P., O'Toole, P.W., De Vos, W.M., 2014. Maintenance of a healthy trajectory of the intestinal microbiome during aging: A dietary approach. Mechanisms of Ageing and Development 136–137, 70-75.

Capuron, L., Schroecksnadel, S., Feart, C., Aubert, A., Higueret, D., Barberger-Gateau, P., Laye, S., Fuchs, D., 2011. Chronic low-grade inflammation in elderly persons is associated with altered tryptophan and tyrosine metabolism: role in neuropsychiatric symptoms. Biol Psychiatry 70, 175-182.

Carrascosa, L.G., Sina, A.A.I., Palanisamy, R., Sepulveda, B., Otte, M.A., Rauf, S., Shiddiky, M.J.A., Trau, M., 2014. Molecular inversion probe-based SPR biosensing for specific, label-free and real-time detection of regional DNA methylation. Chemical Communications 50, 3585-3588.

Cefalu, A.B., Noto, D., Magnolo, L., Pinotti, E., Gomaraschi, M., Martini, S., Vigna, G.B., Calabresi, L., Tarugi, P., Averna, M.R., 2009. Novel mutations of CETP gene in Italian subjects with hyperalphalipoproteinemia. Atherosclerosis 204, 202-207.

Chang, A., Schomburg, I., Placzek, S., Jeske, L., Ulbrich, M., Xiao, M., Sensen, C.W., Schomburg, D., 2015. BRENDA in 2015: exciting developments in its 25th year of existence. Nucleic acids research 43, D439-446.

Chang, B.-Y., Park, S.-M., 2010. Electrochemical Impedance Spectroscopy. Annual Review of Analytical Chemistry 3, 207-229.

Chang, T.-Y., Li, B.-L., Chang, C.C.Y., Urano, Y., 2009. Acyl-coenzyme A:cholesterol acyltransferases. American Journal of Physiology - Endocrinology and Metabolism 297, E1-E9.

Chaplin, M.F., Bucke, C., 1990. Enzyme Technology. Cambridge University Press

Chapman, M.J., Le Goff, W., Guerin, M., Kontush, A., 2010. Cholesteryl ester transfer protein: at the heart of the action of lipid-modulating therapy with statins, fibrates, niacin, and cholesteryl ester transfer protein inhibitors. European heart journal 31, 149-164.

Chasman, D.I., Posada, D., Subrahmanyan, L., Cook, N.R., Stanton, Jr, V.P., Ridker, P., 2004. Pharmacogenetic study of statin therapy and cholesterol reduction. JAMA 291, 2821-2827.

Chédin, F., Lieber, M.R., Hsieh, C.-L., 2002. The DNA methyltransferase-like protein DNMT3L stimulates de novo methylation by Dnmt3a. Proceedings of the National Academy of Sciences 99, 16916-16921.

Chik, F., Szyf, M., 2011. Effects of specific DNMT gene depletion on cancer cell transformation and breast cancer cell invasion; toward selective DNMT inhibitors. Carcinogenesis 32, 224-232.

Chirackal Manavalan, A.P., Kober, A., Metso, J., Lang, I., Becker, T., Hasslitzer, K., Zandl, M., Fanaee-Danesh, E., Pippal, J.B., Sachdev, V., Kratky, D., Stefulj, J., Jauhiainen, M., Panzenboeck, U., 2014. Phospholipid transfer protein is expressed in cerebrovascular endothelial cells and involved in high density lipoprotein biogenesis and remodeling at the blood-brain barrier. The Journal of biological chemistry 289, 4683-4698.

Chistiakov, D.A., Bobryshev, Y.V., Kozarov, E., Sobenin, I.A., Orekhov, A.N., 2015. Role of gut microbiota in the modulation of atherosclerosis-associated immune response. Frontiers in Microbiology 6, 671.

Christensen, B.C., Kelsey, K.T., Zheng, S., Houseman, E.A., Marsit, C.J., Wrensch, M.R., Wiemels, J.L., Nelson, H.H., Karagas, M.R., Kushi, L.H., Kwan, M.L., Wiencke, J.K., 2010. Breast Cancer DNA Methylation Profiles Are Associated with Tumor Size and Alcohol and Folate Intake. PLOS Genetics 6, e1001043.

Citartan, M., Thean-Hock, T., Soo-Choon, T., Chee-Hock, H., Saini, R., Tominaga, J., Gopinath, S.C.B., 2012. Asymmetric PCR for good quality ssDNA generation towards DNA aptamer production. Songklanakarin Journal of Science & Technology 34, 125-131.

Claesson, M.J., Cusack, S., O'Sullivan, O., Greene-Diniz, R., de Weerd, H., Flannery, E., Marchesi, J.R., Falush, D., Dinan, T., Fitzgerald, G., Stanton, C., van Sinderen, D., O'Connor, M., Harnedy, N., O'Connor, K., Henry, C., O'Mahony, D., Fitzgerald, A.P., Shanahan, F., Twomey, C., Hill, C., Ross, R.P., O'Toole, P.W., 2011. Composition, variability, and temporal stability of the intestinal microbiota of the elderly. Proceedings of the National Academy of Sciences of the United States of America 108, 4586-4591.

Claesson, M.J., Jeffery, I.B., Conde, S., Power, S.E., O'Connor, E.M., Cusack, S., Harris, H.M.B., Coakley, M., Lakshminarayanan, B., O'Sullivan, O., Fitzgerald, G.F., Deane, J., O/'Connor, M., Harnedy, N., O'Connor, K., O'Mahony, D., van Sinderen, D., Wallace, M., Brennan, L., Stanton, C., Marchesi, J.R., Fitzgerald, A.P., Shanahan, F., Hill, C., Ross, R.P., O'Toole, P.W., 2012. Gut microbiota composition correlates with diet and health in the elderly. Nature 488, 178-184.

Clio-Infra, 2016. Life Expectancy at Birth (Total).

Cohen, J.C., Pertsemlidis, A., Fahmi, S., Esmail, S., Vega, G.L., Grundy, S.M., Hobbs, H.H., 2006. Multiple rare variants in NPC1L1 associated with reduced sterol absorption and plasma low-density lipoprotein levels. Proceedings of the National Academy of Sciences of the United States of America 103, 1810-1815.

Colman, R.J., Beasley, T.M., Kemnitz, J.W., Johnson, S.C., Weindruch, R., Anderson, R.M., 2014. Caloric restriction reduces age-related and all-cause mortality in rhesus monkeys. Nature Communications 5, 3557.

Colotti, C., Cavallini, G., Vitale, R.L., Donati, A., Maltinti, M., Del Ry, S., Bergamini, E., Giannessi, D., 2005. Effects of Aging and Anti-Aging Caloric Restrictions on Carbonyl and Heat Shock Protein Levels and Expression. Biogerontology 6, 397-406.

Comsa, S., Cimpean, A.M., Raica, M., 2015. The Story of MCF-7 Breast Cancer Cell Line: 40 years of Experience in Research. Anticancer Res 35, 3147-3154.

Connell, J.G., Genorio, B., Lopes, P.P., Strmcnik, D., Stamenkovic, V.R., Markovic, N.M., 2016. Tuning the Reversibility of Mg Anodes via Controlled Surface Passivation by H2O/Cl– in Organic Electrolytes. Chemistry of Materials 28, 8268-8277.

Cooney, M.T., Dudina, A., De Bacquer, D., Wilhelmsen, L., Sans, S., Menotti, A., De Backer, G., Jousilahti, P., Keil, U., Thomsen, T., Whincup, P., Graham, I.M., 2009. HDL cholesterol protects against cardiovascular disease in both genders, at all ages and at all levels of risk. Atherosclerosis 206, 611-616.

Cooper, A.D., 1997. Hepatic uptake of chylomicron remnants. J Lipid Res 38, 2173-2192.

Craddock, A.L., Love, M.W., Daniel, R.W., Kirby, L.C., Walters, H.C., Wong, M.H., Dawson, P.A., 1998. Expression and transport properties of the human ileal and renal sodium-dependent bile acid transporter. The American journal of physiology 274, G157-169.

Crescenti, A., Solà, R., Valls, R.M., Caimari, A., del Bas, J.M., Anguera, A., Anglés, N., Arola, L., 2013. Cocoa Consumption Alters the Global DNA Methylation of Peripheral Leukocytes in Humans with Cardiovascular Disease Risk Factors: A Randomized Controlled Trial. PLOS ONE 8, e65744.

Crider, K.S., Quinlivan, E.P., Berry, R.J., Hao, L., Li, Z., Maneval, D., Yang, T.P., Rasmussen, S.A., Yang, Q., Zhu, J.-H., Hu, D.J., Bailey, L.B., 2011. Genomic DNA Methylation Changes in Response to Folic Acid Supplementation in a Population-Based Intervention Study among Women of Reproductive Age. PLOS ONE 6, e28144.

Crider, K.S., Yang, T.P., Berry, R.J., Bailey, L.B., 2012. Folate and DNA methylation: a review of molecular mechanisms and the evidence for folate's role. Adv Nutr 3, 21-38.

Cui, Q., Ju, X., Yang, T., Zhang, M., Tang, W., Chen, Q., Hu, Y., Haas, J.V., Troutt, J.S., Pickard, R.T., Darling, R., Konrad, R.J., Zhou, H., Cao, G., 2010. Serum PCSK9 is associated with multiple metabolic factors in a large Han Chinese population. Atherosclerosis 213, 632-636.

Cutillas-Marco, E., Prosper, A.F., Grant, W.B., Morales-Suárez-Varela, M.M., 2013. Vitamin D status and hypercholesterolemia in Spanish general population. Dermato-Endocrinology 5, 358-362.

Dalziel, K., Segal, L., de Lorgeril, M., 2006. A mediterranean diet is cost-effective in patients with previous myocardial infarction. The Journal of nutrition 136, 1879-1885.

Damiati, S., Kupcu, S., Peacock, M., Eilenberger, C., Zamzami, M., Qadri, I., Choudhry, H., Sleytr, U.B., Schuster, B., 2017. Acoustic and hybrid 3D-printed electrochemical biosensors for the real-time immunodetection of liver cancer cells (HepG2). Biosens Bioelectron 94, 500-506.

Daoud, M.S., Ataya, F.S., Fouad, D., Alhazzani, A., Shehata, A.I., Al-Jafari, A.A., 2013. Associations of three lipoprotein lipase gene polymorphisms, lipid profiles and coronary artery disease. Biomedical Reports 1, 573-582.

David, L.A., Maurice, C.F., Carmody, R.N., Gootenberg, D.B., Button, J.E., Wolfe, B.E., Ling, A.V., Devlin, A.S., Varma, Y., Fischbach, M.A., Biddinger, S.B., Dutton, R.J., Turnbaugh, P.J., 2014. Diet rapidly and reproducibly alters the human gut microbiome. Nature 505, 559-563.

Dawson, P.A., 2011. Role of the Intestinal Bile Acid Transporters in Bile Acid and Drug Disposition. Handbook of experimental pharmacology, 169-203.

Dawson, P.A., Lan, T., Rao, A., 2009. Bile acid transporters. J Lipid Res 50, 2340-2357.

de Beer, F., Stalenhoef, A.F.H., Hoogerbrugge, N., Kastelein, J.J.P., Gevers Leuven, J.A., van Duijn, C.M., Havekes, L.M., Smelt, A.H.M., 2002. Expression of Type III Hyperlipoproteinemia in Apolipoprotein E2 (Arg158→Cys) Homozygotes Is Associated With Hyperinsulinemia. Arteriosclerosis, Thrombosis, and Vascular Biology 22, 294-299.

de Lorgeril, M., Salen, P., Martin, J.-L., Monjaud, I., Delaye, J., Mamelle, N., 1999. Mediterranean Diet, Traditional Risk Factors, and the Rate of Cardiovascular Complications After Myocardial Infarction: Final Report of the Lyon Diet Heart Study. Circulation 99, 779-785.

de Luca, C., Olefsky, J.M., 2008. Inflammation and insulin resistance. FEBS letters 582, 97-105.

de Magalhães, J.P., Wuttke, D., Wood, S.H., Plank, M., Vora, C., 2012. Genome-Environment Interactions That Modulate Aging: Powerful Targets for Drug Discovery. Pharmacological Reviews 64, 88-101.

De Smedt, D., Kotseva, K., De Bacquer, D., Wood, D., De Backer, G., Dallongeville, J., Seppo, L., Pajak, A., Reiner, Z., Vanuzzo, D., Georgiev, B., Gotcheva, N., Annemans, L., 2012. Cost-effectiveness of optimizing prevention in patients with coronary heart disease: the EUROASPIRE III health economics project. European heart journal 33, 2865-2872.

Demirezen, E.M., Barlas, Y., 2008. A simulation model for blood cholesterol dynamics and related disorders, The 27th International Conference of the System Dynamics Society, Albuquerque, New Mexico.

Devaney, J., Stirzaker, C., Qu, W., Song, J.Z., Statham, A.L., Patterson, K.I., Horvath, L.G., Tabor, B., Coolen, M.W., Hulf, T., Kench, J.G., Henshall, S.M., Pe Benito, R., Haynes, A.-M., Mayor, R., Peinado, M.A., Sutherland, R.L., Clark, S.J., 2011. Epigenetic Deregulation Across Chromosome 2q14.2 Differentiates Normal from Prostate Cancer and Provides a Regional Panel of Novel DNA Methylation Cancer Biomarkers. Cancer Epidemiology Biomarkers & Prevention 20, 148-159.

Dewald, O., Zymek, P., Winkelmann, K., Koerting, A., Ren, G., Abou-Khamis, T., Michael, L.H., Rollins, B.J., Entman, M.L., Frangogiannis, N.G., 2005. CCL2/Monocyte Chemoattractant Protein-1 Regulates Inflammatory Responses Critical to Healing Myocardial Infarcts. Circulation Research 96, 881-889.

Dhingra, R., Vasan, R.S., 2012. Age as a Cardiovascular Risk Factor. The Medical Clinics of North America 96, 87-91.

Diaz, M.E., Mayoral, J.G., Priestap, H., Nouzova, M., Rivera-Perez, C., Noriega, F.G., 2012. Characterization of an isopentenyl diphosphate isomerase involved in the juvenile hormone pathway in Aedes aegypti. Insect biochemistry and molecular biology 42, 751-757.

Ding, V.D., Sheares, B.T., Bergstrom, J.D., Ponpipom, M.M., Perez, L.B., Poulter, C.D., 1991. Purification and characterization of recombinant human farnesyl diphosphate synthase expressed in Escherichia coli. The Biochemical journal 275 (Pt 1), 61-65.

Dobbins, M., Decorby, K., Choi, B.C.K., 2013. The Association between Obesity and Cancer Risk: A Meta-Analysis of Observational Studies from 1985 to 2011. ISRN Preventive Medicine 2013, 16.

Dong, L.M., Weisgraber, K.H., 1996. Human apolipoprotein E4 domain interaction. Arginine 61 and glutamic acid 255 interact to direct the preference for very low density lipoproteins. The Journal of biological chemistry 271, 19053-19057.

Douglas, A., Teaney, D., 1988. Hand-Held Glucose Monitor and Recorder, Engineering in Medicine and Biology Society, 1988. Proceedings of the Annual International Conference of the IEEE. IEEE, pp. 747-748.

Drager, A., Planatscher, H., Wouamba, D.M., Schroder, A., Hucka, A., Endler, L., Golebiewski, M., Zell, A., 2015. SBML Model Report. Model name: "Aguilera 2014 - HIV latency. Interaction between HIV proteins and immune response".

Drinkwater, R.D., Blake, T.J., Morley, A.A., Turner, D.R., 1989. Human lymphocytes aged in vivo have reduced levels of methylation in transcriptionally active and inactive DNA. Mutation Research/DNAging 219, 29-37.

Duan, L.P., Wang, H.H., Ohashi, A., Wang, D.Q., 2006. Role of intestinal sterol transporters Abcg5, Abcg8, and Npc1l1 in cholesterol absorption in mice: gender and age effects. American journal of physiology. Gastrointestinal and liver physiology 290, G269-276.

Dubuc, G., Tremblay, M., Pare, G., Jacques, H., Hamelin, J., Benjannet, S., Boulet, L., Genest, J., Bernier, L., Seidah, N.G., Davignon, J., 2010. A new method for measurement of total plasma PCSK9: clinical applications. J Lipid Res 51, 140-149.

Dujovne, C.A., Ettinger, M.P., McNeer, J.F., Lipka, L.J., LeBeaut, A.P., Suresh, R., Yang, B.o., Veltri, E.P., 2002. Efficacy and safety of a potent new selective cholesterol absorption inhibitor, ezetimibe, in patients with primary hypercholesterolemia. The American Journal of Cardiology 90, 1092-1097.

Edwards, I.J., Rudel, L.L., Terry, J.G., Kemnitz, J.W., Weindruch, R., Cefalu, W.T., 1998. Caloric restriction in rhesus monkeys reduces low density lipoprotein interaction with arterial proteoglycans. J Gerontol A Biol Sci Med Sci 53, B443-448.

Einarsson, K., Nilsell, K., Leijd, B., Angelin, B., 1985. Influence of age on secretion of cholesterol and synthesis of bile acids by the liver. N Engl J Med 313, 277-282.

Elgrishi, N., Rountree, K.J., McCarthy, B.D., Rountree, E.S., Eisenhart, T.T., Dempsey, J.L., 2018. A Practical Beginner's Guide to Cyclic Voltammetry. Journal of Chemical Education 95, 197-206.

EMBL EBI, 2010. SBO:0000436: Ping Pong Bi-Bi mechanism rate law

Engelborghs, S., Dermaut, B., Goeman, J., Saerens, J., Marien, P., Pickut, B., Van den Broeck, M., Serneels, S., Cruts, M., Van Broeckhoven, C., De Deyn, P.P., 2003. Prospective Belgian study of neurodegenerative and vascular dementia: APOE genotype effects. Journal of Neurology, Neurosurgery, and Psychiatry 74, 1148-1151.

Enrique Salcedo-Sora, J., Mc Auley, M.T., 2016. A mathematical model of microbial folate biosynthesis and utilisation: implications for antifolate development. Mol Biosyst 12, 923-933.

Ericsson, S., Eriksson, M., Vitols, S., Einarsson, K., Berglund, L., Angelin, B., 1991. Influence of age on the metabolism of plasma low density lipoproteins in healthy males. Journal of Clinical Investigation 87, 591-596.

Esteves-Villanueva, J.O., Trzeciakiewicz, H., Martic, S., 2014. A protein-based electrochemical biosensor for detection of tau protein, a neurodegenerative disease biomarker. Analyst 139, 2823-2831.

Estruch, R., Ros, E., Salas-Salvadó, J., Covas, M.-I., Corella, D., Arós, F., Gómez-Gracia, E., Ruiz-Gutiérrez, V., Fiol, M., Lapetra, J., Lamuela-Raventos, R.M., Serra-Majem, L., Pintó, X., Basora, J., Muñoz, M.A., Sorlí, J.V., Martínez, J.A., Martínez-González, M.A., 2013. Primary Prevention of Cardiovascular Disease with a Mediterranean Diet. New England Journal of Medicine 368, 1279-1290.

European Medicines Agency, 2017a. Dacogen, Decitabine. Available at http://www.ema.europa.eu/ema/index.jsp?curl=pages/medicines/human/medicines/002221/human_med_001589.jsp&mid=WC0b01ac058001d124.

European Medicines Agency, 2017b. EU/3/01/084. Available at http://www.ema.europa.eu/ema/index.jsp?curl=pages/medicines/human/orphans/2009/11/human_orphan_000230.jsp&mid=WC0b01ac058001d12b.

Everard, A., Lazarevic, V., Gaia, N., Johansson, M., Stahlman, M., Backhed, F., Delzenne, N.M., Schrenzel, J., Francois, P., Cani, P.D., 2014. Microbiome of prebiotic-treated mice reveals novel targets involved in host response during obesity. ISME J 8, 2116-2130.

Fagan-Murphy, A., Hachoumi, L., Yeoman, M.S., Patel, B.A., 2016. Electrochemical sensor for the detection of multiple reactive oxygen and nitrogen species from ageing central nervous system homogenates. Mechanisms of Ageing and Development 160, 28-31.

Fan, Y.-M., Laaksonen, R., Janatuinen, T., Vesalainen, R., Laine, H., Raitakari, O.T., Nuutila, P., Knuuti, J., Rontu, R., Lehtimäki, T., 2006. The influence of hepatic lipase C-480T polymorphism on coronary flow reserve in young men is independent of the plasma cholesterol level. Atherosclerosis 188, 391-397.

Favre, B., Ryder, N.S., 1996. Characterization of squalene epoxidase activity from the dermatophyte Trichophyton rubrum and its inhibition by terbinafine and other antimycotic agents. Antimicrobial agents and chemotherapy 40, 443-447.

Fernandez-Real, J.M., Serino, M., Blasco, G., Puig, J., Daunis, I.E.J., Ricart, W., Burcelin, R., Fernandez-Aranda, F., Portero-Otin, M., 2015. Gut microbiota interacts with brain microstructure and function. J Clin Endocrinol Metab, jc20153076.

Fernandez, M.L., West, K.L., 2005. Mechanisms by which Dietary Fatty Acids Modulate Plasma Lipids1. The Journal of nutrition 135, 2075-2078.

Ferrara, A., Barrett-Connor, E., Shan, J., 1997. Total, LDL, and HDL cholesterol decrease with age in older men and women. The Rancho Bernardo Study 1984-1994. Circulation 96, 37-43.

Field, F.J., Born, E., Mathur, S.N., 2004. Stanol esters decrease plasma cholesterol independently of intestinal ABC sterol transporters and Niemann-Pick C1-like 1 protein gene expression. J Lipid Res 45, 2252-2259.

Field, P.A., Gibbons, G.F., 2000. Decreased hepatic expression of the low-density lipoprotein (LDL) receptor and LDL receptor-related protein in aging rats is associated with delayed clearance of chylomicrons from the circulation. Metabolism 49, 492-498.

Fini, L., Selgrad, M., Fogliano, V., Graziani, G., Romano, M., Hotchkiss, E., Daoud, Y.A., De Vol, E.B., Boland, C.R., Ricciardiello, L., 2007. Annurca Apple Polyphenols Have Potent Demethylating Activity and Can Reactivate Silenced Tumor Suppressor Genes in Colorectal Cancer Cells. The Journal of nutrition 137, 2622-2628.

Finney, A., Sauro, H., Hucka, M., Bolouri, H., 2000. An xml-based model description language for systems biology simulations. Available at http://www.cds.caltech.edu/erato.

Fisher, A., 1996. Electrode Dynamics. New York: Oxford University Press.

Fontana, L., Meyer, T.E., Klein, S., Holloszy, J.O., 2004. Long-term calorie restriction is highly effective in reducing the risk for atherosclerosis in humans. Proceedings of the National Academy of Sciences of the United States of America 101, 6659-6663.

Fradin, D., Boëlle, P.-Y., Belot, M.-P., Lachaux, F., Tost, J., Besse, C., Deleuze, J.-F., De Filippo, G., Bougnères, P., 2017. Genome-Wide Methylation Analysis Identifies Specific Epigenetic Marks In Severely Obese Children. Scientific reports 7, 46311.

Frigola, J., Song, J., Stirzaker, C., Hinshelwood, R.A., Peinado, M.A., Clark, S.J., 2006. Epigenetic remodeling in colorectal cancer results in coordinate gene suppression across an entire chromosome band. 38, 540.

Fu, J., Bonder, M.J., Cenit, M.C., Tigchelaar, E., Maatman, A., Dekens, J.A.M., Brandsma, E., Marczynska, J., Imhann, F., Weersma, R.K., Franke, L., Poon, T.W., Xavier, R.J., Gevers, D., Hofker, M.H., Wijmenga, C., Zhernakova, A., 2015. The Gut Microbiome Contributes to a Substantial Proportion of the Variation in Blood Lipids. Circulation Research.

Fu, Z.D., Csanaky, I.L., Klaassen, C.D., 2012. Gender-Divergent Profile of Bile Acid Homeostasis during Aging of Mice. PLoS ONE 7, e32551.

Fuchs, M., 2003. Bile acid regulation of hepatic physiology: III. Regulation of bile acid synthesis: past progress and future challenges. American journal of physiology. Gastrointestinal and liver physiology 284, G551-557.

Fujiwara, K., Fujimoto, N., Tabata, M., Nishii, K., Matsuo, K., Hotta, K., Kozuki, T., Aoe, M., Kiura, K., Ueoka, H., Tanimoto, M., 2005. Identification of Epigenetic Aberrant Promoter Methylation in Serum DNA Is Useful for Early Detection of Lung Cancer. Clinical Cancer Research 11, 1219-1225.

Funahashi, A., Matsuoka, Y., Jouraku, A., Kitano, H., Kikuchi, N., 2006. Celldesigner: A Modeling Tool for Biochemical Networks, Proceedings of the 2006 Winter Simulation Conference, pp. 1707-1712.

Gale, C.R., Martyn, C.N., Winter, P.D., Cooper, C., 1995. Vitamin C and risk of death from stroke and coronary heart disease in cohort of elderly people. Bmj 310, 1563-1566.

Gamry, 2018. The Basics of Electrochemical Impedance Spectroscopy. 1-18.

Garatachea, N., Emanuele, E., Calero, M., Fuku, N., Arai, Y., Abe, Y., Murakami, H., Miyachi, M., Yvert, T., Verde, Z., Zea, M.A., Venturini, L., Santiago, C., Santos-Lozano, A., Rodríguez-Romo, G., Ricevuti, G., Hirose, N., Rábano, A., Lucia, A., 2014. ApoE gene and exceptional longevity: Insights from three independent cohorts. Experimental Gerontology 53, 16-23.

Garcia-Bellido, A., Santamaria, P., 1972. Developmental Analysis of the Wing Disc in the Mutant Engrailed of Drosophila melanogaster. Genetics 72, 87-104.

García-Escobar, E., Monastero, R., García-Serrano, S., Gómez-Zumaquero, J.M., Lago-Sampedro, A., Rubio-Martín, E., Colomo, N., Rodríguez-Pacheco, F., Soriguer, F., Rojo-Martínez, G., 2017. Dietary fatty acids modulate adipocyte TNFa production via regulation of its DNA promoter methylation levels. The Journal of Nutritional Biochemistry 47, 106-112.

Garrett, R.L., Young, J., 1975. Effect of micelle formation on the absorption of neutral fat and fatty acids by the chicken. The Journal of nutrition 105, 827-838.

Gaudet, F., Hodgson, J.G., Eden, A., Jackson-Grusby, L., Dausman, J., Gray, J.W., Leonhardt, H., Jaenisch, R., 2003. Induction of tumors in mice by genomic hypomethylation. Science 300, 489-492.

Gérard, P., 2014. Metabolism of Cholesterol and Bile Acids by the Gut Microbiota. Pathogens (Basel, Switzerland) 3, 14-24.

Gianchandani, E.P., Brautigan, D.L., Papin, J.A., 2006. Systems analyses characterize integrated functions of biochemical networks. Trends Biochem Sci 31, 284-291.

Gillotte, K.L., Davidson, W.S., Lund-Katz, S., Rothblat, G.H., Phillips, M.C., 1998. Removal of cellular cholesterol by pre-beta-HDL involves plasma membrane microsolubilization. J Lipid Res 39, 1918-1928.

Goldberg, I.J., Eckel, R.H., Abumrad, N.A., 2009. Regulation of fatty acid uptake into tissues: lipoprotein lipase- and CD36-mediated pathways. Journal of Lipid Research 50, S86-S90.

Gould, A.L., Davies, G.M., Alemao, E., Yin, D.D., Cook, J.R., 2007. Cholesterol reduction yields clinical benefits: meta-analysis including recent trials. Clinical Therapeutics 29, 778-794.

Goyal, R., Reinhardt, R., Jeltsch, A., 2006. Accuracy of DNA methylation pattern preservation by the Dnmt1 methyltransferase. Nucleic Acids Research 34, 1182-1188.

Gredilla, R., Sanz, A., Lopez-Torres, M., Barja, G., 2001. Caloric restriction decreases mitochondrial free radical generation at complex I and lowers oxidative damage to mitochondrial DNA in the rat heart. The FASEB Journal 15, 1589-1591.

Gregory, J.C., Buffa, J.A., Org, E., Wang, Z., Levison, B.S., Zhu, W., Wagner, M.A., Bennett, B.J., Li, L., DiDonato, J.A., Lusis, A.J., Hazen, S.L., 2015. Transmission of atherosclerosis susceptibility with gut microbial transplantation. The Journal of biological chemistry 290, 5647-5660.

Groen, A.K., Oude Elferink, R.P., Verkade, H.J., Kuipers, F., 2004. The ins and outs of reverse cholesterol transport. Annals of medicine 36, 135-145.

Guarente, L., 2013. Calorie restriction and sirtuins revisited. Genes Dev 27, 2072-2085.

Guay, S.P., Legare, C., Houde, A.A., Mathieu, P., Bosse, Y., Bouchard, L., 2014. Acetylsalicylic acid, aging and coronary artery disease are associated with ABCA1 DNA methylation in men. Clin Epigenetics 6, 14.

Guthikonda, S., Haynes, W.G., 2006. Homocysteine: role and implications in atherosclerosis. Current atherosclerosis reports 8, 100-106.

Gylling, H., 2004. Cholesterol metabolism and its implications for therapeutic interventions in patients with hypercholesterolaemia. International Journal of Clinical Practice 58, 859-866.

Hahn, O., Grönke, S., Stubbs, T.M., Ficz, G., Hendrich, O., Krueger, F., Andrews, S., Zhang, Q., Wakelam, M.J., Beyer, A., Reik, W., Partridge, L., 2017. Dietary restriction protects from age-associated DNA methylation and induces epigenetic reprogramming of lipid metabolism. Genome Biology 18, 56.

Han, X., Stevens, J., Truesdale, K.P., Bradshaw, P.T., Kucharska-Newton, A., Prizment, A.E., Platz, E.A., Joshu, C.E., 2014. Body mass index at early adulthood, subsequent weight change, and

cancer incidence and mortality. International journal of cancer. Journal international du cancer 135, 2900-2909.

Hansson, G.K., Hermansson, A., 2011. The immune system in atherosclerosis. Nat Immunol 12, 204-212.

Hara, H., Haga, S., Aoyama, Y., Kiriyama, S., 1999. Short-chain fatty acids suppress cholesterol synthesis in rat liver and intestine. The Journal of nutrition 129, 942-948.

Hardison, W.G., 1978. Hepatic taurine concentration and dietary taurine as regulators of bile acid conjugation with taurine. Gastroenterology 75, 71-75.

Harley, C.B., Futcher, A.B., Greider, C.W., 1990. Telomeres shorten during ageing of human fibroblasts. Nature 345, 458.

Harman, D., 1956. Aging: a theory based on free radical and radiation chemistry. J Gerontol 11, 298-300.

Harman, D., 1972. The Biologic Clock: The Mitochondria? Journal of the American Geriatrics Society 20, 145-147.

Harman, D., 2009. Origin and evolution of the free radical theory of aging: a brief personal history, 1954-2009. Biogerontology 10, 773-781.

Harvey, D., 2002. Electrochemical Methods. Current Separations 20, 51-53.

Hasan, S.T., Zingg, J.M., Kwan, P., Noble, T., Smith, D., Meydani, M., 2014. Curcumin modulation of high fat diet-induced atherosclerosis and steatohepatosis in LDL receptor deficient mice. Atherosclerosis 232, 40-51.

Havel, R.J., 1984. The formation of LDL: mechanisms and regulation. J Lipid Res 25, 1570-1576.

Hayashi, H., Sakamoto, M., Kitahara, M., Benno, Y., 2003. Molecular analysis of fecal microbiota in elderly individuals using 16S rDNA library and T-RFLP. Microbiol Immunol 47, 557-570.

Hayatsu, H., Shiraishi, M., Negishi, K., 2008. Bisulfite modification for analysis of DNA methylation. Curr Protoc Nucleic Acid Chem Chapter 6, Unit 6 10.

He, L., Fernandez, M.L., 1998. Saturated fat and simple carbohydrates elevate plasma LDL cholesterol concentrations by specific alterations on hepatic cholesterol metabolism. Nutrition Research 18, 1003-1015.

He, Y., Zhang, L., Li, Z., Gao, H., Yue, Z., Liu, Z., Liu, X., Feng, X., Liu, P., 2015. RIP140 triggers foam-cell formation by repressing ABCA1/G1 expression and cholesterol efflux via liver X receptor. FEBS letters 589, 455-460.

Heiat, M., Ranjbar, R., Latifi, A.M., Rasaee, M.J., Farnoosh, G., 2017. Essential strategies to optimize asymmetric PCR conditions as a reliable method to generate large amount of ssDNA aptamers. Biotechnology and Applied Biochemistry, 1-8.

Heilbronn, L.K., de Jonge, L., Frisard, M.I., DeLany, J.P., Meyer, D.E.L., Rood, J., Nguyen, T., Martin, C.K., Volaufova, J., Most, M.M., Greenway, F.L., Smith, S.R., Williamson, D.A., Deutsch, W.A., Ravussin, E., 2006. Effect of 6-mo. calorie restriction on biomarkers of longevity, metabolic adaptation and oxidative stress in overweight subjects. JAMA : the journal of the American Medical Association 295, 1539-1548.

Henderson, L., Gregory, J., Irving, K., Swan, G., 2003. The National Diet & Nutrition Survey: adults aged 19 to 64 years, Office for National Statistics.

Hennessy, L.K., Osada, J., Ordovas, J.M., Nicolosi, R.J., Stucchi, A.F., Brousseau, M.E., Schaefer, E.J., 1992. Effects of dietary fats and cholesterol on liver lipid content and hepatic apolipoprotein A-I, B, and E and LDL receptor mRNA levels in cebus monkeys. J Lipid Res 33, 351-360.

Herdendorf, T.J., Miziorko, H.M., 2007. Functional evaluation of conserved basic residues in human phosphomevalonate kinase. Biochemistry 46, 11780-11788.

Herman, J.G., Graff, J.R., Myöhänen, S., Nelkin, B.D., Baylin, S.B., 1996. Methylation-specific PCR: a novel PCR assay for methylation status of CpG islands. Proceedings of the National Academy of Sciences of the United States of America 93, 9821-9826.

Herron, K.L., Vega-Lopez, S., Conde, K., Ramjiganesh, T., Shachter, N.S., Fernandez, M.L., 2003. Men classified as hypo- or hyperresponders to dietary cholesterol feeding exhibit differences in lipoprotein metabolism. The Journal of nutrition 133, 1036-1042.

Hindle, J.V., 2010. Ageing, neurodegeneration and Parkinson's disease. Age and ageing 39, 156-161.

Hippe, B., Zwielehner, J., Liszt, K., Lassl, C., Unger, F., Haslberger, A.G., 2011. Quantification of butyryl CoA:acetate CoA-transferase genes reveals different butyrate production capacity in individuals according to diet and age. FEMS Microbiol Lett 316, 130-135.

Hirano, K., Yamashita, S., Nakajima, N., Arai, T., Maruyama, T., Yoshida, Y., Ishigami, M., Sakai, N., Kameda-Takemura, K., Matsuzawa, Y., 1997. Genetic cholesteryl ester transfer protein deficiency is extremely frequent in the Omagari area of Japan. Marked hyperalphalipoproteinemia caused by CETP gene mutation is not associated with longevity. Arterioscler Thromb Vasc Biol 17, 1053-1059.

Hirsch, H.R., 1986. The waste-product theory of aging: cell division rate as a function of waste volume. Mech Ageing Dev 36, 95-107.

Ho, R.H., Leake, B.F., Roberts, R.L., Lee, W., Kim, R.B., 2004. Ethnicity-dependent polymorphism in Na+-taurocholate cotransporting polypeptide (SLC10A1) reveals a domain critical for bile acid substrate recognition. The Journal of biological chemistry 279, 7213-7222.

Hoffman, Jessica M., Lyu, Y., Pletcher, Scott D., Promislow, Daniel E.L., 2017. Proteomics and metabolomics in ageing research: from biomarkers to systems biology. Essays In Biochemistry 61, 379-388.

Hofmann, A.F., Mysels, K.J., 1992. Bile acid solubility and precipitation in vitro and in vivo: the role of conjugation, pH, and Ca2+ ions. J Lipid Res 33, 617-626.

Hollander, D., Morgan, D., 1979. Increase in cholesterol intestinal absorption with aging in the rat. Exp Gerontol 14, 201-204.

Honeychurch, M.J., Rechnitz, G.A., 1998. Voltammetry of Adsorbed Molecules. Part 1: Reversible Redox Systems. Electroanalysis 10, 285-293.

Hoops, S., Sahle, S., Gauges, R., Lee, C., Pahle, J., Simus, N., Singhal, M., Xu, L., Mendes, P., Kummer, U., 2006. COPASI—a COmplex PAthway SImulator. Bioinformatics 22, 3067-3074.

Hopkins, M.J., Macfarlane, G.T., 2002. Changes in predominant bacterial populations in human faeces with age and with Clostridium difficile infection. J Med Microbiol 51, 448-454.

Horakova, D., Kyr, M., Havrdova, E., Dolezal, O., Lelkova, P., Pospisilova, L., Bergsland, N., Dwyer, M.G., Cox, J.L., Hussein, S., Seidl, Z., Vaneckova, M., Krasensky, J., Zivadinov, R., 2010. Apolipoprotein E epsilon4-positive multiple sclerosis patients develop more gray-matter and whole-brain atrophy: a 15-year disease history model based on a 4-year longitudinal study. Folia Biol (Praha) 56, 242-251.

Horton, J.D., Goldstein, J.L., Brown, M.S., 2002. SREBPs: activators of the complete program of cholesterol and fatty acid synthesis in the liver. The Journal of clinical investigation 109, 1125-1131.

Horvath, S., 2013. DNA methylation age of human tissues and cell types. Genome Biol 14, R115.

Hoshino, T., Chiba, A., Abe, N., 2012. Lanosterol biosynthesis: the critical role of the methyl-29 group of 2,3-oxidosqualene for the correct folding of this substrate and for the construction of the five-membered D ring. Chemistry (Weinheim an der Bergstrasse, Germany) 18, 13108-13116.

Hossain, T., Mahmudunnabi, G., Masud, M.K., Islam, M.N., Ooi, L., Konstantinov, K., Hossain, M.S.A., Martinac, B., Alici, G., Nguyen, N.T., Shiddiky, M.J.A., 2017. Electrochemical biosensing strategies for DNA methylation analysis. Biosens Bioelectron 94, 63-73.

Hou, Q., Wang, K., Xu, F., Zhang, W., Ji, K., Liu, Y., 2017. QM/MM studies of the type II isopentenyl diphosphate–dimethylallyl diphosphate isomerase demonstrate a novel role for the flavin coenzyme. RSC Advances 7, 22286-22293.

Hovingh, G.K., Kastelein, J.J.P., van Deventer, S.J.H., Round, P., Ford, J., Saleheen, D., Rader, D.J., Brewer, H.B., Barter, P.J., 2015. Cholesterol ester transfer protein inhibition by TA-8995 in

patients with mild dyslipidaemia (TULIP): a randomised, double-blind, placebo-controlled phase 2 trial. The Lancet.

Hu, J., Zhang, C.Y., 2012. Single base extension reaction-based surface enhanced Raman spectroscopy for DNA methylation assay. Biosens Bioelectron 31, 451-457.

Huang, Y., He, S., Li, J.Z., Seo, Y.K., Osborne, T.F., Cohen, J.C., Hobbs, H.H., 2010. A feed-forward loop amplifies nutritional regulation of PNPLA3. Proceedings of the National Academy of Sciences of the United States of America 107, 7892-7897.

Hubner, K., Schwager, T., Winkler, K., Reich, J.G., Holzhutter, H.G., 2008. Computational lipidology: predicting lipoprotein density profiles in human blood plasma. PLoS computational biology 4, e1000079.

Hucka, M., Finney, A., Bornstein, B.J., Keating, S.M., Shapiro, B.E., Matthews, J., Kovitz, B.L., Schilstra, M.J., Funahashi, A., Doyle, J.C., Kitano, H., 2004. Evolving a lingua franca and associated software infrastructure for computational systems biology: the Systems Biology Markup Language (SBML) project. Systems biology 1, 41-53.

Hucka, M., Finney, A., Sauro, H.M., Bolouri, H., Doyle, J.C., Kitano, H., Forum:, Arkin, A.P., Bornstein, B.J., Bray, D., Cornish-Bowden, A., Cuellar, A.A., Dronov, S., Gilles, E.D., Ginkel, M., Gor, V., Goryanin, I.I., Hedley, W.J., Hodgman, T.C., Hofmeyr, J.-H., Hunter, P.J., Juty, N.S., Kasberger, J.L., Kremling, A., Kummer, U., Le Novère, N., Loew, L.M., Lucio, D., Mendes, P., Minch, E., Mjolsness, E.D., Nakayama, Y., Nelson, M.R., Nielsen, P.F., Sakurada, T., Schaff, J.C., Shapiro, B.E., Shimizu, T.S., Spence, H.D., Stelling, J., Takahashi, K., Tomita, M., Wagner, J., Wang, J., 2003. The systems biology markup language (SBML): a medium for representation and exchange of biochemical network models. Bioinformatics 19, 524-531.

Huebbe, P., Nebel, A., Siegert, S., Moehring, J., Boesch-Saadatmandi, C., Most, E., Pallauf, J., Egert, S., Muller, M.J., Schreiber, S., Nothlings, U., Rimbach, G., 2011. APOE epsilon4 is associated with higher vitamin D levels in targeted replacement mice and humans. FASEB J 25, 3262-3270.

Hyppönen, E., Power, C., 2007. Hypovitaminosis D in British adults at age 45 y: nationwide cohort study of dietary and lifestyle predictors. The American journal of clinical nutrition 85, 860-868.

Ideker, T., Galitski, T., Hood, L., 2001. A new approach to decoding life: systems biology. Annual review of genomics and human genetics 2, 343-372.

Ikeda, I., Matsuoka, R., Hamada, T., Mitsui, K., Imabayashi, S., Uchino, A., Sato, M., Kuwano, E., Itamura, T., Yamada, K., Tanaka, K., Imaizumi, K., 2002. Cholesterol esterase accelerates intestinal cholesterol absorption. Biochimica et Biophysica Acta (BBA) - General Subjects 1571, 34-44.

Ikenoya, M., Yoshinaka, Y., Kobayashi, H., Kawamine, K., Shibuya, K., Sato, F., Sawanobori, K., Watanabe, T., Miyazaki, A., 2007. A selective ACAT-1 inhibitor, K-604, suppresses fatty streak lesions in fat-fed hamsters without affecting plasma cholesterol levels. Atherosclerosis 191, 290-297.

Iqbal, J., Hussain, M.M., 2009. Intestinal lipid absorption. American Journal of Physiology - Endocrinology and Metabolism 296, E1183-E1194.

Ishibashi, S., Brown, M.S., Goldstein, J.L., Gerard, R.D., Hammer, R.E., Herz, J., 1993. Hypercholesterolemia in low density lipoprotein receptor knockout mice and its reversal by adenovirus-mediated gene delivery. Journal of Clinical Investigation 92, 883-893.

Istvan, E.S., Deisenhofer, J., 2001. Structural Mechanism for Statin Inhibition of HMG-CoA Reductase. Science 292, 1160-1164.

Jabbour, E., Short, N.J., Montalban-Bravo, G., Huang, X., Bueso-Ramos, C., Qiao, W., Yang, H., Zhao, C., Kadia, T., Borthakur, G., Pemmaraju, N., Sasaki, K., Estrov, Z., Cortes, J., Ravandi, F., Alvarado, Y., Komrokji, R., Sekeres, M.A., Steensma, D.P., DeZern, A., Roboz, G., Kantarjian, H., Garcia-Manero, G., 2017. Randomized phase 2 study of low-dose decitabine vs low-dose azacitidine in lower-risk MDS and MDS/MPN. Blood 130, 1514-1522.

Jahr, S., Hentze, H., Englisch, S., Hardt, D., Fackelmayer, F.O., Hesch, R.-D., Knippers, R., 2001. DNA Fragments in the Blood Plasma of Cancer Patients: Quantitations and Evidence for Their Origin from Apoptotic and Necrotic Cells. Cancer Research 61, 1659-1665.

Jamil, H., Dickson, J.K., Chu, C.-H., Lago, M.W., Rinehart, J.K., Biller, S.A., Gregg, R.E., Wetterau, J.R., 1995. Microsomal Triglyceride Transfer Protein: Specificity of lipid binding and transport. Journal of Biological Chemistry 270, 6549-6554.

Jansen, S., Lopez-Miranda, J., Castro, P., Lopez-Segura, F., Marin, C., Ordovas, J.M., Paz, E., Jimenez-Pereperez, J., Fuentes, F., Perez-Jimenez, F., 2000. Low-fat and high-monounsaturated fatty acid diets decrease plasma cholesterol ester transfer protein concentrations in young, healthy, normolipemic men. Am J Clin Nutr 72, 36-41.

Jeltsch, A., Jurkowska, R.Z., 2014. New concepts in DNA methylation. Trends in Biochemical Sciences 39, 310-318.

Jenkins, D.A., Jones, P.H., Lamarche, B., et al., 2011. Effect of a dietary portfolio of cholesterol-lowering foods given at 2 levels of intensity of dietary advice on serum lipids in hyperlipidemia: A randomized controlled trial. JAMA 306, 831-839.

Jenkins, D.J.A., Jones, P.J., Frohlich, J., Lamarche, B., Ireland, C., Nishi, S.K., Srichaikul, K., Galange, P., Pellini, C., Faulkner, D., de Souza, R.J., Sievenpiper, J.L., Mirrahimi, A., Jayalath, V.H., Augustin, L.S., Bashyam, B., Leiter, L.A., Josse, R., Couture, P., Ramprasath, V., Kendall, C.W.C., 2015. The effect of a dietary portfolio compared to a DASH-type diet on blood pressure. Nutrition, Metabolism and Cardiovascular Diseases.

Jerby, L., Shlomi, T., Ruppin, E., 2010. Computational reconstruction of tissue-specific metabolic models: application to human liver metabolism. Molecular systems biology 6, 401.

Ji, A., Meyer, J.M., Cai, L., Akinmusire, A., de Beer, M.C., Webb, N.R., van der Westhuyzen, D.R., 2011. Scavenger receptor SR-BI in macrophage lipid metabolism. Atherosclerosis 217, 106-112.

Ji, H., Wang, Y., Jiang, D., Liu, G., Xu, X., Dai, D., Zhou, X., Cui, W., Li, J., Chen, Z., Li, Y., Zhou, D., Zha, Q., Zhuo, R., Jiang, L., Liu, Y., Shen, L., Zhang, B., Xu, L., Hu, H., Zhang, Y., Yin, H., Duan, S., Wang, Q., 2016. Elevated DRD4 promoter methylation increases the risk of Alzheimer's disease in males. Mol Med Rep 14, 2732-2738.

Ji, H., Wang, Y., Liu, G., Chang, L., Chen, Z., Zhou, D., Xu, X., Cui, W., Hong, Q., Jiang, L., Li, J., Zhou, X., Li, Y., Guo, Z., Zha, Q., Niu, Y., Weng, Q., Duan, S., Wang, Q., 2017. Elevated OPRD1 promoter methylation in Alzheimer's disease patients. PLoS ONE 12, e0172335.

Jia, L., Betters, J.L., Yu, L., 2011. Niemann-pick C1-like 1 (NPC1L1) protein in intestinal and hepatic cholesterol transport. Annual review of physiology 73, 239-259.

Johnson, K.A., Goody, R.S., 2011. The Original Michaelis Constant: Translation of the 1913 Michaelis–Menten Paper. Biochemistry 50, 8264-8269.

Johnson, S.C., Rabinovitch, P.S., Kaeberlein, M., 2013. mTOR is a key modulator of ageing and age-related disease. Nature 493, 338-345.

Jones, P.J., Lichtenstein, A.H., Schaefer, E.J., Namchuk, G.L., 1994. Effect of dietary fat selection on plasma cholesterol synthesis in older, moderately hypercholesterolemic humans. Arteriosclerosis, Thrombosis, and Vascular Biology 14, 542-548.

Jones, P.J., Pappu, A.S., Hatcher, L., Li, Z.C., Illingworth, D.R., Connor, W.E., 1996. Dietary cholesterol feeding suppresses human cholesterol synthesis measured by deuterium incorporation and urinary mevalonic acid levels. Arterioscler Thromb Vasc Biol 16, 1222-1228.

Jones, P.J., Schoeller, D.A., 1990. Evidence for diurnal periodicity in human cholesterol synthesis. J Lipid Res 31, 667-673.

Joyce, S.A., MacSharry, J., Casey, P.G., Kinsella, M., Murphy, E.F., Shanahan, F., Hill, C., Gahan, C.G.M., 2014. Regulation of host weight gain and lipid metabolism by bacterial bile acid modification in the gut. Proceedings of the National Academy of Sciences 111, 7421-7426.

Jung, A.Y., Smulders, Y., Verhoef, P., Kok, F.J., Blom, H., Kok, R.M., Kampman, E., Durga, J., 2011. No Effect of Folic Acid Supplementation on Global DNA Methylation in Men and Women with Moderately Elevated Homocysteine. PLOS ONE 6, e24976.

Kandola, K., Bowman, A., Birch-Machin, M.A., 2015. Oxidative stress - a key emerging impact factor in health, ageing, lifestyle and aesthetics. Int J Cosmet Sci 37 Suppl 2, 1-8.

Kawasaki, T., Hamano, Y., Kuzuyama, T., Itoh, N., Seto, H., Dairi, T., 2003. Interconversion of the product specificity of type I eubacterial farnesyl diphosphate synthase and geranylgeranyl diphosphate synthase through one amino acid substitution. Journal of biochemistry 133, 83-91.

Keith, M., Kuliszewski, M.A., Liao, C., Peeva, V., Ahmed, M., Tran, S., Sorokin, K., Jenkins, D.J., Errett, L., Leong-Poi, H., 2015. A modified portfolio diet complements medical management to reduce cardiovascular risk factors in diabetic patients with coronary artery disease. Clinical Nutrition 34, 541-548.

Keleti, T., 1986. Two rules of enzyme kinetics for reversible Michaelis-Menten mechanisms. FEBS letters 208, 109-112.

Kent, E.L., 2012. Sensitivity analysis of biochemical systems using high-throughput computing, Engineering and Physical Sciences. University of Manchester.

Kerenyi, L., Mihalka, L., Csiba, L., Bacso, H., Bereczki, D., 2006. Role of hyperlipidemia in atherosclerotic plaque formation in the internal carotid artery. J Clin Ultrasound 34, 283-288.

Kersten, S., 2014. Physiological regulation of lipoprotein lipase. Biochimica et biophysica acta 1841, 919-933.

Kervizic, G., Corcos, L., 2008. Dynamical modeling of the cholesterol regulatory pathway with Boolean networks. BMC Syst Biol 2, 99.

Kiliaan, A.J., Saunders, P.R., Bijlsma, P.B., Berin, M.C., Taminiau, J.A., Groot, J.A., Perdue, M.H., 1998. Stress stimulates transepithelial macromolecular uptake in rat jejunum. The American journal of physiology 275, G1037-1044.

Kilner, J., Corfe, B.M., McAuley, M.T., Wilkinson, S.J., 2016. A deterministic oscillatory model of microtubule growth and shrinkage for differential actions of short chain fatty acids. Mol Biosyst 12, 93-101.

Kim, C.H., Lee, E.K., Choi, Y.J., An, H.J., Jeong, H.O., Park, D., Kim, B.C., Yu, B.P., Bhak, J., Chung, H.Y., 2016. Short-term calorie restriction ameliorates genomewide, age-related alterations in DNA methylation. Aging Cell 15, 1074-1081.

Kimura-Suda, H., Petrovykh, D.Y., Tarlov, M.J., Whitman, L.J., 2003. Base-dependent competitive adsorption of single-stranded DNA on gold. J Am Chem Soc 125, 9014-9015.

Kimura, M., Okuno, E., Inada, J., Ohyama, H., Kido, R., 1983. Purification and characterization of amino-acid N-choloyltransferase from human liver. Hoppe-Seyler's Zeitschrift fur physiologische Chemie 364, 637-645.

Kirkwood, T.B., Kowald, A., 2012. The free-radical theory of ageing--older, wiser and still alive: modelling positional effects of the primary targets of ROS reveals new support. Bioessays 34, 692-700.

Kirkwood, T.B.L., 2011. Systems biology of ageing and longevity. Philosophical transactions of the Royal Society of London. Series B, Biological sciences 366, 64-70.

Kitano, H., 2002. Computational systems biology. Nature 420, 206-210.

Koeth, R.A., Wang, Z., Levison, B.S., Buffa, J.A., Org, E., Sheehy, B.T., Britt, E.B., Fu, X., Wu, Y., Li, L., Smith, J.D., DiDonato, J.A., Chen, J., Li, H., Wu, G.D., Lewis, J.D., Warrier, M., Brown, J.M., Krauss, R.M., Tang, W.H.W., Bushman, F.D., Lusis, A.J., Hazen, S.L., 2013. Intestinal microbiota metabolism of l-carnitine, a nutrient in red meat, promotes atherosclerosis. Nat Med 19, 576-585.

Koo, K.M., Sina, A.A., Carrascosa, L.G., Shiddiky, M.J., Trau, M., 2014. eMethylsorb: rapid quantification of DNA methylation in cancer cells on screen-printed gold electrodes. Analyst 139, 6178-6184.

Koropatnick, T.A., Kimbell, J., Chen, R., Grove, J.S., Donlon, T.A., Masaki, K.H., Rodriguez, B.L., Willcox, B.J., Yano, K., Curb, J.D., 2008. A prospective study of high-density lipoprotein cholesterol, cholesteryl ester transfer protein gene variants, and healthy aging in very old Japanese-american men. J Gerontol A Biol Sci Med Sci 63, 1235-1240.

Korporaal, S.J.A., Van Eck, M., Adelmeijer, J., Ijsseldijk, M., Out, R., Lisman, T., Lenting, P.J., Van Berkel, T.J.C., Akkerman, J.-W.N., 2007. Platelet Activation by Oxidized Low Density Lipoprotein Is Mediated by Cd36 and Scavenger Receptor-A. Arteriosclerosis, Thrombosis, and Vascular Biology 27, 2476-2483.

Kouzuki, H., Suzuki, H., Ito, K., Ohashi, R., Sugiyama, Y., 1998. Contribution of sodium taurocholate co-transporting polypeptide to the uptake of its possible substrates into rat hepatocytes. The Journal of pharmacology and experimental therapeutics 286, 1043-1050.

Kovacs, K.A., Pamer, Z., Kovacs, A., Fekete, S., Miseta, A., Kovacs, B., Kovacs, G.L., 2007. Association of apolipoprotein E polymorphism with age-related macular degeneration and Alzheimer's disease in south-western Hungary. Ideggyogy Sz 60, 169-172.

Kowala, M.C., Recce, R., Beyer, S., Gu, C., Valentine, M., 2000. Characterization of atherosclerosis in LDL receptor knockout mice: macrophage accumulation correlates with rapid and sustained expression of aortic MCP-1/JE. Atherosclerosis 149, 323-330.

Krause, F., Uhlendorf, J., Lubitz, T., Schulz, M., Klipp, E., Liebermeister, W., 2009. Annotation and merging of SBML models with semanticSBML. Bioinformatics 26, 421-422.

Kromhout, D., Menotti, A., Bloemberg, B., Aravanis, C., Blackburn, H., Buzina, R., Dontas, A.S., Fidanza, F., Giampaoli, S., Jansen, A., et al., 1995. Dietary saturated and trans fatty acids and cholesterol and 25-year mortality from coronary heart disease: the Seven Countries Study. Prev Med 24, 308-315.

Kulanuwat, S., Tungtrongchitr, R., Billington, D., Davies, I.G., 2015. Prevalence of plasma small dense LDL is increased in obesity in a Thai population. Lipids in Health and Disease 14, 8.

Kulis, M., Esteller, M., 2010. DNA methylation and cancer. Adv Genet 70, 27-56.

Kurdyukov, S., Bullock, M., 2016. DNA Methylation Analysis: Choosing the Right Method. Biology 5, 3.

Kutmon, M., van Iersel, M.P., Bohler, A., Kelder, T., Nunes, N., Pico, A.R., Evelo, C.T., 2015. PathVisio 3: An Extendable Pathway Analysis Toolbox. PLoS computational biology 11, e1004085.

Kwiatkowska, M., Norman, G., Parker, D., 2011. PRISM 4.0: Verification of probabilistic real-time systems, International Conference on Computer Aided Verification. Springer, pp. 585-591.

Lamb, R.F., 2012. Negative feedback loops: nutrient starvation employs a new tr(IKK) to inhibit PI3K. Mol Cell 45, 705-706.

Larsen, F., Gundersen, G., Lopez, R., Prydz, H., 1992. CpG islands as gene markers in the human genome. Genomics 13, 1095-1107.

Larson-Meyer, D.E., Heilbronn, L.K., Redman, L.M., Newcomer, B.R., Frisard, M.I., Anton, S., Smith, S.R., Maplstat, A.A., Ravussin, E., Pennington, C.T., 2006. Effect of Calorie Restriction With or Without Exercise on Insulin Sensitivity, β-Cell Function, Fat Cell Size, and Ectopic Lipid in Overweight Subjects. Diabetes care 29, 1337-1344.

Larson, I., Hoffmann, M.M., Ordovas, J.M., Schaefer, E.J., März, W., Kreuzer, J., 1999. The Lipoprotein Lipase HindIII Polymorphism: Association with Total Cholesterol and LDL-Cholesterol, but not with HDL and Triglycerides in 342 Females. Clinical Chemistry 45, 963-968.

Larson, I.A., Ordovas, J.M., DeLuca, C., Barnard, J.R., Feussner, G., Schaefer, E.J., 2000. Association of apolipoprotein (Apo)E genotype with plasma apo E levels. Atherosclerosis 148, 327-335.

Larson, K., Zagkos, L., Mc Auley, M., Roberts, J., Kavallaris, N.I., Matzavinos, A., 2019. Data-driven selection and parameter estimation for DNA methylation mathematical models. J Theor Biol 467, 87-99.

Law, M., 2000. Plant sterol and stanol margarines and health. Bmj 320, 861-864.

Le Novere, N., Bornstein, B., Broicher, A., Courtot, M., Donizelli, M., Dharuri, H., Li, L., Sauro, H., Schilstra, M., Shapiro, B., Snoep, J.L., Hucka, M., 2006. BioModels Database: a free, centralized database of curated, published, quantitative kinetic models of biochemical and cellular systems. Nucleic Acids Res 34, D689-691.

Le Novere, N., Hucka, M., Mi, H., Moodie, S., Schreiber, F., Sorokin, A., Demir, E., Wegner, K., Aladjem, M.I., Wimalaratne, S.M., Bergman, F.T., Gauges, R., Ghazal, P., Kawaji, H., Li, L., Matsuoka, Y., Villeger, A., Boyd, S.E., Calzone, L., Courtot, M., Dogrusoz, U., Freeman, T.C., Funahashi, A., Ghosh, S., Jouraku, A., Kim, S., Kolpakov, F., Luna, A., Sahle, S., Schmidt, E., Watterson, S., Wu, G., Goryanin, I., Kell, D.B., Sander, C., Sauro, H., Snoep, J.L., Kohn, K., Kitano, H., 2009. The Systems Biology Graphical Notation. Nat Biotech 27, 735-741.

Lee, C., Longo, V., 2016. Dietary restriction with and without caloric restriction for healthy aging. F1000Research 5, F1000 Faculty Rev-1117.

Lee, Y.G., Kim, I., Yoon, S.S., Park, S., Cheong, J.W., Min, Y.H., Lee, J.O., Bang, S.M., Yi, H.G., Kim, C.S., Park, Y., Kim, B.S., Mun, Y.C., Seong, C.M., Park, J., Lee, J.H., Kim, S.Y., Lee, H.G., Kim, Y.K., Kim, H.J., 2013. Comparative analysis between azacitidine and decitabine for the treatment of myelodysplastic syndromes. Br J Haematol 161, 339-347.

Li, C., Donizelli, M., Rodriguez, N., Dharuri, H., Endler, L., Chelliah, V., Li, L., He, E., Henry, A., Stefan, M., Snoep, J., Hucka, M., Le Novere, N., Laibe, C., 2010. BioModels Database: An enhanced, curated and annotated resource for published quantitative kinetic models. BMC Systems Biology 4, 92.

Li, J.J., Chen, J.L., 2005. Inflammation may be a bridge connecting hypertension and atherosclerosis. Med Hypotheses 64, 925-929.

Li, X., Hylemon, P., Pandak, W.M., Ren, S., 2006. Enzyme activity assay for cholesterol 27-hydroxylase in mitochondria. J Lipid Res 47, 1507-1512.

Li, X., Zhang, S., Blander, G., Tse, J.G., Krieger, M., Guarente, L., 2007. SIRT1 deacetylates and positively regulates the nuclear receptor LXR. Mol Cell 28, 91-106.

Li, Y., Tollefsbol, T.O., 2011. DNA methylation detection: Bisulfite genomic sequencing analysis. Methods in molecular biology (Clifton, N.J.) 791, 11-21.

Lichtenstein, A.H., Ausman, L.M., Carrasco, W., Jenner, J.L., Ordovas, J.M., Schaefer, E.J., 1993. Hydrogenation impairs the hypolipidemic effect of corn oil in humans. Hydrogenation, trans fatty acids, and plasma lipids. Arterioscler Thromb 13, 154-161.

Lim, D.H.K., Maher, E.R., 2010. DNA methylation: a form of epigenetic control of gene expression. The Obstetrician & Gynaecologist 12, 37-42.

Lim, U., Song, M.A., 2012. Dietary and lifestyle factors of DNA methylation. Methods Mol Biol 863, 359-376.

Lin, D.S., Connor, W.E., 1980. The long term effects of dietary cholesterol upon the plasma lipids, lipoproteins, cholesterol absorption, and the sterol balance in man: the demonstration of feedback inhibition of cholesterol biosynthesis and increased bile acid excretion. J Lipid Res 21, 1042-1052.

Lin, X.C., Zhang, T., Liu, L., Tang, H., Yu, R.Q., Jiang, J.H., 2016. Mass Spectrometry Based Ultrasensitive DNA Methylation Profiling Using Target Fragmentation Assay. Anal Chem 88, 1083-1087.

Lionarons, D.A., Boyer, J.L., Cai, S.Y., 2012. Evolution of substrate specificity for the bile salt transporter ASBT (SLC10A2). J Lipid Res 53, 1535-1542.

Lipsky, M.S., King, M., 2015. Biological theories of aging. Disease-a-Month 61, 460-466.

Liscum, L., 2008. Cholesterol biosynthesis, Biochemistry of Lipids, Lipoproteins, and Membranes, 5th ed. Elsevier, pp. 399-422.

Litovkin, K., Van Eynde, A., Joniau, S., Lerut, E., Laenen, A., Gevaert, T., Gevaert, O., Spahn, M., Kneitz, B., Gramme, P., Helleputte, T., Isebaert, S., Haustermans, K., Bollen, M., 2015. DNA

Methylation-Guided Prediction of Clinical Failure in High-Risk Prostate Cancer. PLOS ONE 10, e0130651.

Liu, J., Ma, K.L., Zhang, Y., Wu, Y., Hu, Z.B., Lv, L.L., Tang, R.N., Liu, H., Ruan, X.Z., Liu, B.C., 2015. Activation of mTORC1 disrupted LDL receptor pathway: a potential new mechanism for the progression of non-alcoholic fatty liver disease. Int J Biochem Cell Biol 61, 8-19.

Liu, J., Zeng, F.F., Liu, Z.M., Zhang, C.X., Ling, W.H., Chen, Y.M., 2013. Effects of blood triglycerides on cardiovascular and all-cause mortality: a systematic review and meta-analysis of 61 prospective studies. Lipids Health Dis 12, 159.

London, D.S., Beezhold, B., 2015. A phytochemical-rich diet may explain the absence of age-related decline in visual acuity of Amazonian hunter-gatherers in Ecuador. Nutrition Research 35, 107-117.

Long, J., Roth, M., 2007. Synthetic microarray data generation with RANGE and NEMO. Bioinformatics 24, 132-134.

Lopatina, N., Haskell, J.F., Andrews, L.G., Poole, J.C., Saldanha, S., Tollefsbol, T., 2002. Differential maintenance and de novo methylating activity by three DNA methyltransferases in aging and immortalized fibroblasts. Journal of Cellular Biochemistry 84, 324-334.

Lowes, D.A., Webster, N.R., Murphy, M.P., Galley, H.F., 2013. Antioxidants that protect mitochondria reduce interleukin-6 and oxidative stress, improve mitochondrial function, and reduce biochemical markers of organ dysfunction in a rat model of acute sepsis. British journal of anaesthesia 110, 472-480.

Lu, J., Hubner, K., Nanjee, M.N., Brinton, E.A., Mazer, N.A., 2014. An in-silico model of lipoprotein metabolism and kinetics for the evaluation of targets and biomarkers in the reverse cholesterol transport pathway. PLoS computational biology 10, e1003509.

Lu, Y., Feskens, E.J., Boer, J.M., Muller, M., 2010. The potential influence of genetic variants in genes along bile acid and bile metabolic pathway on blood cholesterol levels in the population. Atherosclerosis 210, 14-27.

Lund-Katz, S., Lyssenko, N.N., Nickel, M., Nguyen, D., Chetty, P.S., Weibel, G., Phillips, M.C., 2013. Mechanisms responsible for the compositional heterogeneity of nascent high density lipoprotein. The Journal of biological chemistry 288, 23150-23160.

Luthi-Carter, R., Taylor, D.M., Pallos, J., Lambert, E., Amore, A., Parker, A., Moffitt, H., Smith, D.L., Runne, H., Gokce, O., Kuhn, A., Xiang, Z., Maxwell, M.M., Reeves, S.A., Bates, G.P., Neri, C., Thompson, L.M., Marsh, J.L., Kazantsev, A.G., 2010. SIRT2 inhibition achieves neuroprotection by decreasing sterol biosynthesis. Proceedings of the National Academy of Sciences 107, 7927-7932.

Luu, W., Hart-Smith, G., Sharpe, L.J., Brown, A.J., 2015. The terminal enzymes of cholesterol synthesis, DHCR24 and DHCR7, interact physically and functionally. J Lipid Res 56, 888-897.

Lv, Y.-B., Yin, Z.-X., Chei, C.-L., Qian, H.-Z., Kraus, V.B., Zhang, J., Brasher, M.S., Shi, X.-M., Matchar, D.B., Zeng, Y., 2015. Low-density lipoprotein cholesterol was inversely associated with 3-year all-cause mortality among Chinese oldest old: Data from the Chinese Longitudinal Healthy Longevity Survey. Atherosclerosis 239, 137-142.

Mabbott, G.A., 1983. An introduction to cyclic voltammetry. Journal of Chemical Education 60, 697.

Macdonald, D.D., 2006. Reflections on the history of electrochemical impedance spectroscopy. Electrochimica Acta 51, 1376-1388.

Maegawa, S., Lu, Y., Tahara, T., Lee, J.T., Madzo, J., Liang, S., Jelinek, J., Colman, R.J., Issa, J.-P.J., 2017. Caloric restriction delays age-related methylation drift. Nature Communications 8, 539.

Mahley, R.W., Rall, S.C., Jr., 2000. Apolipoprotein E: far more than a lipid transport protein. Annu Rev Genomics Hum Genet 1, 507-537.

Mahmoudi, M.J., Mahmoudi, M., Siassi, F., Shokri, F., Eshraghian, M.R., Zarnani, A.H., Chahardoli, R., Hedayat, M., Khoshnoodi, J., Nayeri, H., Rezaei, N., Saboor-Yaraghi, A.A., 2011. Lymphocyte cytotoxicity of oxLDL in patients with atherosclerosis. Iran J Immunol 8, 27-33.

Makino, S., Ikegami, S., Kume, A., Horiuchi, H., Sasaki, H., Orii, N., 2010. Reducing the risk of infection in the elderly by dietary intake of yoghurt fermented with Lactobacillus delbrueckii ssp. bulgaricus OLL1073R-1. The British journal of nutrition 104, 998-1006.

Makivuokko, H., Tiihonen, K., Tynkkynen, S., Paulin, L., Rautonen, N., 2010. The effect of age and non-steroidal anti-inflammatory drugs on human intestinal microbiota composition. The British journal of nutrition 103, 227-234.

Marciani, L., Cox, E.F., Hoad, C.L., Totman, J.J., Costigan, C., Singh, G., Shepherd, V., Chalkley, L., Robinson, M., Ison, R., Gowland, P.A., Spiller, R.C., 2013. Effects of various food ingredients on gall bladder emptying. Eur J Clin Nutr 67, 1182-1187.

Marino, S., Hogue, I.B., Ray, C.J., Kirschner, D.E., 2008. A Methodology For Performing Global Uncertainty And Sensitivity Analysis In Systems Biology. Journal of theoretical biology 254, 178-196.

Martín, B., Solanas-Barca, M., García-Otín, Á.L., Pampín, S., Cofán, M., Ros, E., Rodríguez-Rey, J.C., Pocoví, M., Civeira, F., 2010. An NPC1L1 gene promoter variant is associated with autosomal dominant hypercholesterolemia. Nutrition, Metabolism and Cardiovascular Diseases 20, 236-242.

Masson, C.J., Plat, J., Mensink, R.P., Namiot, A., Kisielewski, W., Namiot, Z., Füllekrug, J., Ehehalt, R., Glatz, J.F.C., Pelsers, M.M.A.L., 2010. Fatty Acid- and Cholesterol Transporter Protein Expression along the Human Intestinal Tract. PLoS ONE 5, e10380.

Mayor, R., Casadomé, L., Azuara, D., Moreno, V., Clark, S.J., Capellà, G., Peinado, M.A., 2009. Long-range epigenetic silencing at 2q14.2 affects most human colorectal cancers and may have application as a non-invasive biomarker of disease. British Journal of Cancer 100, 1534-1539.

Mazein, A., Watterson, S., Hsieh, W.Y., Griffiths, W.J., Ghazal, P., 2013. A comprehensive machine-readable view of the mammalian cholesterol biosynthesis pathway. Biochem Pharmacol 86, 56-66.

Mc Auley, M., Jones, J., Wilkinson, D., Kirkwood, T., 2005. Modelling Lipid Metabolism to Improve Healthy Ageing. BMC Bioinformatics 6, P21.

Mc Auley, M.T., Choi, H., Mooney, K., Paul, E., Miller, V.M., 2015a. Systems Biology and Synthetic Biology: A New Epoch for Toxicology Research. Advances in Toxicology 2015, 14.

Mc Auley, Mark T., Guimera, Alvaro M., Hodgson, D., McDonald, N., Mooney, Kathleen M., Morgan, Amy E., Proctor, Carole J., 2017. Modelling the molecular mechanisms of aging. Bioscience Reports 37, BSR20160177.

Mc Auley, M.T., Kenny, R.A., Kirkwood, T.B., Wilkinson, D.J., Jones, J.J., Miller, V.M., 2009. A mathematical model of aging-related and cortisol induced hippocampal dysfunction. BMC Neurosci 10, 26.

Mc Auley, M.T., Mooney, K.M., 2014. Lipid metabolism and hormonal interactions: impact on cardiovascular disease and healthy aging. Expert Review of Endocrinology & Metabolism 9, 357-367.

Mc Auley, M.T., Mooney, K.M., 2015a. Computational systems biology for aging research. Interdiscip Top Gerontol 40, 35-48.

Mc Auley, M.T., Mooney, K.M., 2015b. Computationally Modeling Lipid Metabolism and Aging: A Mini-review. Computational and Structural Biotechnology Journal 13, 38-46.

Mc Auley, M.T., Mooney, K.M., 2017. LDL-C levels in older people: Cholesterol homeostasis and the free radical theory of ageing converge. Medical Hypotheses 104, 15-19.

Mc Auley, M.T., Mooney, K.M., Angell, P.J., Wilkinson, S.J., 2015b. Mathematical modelling of metabolic regulation in aging. Metabolites 5, 232-251.

Mc Auley, M.T., Proctor, C.J., Corfe, B.M., Cuskelly, C.J., Mooney, K.M., 2013. Nutrition Research and the Impact of Computational Systems Biology. Journal of Computer Science and Systems Biology 6, 271-285.

Mc Auley, M.T., Wilkinson, D.J., Jones, J.J.L., Kirkwood, T.B.L., 2012. A whole-body mathematical model of cholesterol metabolism and its age-associated dysregulation. BMC Systems Biology 6, 130-130.

McCarthy, R.R., O'Gara, F., 2015. The impact of phytochemicals present in the diet on microbial signalling in the human gut. Journal of Functional Foods 14, 684-691.

McCaskie, P.A., Cadby, G., Hung, J., McQuillan, B.M., Chapman, C.M., Carter, K.W., Thompson, P.L., Palmer, L.J., Beilby, J.P., 2006. The C-480T hepatic lipase polymorphism is associated with HDL-C but not with risk of coronary heart disease. Clin Genet 70, 114-121.

McGovern, A.P., Powell, B.E., Chevassut, T.J., 2012. A dynamic multi-compartmental model of DNA methylation with demonstrable predictive value in hematological malignancies. Journal of theoretical biology 310, 14-20.

McNamara, D.J., Kolb, R., Parker, T.S., Batwin, H., Samuel, P., Brown, C.D., Ahrens, E.H., 1987. Heterogeneity of cholesterol homeostasis in man. Response to changes in dietary fat quality and cholesterol quantity. Journal of Clinical Investigation 79, 1729-1739.

McQueen, M.J., Hawken, S., Wang, X., Ounpuu, S., Sniderman, A., Probstfield, J., Steyn, K., Sanderson, J.E., Hasani, M., Volkova, E., Kazmi, K., Yusuf, S., 2008. Lipids, lipoproteins, and apolipoproteins as risk markers of myocardial infarction in 52 countries (the INTERHEART study): a case-control study. The Lancet 372, 224-233.

Mecocci, P., Polidori, M.C., Troiano, L., Cherubini, A., Cecchetti, R., Pini, G., Straatman, M., Monti, D., Stahl, W., Sies, H., Franceschi, C., Senin, U., 2000. Plasma antioxidants and longevity: a study on healthy centenarians. Free Radical Biology and Medicine 28, 1243-1248.

Meier, P.J., Eckhardt, U., Schroeder, A., Hagenbuch, B., Stieger, B., 1997. Substrate specificity of sinusoidal bile acid and organic anion uptake systems in rat and human liver. Hepatology (Baltimore, Md.) 26, 1667-1677.

Mendizabal, I., Yi, S.V., 2016. Whole-genome bisulfite sequencing maps from multiple human tissues reveal novel CpG islands associated with tissue-specific regulation. Human Molecular Genetics 25, 69-82.

Menotti, A., Blackburn, H., Seccareccia, F., Kromhout, D., Nissinen, A., Karyonen, M., Fidanza, F., Giampaoli, S., Buzina, R., Mohacek, I., Nedeljkovic, S., Aravanis, C., Dontas, A., 1998. Relationship of some risk factors with typical and atypical manifestations of coronary heart disease. Cardiology 89, 59-67.

Menotti, A., Kromhout, D., Blackburn, H., Jacobs, D., Lanti, M., 2004a. Forty-year mortality from cardiovascular diseases and all causes of death in the US Railroad cohort of the Seven Countries Study. Eur J Epidemiol 19, 417-424.

Menotti, A., Lanti, M., Kafatos, A., Nissinen, A., Dontas, A., Nedeljkovic, S., Kromhout, D., 2004b. The role of a baseline casual blood pressure measurement and of blood pressure changes in middle age in prediction of cardiovascular and all-cause mortality occurring late in life: a cross-cultural comparison among the European cohorts of the Seven Countries Study. J Hypertens 22, 1683-1690.

Mercado-Sáenz, S., Ruiz-Gómez, M.J., Morales-Moreno, F., Martínez-Morillo, M., 2010. Cellular aging: theories and technological influence. Brazilian Archives of Biology and Technology 53, 1319-1332.

Merlo, A., Herman, J.G., Mao, L., Lee, D.J., Gabrielson, E., Burger, P.C., Baylin, S.B., Sidransky, D., 1995. 5' CpG island methylation is associated with transcriptional silencing of the tumour suppressor p16/CDKN2/MTS1 in human cancers. Nat Med 1, 686-692.

Merzouk, H., Madani, S., Boualga, A., Prost, J., Bouchenak, M., Belleville, J., 2001. Age-related changes in cholesterol metabolism in macrosomic offspring of rats with streptozotocin-induced diabetes. Journal of Lipid Research 42, 1152-1159.

Messaoudi, M., Lalonde, R., Violle, N., Javelot, H., Desor, D., Nejdi, A., Bisson, J.F., Rougeot, C., Pichelin, M., Cazaubiel, M., Cazaubiel, J.M., 2011. Assessment of psychotropic-like properties

of a probiotic formulation (Lactobacillus helveticus R0052 and Bifidobacterium longum R0175) in rats and human subjects. The British journal of nutrition 105, 755-764.

Micheloni, A., Orsi, G., De Maria, C., Vozzi, G., 2015. ADMET: ADipocyte METabolism mathematical model. Computer methods in biomechanics and biomedical engineering 18, 1386-1391.

Mileo, A.M., Miccadei, S., 2016. Polyphenols as Modulator of Oxidative Stress in Cancer Disease: New Therapeutic Strategies. Oxidative Medicine and Cellular Longevity 2016, 17.

Millan, J., Pinto, X., Munoz, A., Zuniga, M., Rubies-Prat, J., Pallardo, L.F., Masana, L., Mangas, A., Hernandez-Mijares, A., Gonzalez-Santos, P., Ascaso, J.F., Pedro-Botet, J., 2009. Lipoprotein ratios: Physiological significance and clinical usefulness in cardiovascular prevention. Vasc Health Risk Manag 5, 757-765.

Millar, J.S., Lichtenstein, A.H., Cuchel, M., Dolnikowski, G.G., Hachey, D.L., Cohn, J.S., Schaefer, E.J., 1995. Impact of age on the metabolism of VLDL, IDL, and LDL apolipoprotein B-100 in men. J Lipid Res 36, 1155-1167.

Milman, S., Atzmon, G., Crandall, J., Barzilai, N., 2014. Phenotypes and Genotypes of High Density Lipoprotein Cholesterol in Exceptional Longevity. Current vascular pharmacology 12, 690-697.

Mishra, S., Somvanshi, P.R., Venkatesh, K., 2014. Control of cholesterol homeostasis by entero-hepatic bile transport–the role of feedback mechanisms. RSC Advances 4, 58964-58975.

Mita, S., Suzuki, H., Akita, H., Hayashi, H., Onuki, R., Hofmann, A.F., Sugiyama, Y., 2006. Vectorial transport of unconjugated and conjugated bile salts by monolayers of LLC-PK1 cells doubly transfected with human NTCP and BSEP or with rat Ntcp and Bsep. American journal of physiology. Gastrointestinal and liver physiology 290, G550-556.

Mizuno, S.-i., Chijiwa, T., Okamura, T., Akashi, K., Fukumaki, Y., Niho, Y., Sasaki, H., 2001. Expression of DNA methyltransferases DNMT1,3A, and 3B in normal hematopoiesis and in acute and chronic myelogenous leukemia. Blood 97, 1172-1179.

Moebius, F.F., Fitzky, B.U., Lee, J.N., Paik, Y.K., Glossmann, H., 1998. Molecular cloning and expression of the human delta7-sterol reductase. Proceedings of the National Academy of Sciences of the United States of America 95, 1899-1902.

Moelans, C.B., de Groot, J.S., Pan, X., van der Wall, E., van Diest, P.J., 2014. Clonal intratumor heterogeneity of promoter hypermethylation in breast cancer by MS-MLPA. Mod Pathol 27, 869-874.

Montavon, C., Gloss, B.S., Warton, K., Barton, C.A., Statham, A.L., Scurry, J.P., Tabor, B., Nguyen, T.V., Qu, W., Samimi, G., Hacker, N.F., Sutherland, R.L., Clark, S.J., O'Brien, P.M., 2012. Prognostic and diagnostic significance of DNA methylation patterns in high grade serous ovarian cancer. Gynecologic Oncology 124, 582-588.

Moodie, S., Le Novere, N., Demir, E., Mi, H., Villeger, A., 2012. Systems Biology Graphical Notation: Process Description language Level 1 User Manual.

Mooney, K.M., Morgan, A.E., Mc Auley, M.T., 2016. Aging and computational systems biology. Wiley Interdisciplinary Reviews: Systems Biology and Medicine 8, 123-139.

Morgan, A.E., Mooney, K.M., Wilkinson, S.J., Pickles, N.A., Mc Auley, M.T., 2016a. Cholesterol metabolism: A review of how ageing disrupts the biological mechanisms responsible for its regulation. Ageing Research Reviews 27, 108-124.

Morgan, A.E., Mooney, K.M., Wilkinson, S.J., Pickles, N.A., Mc Auley, M.T., 2016b. Investigating cholesterol metabolism and ageing using a systems biology approach. Proceedings of the Nutrition Society 76, 378-391.

Morgan, A.E., Mooney, K.M., Wilkinson, S.J., Pickles, N.A., Mc Auley, M.T., 2016c. Mathematically modelling the dynamics of cholesterol metabolism and ageing. Biosystems 145, 19-32.

Moritz, B., Striegel, K., de Graaf, A.A., Sahm, H., 2000. Kinetic properties of the glucose-6-phosphate and 6 phosphogluconate dehydrogenases from Corynebacterium glutamicum and their

application for predicting pentose phosphate pathway flux in vivo. European Journal of Biochemistry 267, 3442-3452.

Moro-Garcia, M.A., Alonso-Arias, R., Baltadjieva, M., Fernandez Benitez, C., Fernandez Barrial, M.A., Diaz Ruisanchez, E., Alonso Santos, R., Alvarez Sanchez, M., Saavedra Mijan, J., Lopez-Larrea, C., 2013. Oral supplementation with Lactobacillus delbrueckii subsp. bulgaricus 8481 enhances systemic immunity in elderly subjects. Age (Dordr) 35, 1311-1326.

Mousavi, S.A., Berge, K.E., Leren, T.P., 2009. The unique role of proprotein convertase subtilisin/kexin 9 in cholesterol homeostasis. Journal of internal medicine 266, 507-519.

Mueller, S., Saunier, K., Hanisch, C., Norin, E., Alm, L., Midtvedt, T., Cresci, A., Silvi, S., Orpianesi, C., Verdenelli, M.C., Clavel, T., Koebnick, C., Zunft, H.-J.F., Doré, J., Blaut, M., 2006. Differences in Fecal Microbiota in Different European Study Populations in Relation to Age, Gender, and Country: a Cross-Sectional Study. Applied and environmental microbiology 72, 1027-1033.

Muendlein, A., Leiherer, A., Saely, C.H., Rein, P., Zanolin, D., Kinz, E., Brandtner, E.-M., Fraunberger, P., Drexel, H., 2015. Common single nucleotide polymorphisms at the NPC1L1 gene locus significantly predict cardiovascular risk in coronary patients. Atherosclerosis 242, 340-345.

Muñoz-Barrios, S., Guzmán-Guzmán, I.P., Muñoz-Valle, J.F., Salgado-Bernabé, A.B., Salgado-Goytia, L., Parra-Rojas, I., 2012. Association of the Hindiii and S447X Polymorphisms in Lpl Gene with Hypertension and Type 2 Diabetes in Mexican Families. Disease markers 33, 313-320.

Murakami, K., Okada, Y., Okuda, K., 1982. Purification and characterization of 7 alpha-hydroxy-4-cholesten-3-one 12 alpha-monooxygenase. The Journal of biological chemistry 257, 8030-8035.

Murr, C., Grammer, T.B., Kleber, M.E., Meinitzer, A., Marz, W., Fuchs, D., 2015. Low serum tryptophan predicts higher mortality in cardiovascular disease. Eur J Clin Invest 45, 247-254.

Murtomäki, S., Tahvanainen, E., Antikainen, M., Tiret, L., Nicaud, V., Jansen, H., Ehnholm, C., Group, o.b.o.t.E.A.R.S., 1997. Hepatic Lipase Gene Polymorphisms Influence Plasma HDL Levels: Results From Finnish EARS Participants. Arteriosclerosis, Thrombosis, and Vascular Biology 17, 1879-1884.

Nagafuchi, S., Yamaji, T., Kawashima, A., Saito, Y., Takahashi, T., Yamamoto, T., Maruyama, M., Akatsu, H., 2015. Effects of a Formula Containing Two Types of Prebiotics, Bifidogenic Growth Stimulator and Galacto-oligosaccharide, and Fermented Milk Products on Intestinal Microbiota and Antibody Response to Influenza Vaccine in Elderly Patients: A Randomized Controlled Trial. Pharmaceuticals 8, 351-365.

Naik, A., Rozman, D., Belič, A., 2014. SteatoNet: The First Integrated Human Metabolic Model with Multi-layered Regulation to Investigate Liver-Associated Pathologies. PLoS computational biology 10, e1003993.

Nandakumar, V., Vaid, M., Katiyar, S.K., 2011. (-)-Epigallocatechin-3-gallate reactivates silenced tumor suppressor genes, Cip1/p21 and p16INK4a, by reducing DNA methylation and increasing histones acetylation in human skin cancer cells. Carcinogenesis 32, 537-544.

Navarese, E.P., Kolodziejczak, M., Schulze, V., Gurbel, P.A., Tantry, U., Lin, Y., Brockmeyer, M., Kandzari, D.E., Kubica, J.M., D'Agostino, R.B., Sr., Kubica, J., Volpe, M., Agewall, S., Kereiakes, D.J., Kelm, M., 2015. Effects of Proprotein Convertase Subtilisin/Kexin Type 9 Antibodies in Adults With Hypercholesterolemia: A Systematic Review and Meta-analysis. Ann Intern Med 163, 40-51.

Netea, M.G., Demacker, P.N., Kullberg, B.J., Boerman, O.C., Verschueren, I., Stalenhoef, A.F., van der Meer, J.W., 1996. Low-density lipoprotein receptor-deficient mice are protected against lethal endotoxemia and severe gram-negative infections. The Journal of clinical investigation 97, 1366-1372.

Niccoli, T., Partridge, L., 2012. Ageing as a Risk Factor for Disease. Current Biology 22, R741-R752.

Norata, G.D., Banfi, C., Pirillo, A., Tremoli, E., Hamsten, A., Catapano, A.L., Eriksson, P., 2004. Oxidised-HDL3 induces the expression of PAI-1 in human endothelial cells. Role of p38MAPK activation and mRNA stabilization. Br J Haematol 127, 97-104.

O'Sullivan, O., Coakley, M., Lakshminarayanan, B., Conde, S., Claesson, M.J., Cusack, S., Fitzgerald, A.P., O'Toole, P.W., Stanton, C., Ross, R.P., 2013. Alterations in intestinal microbiota of elderly Irish subjects post-antibiotic therapy. J Antimicrob Chemother 68, 214-221.

OFNS, 2013. Mortality Assumptions, 2012-based National Population Projections, in: Statistics, O.f.N. (Ed.).

OFNS, 2017. Deaths registered in England and Wales: 2016.

Ohashi, R., Mu, H., Wang, X., Yao, Q., Chen, C., 2005. Reverse cholesterol transport and cholesterol efflux in atherosclerosis. QJM 98, 845-856.

Ohtani, H., Hayashi, K., Hirata, Y., Dojo, S., Nakashima, K., Nishio, E., Kurushima, H., Saeki, M., Kajiyama, G., 1990. Effects of dietary cholesterol and fatty acids on plasma cholesterol level and hepatic lipoprotein metabolism. J Lipid Res 31, 1413-1422.

Okano, M., Bell, D.W., Haber, D.A., Li, E., 1999. DNA Methyltransferases Dnmt3a and Dnmt3b Are Essential for De Novo Methylation and Mammalian Development. Cell 99, 247-257.

Okuda, A., Okuda, K., 1984. Purification and characterization of delta 4-3-ketosteroid 5 beta-reductase. The Journal of biological chemistry 259, 7519-7524.

Olivecrona, G., Beisiegel, U., 1997. Lipid Binding of Apolipoprotein CII Is Required for Stimulation of Lipoprotein Lipase Activity Against Apolipoprotein CII–Deficient Chylomicrons. Arteriosclerosis, Thrombosis, and Vascular Biology 17, 1545-1549.

Oner, O., Aslim, B., Aydas, S.B., 2014. Mechanisms of cholesterol-lowering effects of lactobacilli and bifidobacteria strains as potential probiotics with their bsh gene analysis. J Mol Microbiol Biotechnol 24, 12-18.

Ozasa, S., Boyd, G.S., 1981. Cholesterol 7 alpha-hydroxylase of rat liver. Studies on the solubilisation, resolution and reconstitution of the enzyme complex. European journal of biochemistry / FEBS 119, 263-272.

Paalvast, Y., Kuivenhoven, J.A., Groen, A.K., 2015. Evaluating computational models of cholesterol metabolism. Biochimica et Biophysica Acta (BBA) - Molecular and Cell Biology of Lipids 1851, 1360-1376.

Pallottini, V., Martini, C., Cavallini, G., Bergamini, E., Mustard, K.J., Hardie, D.G., Trentalance, A., 2007. Age-related HMG-CoA reductase deregulation depends on ROS-induced p38 activation. Mechanisms of Ageing and Development 128, 688-695.

Pallottini, V., Martini, C., Pascolini, A., Cavallini, G., Gori, Z., Bergamini, E., Incerpi, S., Trentalance, A., 2005. 3-Hydroxy-3-methylglutaryl coenzyme A reductase deregulation and age-related hypercholesterolemia: A new role for ROS. Mechanisms of Ageing and Development 126, 845-851.

Papier, K., Jordan, S., D'Este, C., Bain, C., Peungson, J., Banwell, C., Yiengprugsawan, V., Seubsman, S.-a., Sleigh, A., 2016. Incidence and risk factors for type 2 diabetes mellitus in transitional Thailand: results from the Thai cohort study. BMJ Open 6, e014102.

Pappu, A.S., Steiner, R.D., Connor, S.L., Flavell, D.P., Lin, D.S., Hatcher, L., Illingworth, D.R., Connor, W.E., 2002. Feedback inhibition of the cholesterol biosynthetic pathway in patients with Smith-Lemli-Opitz syndrome as demonstrated by urinary mevalonate excretion. J Lipid Res 43, 1661-1669.

Parini, P., Angelin, B., Rudling, M., 1999. Cholesterol and lipoprotein metabolism in aging: reversal of hypercholesterolemia by growth hormone treatment in old rats. Arterioscler Thromb Vasc Biol 19, 832-839.

Park, H.J., Bailey, L.B., Shade, D.C., Hausman, D.B., Hohos, N.M., Meagher, R.B., Kauwell, G.P.A., Lewis, R.D., Smith, A.K., 2017. Distinctions in gene-specific changes in DNA methylation in response to folic acid supplementation between women with normal weight and obesity. Obesity Research & Clinical Practice.

Park, S.-H., Kim, K.-A., Ahn, Y.-T., Jeong, J.-J., Huh, C.-S., Kim, D.-H., 2015. Comparative analysis of gut microbiota in elderly people of urbanized towns and longevity villages. BMC Microbiology 15, 49.

Parton, A., McGilligan, V., O'Kane, M., Baldrick, F.R., Watterson, S., 2015. Computational modelling of atherosclerosis. Briefings in Bioinformatics.

Passarino, G., De Rango, F., Montesanto, A., 2016. Human longevity: Genetics or Lifestyle? It takes two to tango. Immunity & Ageing : I & A 13, 12.

Patel, S., Shukla, R., Goyal, A., 2015. Probiotics in valorization of innate immunity across various animal models. Journal of Functional Foods 14, 549-561.

Patsch, J.R., Prasad, S., Gotto, A.M., Jr., Patsch, W., 1987. High density lipoprotein2. Relationship of the plasma levels of this lipoprotein species to its composition, to the magnitude of postprandial lipemia, and to the activities of lipoprotein lipase and hepatic lipase. The Journal of clinical investigation 80, 341-347.

Patterson, K., Molloy, L., Qu, W., Clark, S., 2011. DNA Methylation: Bisulphite Modification and Analysis. Journal of Visualized Experiments : JoVE, 3170.

Patti, M.E., Kahn, B.B., 2004. Nutrient sensor links obesity with diabetes risk. Nat Med 10, 1049-1050.

Peterson, T.R., Sengupta, S.S., Harris, T.E., Carmack, A.E., Kang, S.A., Balderas, E., Guertin, D.A., Madden, K.L., Carpenter, A.E., Finck, B.N., Sabatini, D.M., 2011. mTOR complex 1 regulates lipin 1 localization to control the SREBP pathway. Cell 146, 408-420.

Pfeifer, G.P., Steigerwald, S.D., Hansen, R.S., Gartler, S.M., Riggs, A.D., 1990. Polymerase chain reaction-aided genomic sequencing of an X chromosome-linked CpG island: methylation patterns suggest clonal inheritance, CpG site autonomy, and an explanation of activity state stability. Proceedings of the National Academy of Sciences 87, 8252-8256.

Phillips, M.C., 2014. Apolipoprotein E isoforms and lipoprotein metabolism. IUBMB Life 66, 616-623.

Piyathilake, C.J., Badiga, S., Borak, S.G., Weragoda, J., Bae, S., Matthews, R., Bell, W.C., Partridge, E.E., 2017. A higher degree of expression of DNA methyl transferase 1 in cervical cancer is associated with poor survival outcome. International Journal of Women's Health 9, 413-420.

Planavila, A., Iglesias, R., Giralt, M., Villarroya, F., 2011. Sirt1 acts in association with PPARalpha to protect the heart from hypertrophy, metabolic dysregulation, and inflammation. Cardiovasc Res 90, 276-284.

Pogribny, I.P., Ross, S.A., Wise, C., Pogribna, M., Jones, E.A., Tryndyak, V.P., James, S.J., Dragan, Y.P., Poirier, L.A., 2006. Irreversible global DNA hypomethylation as a key step in hepatocarcinogenesis induced by dietary methyl deficiency. Mutation Research/Fundamental and Molecular Mechanisms of Mutagenesis 593, 80-87.

Polisecki, E., Peter, I., Simon, J.S., Hegele, R.A., Robertson, M., Ford, I., Shepherd, J., Packard, C., Jukema, J.W., de Craen, A.J.M., Westendorp, R.G.J., Buckley, B.M., Schaefer, E.J., on behalf of the Prospective Study of Pravastatin in the Elderly at Risk, I., 2010. Genetic variation at the NPC1L1 gene locus, plasma lipoproteins, and heart disease risk in the elderly. Journal of Lipid Research 51, 1201-1207.

Polo, M., de Bravo, M.G., Carbone, C., 1999. 3-Hydroxy-3-methylglutaryl coenzyme a reductase activity in liver of athymic mice with or without an implanted human carcinoma. Comparative biochemistry and physiology. Part B, Biochemistry & molecular biology 122, 433-437.

Polokoff, M.A., Bell, R.M., 1977. Characterization of liver cholic acid coenzyme A ligase activity. Evidence that separate microsomal enzymes are responsible for cholic acid and fatty acid activation. The Journal of biological chemistry 252, 1167-1171.

Pool, F., Currie, R., Sweby, P.K., Salazar, J.D., Tindall, M.J., 2018. A mathematical model of the mevalonate cholesterol biosynthesis pathway. Journal of Theoretical Biology 443, 157-176.

Popov, D., 2010. Endothelial cell dysfunction in hyperglycemia: Phenotypic change, intracellular signaling modification, ultrastructural alteration, and potential clinical outcomes. International Journal of Diabetes Mellitus 2, 189-195.

Potter, D., Miziorko, H.M., 1997. Identification of catalytic residues in human mevalonate kinase. The Journal of biological chemistry 272, 25449-25454.

Pratt, A.C., Wattis, J.A.D., Salter, A.M., 2015. Mathematical modelling of hepatic lipid metabolism. Mathematical Biosciences 262, 167-181.

Prince, M.J., Wu, F., Guo, Y., Gutierrez Robledo, L.M., O'Donnell, M., Sullivan, R., Yusuf, S., 2015. The burden of disease in older people and implications for health policy and practice. The Lancet 385, 549-562.

Pufulete, M., Al-Ghnaniem, R., Khushal, A., Appleby, P., Harris, N., Gout, S., Emery, P.W., Sanders, T.A.B., 2005. Effect of folic acid supplementation on genomic DNA methylation in patients with colorectal adenoma. Gut 54, 648-653.

Puska, P., 1973. The North Karelia project: an attempt at community prevention of cardiovascular disease. WHO Chron 27, 55-58.

Puska, P., 2008. The North Karelia Project: 30 years successfully preventing chronic diseases. Diabetes Voice 53, 26-29.

Puska, P., Tuomilehto, J., Salonen, J., Neittaanmäki, L., Maki, J., Virtamo, J., Nissinen, A., Koskela, K., Takalo, T., 1979. Changes in coronary risk factors during comprehensive five-year community programme to control cardiovascular diseases (North Karelia project). British Medical Journal 2, 1173-1178.

Qiu, X., Brown, K., Hirschey, M.D., Verdin, E., Chen, D., 2010. Calorie restriction reduces oxidative stress by SIRT3-mediated SOD2 activation. Cell Metab 12, 662-667.

Quek, K., Li, J., Estecio, M., Zhang, J., Fujimoto, J., Roarty, E., Little, L., Chow, C.-W., Song, X., Behrens, C., Chen, T., William, W.N., Swisher, S., Heymach, J., Wistuba, I., Zhang, J., Futreal, A., Zhang, J., 2017. DNA methylation intratumor heterogeneity in localized lung adenocarcinomas. Oncotarget 8, 21994-22002.

Quintao, E., Grundy, S.M., Ahrens, E.H., Jr., 1971. Effects of dietary cholesterol on the regulation of total body cholesterol in man. J Lipid Res 12, 233-247.

Rader, D.J., Schaefer, J.R., Lohse, P., Ikewaki, K., Thomas, F., Harris, W.A., Zech, L.A., Dujovne, C.A., Brewer, H.B., Jr., 1993. Increased production of apolipoprotein A-I associated with elevated plasma levels of high-density lipoproteins, apolipoprotein A-I, and lipoprotein A-I in a patient with familial hyperalphalipoproteinemia. Metabolism 42, 1429-1434.

Radhakrishnan, S., Krishnamoorthy, K., Sekar, C., Wilson, J., Kim, S.J., 2014. A highly sensitive electrochemical sensor for nitrite detection based on Fe2O3 nanoparticles decorated reduced graphene oxide nanosheets. Applied Catalysis B: Environmental 148-149, 22-28.

Rampelli, S., Candela, M., Turroni, S., Biagi, E., Collino, S., Franceschi, C., O'Toole, P.W., Brigidi, P., 2013. Functional metagenomic profiling of intestinal microbiome in extreme ageing. Aging 5, 902-912.

Rasmussen, K.D., Helin, K., 2016. Role of TET enzymes in DNA methylation, development, and cancer. Genes & Development 30, 733-750.

Rauch, T., Pfeifer, G.P., 2005. Methylated-CpG island recovery assay: a new technique for the rapid detection of methylated-CpG islands in cancer. Lab Invest 85, 1172-1180.

Renfurm, L.N., Bandsma, R.H., Verkade, H.J., Hulzebos, C.V., van Dijk, T., Boer, T., Stellaard, F., Kuipers, F., Sauer, P.J., 2004. Cholesterol synthesis and de novo lipogenesis in premature infants determined by mass isotopomer distribution analysis. Pediatr Res 56, 602-607.

Repa, J.J., Berge, K.E., Pomajzl, C., Richardson, J.A., Hobbs, H., Mangelsdorf, D.J., 2002. Regulation of ATP-binding Cassette Sterol Transporters ABCG5 and ABCG8 by the Liver X Receptors α and β. Journal of Biological Chemistry 277, 18793-18800.

Retter, U., Lohse, H., 2010. Electrochemical Impedance Spectroscopy, in: Scholz, F., Bond, A.M., Compton, R.G., Fiedler, D.A., Inzelt, G., Kahlert, H., Komorsky-Lovrić, Š., Lohse, H., Lovrić, M., Marken, F., Neudeck, A., Retter, U., Scholz, F., Stojek, Z. (Eds.), Electroanalytical Methods: Guide to Experiments and Applications. Springer Berlin Heidelberg, Berlin, Heidelberg, pp. 159-177.

Rhinn, H., Fujita, R., Qiang, L., Cheng, R., Lee, J.H., Abeliovich, A., 2013. Integrative genomics identifies APOE ε4 effectors in Alzheimer's disease. Nature 500, 45-50.

Richard, C., Couture, P., Desroches, S., Benjannet, S., Seidah, N.G., Lichtenstein, A.H., Lamarche, B., 2012. Effect of the Mediterranean diet with and without weight loss on surrogate markers of cholesterol homeostasis in men with the metabolic syndrome. The British journal of nutrition 107, 705-711.

Richardson, B., 2003. DNA methylation and autoimmune disease. Clin Immunol 109, 72-79.

Ridaura, V.K., Faith, J.J., Rey, F.E., Cheng, J., Duncan, A.E., Kau, A.L., Griffin, N.W., Lombard, V., Henrissat, B., Bain, J.R., Muehlbauer, M.J., Ilkayeva, O., Semenkovich, C.F., Funai, K., Hayashi, D.K., Lyle, B.J., Martini, M.C., Ursell, L.K., Clemente, J.C., Van Treuren, W., Walters, W.A., Knight, R., Newgard, C.B., Heath, A.C., Gordon, J.I., 2013. Gut Microbiota from Twins Discordant for Obesity Modulate Metabolism in Mice. Science 341.

Ridker, P.M., Mora, S., Rose, L., 2016. Percent reduction in LDL cholesterol following high-intensity statin therapy: potential implications for guidelines and for the prescription of emerging lipid-lowering agents. European heart journal 37, 1373-1379.

Ridlon, J.M., Kang, D.-J., Hylemon, P.B., 2006. Bile salt biotransformations by human intestinal bacteria. Journal of Lipid Research 47, 241-259.

Rifai, L., Silver, M.A., 2015. A Review of the DASH Diet as an Optimal Dietary Plan for Symptomatic Heart Failure. Progress in Cardiovascular Diseases.

Riggs, A.D., Xiong, Z., 2004. Methylation and epigenetic fidelity. Proceedings of the National Academy of Sciences 101, 4-5.

Risley, J.M., 2002. Cholesterol Biosynthesis: Lanosterol to Cholesterol. Journal of Chemical Education 79, 377.

Ristow, M., Zarse, K., 2010. How increased oxidative stress promotes longevity and metabolic health: The concept of mitochondrial hormesis (mitohormesis). Exp Gerontol 45, 410-418.

Rodriguez-Silva, A.A., Movil-Cabrera, O., Oliveira dos Anjos, C.T., Staser, J.A., 2016. Supercapacitor-Based Biosensor for Low Density Lipoprotein Detection. Journal of The Electrochemical Society 163, B256-B263.

Rodriguez, N., Donizelli, M., Le Novère, N., 2007. SBMLeditor: effective creation of models in the Systems Biology Markup Language (SBML). BMC Bioinformatics 8, 79-79.

Rohn, H., Junker, A., Hartmann, A., Grafahrend-Belau, E., Treutler, H., Klapperstuck, M., Czauderna, T., Klukas, C., Schreiber, F., 2012. VANTED v2: a framework for systems biology applications. BMC Syst Biol 6, 139.

Rosenfeld, M.E., Campbell, L.A., 2011. Pathogens and atherosclerosis: update on the potential contribution of multiple infectious organisms to the pathogenesis of atherosclerosis. Thromb Haemost 106, 858-867.

Ross, R., Masuda, J., Raines, E., Gown, A., Katsuda, S., Sasahara, M., Malden, L., Masuko, H., Sato, H., 1990. Localization of PDGF-B protein in macrophages in all phases of atherogenesis. Science 248, 1009-1012.

Rosty, C., Ueki, T., Argani, P., Jansen, M., Yeo, C.J., Cameron, J.L., Hruban, R.H., Goggins, M., 2002. Overexpression of S100A4 in Pancreatic Ductal Adenocarcinomas Is Associated with Poor Differentiation and DNA Hypomethylation. The American Journal of Pathology 160, 45-50.

Russell, D.W., 2003. The enzymes, regulation, and genetics of bile acid synthesis. Annual review of biochemistry 72, 137-174.

Rzehak, P., Covic, M., Saffery, R., Reischl, E., Wahl, S., Grote, V., Weber, M., Xhonneux, A., Langhendries, J.-P., Ferre, N., Closa-Monasterolo, R., Escribano, J., Verduci, E., Riva, E., Socha, P., Gruszfeld, D., Koletzko, B., 2017. DNA-Methylation and Body Composition in Preschool Children: Epigenome-Wide-Analysis in the European Childhood Obesity Project (CHOP)-Study. Scientific reports 7, 14349.

Saheb, A., Patterson, S., Josowicz, M., 2014. Probing for DNA methylation with a voltammetric DNA detector. Analyst 139, 786-792.

Sakurai, S., Fukao, T., Haapalainen, A.M., Zhang, G., Yamada, K., Lilliu, F., Yano, S., Robinson, P., Gibson, M.K., Wanders, R.J., Mitchell, G.A., Wierenga, R.K., Kondo, N., 2007. Kinetic and

expression analyses of seven novel mutations in mitochondrial acetoacetyl-CoA thiolase (T2): identification of a Km mutant and an analysis of the mutational sites in the structure. Molecular genetics and metabolism 90, 370-378.

Salas-Salvadó, J., Bulló, M., Babio, N., Martínez-González, M.Á., Ibarrola-Jurado, N., Basora, J., Estruch, R., Covas, M.I., Corella, D., Arós, F., Ruiz-Gutiérrez, V., Ros, E., Investigators, f.t.P.S., 2011. Reduction in the Incidence of Type 2 Diabetes With the Mediterranean Diet: Results of the PREDIMED-Reus nutrition intervention randomized trial. Diabetes Care 34, 14-19.

Salcedo-Sora, J.E., Mc Auley, M.T., 2016. A mathematical model of microbial folate biosynthesis and utilisation: implications for antifolate development. Mol Biosyst 12, 923-933.

Salemans, J.M., Nagengast, F.M., Tangerman, A., van Schaik, A., Hopman, W.P., de Haan, A.F., Jansen, J.B., 1993. Effect of ageing on postprandial conjugated and unconjugated serum bile acid levels in healthy subjects. Eur J Clin Invest 23, 192-198.

Sanchez-Mut, J.V., Heyn, H., Vidal, E., Moran, S., Sayols, S., Delgado-Morales, R., Schultz, M.D., Ansoleaga, B., Garcia-Esparcia, P., Pons-Espinal, M., de Lagran, M.M., Dopazo, J., Rabano, A., Avila, J., Dierssen, M., Lott, I., Ferrer, I., Ecker, J.R., Esteller, M., 2016. Human DNA methylomes of neurodegenerative diseases show common epigenomic patterns. Transl Psychiatry 6, e718.

Sane, A.T., Sinnett, D., Delvin, E., Bendayan, M., Marcil, V., Menard, D., Beaulieu, J.F., Levy, E., 2006. Localization and role of NPC1L1 in cholesterol absorption in human intestine. J Lipid Res 47, 2112-2120.

Saneei, P., Salehi-Abargouei, A., Esmaillzadeh, A., Azadbakht, L., 2014. Influence of Dietary Approaches to Stop Hypertension (DASH) diet on blood pressure: A systematic review and meta-analysis on randomized controlled trials. Nutrition, Metabolism and Cardiovascular Diseases 24, 1253-1261.

Santoro, A., Pini, E., Scurti, M., Palmas, G., Berendsen, A., Brzozowska, A., Pietruszka, B., Szczecinska, A., Cano, N., Meunier, N., de Groot, C.P.G.M., Feskens, E., Fairweather-Tait, S., Salvioli, S., Capri, M., Brigidi, P., Franceschi, C., Fabbri, C., Bertarelli, C., Izzi, M., Mazzocchi, M., Chardigny, J.M., Morio, B., Rossi, D., Notarfonso, M., O'Toole, P.W., Cashman, K., Carding, S.R., Nicoletti, C., Jacobs, D., Xipsiti, M., Fernandez, L., Wills, J., Irz, X., Kuosmanen, N., Gonos, E.S., Voutetakis, K., Salmon, M., Toussaint, O., Traill, B.W., Nocella, G., Caracciolo, B., Xu, W., Mikko, I., Tuure, T., Brummer, R., Kadi, F., Breton, S., Triomphe, M., Magario, G., Villani, F., Pancrazio, A., Teufner, B., Stocker, J., Echevarría, F.J., Iglesias, J.R., Smrž, F., Krejcirova, L., Koytsomitropoulou, E., Georgakidis, K., Yornuk, R., Ucar, C., Van Ommen, B., Bouwman, J., Collino, S., Jankovics, C., Losó, A., de Vos, W., Fuentes, S., Commelin, E., 2014. Combating inflammaging through a Mediterranean whole diet approach: The NU-AGE project's conceptual framework and design. Mechanisms of Ageing and Development 136–137, 3-13.

Satoh, A., Stein, L., Imai, S., 2011. The role of mammalian sirtuins in the regulation of metabolism, aging, and longevity. Handb Exp Pharmacol 206, 125-162.

Savignac, H.M., Tramullas, M., Kiely, B., Dinan, T.G., Cryan, J.F., 2015. Bifidobacteria modulate cognitive processes in an anxious mouse strain. Behav Brain Res 287, 59-72.

Saxonov, S., Berg, P., Brutlag, D.L., 2006. A genome-wide analysis of CpG dinucleotides in the human genome distinguishes two distinct classes of promoters. Proceedings of the National Academy of Sciences of the United States of America 103, 1412-1417.

Sayin, Sama I., Wahlström, A., Felin, J., Jäntti, S., Marschall, H.-U., Bamberg, K., Angelin, B., Hyötyläinen, T., Orešič, M., Bäckhed, F., 2013. Gut Microbiota Regulates Bile Acid Metabolism by Reducing the Levels of Tauro-beta-muricholic Acid, a Naturally Occurring FXR Antagonist. Cell Metabolism 17, 225-235.

Sbarra, V., Ristorcelli, E., Petit-Thevenin, J.L., Teissedre, P.L., Lombardo, D., Verine, A., 2005. In vitro polyphenol effects on activity, expression and secretion of pancreatic bile salt-dependent lipase. Biochimica et biophysica acta 1736, 67-76.

Scheibner, J., Fuchs, M., Hormann, E., Tauber, G., Stange, E.F., 1994. Biliary cholesterol secretion and bile acid formation in the hamster: the role of newly synthesized cholesterol. J Lipid Res 35, 690-697.

Schjoldager, B.T., 1994. Role of CCK in gallbladder function. Annals of the New York Academy of Sciences 713, 207-218.

Schomburg, D., Chang, A., Schomburg, I., 2006. Class 2 Transferases II: EC 2.1. 2.1-2.3. 1.59. Springer.

Schuijt, T.J., Lankelma, J.M., Scicluna, B.P., de Sousa e Melo, F., Roelofs, J.J.T.H., de Boer, J.D., Hoogendijk, A.J., de Beer, R., de Vos, A., Belzer, C., de Vos, W.M., van der Poll, T., Wiersinga, W.J., 2015. The gut microbiota plays a protective role in the host defence against pneumococcal pneumonia. Gut.

Schulz, T.J., Zarse, K., Voigt, A., Urban, N., Birringer, M., Ristow, M., 2007. Glucose restriction extends Caenorhabditis elegans life span by inducing mitochondrial respiration and increasing oxidative stress. Cell Metab 6, 280-293.

Schumacher, A., Kapranov, P., Kaminsky, Z., Flanagan, J., Assadzadeh, A., Yau, P., Virtanen, C., Winegarden, N., Cheng, J., Gingeras, T., Petronis, A., 2006. Microarray-based DNA methylation profiling: technology and applications. Nucleic Acids Research 34, 528-542.

Schupf, N., Barral, S., Perls, T., Newman, A., Christensen, K., Thyagarajan, B., Province, M., Rossi, W.K., Mayeux, R., 2013. Apolipoprotein E and Familial Longevity. Neurobiology of aging 34, 1287-1291.

Schwarz, M., Russell, D.W., Dietschy, J.M., Turley, S.D., 2001. Alternate pathways of bile acid synthesis in the cholesterol 7alpha-hydroxylase knockout mouse are not upregulated by either cholesterol or cholestyramine feeding. J Lipid Res 42, 1594-1603.

Schwetz, V., Scharnagl, H., Trummer, C., Stojakovic, T., Pandis, M., Grübler, M.R., Verheyen, N., Gaksch, M., Zittermann, A., Aberer, F., Lerchbaum, E., Obermayer-Pietsch, B., Pieber, T.R., März, W., Tomaschitz, A., Pilz, S., 2018. Vitamin D supplementation and lipoprotein metabolism: A randomized controlled trial. Journal of Clinical Lipidology 12, 588-596.e584.

Shammas, M.A., 2011. Telomeres, lifestyle, cancer, and aging. Current Opinion in Clinical Nutrition and Metabolic Care 14, 28-34.

Shankaran, H., Resat, H., Wiley, H.S., 2007. Cell Surface Receptors for Signal Transduction and Ligand Transport: A Design Principles Study. PLoS computational biology 3, e101.

Shayganni, E., Bahmani, M., Asgary, S., Rafieian-Kopaei, M., 2015. Inflammaging and cardiovascular disease: Management by medicinal plants. Phytomedicine.

Shen, L., Peng, H., Peng, R., Fan, Q., Zhao, S., Xu, D., Morisseau, C., Chiamvimonvat, N., Hammock, B.D., 2015. Inhibition of soluble epoxide hydrolase in mice promotes reverse cholesterol transport and regression of atherosclerosis. Atherosclerosis 239, 557-565.

Shiomi, M., Ito, T., Fujioka, T., Tsujita, Y., 2000. Age-associated decrease in plasma cholesterol and changes in cholesterol metabolism in homozygous Watanabe heritable hyperlipidemic rabbits. Metabolism 49, 552-556.

Shorten, P.R., Upreti, G.C., 2005. A mathematical model of fatty acid metabolism and VLDL assembly in human liver. Biochimica et biophysica acta 1736, 94-108.

Simon, J.S., Karnoub, M.C., Devlin, D.J., Arreaza, M.G., Qiu, P., Monks, S.A., Severino, M.E., Deutsch, P., Palmisano, J., Sachs, A.B., Bayne, M.L., Plump, A.S., Schadt, E.E., 2005. Sequence variation in NPC1L1 and association with improved LDL-cholesterol lowering in response to ezetimibe treatment. Genomics 86, 648-656.

Sina, A.A.I., Carrascosa, L.G., Liang, Z., Grewal, Y.S., Wardiana, A., Shiddiky, M.J.A., Gardiner, R.A., Samaratunga, H., Gandhi, M.K., Scott, R.J., Korbie, D., Trau, M., 2018. Epigenetically reprogrammed methylation landscape drives the DNA self-assembly and serves as a universal cancer biomarker. Nature Communications 9, 4915.

Sina, A.A.I., Howell, S., Carrascosa, L.G., Rauf, S., Shiddiky, M.J.A., Trau, M., 2014. eMethylsorb: electrochemical quantification of DNA methylation at CpG resolution using DNA-gold affinity interactions. Chemical Communications 50, 13153-13156.

Singh, R.B., Ghosh, S., Niaz, M.A., Singh, R., Beegum, R., Chibo, H., Shoumin, Z., Postiglione, A., 1995. Dietary intake, plasma levels of antioxidant vitamins, and oxidative stress in relation to coronary artery disease in elderly subjects. The American Journal of Cardiology 76, 1233-1238.

Sips, F.L., Tiemann, C.A., Oosterveer, M.H., Groen, A.K., Hilbers, P.A., van Riel, N.A., 2014. A computational model for the analysis of lipoprotein distributions in the mouse: translating FPLC profiles to lipoprotein metabolism. PLoS computational biology 10, e1003579.

Sirtori, C.R., 2014. The pharmacology of statins. Pharmacological Research 88, 3-11.

Soltis, D.A., McMahon, G., Caplan, S.L., Dudas, D.A., Chamberlin, H.A., Vattay, A., Dottavio, D., Rucker, M.L., Engstrom, R.G., Cornell-Kennon, S.A., et al., 1995. Expression, purification, and characterization of the human squalene synthase: use of yeast and baculoviral systems. Archives of biochemistry and biophysics 316, 713-723.

Song, F., Poljak, A., Crawford, J., Kochan, N.A., Wen, W., Cameron, B., Lux, O., Brodaty, H., Mather, K., Smythe, G.A., Sachdev, P.S., 2012. Plasma Apolipoprotein Levels Are Associated with Cognitive Status and Decline in a Community Cohort of Older Individuals. PLOS ONE 7, e34078.

Sorci-Thomas, M., Babiak, J., Rudel, L.L., 1990. Lecithin-cholesterol acyltransferase (LCAT) catalyzes transacylation of intact cholesteryl esters. Evidence for the partial reversal of the forward LCAT reaction. The Journal of biological chemistry 265, 2665-2670.

Soroka, C.J., Boyer, J.L., 2014. Biosynthesis and trafficking of the bile salt export pump, BSEP: therapeutic implications of BSEP mutations. Mol Aspects Med 37, 3-14.

Sorokin, A., Paliy, K., Selkov, A., Demin, O.V., Dronov, S., Ghazal, P., Goryanin, I., 2006. The Pathway Editor: A tool for managing complex biological networks. IBM Journal of Research and Development 50, 561-573.

Soule, H.D., Vazquez, J., Long, A., Albert, S., Brennan, M., 1973. A Human Cell Line From a Pleural Effusion Derived From a Breast Carcinoma2. JNCI: Journal of the National Cancer Institute 51, 1409-1416.

Soumyarani, V.S., Jayakumari, N., 2012. Oxidatively modified high density lipoprotein promotes inflammatory response in human monocytes-macrophages by enhanced production of ROS, TNF-alpha, MMP-9, and MMP-2. Mol Cell Biochem 366, 277-285.

Spady, D.K., Cuthbert, J.A., 1992. Regulation of hepatic sterol metabolism in the rat. Parallel regulation of activity and mRNA for 7 alpha-hydroxylase but not 3-hydroxy-3-methylglutaryl-coenzyme A reductase or low density lipoprotein receptor. The Journal of biological chemistry 267, 5584-5591.

Spady, D.K., Turley, S.D., Dietschy, J.M., 1985. Receptor-independent low density lipoprotein transport in the rat in vivo. Quantitation, characterization, and metabolic consequences. The Journal of clinical investigation 76, 1113-1122.

Steenbergen, L., Sellaro, R., van Hemert, S., Bosch, J.A., Colzato, L.S., 2015. A randomized controlled trial to test the effect of multispecies probiotics on cognitive reactivity to sad mood. Brain, Behavior, and Immunity 48, 258-264.

Stevens, M., Cheng, J.B., Li, D., Xie, M., Hong, C., Maire, C.L., Ligon, K.L., Hirst, M., Marra, M.A., Costello, J.F., Wang, T., 2013. Estimating absolute methylation levels at single-CpG resolution from methylation enrichment and restriction enzyme sequencing methods. Genome Research 23, 1541-1553.

Stewart, T.M., Bhapkar, M., Das, S., Galan, K., Martin, C.K., McAdams, L., Pieper, C., Redman, L., Roberts, S., Stein, R.I., Rochon, J., Williamson, D.A., 2013. Comprehensive Assessment of Long-term Effects of Reducing Intake of Energy Phase 2 (CALERIE Phase 2) screening and recruitment: methods and results. Contemp Clin Trials 34, 10-20.

Stitziel, N.O., Won, H.-H., Morrison, A.C., Peloso, G.M., Do, R., Lange, L.A., Fontanillas, P., Gupta, N., Duga, S., Goel, A., 2014. Inactivating mutations in NPC1L1 and protection from coronary heart disease. The New England journal of medicine 371, 2072-2082.

Streppel, M.T., Ocke, M.C., Boshuizen, H.C., Kok, F.J., Kromhout, D., 2008. Dietary fiber intake in relation to coronary heart disease and all-cause mortality over 40 y: the Zutphen Study. Am J Clin Nutr 88, 1119-1125.

Stresemann, C., Lyko, F., 2008. Modes of action of the DNA methyltransferase inhibitors azacytidine and decitabine. Int J Cancer 123, 8-13.

Sun, D., Luo, M., Jeong, M., Rodriguez, B., Xia, Z., Hannah, R., Wang, H., Le, T., Faull, Kym F., Chen, R., Gu, H., Bock, C., Meissner, A., Göttgens, B., Darlington, Gretchen J., Li, W., Goodell, Margaret A., 2014. Epigenomic Profiling of Young and Aged HSCs Reveals Concerted Changes during Aging that Reinforce Self-Renewal. Cell Stem Cell 14, 673-688.

Tancharoenrat, P., Ravindran, V., Zaefarian, F., Ravindran, G., 2014. Digestion of fat and fatty acids along the gastrointestinal tract of broiler chickens. Poultry Science 93, 371-379.

Tannock, G.W., Dashkevicz, M.P., Feighner, S.D., 1989. Lactobacilli and bile salt hydrolase in the murine intestinal tract. Applied and environmental microbiology 55, 1848-1851.

Tao, R., Xiong, X., DePinho, R.A., Deng, C.X., Dong, X.C., 2013. Hepatic SREBP-2 and cholesterol biosynthesis are regulated by FoxO3 and Sirt6. J Lipid Res 54, 2745-2753.

Taormina, G., Mirisola, M.G., 2014. Calorie Restriction in Mammals and Simple Model Organisms. BioMed Research International 2014, 10.

Tassi, S., Carta, S., Vene, R., Delfino, L., Ciriolo, M.R., Rubartelli, A., 2009. Pathogen-induced interleukin-1beta processing and secretion is regulated by a biphasic redox response. J Immunol 183, 1456-1462.

Tavakoli, F., Namakin, K., Zardast, M., 2016. Vitamin D Supplementation and High-Density Lipoprotein Cholesterol: A Study in Healthy School Children. Iranian Journal of Pediatrics 26, e3311.

Teare, J., Islam, R., Flanagan, R., Gallagher, S., Davies, M., Grabau, C., 1997. Measurement of nucleic acid concentrations using the DyNA Quant™ and the GeneQuant™. Biotechniques 22, 1170-1174.

Thomas, C., Pellicciari, R., Pruzanski, M., Auwerx, J., Schoonjans, K., 2008. Targeting bile-acid signalling for metabolic diseases. Nature reviews. Drug discovery 7, 678-693.

Thompson, G., Davies, T., Mc Auley, M., Halpern, J., 2016. Electrochemical Detection of DNA Methylation and Application to Breast Cancer Screening. Oral Presentation Abstracts Electrochemical Sensing Electrochem 19.

Tikellis, G., Sun, C., Gorin, M.B., Klein, R., Klein, B.E., Larsen, E.K., Siscovick, D.S., Hubbard, L.D., Wong, T.Y., 2007. Apolipoprotein e gene and age-related maculopathy in older individuals: the cardiovascular health study. Arch Ophthalmol 125, 68-73.

Tobi, E.W., Goeman, J.J., Monajemi, R., Gu, H., Putter, H., Zhang, Y., Slieker, R.C., Stok, A.P., Thijssen, P.E., Müller, F., van Zwet, E.W., Bock, C., Meissner, A., Lumey, L.H., Eline Slagboom, P., Heijmans, B.T., 2014. DNA methylation signatures link prenatal famine exposure to growth and metabolism. Nature Communications 5, 5592.

Topkaya, S.N., Ozkan-Ariksoysal, D., Kosova, B., Ozel, R., Ozsoz, M., 2012. Electrochemical DNA biosensor for detecting cancer biomarker related to glutathione S-transferase P1 (GSTP1) hypermethylation in real samples. Biosensors and Bioelectronics 31, 516-522.

Tosato, M., Zamboni, V., Ferrini, A., Cesari, M., 2007. The aging process and potential interventions to extend life expectancy. Clinical Interventions in Aging 2, 401-412.

Tost, J., Gut, I.G., 2007. DNA methylation analysis by pyrosequencing. Nat Protoc 2, 2265-2275.

Townsend, N., Bhatnagar, P., Wilkins, E., Wickramasinghe, K., Rayner, M., 2015. Cardiovascular disease statistics, 2015. British Heart Foundation, London.

Trasatti, S., 1986. The absolute electrode potential: an explanatory note (Recommendations 1986). Pure and Applied Chemistry 58, 955-966.

Trautwein, E.A., Siddiqui, A., Hayes, K.C., 1999. Characterization of the bile acid profile in developing male and female hamsters in response to dietary cholesterol challenge. Comparative biochemistry and physiology. Part A, Molecular & integrative physiology 124, 93-103.

Trichopoulou, A., Lagiou, P., 1997. Healthy traditional Mediterranean diet: an expression of culture, history, and lifestyle. Nutr Rev 55, 383-389.

Tuohy, K.M., Probert, H.M., Smejkal, C.W., Gibson, G.R., 2003. Using probiotics and prebiotics to improve gut health. Drug Discovery Today 8, 692-700.

Uchida, K., Satoh, T., Chikai, T., Takase, H., Nomura, Y., Nakao, H., Takeuchi, N., 1996. Influence of cholesterol feeding on bile acid metabolism in young and aged germ-free rats. Jpn J Pharmacol 71, 113-118.

UNSD, 2016. Population by age, sex and urban/rural residence.

Valencia-Morales, M.d.P., Zaina, S., Heyn, H., Carmona, F.J., Varol, N., Sayols, S., Condom, E., Ramírez-Ruz, J., Gomez, A., Moran, S., Lund, G., Rodríguez-Ríos, D., López-González, G., Ramírez-Nava, M., de la Rocha, C., Sanchez-Flores, A., Esteller, M., 2015. The DNA methylation drift of the atherosclerotic aorta increases with lesion progression. BMC Medical Genomics 8, 7.

Valentini, E., Zampieri, M., Malavolta, M., Bacalini, M.G., Calabrese, R., Guastafierro, T., Reale, A., Franceschi, C., Hervonen, A., Koller, B., Bernhardt, J., Slagboom, P.E., Toussaint, O., Sikora, E., Gonos, E.S., Breusing, N., Grune, T., Jansen, E., Dollé, M.E.T., Moreno-Villanueva, M., Sindlinger, T., Bürkle, A., Ciccarone, F., Caiafa, P., 2016. Analysis of the machinery and intermediates of the 5hmC-mediated DNA demethylation pathway in aging on samples from the MARK-AGE Study. Aging 8, 1896-1915.

van de Pas, N.C., Woutersen, R.A., van Ommen, B., Rietjens, I.M., de Graaf, A.A., 2012. A physiologically based in silico kinetic model predicting plasma cholesterol concentrations in humans. J Lipid Res 53, 2734-2746.

Van Dyck, F., Braem, C.V., Chen, Z., Declercq, J., Deckers, R., Kim, B.-M., Ito, S., Wu, M.K., Cohen, D.E., Dewerchin, M., Derua, R., Waelkens, E., Fiette, L., Roebroek, A., Schuit, F., Van de Ven, W.J.M., Shivdasani, R.A., 2007. Loss of the PlagL2 Transcription Factor Affects Lacteal Uptake of Chylomicrons. Cell Metabolism 6, 406-413.

van Iersel, M.P., Villéger, A.C., Czauderna, T., Boyd, S.E., Bergmann, F.T., Luna, A., Demir, E., Sorokin, A., Dogrusoz, U., Matsuoka, Y., Funahashi, A., Aladjem, M.I., Mi, H., Moodie, S.L., Kitano, H., Le Novère, N., Schreiber, F., 2012. Software support for SBGN maps: SBGN-ML and LibSBGN. Bioinformatics 28, 2016-2021.

Varley, K.E., Mutch, D.G., Edmonston, T.B., Goodfellow, P.J., Mitra, R.D., 2009. Intra-tumor heterogeneity of MLH1 promoter methylation revealed by deep single molecule bisulfite sequencing. Nucleic Acids Research 37, 4603-4612.

Vartiainen, E., Laatikainen, T., Peltonen, M., Juolevi, A., Mannisto, S., Sundvall, J., Jousilahti, P., Salomaa, V., Valsta, L., Puska, P., 2010. Thirty-five-year trends in cardiovascular risk factors in Finland. International journal of epidemiology 39, 504-518.

Veniant, M.M., Zlot, C.H., Walzem, R.L., Pierotti, V., Driscoll, R., Dichek, D., Herz, J., Young, S.G., 1998. Lipoprotein clearance mechanisms in LDL receptor-deficient "Apo-B48-only" and "Apo-B100-only" mice. The Journal of clinical investigation 102, 1559-1568.

Vetter, K.J., 2013. Electrochemical kinetics: theoretical aspects. Elsevier.

Vitezova, A., Voortman, T., Zillikens, M.C., Jansen, P.W., Hofman, A., Uitterlinden, A.G., Franco, O.H., Kiefte-de Jong, J.C., 2015. Bidirectional associations between circulating vitamin D and cholesterol levels: The Rotterdam Study. Maturitas 82, 411-417.

Vogiatzi, G., Tousoulis, D., Stefanadis, C., 2009. The role of oxidative stress in atherosclerosis. Hellenic J Cardiol 50, 402-409.

Voit, E.O., Martens, H.A., Omholt, S.W., 2015. 150 Years of the Mass Action Law. PLoS computational biology 11, e1004012.

Voynova, N.E., Fu, Z., Battaile, K.P., Herdendorf, T.J., Kim, J.J., Miziorko, H.M., 2008. Human mevalonate diphosphate decarboxylase: characterization, investigation of the mevalonate diphosphate binding site, and crystal structure. Archives of biochemistry and biophysics 480, 58-67.

Vucetic, Z., Kimmel, J., Reyes, T.M., 2011. Chronic High-Fat Diet Drives Postnatal Epigenetic Regulation of μ-Opioid Receptor in the Brain. Neuropsychopharmacology 36, 1199-1206.

Wang, B.T., Ducker, G.S., Barczak, A.J., Barbeau, R., Erle, D.J., Shokat, K.M., 2011. The mammalian target of rapamycin regulates cholesterol biosynthetic gene expression and exhibits a rapamycin-resistant transcriptional profile. Proceedings of the National Academy of Sciences of the United States of America 108, 15201-15206.

Wang, H.H., Patel, S.B., Carey, M.C., Wang, D.Q.H., 2007. Quantifying Anomalous Intestinal Sterol Uptake, Lymphatic Transport, and Biliary Secretion in Abcg8(-/-) Mice. Hepatology (Baltimore, Md.) 45, 998-1006.

Wang, J., Qiang, H., Chen, D., Zhang, C., Zhuang, Y., 2002. CETP gene mutation (D442G) increases low-density lipoprotein particle size in patients with coronary heart disease. Clin Chim Acta 322, 85-90.

Wang, J.C., Bennett, M., 2012. Aging and Atherosclerosis: Mechanisms, Functional Consequences, and Potential Therapeutics for Cellular Senescence. Circulation Research 111, 245-259.

Wang, T., Tsui, B., Kreisberg, J.F., Robertson, N.A., Gross, A.M., Yu, M.K., Carter, H., Brown-Borg, H.M., Adams, P.D., Ideker, T., 2017. Epigenetic aging signatures in mice livers are slowed by dwarfism, calorie restriction and rapamycin treatment. Genome Biology 18, 57.

Wang, Y., Ji, L., Jiang, R., Zheng, L., Liu, D., 2014. Oxidized high-density lipoprotein induces the proliferation and migration of vascular smooth muscle cells by promoting the production of ROS. J Atheroscler Thromb 21, 204-216.

Wang, Y.M., Zhang, B., Xue, Y., Li, Z.J., Wang, J.F., Xue, C.H., Yanagita, T., 2010. The mechanism of dietary cholesterol effects on lipids metabolism in rats. Lipids Health Dis 9, 4.

Warton, K., Samimi, G., 2015. Methylation of cell-free circulating DNA in the diagnosis of cancer. Frontiers in Molecular Biosciences 2.

Watterson, S., Guerriero, M.L., Blanc, M., Mazein, A., Loewe, L., Robertson, K.A., Gibbs, H., Shui, G., Wenk, M.R., Hillston, J., Ghazal, P., 2013. A model of flux regulation in the cholesterol biosynthesis pathway: Immune mediated graduated flux reduction versus statin-like led stepped flux reduction. Biochimie 95, 613-621.

Wattis, J.A., O'Malley, B., Blackburn, H., Pickersgill, L., Panovska, J., Byrne, H.M., Jackson, K.G., 2008. Mathematical model for low density lipoprotein (LDL) endocytosis by hepatocytes. Bull Math Biol 70, 2303-2333.

Wei, D., Tao, R., Zhang, Y., White, M.F., Dong, X.C., 2011. Feedback regulation of hepatic gluconeogenesis through modulation of SHP/Nr0b2 gene expression by Sirt1 and FoxO1. Am J Physiol Endocrinol Metab 300, E312-320.

Weinman, S.A., Carruth, M.W., Dawson, P.A., 1998. Bile acid uptake via the human apical sodium-bile acid cotransporter is electrogenic. The Journal of biological chemistry 273, 34691-34695.

Westerterp, M., van der Hoogt, C.C., de Haan, W., Offerman, E.H., Dallinga-Thie, G.M., Jukema, J.W., Havekes, L.M., Rensen, P.C.N., 2006. Cholesteryl Ester Transfer Protein Decreases High-Density Lipoprotein and Severely Aggravates Atherosclerosis in APOE*3-Leiden Mice. Arteriosclerosis, Thrombosis, and Vascular Biology 26, 2552-2559.

White, M.C., Holman, D.M., Boehm, J.E., Peipins, L.A., Grossman, M., Henley, S.J., 2014. Age and Cancer Risk: A Potentially Modifiable Relationship. American journal of preventive medicine 46, S7-15.

WHO, 2014. Aging and Life Course: Facts about Aging. WHO.

WHO, 2015. Life expectancy data by country.

Wikgren, M., Karlsson, T., Nilbrink, T., Nordfjall, K., Hultdin, J., Sleegers, K., Van Broeckhoven, C., Nyberg, L., Roos, G., Nilsson, L.G., Adolfsson, R., Norrback, K.F., 2012. APOE epsilon4 is associated with longer telomeres, and longer telomeres among epsilon4 carriers predicts worse episodic memory. Neurobiol Aging 33, 335-344.

Wilson, P.W., Anderson, K.M., Harris, T., Kannel, W.B., Castelli, W.P., 1994. Determinants of change in total cholesterol and HDL-C with age: the Framingham Study. J Gerontol 49, M252-257.

Wilson, S.L., Kalinovsky, A., Orvis, G.D., Joyner, A.L., 2011. Spatially Restricted and Developmentally Dynamic Expression of Engrailed Genes in Multiple Cerebellar Cell Types. Cerebellum (London, England) 10, 356-372.

Wilson, V.L., Smith, R.A., Ma, S., Cutler, R.G., 1987. Genomic 5-methyldeoxycytidine decreases with age. Journal of Biological Chemistry 262, 9948-9951.

Winter, P.C., 2005. Polymerase Chain Reaction (PCR), eLS. John Wiley & Sons, Ltd.

Wittenberg, R., Hu, B., Comas-Herrera, A., J.-L., F., 2012. Care for older people: Projected expenditure to 2022 on social care and continuing health care for England's older population. nuffieldtrust.

Woodside, J.V., McGrath, A.J., Lyner, N., McKinley, M.C., 2015. Carotenoids and health in older people. Maturitas 80, 63-68.

Woollett, L.A., Spady, D.K., Dietschy, J.M., 1992. Saturated and unsaturated fatty acids independently regulate low density lipoprotein receptor activity and production rate. J Lipid Res 33, 77-88.

Woollett, L.A., Wang, Y., Buckley, D.D., Yao, L., Chin, S., Granholm, N., Jones, P.J., Setchell, K.D., Tso, P., Heubi, J.E., 2006. Micellar solubilisation of cholesterol is essential for absorption in humans. Gut 55, 197-204.

Xiao, D., Mo, Y., Choi, M.M., 2003. A hand-held optical sensor for dissolved oxygen measurement. Measurement Science and Technology 14, 862.

Xie, M., Jiang, Q., Xie, Y., 2015. Comparison Between Decitabine and Azacitidine for the Treatment of Myelodysplastic Syndrome: A Meta-Analysis With 1392 Participants. Clinical Lymphoma Myeloma and Leukemia 15, 22-28.

Xu, X., Su, S., Barnes, V.A., De Miguel, C., Pollock, J., Ownby, D., Shi, H., Zhu, H., Snieder, H., Wang, X., 2013. A genome-wide methylation study on obesity: Differential variability and differential methylation. Epigenetics 8, 522-533.

Yang, B.T., Dayeh, T.A., Kirkpatrick, C.L., Taneera, J., Kumar, R., Groop, L., Wollheim, C.B., Nitert, M.D., Ling, C., 2011. Insulin promoter DNA methylation correlates negatively with insulin gene expression and positively with HbA(1c) levels in human pancreatic islets. Diabetologia 54, 360-367.

Yang, D., Elner, S.G., Bian, Z.-M., Till, G.O., Petty, H.R., Elner, V.M., 2007. Pro-inflammatory Cytokines Increase Reactive Oxygen Species through Mitochondria and NADPH Oxidase in Cultured RPE Cells. Experimental eye research 85, 462-472.

Yang, X., Han, H., De Carvalho, D.D., Lay, F.D., Jones, P.A., Liang, G., 2014. Gene body methylation can alter gene expression and is a therapeutic target in cancer. Cancer Cell 26, 577-590.

Yavari, A., Javadi, M., Mirmiran, P., Bahadoran, Z., 2015. Exercise-induced oxidative stress and dietary antioxidants. Asian journal of sports medicine 6, e24898-e24898.

Yavuz, B., Ertugrul, D.T., Cil, H., Ata, N., Akin, K.O., Yalcin, A.A., Kucukazman, M., Dal, K., Hokkaomeroglu, M.S., Yavuz, B.B., Tutal, E., 2009. Increased Levels of 25 Hydroxyvitamin D and 1,25-Dihydroxyvitamin D After Rosuvastatin Treatment: A Novel Pleiotropic Effect of Statins? Cardiovascular Drugs and Therapy 23, 295-299.

Yu, X.-H., Qian, K., Jiang, N., Zheng, X.-L., Cayabyab, F.S., Tang, C.-K., 2014. ABCG5/ABCG8 in cholesterol excretion and atherosclerosis. Clinica Chimica Acta 428, 82-88.

Zagkos, L., Auley, M.M., Roberts, J., Kavallaris, N.I., 2019. Mathematical models of DNA methylation dynamics: Implications for health and ageing. J Theor Biol 462, 184-193.

Zec, N., Rowitch, D.H., Bitgood, M.J., Kinney, H.C., 1997. Expression of the homeobox-containing genes EN1 and EN2 in human fetal midgestational medulla and cerebellum. J Neuropathol Exp Neurol 56, 236-242.

Zende, P.D., Bankar, M.P., Kamble, P.S., Momin, A.A., 2013. Apolipoprotein e gene polymorphism and its effect on plasma lipids in arteriosclerosis. J Clin Diagn Res 7, 2149-2152.

Zhang, H., Tsao, R., 2016. Dietary polyphenols, oxidative stress and antioxidant and anti-inflammatory effects. Current Opinion in Food Science 8, 33-42.

Zhang, L., Long, X., 2015. Association of BRCA1 promoter methylation with sporadic breast cancers: Evidence from 40 studies. Scientific reports 5, 17869.

Zhang, M., Charles, R., Tong, H., Zhang, L., Patel, M., Wang, F., Rames, M.J., Ren, A., Rye, K.A., Qiu, X., Johns, D.G., Charles, M.A., Ren, G., 2015. HDL surface lipids mediate CETP binding as revealed by electron microscopy and molecular dynamics simulation. Scientific reports 5, 8741.

Zhang, P., Chu, T., Dedousis, N., Mantell, B.S., Sipula, I., Li, L., Bunce, K.D., Shaw, P.A., Katz, L.S., Zhu, J., Argmann, C., O'Doherty, R.M., Peters, D.G., Scott, D.K., 2017. DNA methylation alters transcriptional rates of differentially expressed genes and contributes to pathophysiology in mice fed a high fat diet. Molecular Metabolism 6, 327-339.

Zhao, J., Goldberg, J., Vaccarino, V., 2012. Promoter methylation of serotonin transporter gene is associated with obesity measures: a monozygotic twin study. International Journal Of Obesity 37, 140.

Zhong, S., Sharp, D.S., Grove, J.S., Bruce, C., Yano, K., Curb, J.D., Tall, A.R., 1996. Increased coronary heart disease in Japanese-American men with mutation in the cholesteryl ester transfer protein gene despite increased HDL levels. The Journal of clinical investigation 97, 2917-2923.

Zou, B., Chim, C.S., Zeng, H., Leung, S.Y., Yang, Y., Tu, S.P., Lin, M.C.M., Wang, J., He, H., Jiang, S.H., Sun, Y.W., Yu, L.F., Yuen, S.T., Kung, H.F., Wong, B.C.Y., 2006. Correlation Between the Single-Site CpG Methylation and Expression Silencing of the XAF1 Gene in Human Gastric and Colon Cancers. Gastroenterology 131, 1835-1843.

Appendix

Section 1 Model overview

Model abbreviations

AACT: Acetoacetyl CoA thiolase

ABC1D: ATP-binding cassette subfamily A member 1 degradation

ABC1S: ATP-binding cassette subfamily A member 1 synthesis

ABCA1: ATP-binding cassette subfamily A member 1

ABCG5G8: ATP-binding cassette transporters G8/G8

ABCG5G8D: ATP-binding cassette transporters G8/G8 degradation

ABCG5G8S: ATP-binding cassette transporters G8/G8 synthesis

ABST: Apical-dependent bile acid transporter

ABSTD: Apical-dependent bile acid transporter degradation

ABSTS: Apical-dependent bile acid transporter synthesis

ACAT1: Acetyl-coenzyme A: cholesterol acetyltransferase 1

ACAT2: Acetyl-coenzyme A: cholesterol acetyltransferase 2

AKR1D1: Aldo-keto reductase family 1 member D1

APOAI: Apolipoprotein A-I

BACS: Bile acid: CoA synthase

BAT: Bile acid CoA: amino acid N-acyltransferase

BCBA: Blood conjugated bile acids

BSEP: Bile salt export pump

BSEPD: Bile salt export pump degradation

BSEPS: Bile salt export pump synthesis

BSH: Bile salt hydrolase

BUBA: Blood unconjugated bile acids

C1: 7α-hydroxycholesterol

C10: 7α-hydroxy-3-oxo-4-cholestenoate

C2: 7α-hydroxycholest-4-en-3-one

C3: 7α-hydroxy-5β-cholestan-3-one

C4: 3α, 7α-dihydroxy-5β-cholestanate

C5: 4-cholesten-7α, 12α-diol-3-one

C6: 5β-cholesten-7α, 12α-diol-3one

C7: 3α, 7α, 12α-trihydroxy-5β-cholestanoate

C8: 3β-hydroxy-5-cholestenoate

C9: 3β, 7α-dihydroxy-5-cholestenoate

CEH: Cholesterol ester hydrolase

CETP: Cholesteryl ester transfer protein

CYP27A1: Sterol 27-hydroxylase

CYP7A1: Cholesterol 7α-hydroxylase

CYP7B1: 25-hydroxycholesterol 7α-hydroxylase

CYP8B1: 12α-hydroxylase

DCE: Dietary cholesterol esters

DFC: Dietary free cholesterol

DHCR7: 7-Dehydrocholesterol reductase

DHCR24: 24-Dehydrocholesterol reductase

EFC: Excreted free cholesterol

EUBA: Excreted unconjugated bile acids

FDPS: Farnesyl diphosphate synthase

H7DHC: Hepatic 7-dehydrocholesterol

H7DHDES: Hepatic 7-dehydrodesmosterol

HAACoA: Hepatic acetoAcetyl CoA

HACoA: Hepatic acetyl CoA

HACoAS: Hepatic acetyl CoA synthesis

HAPOAIS: Hepatic apolipoprotein A-I synthesis

HCBA: Hepatic conjugated bile acids

HCE: Hepatic cholesterol esters

HCH: Hepatic chylomicron

HDES: Hepatic desmosterol

HDL2: High density lipoprotein subclass 2

HDL3: High density lipoprotein subclass 3

HDMAPP: Hepatic dimethylallyl pyrophosphate

HFC: Hepatic free cholesterol

HFPP: Hepatic farnesyl pyrophosphate

HGPP: Hepatic geranyl pyrophosphate

HHMGCoA: Hepatic HMG CoA

HIPP: Hepatic isopentenyl pyrophosphate

HL: Hepatic lipase

HLAN: Hepatic lanosterol

HLDLR: Hepatic low density lipoprotein receptor

HLDLRD: Hepatic low density lipoprotein receptor degradation

HLDLRS: Hepatic low density lipoprotein receptor synthesis

HMG-CoA reductase: 3-Hydroxy-3-methylglutaryl reductase

HMG-CoA synthase: 3-Hydroxy-3-methylglutaryl CoA synthase

HMV: Hepatic mevalonate

HMV5P: Hepatic mevalonate-5-phosphate

HMV5PP: Hepatic mevalonate diphosphate

HSD3B7: Cholest-5-ene-3β, 7α-diol 3β-dehydrogenase

HSL: Hormone sensitive lipase

HSQ: Hepatic squalene

HSQE: Hepatic squalene epoxide

HSRB1: Hepatic scavenger receptor class B member 1

HSRB1D: Hepatic scavenger receptor class B member 1 degradation

HSRB1S: Hepatic scavenger receptor class B member 1 synthesis

HUBA: Hepatic unconjugated bile acids

HUBACoA: Hepatic unconjugated bile acid -CoA

IAPOAIS: Intestinal Apolipoprotein A-I synthesis

ICBA: Ileocyte conjugated bile acids

IDI: Isopentenyl diphosphate delta isomerase

IDLC: Intermediate density lipoprotein cholesterol

IUBA: Ileocyte unconjugated bile acids

J7DHC: Jejunocyte 7-dehydrocholesterol

J7DHDES: Jejunocyte 7-dehydrodesmosterol

JAACoA: Jejunocyte acetoAcetyl CoA

JACoA: Jejunocyte acetyl CoA

JACoAS: Jejunocyte acetyl CoA synthesis

JCE: Jejunocyte cholesterol esters

JCH: Jejunocyte chylomicron

JDES: Jejunocyte desmosterol

JDMAPP: Jejunocyte dimethylallyl pyrophosphate

JFC: Jejunocyte free cholesterol

JFPP: jejunocyte farnesyl pyrophosphate

JGPP: Jejunocyte geranyl pyrophosphate

JHMGCoA: Jejunocyte HMG CoA

JIPP: Jejunocyte isopentenyl pyrophosphate

JLAN: Jejunocyte lanosterol

JMV: Jejunocyte mevalonate

JMV5P: Jejunocyte mevalonate-5-phosphate

JMV5PP: Jejunocyte mevalonate diphosphate

JSQ: Jejunocyte squalene

JSQE: Jejunocyte squalene epoxide

LCAT: Lecithin-cholesterol acyltransferase

LCBA: Lumen conjugated bile acids

LCE: Lumen cholesterol esters

LDLC: Low density lipoprotein

LFC: Lumen free cholesterol

LPL: Lipoprotein lipase

LRP: Lipoprotein receptor related protein

LRPD: Lipoprotein receptor related protein degradation

LRPS: Lipoprotein receptor related protein synthesis

LUBA: Lumen unconjugated bile acids

MTP: Microsomal triglyceride transfer protein

MVD: Mevalonate-5PP decarboxylase

MVK: Mevalonate kinase

ndHDL: Nascent high density lipoprotein

ndHDLC: Nascent high density lipoprotein cholesterol

NPC1L1: Neimann-Pick C1-Like 1

NPC1L1: Neimann-Pick C1-Like 1 degradation

NPC1L1S: Neimann-Pick C1-Like 1 synthesis

NTCP: Na+-taurocholate cotransporting polypeptide

NTCPD: Na+-taurocholate cotransporting polypeptide degradation

NTCPS: Na+-taurocholate cotransporting polypeptide synthesis

OST: Organic solute transporter α/β

OSTD: Organic solute transporter α/β degradation

OSTS: Organic solute transporter α/β synthesis

OSC: Oxidosqualene cyclase

P7DHC: Peripheral 7-dehydrocholesterol

P7DHDES: Peripheral 7-dehydrodesmosterol

PAACoA: Peripheral acetoAcetyl CoA

PACoA: Peripheral acetyl CoA

PACoAS: Peripheral acetyl CoA synthesis

PCE: Peripheral cholesterol esters

PDES: Peripheral desmosterol

PDMAPP: Peripheral dimethylallyl pyrophosphate

PFC: Peripheral free cholesterol

PFPP: Peripheral farnesyl pyrophosphate

PGPP: Peripheral geranyl pyrophosphate

PHMGCoA: Peripheral HMG CoA

PIPP: Peripheral isopentenyl pyrophosphate

PL: Phospholipids

PLAN: Peripheral lanosterol

PLDLR: Peripheral low density lipoprotein receptor

PLDLRD: Peripheral low density lipoprotein receptor degradation

PLDLRS: Peripheral low density lipoprotein receptor synthesis

PLPT: Phospholipid transfer protein

PLS: Phospholipid source

PMV: Peripheral mevalonate

PMV5P: Peripheral mevalonate-5-phosphate

PMV5PP: Peripheral mevalonate diphosphate

PMVK: Peripheral phosphomevalonate kinase

PSQ: Peripheral squalene

PSQE: Peripheral squalene epoxide

PSRB1: Peripheral scavenger receptor class B member 1

PSRB1D : Peripheral scavenger receptor class B member 1 degradation

PSRB1S: Peripheral scavenger receptor class B member 1 synthesis

PSS: Peripheral steroid synthesis

SE: Squalene epoxidase

SS: Squalene synthase

VLDLC: Very low density lipoprotein cholesterol

Table A.1 Initial values and abbreviation of species

Species	Abbreviation	Initial Value (mg)
Dietary Intake		
Free cholesterol	DFC	0
Cholesterol esters	DCE	0
Intestinal Lumen		
Free cholesterol	LFC	0
Cholesterol esters	LCE	0
Conjugated bile acids	LCBA	200
Unconjugated bile acids	LUBA	50
Jejunocytes		
Acetyl CoA synthesis	JACoAS	210
Acetyl CoA	JACoA	210
AcetoAcetyl CoA	JAACoA	210
HMG CoA	JHMGCoA	210
Mevalonate	JMV	210
Mevalonate-5-phosphate	JMV5P	210
Mevalonate diphosphate	JMV5PP	210
Isopentenyl pyrophosphate	JIPP	210
Dimethylallyl pyrophosphate	JDMAPP	210
Geranyl pyrophosphate	JGPP	210
Farnesyl pyrophosphate	JFPP	210
Squalene	JSQ	210
Squalene epoxide	JSQE	210
Lanosterol	JLAN	210
7-Dehydrodesmosterol	J7DHDES	210
7-Dehydrocholesterol	J7DHC	210
Desmosterol	JDES	210
Free cholesterol	JFC	1575
Cholesterol esters	JCE	1575
Chylomicron	JCH	948

Species	Species	Species
Neimann-Pick C1-Like 1	NPC1L1	100
Neimann-Pick C1-Like 1 synthesis	NPC1L1S	1
Neimann-Pick C1-Like 1 degradation	NPC1L1D	0

Ileocytes

Conjugated bile acids	ICBA	50
Unconjugated bile acids	IUBA	50
Apical-dependent bile acid transporter	ABST	100
Apical-dependent bile acid transporter	ABSTS	1
Apical-dependent bile acid transporter	ABSTD	0
Organic solute transporter α/β	OST	100
Organic solute transporter α/β synthesis	OSTS	1
Organic solute transporter α/β degradation	OSTD	0
Intestinal Apolipoprotein A-I synthesis	IAPOAIS	1657

Blood

Apolipoprotein A-I	APOAI	8286
Nascent high density lipoprotein	ndHDL	1657
Nascent high density lipoprotein cholesterol	ndHDLC	1228
High density lipoprotein subclass 2	HDL2	409
High density lipoprotein subclass 3	HDL3	409
Very low density lipoprotein cholesterol	VLDLC	948
Intermediate density lipoprotein cholesterol	IDLC	949
Low density lipoprotein	LDLC	3209
Unconjugated bile acids	BUBA	1
Conjugated bile acids	BCBA	1
Phospholipids	PL	1657
Phospholipid source	PLS	10

Species	Species	Species

Hepatic Tissue

Acetyl CoA synthesis	HACoAS	303
Acetyl CoA	HACoA	303
AcetoAcetyl CoA	HAACoA	303
HMG CoA	HHMGCoA	303
Mevalonate	HMV	303
Mevalonate-5-phosphate	HMV5P	303
Mevalonate diphosphate	HMV5PP	303
Isopentenyl pyrophosphate	HIPP	303
Dimethylallyl pyrophosphate	HDMAPP	303
Geranyl pyrophosphate	HGPP	303
Farnesyl pyrophosphate	HFPP	303
Squalene	HSQ	303
Squalene epoxide	HSQE	303
Lanosterol	HLAN	303
7-Dehydrodesmosterol	H7DHDES	303
7-Dehydrocholesterol	H7DHC	303
Desmosterol	HDES	303
Free cholesterol	HFC	38917
Cholesterol esters	HCE	18012
Chylomicron	HCH	200
Hepatic Apolipoprotein A-I synthesis	HAPOAIS	1657
Low density lipoprotein receptor	HLDLR	100
Low density lipoprotein receptor synthesis	HLDLRS	1
Low density lipoprotein receptor degradation	HLDLRD	0
Scavenger receptor class B member 1	HSRB1	100
Scavenger receptor class B member 1 synthesis	HSRB1S	1
Scavenger receptor class B member 1 degradation	HSRB1D	0
Lipoprotein receptor related protein	LRP	100
Lipoprotein receptor related protein synthesis	LRPS	1
Lipoprotein receptor related protein degradation	LRPD	0
ATP-binding cassette transporters G8/G8	ABCG5G8	100

Species	Species	Species
ATP-binding cassette transporters G8/G8 synthesis	ABCG5G8S	1
ATP-binding cassette transporters G8/G8 degradation	ABCG5G8D	0
Na$^+$-taurocholate cotransporting polypeptide	NTCP	100
Na$^+$-taurocholate cotransporting polypeptide synthesis	NTCPS	1
Na$^+$-taurocholate cotransporting polypeptide degradation	NTCPD	0
Bile salt export pump	BSEP	100
Bile salt export pump synthesis	BSEPS	1
Bile salt export pump degradation	BSEPD	0
7α-hydroxycholesterol	C1	200
7α-hydroxycholest-4-en-3-one	C2	200
7α-hydroxy-5β-cholestan-3-one	C3	200
3α, 7α-dihydroxy-5β-cholestanate	C4	200
4-cholesten-7α, 12α-diol-3-one	C5	200
5β-cholesten-7α, 12α-diol-3one	C6	200
3α, 7α, 12α-trihydroxy-5β-cholestanoate	C7	200
3β-hydroxy-5-cholestenoate	C8	200
3β, 7α-dihydroxy-5-cholestenoate	C9	200
7α-hydroxy-3-oxo-4-cholestenoate	C10	200
Unconjugated bile acid -CoA	HUBACoA	200
Conjugated bile acids	HCBA	220
Unconjugated bile acids	HUBA	180

Peripheral Tissue

Acetyl CoA synthesis	PACoAS	21
Acetyl CoA	PACoA	21
AcetoAcetyl CoA	PAACoA	21
HMG CoA	PHMGCoA	21
Mevalonate	PMV	21
Mevalonate-5-phosphate	PMV5P	21
Mevalonate diphosphate	PMV5PP	21
Isopentenyl pyrophosphate	PIPP	21
Dimethylallyl pyrophosphate	PDMAPP	21

Species	Species	Species
Geranyl pyrophosphate	PGPP	21
Farnesyl pyrophosphate	PFPP	21
Squalene	PSQ	21
Squalene epoxide	PSQE	21
Lanosterol	PLAN	21
7-Dehydrodesmosterol	P7DHDES	21
7-Dehydrocholesterol	P7DHC	21
Desmosterol	PDES	21
Free cholesterol	PFC	25914
Cholesterol esters	PCE	4218
ATP-binding cassette subfamily A member 1	ABCA1	100
ATP-binding cassette subfamily A member 1 synthesis	ABC1S	1
ATP-binding cassette subfamily A member 1 degradation	ABC1D	0
Scavenger receptor class B member 1	PSRB1	100
Scavenger receptor class B member 1 synthesis	PSRB1S	1
Scavenger receptor class B member 1 degradation	PSRB1D	0
Low density lipoprotein receptor	PLDLR	100
Low density lipoprotein receptor synthesis	PLDLRS	1
Low density lipoprotein receptor degradation	PLDLRD	0
Steroid synthesis	PSS	1
Excreted		
Free cholesterol	EFC	0
Unconjugated bile acids	EUBA	0

Table A.2 Reactions and their rate laws

	Reaction	Reaction	Compartments	Enzyme/Receptor	EC Number	Rate Law
	Intestinal Cholesterol Absorption					
1	Ingestion FC	DFC -> LFC	INTAKE -> LUMEN		-	Mass action
2	Counter for FC ingestion	counter1 -> counter2			-	Constant Flux
3	Ingestion CE	DCE -> LCE	INTAKE -> LUMEN		-	Mass action
4	Counter for CE ingestion	counter3 -> counter4			-	Constant Flux
5	CEH conversion of dietary esters	LCE -> LFC	LUMEN	CEH	3.1.1.13	Michaelis Menten
6	Jejunocyte Absorption of FC	LFC -> JFC	LUMEN -> JEJUNOCYTE	NPC1L1	-	$K_{abs}[LFC][LCBA][LUBA][NPC1L1]$
7	Esterification of Jejunocyte FC	JFC -> JCE	JEJUNOCYTE	ACAT2	2.3.1.26	Michaelis Menten
8	CE uptake into Chylomicron	JCE -> JCH	JEJUNOCYTE	MTP	-	Mass Action
9	FC uptake into Chylomicron	JFC -> JCH	JEJUNOCYTE	MTP	-	Mass Action
10	Chylomicron FC uptake by Liver (LRP)	HCH -> HFC	HEPATOCYTE	LRP	-	$K_{ch4}[HCH][LRP]$
11	Chylomicron transport to liver	JCH -> HCH	JEJUNOCYTE -> HEPATOCYTE		-	Mass action
12	Chylomicron CE uptake by Liver (LRP)	HCH -> HCE	HEPATOCYTE	LRP	-	$K_{ch1}[HCH][LRP]$
13	Chylomicron FC uptake by Liver (HLRLR)	HCH -> HFC	HEPATOCYTE	HLDLR	-	$K_{ch3}[HCH][HLDLR]$
14	Chylomicron CE uptake by Liver (HLDLR)	HCH -> HCE	HEPATOCYTE	HLDLR	-	$K_{ch1}[HCH][HLDLR]$
15	Biliary Cholesterol Release	HFC -> LFC	HEPATOCYTE -> LUMEN	ABC G5/G8	-	$BCR_{max}/(1+(BCRt/HFC)^{BS})$
16	Conversion of hepatic FC to CE	HFC -> HCE	HEPATOCYTE	ACAT2	2.3.1.26	Michaelis Menten
17	Conversion of hepatic CE to FC	HCE -> HFC	HEPATOCTE	CEH	3.1.1.13	Michaelis Menten
	Lipoproteins, Reverse Cholesterol Transport and Excretion of Cholesterol					
18	VLDLC formation	HCE -> VLDLC	HEPATOCYE -> BLOOD		-	Mass action
19	Excreted Cholesterol	LFC -> EFC	LUMEN -> EXCRETED		-	$K_{efc}[LFC][LCBA][LUBA]$
20	VLDLC Reuptake	VLDLC -> HCE	BLOOD -> HEPATOCYTE	HLDLR	-	$K_{vldl}[VLDLC][HLDLR]$
21	IDLC formation	VLDLC -> IDLC	BLOOD	LPL	3.1.1.34	$K_{idlf}[VLDLC][LPL]$
22	IDLC Reuptake	IDLC -> HCE	BLOOD -> HEPATOCYTE	HLDLR	-	$K_{idlu}[IDLC][HLDLR]$
23	LDLC formation	IDLC -> LDLC	BLOOD	HL	3.1.1.79	$K_{ldl}[IDLC][HSL]$
24	Receptor dependent hepatic LDLC uptake	LDLC -> HCE	BLOOD -> HEPATOCYTE	HDLR	-	$K_{hldlu}[HLDLR][LDLC]$
25	Receptor independent hepatic LDLC uptake	LDLC -> HCE	BLOOD HEPATOCYTE		-	Mass action
26	Receptor dependent peripheral LDLC uptake	LDLC -> PCE	BLOOD -> PERIPHERAL	PLDLR	-	$K_{pldlu}[LDLC][PLDLR]$
27	Receptor independent peripheral LDLC uptake	LDLC -> PCE	BLOOD -> PERIPHERAL		-	Mass action

	Reaction	Reaction	Compartments	Enzyme/Receptor	EC Number	Rate Law
28	Peripheral CE conversion to FC	PCE -> PFC	PERIPHERAL TISSUE	CEH	3.1.1.13	Michaelis Menten
29	Peripheral FC conversion to CE	PFC -> PCE	PERIPHERAL TISSUE	ACAT1	2.3.1.26	Michaelis Menten
30	Hepatic APOAI synthesis	HAPOAIS -> APOAI	HEPATOCYTE -> BLOOD			Mass action
31	Intestinal APOAI synthesis	IAPOAIS -> APOAI	ILEOCYTES -> BLOOD			Mass action
32	ndHDL formation	APOA1 + PL -> ndHDL	BLOOD			Mass action
33	ABCA1 release of PFC	PFC + ndHDL -> ndHDLC	PERIPHERAL -> BLOOD	ABCA1	-	K_{a1e}[PFC][ndHDL][ABCA1]
34	SRB1 release of PFC	PFC + ndHDL -> ndHDLC	PERIPHERAL -> BLOOD	SRB1	-	K_{psrb1}[PFC][ndHDL][PSRB1]
35	Receptor independent release of PFC	PFC + ndHDL -> ndHDLC	PERIPHERAL -> BLOOD			Mass action
36	HDL3 Formation	ndHDLC -> HDL3	BLOOD	LCAT	2.3.1.43	K_{hdl3}[PFC][LCAT][ndHDLC]
37	HDL3 to HDL2	HDL3 -> HDL2	BLOOD	PLTP		Michaelis Menten
38	HDL2 to HDL3	HDL2 -> HDL3	BLOOD	HL	3.1.1.3	Michaelis Menten
39	CETP mediated transfer to VLDL	HDL2 -> VLDLC	BLOOD	CETP	-	K_{cetp2}[HDL2][CETP]
40	CETP mediated transfer to LDL	HDL2 -> LDLC	BLOOD	CETP	-	K_{cetp1}[HDL2][CETP]
41	Reverse cholesterol Transport	HDL2 -> HCE	BLOOD -> HEPATOCYTE	SRB1	-	K_{rct}[HDL2][HSRB1]
42	Peripheral steroid production	PFC -> PSS	PERIPHERAL TISSUE			Mass action
43	Phospholipid source	PLS -> PL				Mass action

Intestinal and Hepatic Movement of Bile Acids

	Reaction	Reaction	Compartments	Enzyme/Receptor	EC Number	Rate Law
44	Bile Acid Release	HCBA -> LCBA	HEPATOCYTE -> LUMEN	BSEP	-	Michaelis Menten
45	Deconjugation of CBA	LCBA -> LUBA	LUMEN	BSH	3.5.1.24	Michaelis Menten
46	Excretion of UBA	LUBA -> EUBA	LUMEN -> EXCRETED		-	Mass action
47	Receptor dependent UBA uptake	LUBA -> IUBA	LUMEN -> ILEOCYTE	ABST	-	Michaelis Menten
48	Receptor independent UBA uptake	LUBA -> IUBA	LUMEN -> ILEOCYTE			Mass action
49	CBA uptake	LCBA -> ICBA	LUMEN -> ILEOCYTE	ABST	-	Michaelis Menten
50	Efflux of UBA out of ileocyte	IUBA -> BUBA	ILEOCYTE -> BLOOD	OSTα/β	-	Michaelis Menten
51	Efflux of CBA out of ileocyte	ICBA -> BCBA	ILEOCYTE -> BLOOD	OSTα/β	-	Michaelis Menten
52	Hepatic uptake of UBA	BUBA -> HUBA	BLOOD -> HEPATOCYTE	NTCP	-	Michaelis Menten
53	Hepatic uptake of CBA	BCBA -> HCBA	BLOOD -> HEPATOCYTE	NTCP	-	Michaelis Menten

Receptor Synthesis and Degradation

	Reaction	Reaction	Compartments	Enzyme/Receptor	EC Number	Rate Law
54	NPC1L1 degradation	NPC1L1 -> NPC1L1D	JEJUNOCYTE		-	Mass action
55	ASBT degradation	ASBT -> ASBTD	ILEOCYTE		-	Mass action
56	OSTαβ degradation	OST -> OSTD	ILEOCYTE		-	Mass action
57	LRP synthesis	LRPS -> LRP	HEPATOCYTE		-	$(K_{lrps}$[LRPS])/[HFC]

	Reaction	Reaction	Compartments	Enzyme/Receptor	EC Number	Rate Law
58	LRP degradation	LRP -> LRPD	HEPATOCYTE		-	Mass action
59	HLDLR synthesis	HLDLRS -> HLDLR	HEPATOCYTE		-	$(K_{hdlrs}[HLDLRS])/[HFC]$
60	HLDLR degradation	HLDLR -> HLDLRD	HEPATOCYTE		-	Mass action
61	HSRB1 synthesis	HSRB1S -> HSRB1	HEPATOCYTE		-	$(K_{hsrb1s}[HSRB1S])/[HCE]$
62	HSRB1 degradation	HSRB1 -> HSRB1D	HEPATOCYTE		-	Mass action
63	ABCG5G8 degradation	ABCG5G8 -> ABCG5G8D	HEPATOCYTE		-	Mass action
64	NTCP degradation	NTCP -> NTCPD	HEPATOCYTE		-	Mass action
65	BSEP synthesis	BSEPS -> BSEP	HEPATOCYTE		-	$(K_{bseps}[BSEPS])/[HCBA]$
66	BSEP degradation	BSEP -> BSEPD	HEPATOCYTE		-	Mass action
67	ABCA1 degradation	ABCA1 -> ABCA1D	PERIPHERAL TISSUE		-	Mass action
68	PSRB1 synthesis	PSRB1S -> PSRB1	PERIPHERAL TISSUE		-	$(K_{psrb1s}[PSRB1S])/[PFC]$
69	PSRB1 degradation	PSRB1 -> PSRB1D	PERIPHERAL TISSUE		-	Mass action
70	PLDLR synthesis	PLDLRS -> PLDLR	PERIPHERAL TISSUE		-	$(Kpldlrs[PLDLRS])/[PFC]$
71	PLDLR degradation	PLDLR -> PLDLRD	PERIPHERAL TISSUE		-	Mass action
72	OSTαβ synthesis	OSTS -> OST	ILEOCYTE		-	$(K_{osts}[OSTS])/(ICBA]+[IUBA])$
73	ABCG5G8 synthesis	ABCG5G8S -> ABCG55G8	HEPATOCYTE		-	$(K_{g5g8s}[ABCG5G8S])/[HFC]$
74	ABCA1 synthesis	ABCA1S -> ABCA1	PERIPHERAL TISSUE		-	$(K_{a1s}[ABCA1S])/[PFC]$
75	NTCP synthesis	NTCPS -> NTCP	HEPATOCYTE		-	$(Kntcps[NTCPS])/([HUBA]+[HCBA])$
76	ASBT synthesis	ASBTS -> ASBT	ILEOCYTE		-	$(K_{asbts}[ASBTS])/(ICBA+IUBA)$
77	NPC1L1 synthesis	NPC1L1S -> NPC1L1	JEJUNOCYTE		-	$(K_{npc1l1s}[NPC1L1S])/[JFC]$
	Cholesterol synthesis – Hepatic					
78	Acetyl CoA synthesis	HACoAS -> HACoA	HEPATOCYTE			Mass action
79	Interconversion of Acetyl CoA and Acetoacetyl CoA	2 * HACoA = HAACoA + HCoASH	HEPATOCYTE	AACT	2.3.1.9	Ping Pong Bi Bi
80	HMG CoA formation	HACoA + HAACoA -> HHMGCoA	HEPATOCYTE	HMGCoAS	2.3.3.10	Bi
81	Mevalonate formation	HHMGCoA -> HMV	HEPATOCYTE	HMGCoAR	1.1.1.34	Michaelis Menten
82	Mevalonate5P formation	HMV -> HMV5P	HEPATOCYTE	MVK	2.7.1.36	Michaelis Menten
83	IPP formation	HMV5PP -> HIPP	HEPATOCYTE	MVD	4.1.1.33	Michaelis Menten
84	Mevalonate5PP formation	HMV5P = HMV5PP	HEPATOCYTE	PMVK	2.7.4.2	Reversible Michaelis Menten
85	DMAPP interconversion	HIPP = HDMAPP	HEPATOCYTE	IDI	5.3.3.2	Reversible Michaelis Menten
86	GeranylPP formation	HDMAPP + HIPP -> HGPP	HEPATOCYTE	FDPS	2.5.1.10	Bi
87	FarnesylPP formation	HGPP + HIPP -> HFPP	HEPATOCYTE	FDPS	2.5.1.10	Bi
88	Squalene formation	HFPP -> HSQ	HEPATOCYTE	SS	2.5.1.21	Michaelis Menten

	Reaction	Reaction	Compartments	Enzyme/Receptor	EC Number	Rate Law
89	Squalene epoxide formation	HSQ -> HSQE	HEPATOCYTE	SE	1.14.13.132	Michaelis Menten
90	Lanosterol formation	HSQE -> HLAN	HEPATOCYTE	OSC	5.4.99.7	Michaelis Menten
91	7 Dehydrodesmosterol formation	HLAN -> H7DHDES	HEPATOCYTE		-	Mass action
92	7DHC formation	H7DHDES -> H7DHC	HEPATOCYTE	DHCR24	1.3.1.72	Michaelis Menten
93	Desmosterol formation	H7DHDES -> HDES	HEPATOCYTE	DHCR7	1.3.1.21	Michaelis Menten
94	FC formation from 7DHC	H7DHC -> HFC	HEPATOCYTE	DHCR7	1.3.1.21	Michaelis Menten
95	FC formation from desmosterol	HDES -> HFC	HEPATOCYTE	DHCR24	1.3.1.72	Michaelis Menten
	Cholesterol synthesis – Peripheral Tissue					
96	Acetyl CoA synthesis	PACoAS -> PACoA	PERIPHERAL TISSUE			Mass action
97	Interconversion of Acetyl CoA and Acetoacetyl CoA	2 * PACoA = PAACoA + PCoASH	PERIPHERAL TISSUE	AACT	2.3.1.9	Ping Pong Bi Bi
98	HMG CoA formation	PACoA + PAACoA -> PHMGCoA	PERIPHERAL TISSUE	HMGCoAS	2.3.3.10	Bi
99	Mevalonate formation	PHMGCoA -> PMV	PERIPHERAL TISSUE	HMGCoAR	1.1.1.34	Michaelis Menten
100	Mevalonate5P formation	PMV -> PMV5P	PERIPHERAL TISSUE	MVK	2.7.1.36	Michaelis Menten
101	Mevalonate5PP formation	PMV5P = PMV5PP	PERIPHERAL TISSUE	PMVK	2.7.4.2	Reversible Michaelis Menten
102	IPP formation	PMV5PP -> PIPP	PERIPHERAL TISSUE	MVD	4.1.1.33	Michaelis Menten
103	DMAPP interconversion	PIPP = PDMAPP	PERIPHERAL TISSUE	IDI	5.3.3.2	Reversible Michaelis Menten
104	GeranylPP formation	PDMAPP + PIPP -> PGPP	PERIPHERAL TISSUE	FDPS	2.5.1.10	Bi
105	FarnesylPP formation	PGPP + PIPP -> PFPP	PERIPHERAL TISSUE	FDPS	2.5.1.10	Bi
106	Squalene formation	PFPP -> PSQ	PERIPHERAL TISSUE	SS	2.5.1.21	Michaelis Menten
107	Squalene epoxide formation	PSQ -> PSQE	PERIPHERAL TISSUE	SE	1.14.13.132	Michaelis Menten
108	Lanosterol formation	PSQE -> PLAN	PERIPHERAL TISSUE	OSC	5.4.99.7	Michaelis Menten
109	7 Dehydrodesmosterol formation	PLAN -> P7DHDES	PERIPHERAL TISSUE		-	Mass action
110	7DHC formation	P7DHDES -> P7DHC	PERIPHERAL TISSUE	DHCR24	1.3.1.72	Michaelis Menten
111	Desmosterol formation	P7DHDES -> PDES	PERIPHERAL TISSUE	DHCR7	1.3.1.21	Michaelis Menten
112	FC formation from 7DHC	P7DHC -> PFC	PERIPHERAL TISSUE	DHCR7	1.3.1.21	Michaelis Menten
113	FC formation from desmosterol	PDES -> PFC	PERIPHERAL TISSUE	DHCR24	1.3.1.72	Michaelis Menten
	Cholesterol Synthesis – intestinal (stated as jejunocytes)					
114	Acetyl CoA synthesis	JACoAS -> JACoA	JEJUNOCYTE		-	Mass action
115	Interconversion of Acetyl CoA and Acetoacetyl CoA	2 * JACoA = JAACoA + JCoASH	JEJUNOCYTE	AACT	2.3.1.9	Ping Pong Bi Bi
116	HMG CoA formation	JACoA + JAACoA -> JHMGCoA	JEJUNOCYTE	HMGCoAS	2.3.3.10	Bi

303

	Reaction	Reaction	Compartments	Enzyme/Receptor	EC Number	Rate Law
117	Mevalonate formation	JHMGCoA -> JMV	JEJUNOCYTE	HMGCoAR	1.1.1.34	Michaelis Menten
118	Mevalonate5P formation	JMV -> JMV5P	JEJUNOCYTE	MVK	2.7.1.36	Michaelis Menten
119	Mevalonate5PP formation	JMV5P = JMV5PP	JEJUNOCYTE	PMVK	2.7.4.2	Reversible Michaelis Menten
120	IPP formation	JMV5PP -> JIPP	JEJUNOCYTE	MVD	4.1.1.33	Michaelis Menten
121	DMAPP interconversion	JIPP = JDMAPP	JEJUNOCYTE	IDI	5.3.3.2	Reversible Michaelis Menten
122	GeranylPP formation	JDMAPP + JIPP -> JGPP	JEJUNOCYTE	FDPS	2.5.1.10	Bi
123	FarnesylPP formation	JGPP + JIPP -> JFPP	JEJUNOCYTE	FDPS	2.5.1.10	Bi
124	Squalene formation	JFPP -> JSQ	JEJUNOCYTE	SS	2.5.1.21	Michaelis Menten
125	Squalene epoxide formation	JSQ -> JSQE	JEJUNOCYTE	SE	1.14.13.132	Michaelis Menten
126	Lanosterol formation	JSQE -> JLAN	JEJUNOCYTE	OSC	5.4.99.7	Michaelis Menten
127	7 Dehydrodesmosterol formation	JLAN -> J7DHDES	JEJUNOCYTE		-	Mass action
128	7DHC formation	J7DHDES -> J7DHC	JEJUNOCYTE	DHCR24	1.3.1.72	Michaelis Menten
129	Desmosterol formation	J7DHDES -> JDES	JEJUNOCYTE	DHCR7	1.3.1.21	Michaelis Menten
130	FC formation from 7DHC	J7DHC -> JFC	JEJUNOCYTE	DHCR7	1.3.1.21	Michaelis Menten
131	FC formation from desmosterol	JDES -> JFC	JEJUNOCYTE	DHCR24	1.3.1.72	Michaelis Menten
	Bile Acid Synthesis					
132	BASC C1 formation CYP7AI	HFC -> C1	HEPATOCYTE	CYP7A1	1.14.13.17	Michaelis Menten
133	BASC C2 formation HSD3B7	C1 ->C2	HEPATOCYTE	HSD3B7	1.1.1.181	Michaelis Menten
134	BASC C3 formation AKR1D1	C2 -> C3	HEPATOCYTE	AKR1D1	1.3.1.3	Michaelis Menten
135	BASC C4 formation CYP27A1	C3 -> C4	HEPATOCYTE	CYP27A1	1.14.13.15	Michaelis Menten
136	BASC C5 formation CYP8B1	C2 -> C5	HEPATOCYTE	CYP8B1	1.14.13.95	Michaelis Menten
137	BASC C6 formation AKR1D1	C5 -> C6	HEPATOCYTE	AKR1D1	1.3.1.3	Michaelis Menten
138	BASC C7 formation CYP27A1	C6 -> C7	HEPATOCYTE	CYP27A1	1.14.13.15	Michaelis Menten
139	BASA C8 formation CYP27A1	HFC -> C8	HEPATOCYTE	CYP27A1	1.14.13.15	Michaelis Menten
140	BASA C9 formation CYP7B1	C8 -> C9	HEPATOCYTE	CYP7B1	1.14.13.100	Michaelis Menten
141	BASA C10 formation HSD3b7	C9 -> C10	HEPATOCYTE	HSD3B7	1.1.1.181	Michaelis Menten
142	BASC HUBA formation C4	C4 -> HUBA	HEPATOCYTE		-	Mass action
143	BASC HUBA formation C7	C7 -> HUBA	HEPATOCYTE		-	Mass action
144	BAS UBA-CoA formation	HUBA -> HUBACoA	HEPATOCYTE	BACS	6.2.1.7	Michaelis Menten
145	BAS CBA formation	HUBACoA -> HCBA	HEPATOCYTE	BAT	2.3.1.65	Michaelis Menten
146	BASA HUBA formation C10	C10 -> HUBA	HEPATOCYTE		-	Mass action

Table A.3 Summary of parameter values

Reaction	Parameter	Value*	Reference
Assumed			
ABCA1 release of peripheral free cholesterol	K_{a1e}	0.1	Assumed
ABCA1 synthesis	K_{a1s}	1	Assumed
ABCG5/G8 synthesis	K_{g5g8s}	10	Assumed
ASBT synthesis	K_{asbts}	1	Assumed
BSEP synthesis	K_{bseps}	1	Assumed
Biliary cholesterol maximum release rate	BCR_{max}	1.7	Adapted (Mc Auley et al., 2012)
Biliary cholesterol release threshold	BCT_t	1	Adapted (Mc Auley et al., 2012)
Biliary cholesterol feedback equation sensitivity	BS	1	Adapted (Mc Auley et al., 2012)
CEPT mediated transfer of cholesterol to LDL from HDL_2	K_{cetp1}	1×10^{-7}	Adapted (Mc Auley et al., 2012)
CEPT mediated transfer of cholesterol to VLDL from HDL_2	K_{cept2}	1×10^{-7}	Adapted (Mc Auley et al., 2012)
Chylomicron cholesterol esters uptake by liver HLDLR	K_{ch1}	0.0001	Assumed
Chylomicron cholesterol esters uptake by liver LRP	K_{ch2}	0.0001	Assumed
Chylomicron free cholesterol uptake by liver HLDLR	K_{ch3}	5	Assumed
Chylomicron free cholesterol uptake by liver LRP	K_{ch4}	5	Assumed
Excreted free cholesterol	K_{efc}	0.9	Adapted (Mc Auley et al., 2012)
HDL_3 formation	K_{hdl3}	0.0004	Adapted from (Mc Auley et al., 2012)
HLDLR synthesis	K_{hldlrs}	100	Adapted (Mc Auley et al., 2012)
Hepatic SRB1 synthesis	K_{hsrb1s}	0.001	Adapted (Mc Auley et al., 2012)
ILDLC formation	K_{idlf}	0.04	Adapted (Mc Auley et al., 2012)
ILDLC reuptake by liver	K_{idlu}	0.0045	Adapted (Mc Auley et al., 2012)
Jejunocyte absorption of free cholesterol	K_{abs}	10	Assumed
LDLC formation	K_{ldl}	1.01×10^{-5}	Adapted (Mc Auley et al., 2012)
LRP synthesis	K_{lrps}	100	Assumed
NPC1L1 synthesis	$K_{npc1l1s}$	1	Assumed
NTCP synthesis	K_{ntcps}	1	Assumed
OSTα/β synthesis	K_{osts}	1	Assumed
Peripheral LDLR synthesis	K_{pldlrs}	1	Adapted (Mc Auley et al., 2012)
Peripheral SRB1 synthesis	K_{psrb1s}	100	Assumed
Receptor dependent hepatic LDLC uptake	K_{hldlu}	2.9×10^{-7}	Adapted (Mc Auley et al., 2012)
Receptor dependent peripheral LDLC uptake	K_{pldlu}	7×10^{-8}	Adapted (Mc Auley et al., 2012)
Reverse cholesterol transport	K_{rct}	1×10^{-12}	Adapted (Mc Auley et al., 2012)
SRB1 release of peripheral free cholesterol	K_{psrb1}	0.1	Assumed
VLDL reuptake	K_{vldl}	0.0026	Adapted (Mc Auley et al., 2012)
Mass Action			
Ingestion of DFC	K_1	1	Adapted (Mc Auley et al., 2012)
Ingestion of DCE	K_1	1	Adapted (Mc Auley et al., 2012)
CE uptake into chylomicron	K_1	4×10^{-5}	Assumed
FC uptake into chylomicron	K_1	0.0012	Assumed

Reaction	Parameter	Value	Reference
Chylomicron transport to liver	K_1	0.001	Assumed
VLDLC formation	K_1	0.4	Adapted (Mc Auley et al., 2012)
Receptor independent hepatic LDLC uptake	K_1	5×10^{-9}	Adapted (Mc Auley et al., 2012)
Receptor independent peripheral LDLC uptake	K_1	5×10^{-8}	Adapted (Mc Auley et al., 2012)
Hepatic APOAI synthesis	K_1	1×10^{14}	Assumed
Intestinal APOAI synthesis	K_1	1×10^{10}	Assumed
ndHDL formation	K_1	5×10^{-15}	Assumed
Receptor independent release of PFC	K_1	1	Assumed
Peripheral steroid production	K_1	9×10^{-7}	Adapted (Mc Auley et al., 2012)
Phospholipid source	K_1	0.1	Assumed
Excretion of UBA	K_1	2×10^{-5}	Adapted (Mc Auley et al., 2012)
Receptor independent UBA uptake	K_1	1×10^{-20}	Assumed
NPC1L1 degradation	K_1	1×10^{-7}	Assumed
ASBT degradation	K_1	1×10^{-7}	Assumed
OSTα/β degradation	K_1	1×10^{-7}	Assumed
LRP degradation	K_1	1×10^{-7}	Assumed
HLDLR degradation	K_1	1×10^{-7}	Adapted (Mc Auley et al., 2012)
HSRB1 degradation	K_1	1×10^{-8}	Adapted (Mc Auley et al., 2012)
ABCG5/G8 degradation	K_1	1×10^{-6}	Assumed
NTCP degradation	K_1	1×10^{-7}	Assumed
BSEP degradation	K_1	1×10^{-7}	Assumed
ABCA1 degradation	K_1	1×10^{-6}	Assumed
PSRB1 degradation	K_1	1×10^{-7}	Assumed
PLDLR degradation	K_1	1×10^{-6}	Adapted (Mc Auley et al., 2012)
Hepatic Acetyl CoA synthesis	K_1	1	Assumed
Hepatic 7 dehydrodesmosterol formation	K_1	1000	Assumed
Peripheral Acetyl CoA synthesis	K_1	1×10^{-5}	Assumed
Peripheral 7 dehydrodesmosterol formation	K_1	1	Assumed
Intestinal Acetyl CoA synthesis	K_1	1	Assumed
Intestinal 7 dehydrodesmosterol formation	K_1	0.1	Assumed
BASC HUBA formation from C4	K_1	1.9×10^{-6}	Assumed
BASC HUBA formation from C7	K_1	1×10^{-7}	Assumed
Bi			
Hepatic HMG CoA formation	K_{ma}	59.0986	(Andrew Skaff and Miziorko, 2010)
	K_{mb}	4.25805	(Andrew Skaff and Miziorko, 2010)
	V_{max}	0.542412	(Andrew Skaff and Miziorko, 2010)
Hepatic Geranyl-PP formation	K_{ma}	7.80105	(Kawasaki et al., 2003)
	K_{mb}	13.0674	(Kawasaki et al., 2003)
	V_{max}	4700.32	(Kawasaki et al., 2003)
Hepatic Farnesyl-PP formation	K_{ma}	0.13511	(Ding et al., 1991)
	K_{mb}	0.00470032	(Ding et al., 1991)
	V_{max}	0.339347	(Ding et al., 1991)

Reaction	Parameter	Value	Reference
Peripheral HMG CoA formation	K_{ma}	59.0986	(Andrew Skaff and Miziorko, 2010)
	K_{mb}	4.25805	(Andrew Skaff and Miziorko, 2010)
	V_{max}	0.542412	(Andrew Skaff and Miziorko, 2010)
Peripheral Geranyl-PP formation	K_{ma}	7.80105	(Kawasaki et al., 2003)
	K_{mb}	13.0674	(Kawasaki et al., 2003)
	V_{max}	4700.32	(Kawasaki et al., 2003)
Peripheral Farnesyl-PP formation	K_{ma}	0.13511	(Ding et al., 1991)
	K_{mb}	0.00470032	(Ding et al., 1991)
	V_{max}	0.339347	(Ding et al., 1991)
Intestinal HMG CoA formation	K_{ma}	59.0986	(Andrew Skaff and Miziorko, 2010)
	K_{mb}	4.25805	(Andrew Skaff and Miziorko, 2010)
	V_{max}	0.542412	(Andrew Skaff and Miziorko, 2010)
Intestinal Geranyl-PP formation	K_{ma}	7.80105	(Kawasaki et al., 2003)
	K_{mb}	13.0674	(Kawasaki et al., 2003)
	V_{max}	4700.32	(Kawasaki et al., 2003)
Intestinal Farnesyl-PP formation	K_{ma}	0.13511	(Ding et al., 1991)
	K_{mb}	0.00470032	(Ding et al., 1991)
	V_{max}	0.339347	(Ding et al., 1991)
Michaelis Menten			
CEH conversion of dietary esters	K_m	9.21694	(Sbarra et al., 2005)
	V_{max}	0.214196	(Sbarra et al., 2005)
Esterification of Jejunocyte FC	K_m	3.68273	(Ikenoya et al., 2007)
	V_{max}	0.00154664	(Ikenoya et al., 2007)
Conversion of hepatic FC to CE	K_m	3.86273	(Ikenoya et al., 2007)
	V_{max}	0.0154664	Adapted (Ikenoya et al., 2007)
Conversion of hepatic CE to FC	K_m	9.21694	(Sbarra et al., 2005)
	V_{max}	0.00214196	Adapted (Sbarra et al., 2005)
Peripheral CE conversion to FC	K_m	9.21694	(Sbarra et al., 2005)
	V_{max}	0.214196	(Sbarra et al., 2005)
Peripheral FC conversion to CE	K_m	1.78637	(Ikenoya et al., 2007)
	V_{max}	0.00842919	(Ikenoya et al., 2007)
HDL_3 to HDL_2	K_m	0.504	Assumed
	V_{max}	0.504	Assumed
HDL_2 to HDL_3	K_m	0.5	Assumed
	V_{max}	0.5	Assumed
Bile acid release	K_m	1.0×10^{-5}	Adapted (Mita et al., 2006)
	V_{max}	0.0001	Adapted (Mita et al., 2006)

Reaction	Parameter	Value	Reference
Deconjugation of CBA			
	K_m	0.0001	Adapted (Gopal-Srivastava and Hylemon, 1988; Kumar et al., 2006; Lundeen and Savage, 1990, 1992; Nair et al., 1967; Patel et al., 2010; Stellwag and Hylemon, 1976)
	V_{max}	5×10^{-6}	Adapted (Gopal-Srivastava and Hylemon, 1988; Kumar et al., 2006; Lundeen and Savage, 1990, 1992; Nair et al., 1967; Patel et al., 2010; Stellwag and Hylemon, 1976)
Receptor dependent UBA uptake	K_m	1×10^{-6}	Assumed
	V_{max}	1×10^{-15}	Assumed
CBA uptake	K_m	6.80724×10^{-6}	(Lionarons et al., 2012)
	V_{max}	2.63007×10^{-15}	(Lionarons et al., 2012)
Efflux of UBA out of ileocyte	K_m	0.0001	Assumed
	V_{max}	0.0001	Assumed
Efflux of CBA out of ileocyte	K_m	0.0001	Assumed
	V_{max}	0.0001	Assumed
Hepatic uptake of UBA	K_m	9.47882	(Ho et al., 2004)
	V_{max}	2.18994×10^{-5}	(Ho et al., 2004)
Hepatic uptake of CBA	K_m	0.010314	(Mita et al., 2006)
	V_{max}	0.000196997	(Mita et al., 2006)
Hepatic Mevalonate formation	K_m	22.0622	(Polo et al., 1999)
	V_{max}	0.000284894	Adapted (Polo et al., 1999)
Hepatic Mevalonate5P formation	K_m	3.5316	(Potter and Miziorko, 1997)
	V_{max}	5.44455	(Potter and Miziorko, 1997)
Hepatic IPP formation	K_m	0.00890467	(Voynova et al., 2008)
	V_{max}	1.87953	(Voynova et al., 2008)
Hepatic Squalene formation	K_m	0.879359	(Soltis et al., 1995)
	V_{max}	1.83518	(Soltis et al., 1995)
Hepatic Squalene epoxide formation	K_m	5.46244	(Favre and Ryder, 1996)
	V_{max}	4.8587×10^{-6}	(Favre and Ryder, 1996)
Hepatic Lanosterol formation	K_m	32.004	(Hoshino et al., 2012)
	V_{max}	0.140818	(Hoshino et al., 2012)
Hepatic 7 DHC formation	K_m	62.6963	(Bae and Paik, 1997)
	V_{max}	0.000553882	(Bae and Paik, 1997)
Hepatic Desmosterol formation	K_m	11.5389	(Moebius et al., 1998)
	V_{max}	0.000326936	Adapted (Moebius et al., 1998)
Hepatic FC formation from 7 DHC	K_m	11.5389	(Moebius et al., 1998)
	V_{max}	0.000326936	(Moebius et al., 1998)
Hepatic FC formation from desmosterol	K_m	62.6963	(Bae and Paik, 1997)
	V_{max}	0.000553882	(Bae and Paik, 1997)
Peripheral Mevalonate formation	K_m	22.0622	(Polo et al., 1999)
	V_{max}	0.000569788	(Polo et al., 1999)
Peripheral Mevalonate5P formation	K_m	3.5316	(Potter and Miziorko, 1997)
	V_{max}	5.44455	(Potter and Miziorko, 1997)

Reaction	Parameter	Value	Reference
Peripheral IPP formation	K_m	0.00890467	(Voynova et al., 2008)
	V_{max}	1.87953	(Voynova et al., 2008)
Peripheral Squalene formation	K_m	0.879359	(Soltis et al., 1995)
	V_{max}	1.83518	(Soltis et al., 1995)
Peripheral Squalene epoxide formation	K_m	5.46244	(Favre and Ryder, 1996)
	V_{max}	4.8587×10^{-6}	(Favre and Ryder, 1996)
Peripheral Lanosterol formation	K_m	32.004	(Hoshino et al., 2012)
	V_{max}	0.140818	(Hoshino et al., 2012)
Peripheral 7 DHC formation	K_m	62.6963	(Bae and Paik, 1997)
	V_{max}	0.000553882	(Bae and Paik, 1997)
Peripheral Desmosterol formation	K_m	11.5389	(Moebius et al., 1998)
	V_{max}	0.000326939	(Moebius et al., 1998)
Peripheral FC formation from 7 DHC	K_m	11.5389	(Moebius et al., 1998)
	V_{max}	0.000326936	(Moebius et al., 1998)
Peripheral FC formation from desmosterol	K_m	62.6963	(Bae and Paik, 1997)
	V_{max}	0.000553882	(Bae and Paik, 1997)
Intestinal Mevalonate formation	K_m	22.0622	(Polo et al., 1999)
	V_{max}	0.000569788	(Polo et al., 1999)
Intestinal Mevalonate5P formation	K_m	3.5316	(Potter and Miziorko, 1997)
	V_{max}	5.44455	(Potter and Miziorko, 1997)
Intestinal IPP formation	K_m	0.00890467	(Voynova et al., 2008)
	V_{max}	1.87953	(Voynova et al., 2008)
Intestinal Squalene formation	K_m	0.879359	(Soltis et al., 1995)
	V_{max}	1.83518	(Soltis et al., 1995)
Intestinal Squalene epoxide formation	K_m	5.46244	(Favre and Ryder, 1996)
	V_{max}	4.8587×10^{-6}	(Favre and Ryder, 1996)
Intestinal Lanosterol formation	K_m	32.004	(Hoshino et al., 2012)
	V_{max}	0.140818	(Hoshino et al., 2012)
Intestinal 7 DHC formation	K_m	62.6963	(Bae and Paik, 1997)
	V_{max}	0.000553882	(Bae and Paik, 1997)
Intestinal Desmosterol formation	K_m	11.5389	(Moebius et al., 1998)
	V_{max}	62.6963	(Moebius et al., 1998)
Intestinal FC formation from 7 DHC	K_m	11.5389	(Moebius et al., 1998)
	V_{max}	0.000326936	(Moebius et al., 1998)
Intestinal FC formation from desmosterol	K_m	62.6963	(Bae and Paik, 1997)
	V_{max}	0.000553882	(Bae and Paik, 1997)
BASC C1 formation CYP7AI	K_m	5.7999	(Ozasa and Boyd, 1981)
	V_{max}	0.00055679	(Ozasa and Boyd, 1981)
BASC C2 formation HSD3B7	K_m	5	Assumed
	V_{max}	0.0005	Assumed
BASC C3 formation AKR1D1	K_m	4.9595	(Okuda and Okuda, 1984)
	V_{max}	0.0004	Assumed
BASC C4 formation CYP27A1	K_m	4.0265	(Atsuta and Okuda, 1982)
	V_{max}	0.0004	Adapted from (Atsuta and Okuda, 1982)
BASC C5 formation CYP8B1	K_m	14.715	(Murakami et al., 1982)
	V_{max}	0.763305	(Murakami et al., 1982)
BASC C6 formation AKR1D1	K_m	5.08289	(Okuda and Okuda, 1984)
	V_{max}	0.5×10^{-5}	Assumed

Reaction	Parameter	Value	Reference
BASC C7 formation CYP27A1	K_m	1.87488	(Atsuta and Okuda, 1982)
	V_{max}	2.24986×10^{-5}	(Atsuta and Okuda, 1982)
BASA C8 formation CYP27A1	K_m	154.664	(Li et al., 2006)
	V_{max}	0.000502658	(Li et al., 2006)
BASA C9 formation CYP7B1	K_m	5	Assumed
	V_{max}	0.0005	Assumed
BASA C10 formation HSD3b7	K_m	5	Assumed
	V_{max}	0.0005	Assumed
BAS UBA-CoA formation	K_m	4.0857	(Polokoff and Bell, 1977)
	V_{max}	0.000902	(Polokoff and Bell, 1977)
BAS CBA formation	K_m	3.70589	(Kimura et al., 1983)
	V_{max}	0.0009	Assumed
Reversible Michaelis Menten			
Hepatic Mevalonate5PP formation	K_{ms}	7.75676	(Herdendorf and Miziorko, 2007)
	K_{mp}	12.6329	(Herdendorf and Miziorko, 2007)
	V_f	10.5857	(Herdendorf and Miziorko, 2007)
	V_r	3.48176	(Herdendorf and Miziorko, 2007)
Hepatic DMAPP formation	K_{ms}	68.1177	(Diaz et al., 2012)
	K_{mp}	68.1177	(Diaz et al., 2012)
	V_f	0.147654	(Diaz et al., 2012)
	V_r	0.147654	(Diaz et al., 2012)
Peripheral Mevalonate5PP formation	K_{ms}	7.75676	(Herdendorf and Miziorko, 2007)
	K_{mp}	12.6329	(Herdendorf and Miziorko, 2007)
	V_f	10.5857	(Herdendorf and Miziorko, 2007)
	V_r	3.48176	(Herdendorf and Miziorko, 2007)
Peripheral DMAPP formation	K_{ms}	68.1177	(Diaz et al., 2012)
	K_{mp}	68.1177	(Diaz et al., 2012)
	V_f	0.147654	(Diaz et al., 2012)
	V_r	0.147654	(Diaz et al., 2012)
Intestinal Mevalonate5PP formation	K_{ms}	7.75676	(Herdendorf and Miziorko, 2007)
	K_{mp}	12.6329	(Herdendorf and Miziorko, 2007)
	V_f	10.5857	(Herdendorf and Miziorko, 2007)
	V_r	3.48176	(Herdendorf and Miziorko, 2007)

Reaction	Parameter	Value	Reference
Intestinal DMAPP formation	K_{ms}	68.1177	(Diaz et al., 2012)
	K_{mp}	68.1177	(Diaz et al., 2012)
	V_f	0.147654	(Diaz et al., 2012)
	V_r	0.147654	(Diaz et al., 2012)
Ping Pong Bi Bi			
Hepatic Interconversion of Acetyl CoA and Acetoacetyl CoA	K_{eq}	0.1	Assumed
	V_f	0.469551	(Sakurai et al., 2007)
	V_r	0.469551	Assumed
	K_{ma}	22.668	(Sakurai et al., 2007)
	K_{mb}	22.668	Assumed
	K_{mp}	4.25805	(Sakurai et al., 2007)
	K_{mq}	4.91226	(Sakurai et al., 2007)
	K_{ia}	0.1	Assumed
	K_{iq}	0.1	Assumed
Peripheral Interconversion of Acetyl CoA and Acetoacetyl CoA	K_{eq}	0.1	Assumed
	V_f	0.469551	(Sakurai et al., 2007)
	V_r	0.469551	Assumed
	K_{ma}	22.668	(Sakurai et al., 2007)
	K_{mb}	22.668	Assumed
	K_{mp}	4.25805	(Sakurai et al., 2007)
	K_{mq}	4.91226	(Sakurai et al., 2007)
	K_{ia}	0.1	Assumed
	K_{iq}	0.1	Assumed
Intestinal Interconversion of Acetyl CoA and Acetoacetyl CoA	K_{eq}	0.1	Assumed
	V_f	0.469551	(Sakurai et al., 2007)
	V_r	0.469551	Assumed
	K_{ma}	22.668	(Sakurai et al., 2007)
	K_{mb}	22.668	Assumed
	K_{mp}	4.25805	(Sakurai et al., 2007)
	K_{mq}	4.91226	(Sakurai et al., 2007)
	K_{ia}	0.1	Assumed
	K_{iq}	0.1	Assumed

* Values converted to mg/min. Units: K_M = 1, V_{max} = 1/min

Table A.4 Ranked LDL-C sensitivity

Parameter	S_i
LDLC_formation_Kldl	0.810567912
VLDLC_formation_k1	0.727156176
HDL3_to_HDL2_V	0.564222571
IDLC_formation_Kidlf	0.329764491
Conversion_of_hepatic_FC_to_CE_V	3.74E-02
HLDLR_degradation_k1	1.09E-02
CETP_mediated_transfer_to_LDL_Kcetp1	5.89E-03
CETP_mediated_transfer_to_VLDL_Kcetp2	3.72E-03
PLDLR_degradation_k1	2.62E-03
HDL2_to_HDL3_Km	8.52E-04
Chylomicron_CE_uptake_by_liver__HLDLR_Kch1	8.45E-05
Biliary_Cholesterol_release_BCRmax	7.94E-05
HDL3_formation_Khdl3	1.03E-05
Chylomicron_CE_uptake_by_liver__LRP_Kch2	8.53E-06
Peripheral_CE_conversion_to_FC_V	3.11E-06
Conversion_of_hepatic_CE_to_FC_Km	2.69E-06
Chylomicron_transport_to_liver_k1	1.71E-06
FC_uptake_into_chylomicron_k1	1.42E-06
HLDLR_synthesis_Khldlrs	7.90E-07
CE_uptake_into_Chylomicron_k1	3.63E-07
Jejunocyte_absorption_of_FC_Kabs	8.27E-08
Reverse_cholesterol_transport_Krct	3.66E-08
Per_FC_formation_from_7_DHC_V	3.09E-08
Int_FC_formation_from_desmosterol_V	2.43E-08
Per_FC_formation_from_desmosterol_V	2.02E-08
Biliary_Cholesterol_release_BS	1.92E-08
Int_FC_formation_from_7_DHC_V	1.42E-08
Per_7DHC_formation_V	3.76E-09
Per_7_Dehydrodesmosterol_formation_k1	2.96E-09
Per_Desmosterol_formation_V	2.91E-09
Hep_Interconversion_of_Acetyl_CoA_and_Acetoacetyl_CoA_Kiq	2.77E-09
Hep_FC_formation_from_7DHC_V	2.26E-09
Int_Interconversion_of_Acetyl_CoA_and_Acetoacetyl_CoA_Vr	1.99E-09
Hep_FC_formation_from_desmosterol_V	1.83E-09
Int_GeranylPP_formation_Kma	1.74E-09
PSRB1_synthesis_Kpsrb1s	1.70E-09
CEH_conversion_of_dietary_esters_V	1.65E-09
Int_IPP_formation_V	1.64E-09
Per_Lanosterol_formation_V	1.62E-09
Per_DMAPP_interconversion_Vf	1.60E-09
Hep_FC_formation_from_7DHC_Km	1.52E-09
Int_DMAPP_interconversion_Kms	1.42E-09
Hep_GeranylPP_formation_Kmb	1.37E-09
Int_HMG_CoA_formation_Kmb	1.19E-09
Int_Interconversion_of_Acetyl_CoA_and_Acetoacetyl_CoA_Kmp	1.08E-09
Per_Mevalonate_5PP_formation_Vf	1.04E-09
Per_DMAPP_interconversion_Kmp	1.02E-09

Parameter	S_i
Int_Squalene_formation_Km	9.90E-10
Per_Squalene_epoxide_formation_V	9.51E-10
Int_7_Dehydrodesmosterol_formation_k1	9.06E-10
Per_HMG_CoA_formation_Kma	8.87E-10
Int_HMG_CoA_formation_vmax	8.74E-10
Int_Mevalonate_5PP_formation_Kmp	8.60E-10
Hep_Lanosterol_formation_V	8.58E-10
Hep_Lanosterol_formation_Km	8.11E-10
Hep_Mevalonate5PP_formation_Vf	7.96E-10
Hep_7_dehydrodesmosterol_formation_k1	7.95E-10
Hep_Squalene_formation_Km	7.85E-10
Hep_Interconversion_of_Acetyl_CoA_and_Acetoacetyl_CoA_Keq	7.82E-10
Hep_Mevalonate5PP_formation_Vr	7.35E-10
Int_Mevalonate_formation_V	6.72E-10
Int_GeranylPP_formation_Kmb	6.72E-10
Int_Lanosterol_formation_Km	6.26E-10
Hep_HMG_CoA_formation_vmax	6.15E-10
Int_Squalene_epoxide_formation_V	6.09E-10
Int_FarnesylPP_formation_Kmb	5.95E-10
Hep_Mevalonate_formation_V	5.72E-10
Int_Interconversion_of_Acetyl_CoA_and_Acetoacetyl_CoA_Kiq	5.60E-10
Per_Mevalonate_formation_V	5.54E-10
Int_Mevalonate_formation_Km	4.84E-10
Int_DMAPP_interconversion_Vf	4.61E-10
Per_Mevalonate5P_formation_V	4.08E-10
Hep_Mevalonate5P_formation_V	4.03E-10
Per_HMG_CoA_formation_vmax	3.90E-10
ndHDL_formation_k1	3.86E-10
Per_interconversion_of_Acetyl_CoA_and_Acetoacetyl_CoA_Kmb	3.75E-10
Int_DMAPP_interconversion_Vr	3.73E-10
Hep_squalene_epoxide_formation_Km	3.70E-10
Per_IPP_formation_Km	3.69E-10
Int_Interconversion_of_Acetyl_CoA_and_Acetoacetyl_CoA_Keq	3.59E-10
Hep_Interconversion_of_Acetyl_CoA_and_Acetoacetyl_CoA_Vf	3.57E-10
Hep_Mevalonate_formation_Km	3.13E-10
Per_IPP_formation_V	3.05E-10
Per_FarnesylPP_formation_Kma	2.93E-10
Hep_desmosterol_formation_Km	2.84E-10
ABCA1_synthesis_Ka1s	2.68E-10
Hepatic_APOAI_synthesis_k1	2.46E-10
Hep_squalene_epoxide_formation_V	2.29E-10
Per_interconversion_of_Acetyl_CoA_and_Acetoacetyl_CoA_Vr	2.09E-10
Int_Interconversion_of_Acetyl_CoA_and_Acetoacetyl_CoA_Kia	1.85E-10
BASC_C6_formation_AKR1D1_Km	1.84E-10
Int_Lanosterol_formation_V	1.82E-10
Per_interconversion_of_Acetyl_CoA_and_Acetoacetyl_CoA_Kmp	1.80E-10
Hepatic_uptake_of_UBA_V	1.72E-10
Int_HMG_CoA_formation_Kma	1.56E-10
BASA_HUBA_formation_C10_k1	1.54E-10

Parameter	S_i
BASC_C7_formation_CYP27A1_V	1.53E-10
Hepatic_uptake_of_CBA_Km	1.46E-10
Per_FarnesylPP_formation_vmax	1.39E-10
LRP_degradation_k1	1.23E-10
Per_Acetyl_CoA_synthesis_k1	1.20E-10
Per_Geranyl_formation_Kmb	1.14E-10
BASC_C5_formation_CYP8B1_Km	1.13E-10
Hep_7_DHC_formation_Km	1.12E-10
Hep_Interconversion_of_Acetyl_CoA_and_Acetoacetyl_CoA_Kmq	1.05E-10
Int_Squalene_epoxide_formation_Km	1.03E-10
BASC_C2_formation_HSD3B7_Km	1.03E-10
Int_GeranylPP_formation_vmax	9.93E-11
Per_DMAPP_interconversion_Kms	9.91E-11
Hep_desmosterol_formation_V	9.71E-11
Hep_FarnesylPP_formation_Kmb	9.04E-11
BASC_C3_formation_AKR1D1_V	8.78E-11
Hep_IPP_formation_Km	8.45E-11
Receptor_independent_UBA_uptake_k1	7.98E-11
Hep_Squalene_formation_V	7.85E-11
Receptor_dependent_UBA_uptake_V	7.07E-11
BASA_C9_formation_CYP7B1_V	6.05E-11
Int_Interconversion_of_Acetyl_CoA_and_Acetoacetyl_CoA_Kma	5.28E-11
Hepatic_uptake_of_UBA_Km	5.07E-11
BASC_C5_formation_CYP8B1_V	5.01E-11
BASC_C4_formation_CYP27A1_V	4.80E-11
BASA_C10_formation_HSD4B7_Km	4.49E-11
Int_Mevalonate_5PP_formation_Vf	3.93E-11
Hep_Interconversion_of_Acetyl_CoA_and_Acetoacetyl_CoA_Vr	3.37E-11
Per_Mevalonate_5PP_formation_Kmp	3.20E-11
Efflux_of_CBA_out_of_ileocyte_Km	2.84E-11
HSRB1_degradation_k1	2.63E-11
BAS_CBA_formation_V	2.41E-11
BASC_HUBA_formation_C4_k1	2.00E-11
BASC_HUBA_formation_C7_k1	2.08E-12
Counter_for_DFC_ingestion_v	0
Counter_for_DCE_ingestion_v	0
Phospholipid_source_k1	0
Receptor_dependent_UBA_uptake_Km	0
CBA_uptake_Km	0
ASBT_degradation_k1	0
OSTalphabeta_degradation_k1	0
ABCG5G8_degradation_k1	0
NTCP_degradation_k1	0
BSEP_synthesis_Kbseps	0
BSEP_degradation_k1	0
OST_synthesis_Kosts	0
ABCG5G8_synthesis_Kg5g8s	0
NTCP_synthesis_Kntcps	0
ASBT_synthesis_Kasbts	0

Parameter	S_i
BASC_C4_formation_CYP27A1_Km	-2.84E-12
BASC_C6_formation_AKR1D1_V	-3.81E-12
Bile_acid_release_Km	-1.01E-11
CBA_uptake_V	-1.44E-11
BASC_C7_formation_CYP27A1_Km	-1.53E-11
BASC_C2_formation_HSD3B7_V	-1.77E-11
BASA_C9_formation_CYP7B1_Km	-2.25E-11
BASA_C8_formation_CYP27A1_Km	-4.03E-11
Hep_Interconversion_of_Acetyl_CoA_and_Acetoacetyl_CoA_Kmp	-4.22E-11
Per_interconversion_of_Acetyl_CoA_and_Acetoacetyl_CoA_Keq	-5.20E-11
Efflux_of_UBA_out_of_ileocyte_Km	-5.53E-11
Hepatic_uptake_of_CBA_V	-6.94E-11
ABCA1_degradation_k1	-7.28E-11
BAS_UBA_CoA_formation_V	-8.65E-11
BASA_C10_formation_HSD4B7_V	-8.78E-11
NPC1L1_degradation_k1	-8.79E-11
Efflux_of_UBA_out_of_ileocyte_V	-8.99E-11
Int_Mevalonate_5PP_formation_Vr	-9.66E-11
BASC_C3_formation_AKR1D1_Km	-1.08E-10
Hep_Mevalonate5P_formation_Km	-1.19E-10
HSRB1_synthesis_Khsrb1s	-1.34E-10
Bile_acid_release_V	-1.37E-10
BAS_UBA_CoA_formation_Km	-1.50E-10
BAS_CBA_formation_Km	-1.52E-10
Per_Squalene_formation_V	-1.54E-10
Hep_7_DHC_formation_V	-1.77E-10
Int_Mevalonate_5P_V	-1.84E-10
PSRB1_degradation_k1	-2.04E-10
Deconjugation_of_CBA_Km	-2.17E-10
Hep_HMG_CoA_formation_Kma	-2.18E-10
Hep_FarnesylPP_formation_Kma	-2.29E-10
Int_7DHC_formation_Km	-2.32E-10
NPC1L1_synthesis_Knpc1l1s	-2.47E-10
Per_Mevalonate_formation_Km	-2.48E-10
Hep_FarnesylPP_formation_vmax	-2.54E-10
Ingestion_of_DFC_k1	-2.58E-10
Hep_IPP_formation_V	-2.79E-10
Hep_Mevalonate5PP_formation_Kmp	-2.98E-10
Hep_FC_formation_from_desmosterol_Km	-3.01E-10
Hep_DMAPP_interconversion_Kms	-3.03E-10
Esterification_of_Jejunocyte_FC_Km	-3.08E-10
Per_HMG_CoA_formation_Kmb	-3.16E-10
Int_Squalene_formation_V	-3.20E-10
LRP_synthesis_Klrps	-3.25E-10
Int_7DHC_formation_V	-3.37E-10
Per_Mevalonate5P_formation_Km	-3.47E-10
Int_FarnesylPP_formation_vmax	-3.59E-10
Intestinal_APOAI_synthesis_k1	-3.73E-10
Per_Geranyl_formation_Kma	-4.02E-10

Parameter	S_i
Peripheral_FC_conversion_to_CE_Km	-4.32E-10
Hep_Interconversion_of_Acetyl_CoA_and_Acetoacetyl_CoA_Kmb	-4.34E-10
Per_interconversion_of_Acetyl_CoA_and_Acetoacetyl_CoA_Vf	-4.47E-10
Int_Interconversion_of_Acetyl_CoA_and_Acetoacetyl_CoA_Kmb	-4.58E-10
Int_Desmosterol_formation_Km	-4.75E-10
Hep_Mevalonate5PP_formation_Kms	-4.78E-10
Per_7DHC_formation_Km	-4.79E-10
Hep_Acetyl_CoA_synthesis_k1	-4.83E-10
Hep_DMAPP_interconversion_Kmp	-4.89E-10
Per_Squalene_epoxide_formation_Km	-4.99E-10
Hep_DMAPP_interconversion_Vr	-5.01E-10
Hep_DMAPP_interconversion_Vf	-5.04E-10
Int_Interconversion_of_Acetyl_CoA_and_Acetoacetyl_CoA_Kmq	-5.12E-10
Per_Mevalonate_5PP_formation_Vr	-5.15E-10
Hep_HMG_CoA_formation_Kmb	-5.55E-10
Per_interconversion_of_Acetyl_CoA_and_Acetoacetyl_CoA_Kia	-5.56E-10
Deconjugation_of_CBA_V	-5.74E-10
Int_FarnesylPP_formation_Kma	-5.78E-10
Hep_Interconversion_of_Acetyl_CoA_and_Acetoacetyl_CoA_Kia	-6.26E-10
Per_Geranyl_formation_vmax	-6.28E-10
Per_Mevalonate_5PP_formation_Kms	-6.50E-10
BASC_C1_formation_CYP7A1_Km	-6.72E-10
Int_Mevalonate_5PP_formation_Kms	-6.94E-10
Hep_Interconversion_of_Acetyl_CoA_and_Acetoacetyl_CoA_Kma	-7.29E-10
Efflux_of_CBA_out_of_ileocyte_V	-7.49E-10
Per_Lanosterol_formation_Km	-7.50E-10
Int_Acetyl_CoA_synthesis_k1	-7.88E-10
Int_FC_formation_from_desmosterol_Km	-8.15E-10
Int_IPP_formation_Km	-8.63E-10
Int_Interconversion_of_Acetyl_CoA_and_Acetoacetyl_CoA_Vf	-9.00E-10
Per_Squalene_formation_Km	-9.87E-10
Hep_GeranylPP_formation_vmax	-1.02E-09
BASC_C1_formation_CYP7A1_V	-1.09E-09
Int_Mevalonate_5P_Km	-1.12E-09
Excretion_of_UBA_k1	-1.30E-09
BASA_C8_formation_CYP27A1_V	-1.32E-09
Per_Desmosterol_formation_Km	-1.37E-09
Biliary_Cholesterol_release_BCRt	-1.39E-09
Hep_GeranylPP_formation_Kma	-1.41E-09
Per_DMAPP_interconversion_Vr	-1.41E-09
Int_DMAPP_interconversion_Kmp	-1.44E-09
Ingestion_of_DCE_k1	-1.45E-09
Int_Desmosterol_formation_V	-1.49E-09
Int_FC_formation_from_7_DHC_Km	-1.53E-09
Per_FarnesylPP_formation_Kmb	-1.54E-09
CEH_conversion_of_dietary_esters_Km	-1.70E-09
Per_interconversion_of_Acetyl_CoA_and_Acetoacetyl_CoA_Kma	-3.88E-09
Per_interconversion_of_Acetyl_CoA_and_Acetoacetyl_CoA_Kmq	-5.07E-09
Per_interconversion_of_Acetyl_CoA_and_Acetoacetyl_CoA_Kiq	-5.81E-09

Parameter	S_i
Peripheral_CE_conversion_to_FC_Km	-6.14E-09
Per_FC_formation_from_7_DHC_Km	-1.01E-08
Per_FC_formation_from_desmosterol_Km	-1.34E-08
Esterification_of_Jejunocyte_FC_V	-3.01E-08
Excreted_Cholesterol_Kefc	-8.50E-08
Receptor_independent_release_of_PFC_k1	-4.89E-07
Peripheral_FC_conversion_to_CE_V	-1.23E-06
Peripheral_steroid_production_k1	-3.16E-06
Conversion_of_hepatic_FC_to_CE_Km	-3.25E-06
SRB1_release_of_PFC_Kpsrb1	-4.90E-06
ABCA1_release_of_PFC_Ka1e	-4.90E-06
Chylomicron_FC_uptake_by_liver__LRP_Kch4	-8.53E-06
Receptor_independent_hepatic_LDLC_uptake_k1	-1.38E-05
Chylomicron_FC_uptake_by_liver__HLDLR_Kch3	-8.45E-05
PLDLR_synthesis_Kpldlrs	-1.94E-04
Receptor_independent_peripheral_LDLC_uptake_k1	-5.33E-04
HDL3_to_HDL2_Km	-9.41E-04
Conversion_of_hepatic_CE_to_FC_V	-5.18E-03
Receptor_dependent_peripheral_LDLC_uptake_Kpldlu	-7.25E-02
VLDLC_reuptake_Kvldl	-0.285609926
HDL2_to_HDL3_V	-0.559833842
IDLC_reuptake_Kidlu	-0.771136708
Receptor_dependent_hepatic_LDLC_uptake_Khldlu	-0.794330576

Section 2 Cholesterol model ordinary differential equations

1. $\dfrac{d([LFC]V_{"Intestinal\ Lumen"})}{dt} = +(K_1[DFC])$

   $+\left(\dfrac{BCR_{max}}{1+\left(\dfrac{BCR_t}{[HFC]}\right)^{BS}}\right)$

   $-\left(K_{efc}[LFC][LCBA][LUBA]\right)$

   $+V_{"Intestinal\ Lumen"}\left(\dfrac{V_{max}[LCE]}{K_M+[LCE]}\right)$

   $-\left(K_{abs}[LFC][LCBA][LUBA][NPC1L1]\right)$

2. $\dfrac{d([LCE]V_{"Intestinal\ Lumen"})}{dt} = +(K_1[DCE])$

   $-V_{"Intestinal\ Lumen"}\left(\dfrac{V_{max}[LCE]}{K_M+[LCE]}\right)$

3. $\dfrac{d([counter4]V_{"Intestinal\ Lumen"})}{dt} = V_{"Intestinal\ Lumen"}(v)$

4. $\dfrac{d([LCBA]V_{"Intestinal\ Lumen"})}{dt} = +\left(\dfrac{V_{max}[HCBA]}{K_M+[HCBA]}\right)$

   $-V_{"Intestinal\ Lumen"}\left(\dfrac{V_{max}[LCBA]}{K_M+[LCBA]}\right)$

   $-\left(\dfrac{V_{max}[LCBA]}{K_M+[LCBA]}\right)$

5. $\dfrac{d([LUBA]V_{"Intestinal\ Lumen"})}{dt} = +V_{"Intestinal\ Lumen"}\left(\dfrac{V_{max}[LCBA]}{K_M+[LCBA]}\right)$

   $-(K_1[LUBA])$

   $-\left(\dfrac{V_{max}[LUBA]}{K_M+[LUBA]}\right)$

   $-(K_1[LUBA])$

6.
$$\frac{d([NPC1L1D]V_{"Jejunocytes"})}{dt} = +V_{"Jejunocytes"}(K_1[NPC1L1])$$

7.
$$\frac{d[JIPP]V_{"Jejunocytes"}}{dt} = +V_{"Jejunocytes"}\left(\frac{V_{max}[JMV5PP]}{K_M + [JMV5PP]}\right)$$

$$-V_{"Jejunocytes"}\left(\frac{\frac{V_f[JIPP]}{K_M^S} - \frac{V_r[JDMAPP]}{K_M^P}}{1 + \frac{[JIPP]}{K_M^S} + \frac{[JDMAPP]}{K_M^P}}\right)$$

$$-V_{"Jejunocytes"}\left(\frac{V_{max}[JDMAPP][JIPP]}{K_M^A K_M^B + [JDMAPP]K_M^B + [JIPP]K_M^A + [JDMAPP][JIPP]}\right)$$

$$-V_{"Jejunocytes"}\left(\frac{V_{max}[JGPP][JIPP]}{K_M^A K_M^B + [JGPP]K_M^B + [JIPP]K_M^A + [JGPP][JIPP]}\right)$$

8.
$$\frac{d([JACoA]V_{"Jejunocytes"})}{dt} = V_{"Jejunocytes"}(K_1[JACoAS])$$

$$-n_{jacoa}V_{"Jejunocytes"}\left(\frac{V_f\left([JACoA][JACoA] - \frac{[JAACoA][JACoASH]}{K_{eq}}\right)}{[JACoA][JACoA] + K_M^B[JACoA] + K_M^A[JACoA]\left(1 + \frac{[JCoASH]}{K_{iq}}\right) + \frac{V_f}{V_r K_{eq}}\left(K_M^Q[JAACoA]\left(1 + \frac{[JACoA]}{K_{ia}}\right) + [JCoASH](K_M^P + [JAACoA])\right)}\right)$$

$$-V_{"Jejunocytes"}\left(\frac{V_{max}[JACoA][JAACoA]}{K_M^A K_M^B + [JACoA]K_M^B + [JAACoA]K_M^A + [JACoA][JAACoA]}\right)$$

9.
$$\frac{d([JCoASH]V_{"Jejunocytes"})}{dt} = +V_{"Jejunocytes"}\left(\frac{V_f\left([JACoA][JACoA] - \frac{[JAACoA][JACoASH]}{K_{eq}}\right)}{[JACoA][JACoA] + K_M^B[JACoA] + K_M^A[JACoA]\left(1 + \frac{[JCoASH]}{K_{iq}}\right) + \frac{V_f}{V_r K_{eq}}\left(K_M^Q[JAACoA]\left(1 + \frac{[JACoA]}{K_{ia}}\right) + [JCoASH](K_M^P + [JAACoA])\right)}\right)$$

10.
$$\frac{d([JDES]V_{"Jejunocytes"})}{dt} = +V_{"Jejunocytes"}\left(\frac{V_{max}[J7DHDES]}{K_M + [J7DHDES]}\right)$$
$$-V_{"Jejunocytes"}\left(\frac{V_{max}[JDES]}{K_M + [JDES]}\right)$$

11.
$$\frac{d([JACoAS]V_{"Jejunocytes"})}{dt} = -V_{"Jejunocytes"}(K_1[JACoAS])$$

12.
$$\frac{d([JMV]V_{"Jejunocytes"})}{dt} = +V_{"Jejunocytes"}\left(\frac{V_{max}[JHMGCoA]}{K_M + [JHMGCoA]}\right)$$
$$-\left(\frac{V_{max}[JMV]}{K_M + [JMV]}\right)$$

13.
$$\frac{d([JAACoA]V_{"Jejunocytes"})}{dt} = +V_{"Jejunocytes"}\left(\frac{V_f\left([JACoA][JACoA] - \frac{[JAACoA][JACoASH]}{K_{eq}}\right)}{[JACoA][JACoA] + K_M^B[JACoA] + K_M^A[JACoA]\left(1 + \frac{[JCoASH]}{K_{iq}}\right) + \frac{V_f}{V_r K_{eq}}\left(K_M^Q[JAACoA]\left(1 + \frac{[JACoA]}{K_{ia}}\right) + [JCoASH](K_M^P + [JAACoA])\right)}\right)$$

$$-V_{"Jejunocytes"}\left(\frac{V_{max}[JACoA][JAACoA]}{K_M^A K_M^B + [JACoA]K_M^B + [JAACoA]K_M^A + [JACoA][JAACoA]}\right)$$

14. $$\frac{d\left([JMV5PP]V_{"Jejunocytes"}\right)}{dt} = +\left(\frac{\frac{V_f[JMV5P]}{K_M^S} - \frac{V_r[JMV5PP]}{K_M^P}}{1 + \frac{[JMV5P]}{K_M^S} + \frac{[JMV5PP]}{K_M^P}}\right)$$

$$-V_{"Jejunocytes"}\left(\frac{V_{max}[JMV5PP]}{K_M + [JMV5PP]}\right)$$

15. $$\frac{d\left([JDMAPP]V_{"Jejunocytes"}\right)}{dt} = +V_{"Jejunocytes"}\left(\frac{\frac{V_f[JIPP]}{K_M^S} - \frac{V_r[JDMAPP]}{K_M^P}}{1 + \frac{[JIPP]}{K_M^S} + \frac{[JDMAPP]}{K_M^P}}\right)$$

$$-V_{"Jejunocytes"}\left(\frac{V_{max}[JDMAPP][JIPP]}{K_M^A K_M^B + [JDMAPP]K_M^B + [JIPP]K_M^A + [JDMAPP][JIPP]}\right)$$

16. $$\frac{d\left([JHMGCoA]V_{"Jejunocytes"}\right)}{dt} = +V_{"Jejunocytes"}\left(\frac{V_{max}[JACoA][JAACoA]}{K_M^A K_M^B + [JACoA]K_M^B + [JAACoA]K_M^A + [JACoA][JAACoA]}\right)$$

$$-V_{"Jejunocytes"}\left(\frac{V_{max}[JHMGCoA]}{K_M + [JHMGCoA]}\right)$$

17. $$\frac{d\left([JSQ]V_{"Jejunocytes"}\right)}{dt} = +V_{"Jejunocytes"}\left(\frac{V_{max}[JFPP]}{K_M + [JFPP]}\right)$$

$$-V_{"Jejunocytes"}\left(\frac{V_{max}[JSQ]}{K_M + [JSQ]}\right)$$

18. $$\frac{d\left([JGPP]V_{"Jejunocytes"}\right)}{dt} = +V_{"Jejunocytes"}\left(\frac{V_{max}[JDMAPP][JIPP]}{K_M^A K_M^B + [JDMAPP]K_M^B + [JIPP]K_M^A + [JDMAPP][JIPP]}\right)$$

$$-V_{"Jejunocytes"}\left(\frac{V_{max}[JGPP][JIPP]}{K_M^A K_M^B + [JGPP]K_M^B + [JIPP]K_M^A + [JGPP][JIPP]}\right)$$

19. $$\frac{d\left([JSQE]V_{"Jejunocytes"}\right)}{dt} = +V_{"Jejunocytes"}\left(\frac{V_{max}[JSQ]}{K_M + [JSQ]}\right)$$

$$-V_{"Jejunocytes"}\left(\frac{V_{max}[JSQE]}{K_M + [JSQE]}\right)$$

20. $$\frac{d\left([J7DHDES]V_{"Jejunocytes"}\right)}{dt} = +V_{"Jejunocytes"}(K_1[JLAN])$$

$$-V_{"Jejunocytes"}\left(\frac{V_{max}[J7DHDES]}{K_M + [J7DHDES]}\right)$$

$$-V_{"Jejunocytes"}\left(\frac{V_{max}[J7DHDES]}{K_M + [J7DHDES]}\right)$$

21. $$\frac{d\left([JFPP]V_{"Jejunocytes"}\right)}{dt} = +V_{"Jejunocytes"}\left(\frac{V_{max}[JGPP][JIPP]}{K_M^A K_M^B + [JGPP]K_M^B + [JIPP]K_M^A + [JGPP][JIPP]}\right)$$

$$-V_{"Jejunocytes"}\left(\frac{V_{max}[JFPP]}{K_M + [JFPP]}\right)$$

22. $$\frac{d([J7DHC]V_{"Jejunocytes"})}{dt} = +V_{"Jejunocytes"}\left(\frac{V_{max}[J7DHDES]}{K_M+[J7DHDES]}\right)$$

$$-V_{"Jejunocytes"}\left(\frac{V_{max}[J7DHC]}{K_M + [J7DHC]}\right)$$

23. $$\frac{d([JLAN]V_{"Jejunocytes"})}{dt} = +V_{"Jejunocytes"}\left(\frac{V_{max}[JSQE]}{K_M+[JSQE]}\right)$$

$$-V_{"Jejunocytes"}(K_1[JLAN])$$

24. $$\frac{d([JCE]V_{"Jejunocytes"})}{dt} = +V_{"Jejunocytes"}\left(\frac{V_{max}[JFC]}{K_M+[JFC]}\right)$$

$$-V_{"Jejunocytes"}(K_1[JCE])$$

25. $$\frac{d([JFC]V_{"Jejunocytes"})}{dt} = +V_{"Jejunocytes"}\left(\frac{V_{max}[J7DHC]}{K_M+[J7DHC]}\right)$$

$$+V_{"Jejunocytes"}\left(\frac{V_{max}[JDES]}{K_M + [JDES]}\right)$$

$$-(K_{abs}[LFC][LCBA][LUBA][NPC1L1]$$

$$-V_{"Jejunocytes"}\left(\frac{V_{max}[JFC]}{K_M + [JFC]}\right)$$

$$-(K_1[JFC])$$

26. $$\frac{d([NPC1L1S]V_{"Jejunocytes"})}{dt} = -V_{"Jejunocytes"}\left(\frac{K_{npc1l1s}[NPC1L1S]}{[JFC]}\right)$$

27. $$\frac{d([NPC1L1]V_{"Jejunocytes"})}{dt} = -V_{"Jejunocytes"}(K_1[NPC1L1])$$

$$+V_{"Jejunocytes"}\left(\frac{K_{npc1l1s}[NPC1L1S]}{[JFC]}\right)$$

28. $$\frac{d([JMV5P]V_{"Jejunocytes"})}{dt} = +V_{"Jejunocytes"}\left(\frac{V_{max}[JMV]}{K_M+[JMV]}\right)$$

$$-V_{"Jejunocytes"}\left(\frac{\frac{V_f[JMV5P]}{K_M^S} - \frac{V_r[JMV5PP]}{K_M^P}}{1 + \frac{[JMV5P]}{K_M^S} + \frac{[JMV5PP]}{K_M^P}}\right)$$

29. $\dfrac{d\left([JCH]V_{"Jejunocytes"}\right)}{dt} = -(K_1[JCH])$

$+V_{"Jejunocytes"}(K_1[JCE])$

$+V_{"Jejunocytes"}(K_1[JFC])$

30. $\dfrac{d\left([IAPOAIS]V_{"Ileocytes"}\right)}{dt} = -(K_1[IAPOAIS])$

31. $\dfrac{d\left([IUBA]V_{"Ileocytes"}\right)}{dt} = +\left(\dfrac{V_{max}[LUBA]}{K_M+[LUBA]}\right)$

$+(K_1[LUBA])$

$-\left(\dfrac{V_{max}[IUBA]}{K_M+[IUBA]}\right)$

32. $\dfrac{d\left([ICBA]V_{"Ileocytes"}\right)}{dt} = +\left(\dfrac{V_{max}[LCBA]}{K_M+[LCBA]}\right)$

$-\left(\dfrac{V_{max}[ICBA]}{K_M+[ICBA]}\right)$

33. $\dfrac{d\left([OST]V_{"Ileocytes"}\right)}{dt} = -V_{"Ileocytes"}(K_1[OST])$

$+V_{"Ileocytes"}\left(\dfrac{K_{osts}[OSTS]}{[ICBA]+[IUBA]}\right)$

34. $\dfrac{d\left([ASBTS]V_{"Ileocytes"}\right)}{dt} = -V_{"Ileocytes"}\left(\dfrac{K_{asbts}[ASBTS]}{[ICBA]+[IUBA]}\right)$

35. $\dfrac{d\left([OSTD]V_{"Ileocytes"}\right)}{dt} = +V_{"Ileocytes"}(K_1[OST])$

36. $\dfrac{d\left([OSTS]V_{"Ileocytes"}\right)}{dt} = -V_{"Ileocytes"}\left(\dfrac{K_{osts}[OSTS]}{[ICBA]+[IUBA]}\right)$

37. $\dfrac{d\left([ASBTD]V_{"Ileocytes"}\right)}{dt} = +V_{"Ileocytes"}(K_1[ASBT])$

38. $\dfrac{d\left([ASBT]V_{"Ileocytes"}\right)}{dt} = -V_{"Ileocytes"}(K_1[ASBT])$

$+V_{"Ileocytes"}\left(\dfrac{K_{asbts}[ASBTS]}{[ICBA]+[IUBA]}\right)$

39. $\dfrac{d\left([HCH]V_{"Hepatic\ Tissue"}\right)}{dt} = +(K_1[JCH])$

$-V_{"Hepatic\ Tissue"}(K_{ch2}[HCH][LRP])$

$-V_{"Hepatic\ Tissue"}(K_{ch3}[HCH][HLDLR])$

$-V_{"Hepatic\ Tissue"}(K_{ch1}[HCH][HLDLR])$

$-V_{"Hepatic\ Tissue"}(K_{ch4}[HCH][LRP])$

40. $\dfrac{d\left([LRP]V_{"Hepatic\ Tissue"}\right)}{dt} = +V_{"Hepatic\ Tissue"}\left(\dfrac{K_{lrps}[LRPS]}{[HFC]}\right)$

$-V_{"Hepatic\ Tissue"}(K_1[LRP])$

41. $\dfrac{d\left([HLDLR]V_{"Hepatic\ Tissue"}\right)}{dt} = +V_{"Hepatic\ Tissue"}\left(\dfrac{K_{hldlrs}[HLDLRS]}{[HFC]}\right)$

$-V_{"Hepatic\ Tissue"}(K_1[HLDLR])$

42. $\dfrac{d\left([HFC]V_{"Hepatic\ Tissue"}\right)}{dt} = +V_{"Hepatic\ Tissue"}(K_{ch3}[HCH][HLDLR])$

$-V_{"Hepatic\ Tissue"}\left(\dfrac{V_{max}[HFC]}{K_M + [HFC]}\right)$

$-V_{"Hepatic\ Tissue"}\left(\dfrac{V_{max}[HFC]}{K_M + [HFC]}\right)$

$-\left(\dfrac{BCR_{max}}{1 + \left(\dfrac{BCR_t}{[HFC]}\right)^{BS}}\right)$

$-V_{"Hepatic\ Tissue"}\left(\dfrac{V_{max}[HFC]}{K_M + [HFC]}\right)$

$+V_{"Hepatic\ Tissue"}\left(\dfrac{V_{max}[HCE]}{K_M + [HCE]}\right)$

$+V_{"Hepatic\ Tissue"}(K_{ch4}[HCH][LRP])$

$+V_{"Hepatic\ Tissue"}\left(\dfrac{V_{max}[H7DHC]}{K_M + [H7DHC]}\right)$

$+V_{"Hepatic\ Tissue"}\left(\dfrac{V_{max}[HDES]}{K_M + [HDES]}\right)$

43. $\dfrac{d\left([HCE]V_{"Hepatic\ Tissue"}\right)}{dt} = +V_{"Hepatic\ Tissue"}(K_{ch2}[HCH][LRP])$

$+V_{"Hepatic\ Tissue"}(K_{ch1}[HCH][HLDLR])$

$+V_{"Hepatic\ Tissue"}\left(\dfrac{V_{max}[HFC]}{K_M + [HFC]}\right)$

$-V_{"Hepatic\ Tissue"}\left(\dfrac{V_{max}[HCE]}{K_M + [HCE]}\right)$

$-(K_1[HCE])$

$+(K_{vldl}[VLDLC][HLDLR])$

$+(K_{idlu}[IDLC][HLDLR])$

$+(K_{hldlu}[HLDLR][LDLC])$

$+(K_1[LDLC])$

$+(K_{rct}[HDL2][HSRB1])$

44. $\dfrac{d\left([HAPOAIS]V_{"Hepatic\ Tissue"}\right)}{dt} = -V_{"Hepatic\ Tissue"}(K_1[HAPOAIS])$

45. $\dfrac{d\left([HUBA]V_{"Hepatic\ Tissue"}\right)}{dt} = +V_{"Hepatic\ Tissue"}(K_1[C4])$

$+V_{"Hepatic\ Tissue"}(K_1[C7])$

$-V_{"Hepatic\ Tissue"}\left(\dfrac{V_{max}[HUBA]}{K_M + [HUBA]}\right)$

$+V_{"Hepatic\ Tissue"}(K_1[C10])$

$+\left(\dfrac{V_{max}[BUBA]}{K_M + [BUBA]}\right)$

46. $\dfrac{d\left([NTCP]V_{"Hepatic\ Tissue"}\right)}{dt} = -V_{"Hepatic\ Tissue"}(K_1[NTCP])$

$+V_{"Hepatic\ Tissue"}\left(\dfrac{K_{ntcps}[NTCPS]}{[HUBA] + [HCBA]}\right)$

47. $\dfrac{d\left([LRPD]V_{"Hepatic\ Tissue"}\right)}{dt} = +V_{"Hepatic\ Tissue"}(K_1[LRP])$

48. $\dfrac{d\left([LRPS]V_{"Hepatic\ Tissue"}\right)}{dt} = -V_{"Hepatic\ Tissue"}\left(\dfrac{K_{lrps}[LRPS]}{[HFC]}\right)$

49. $\dfrac{d\left([HLDLRD]V_{"Hepatic\,Tissue"}\right)}{dt} = +V_{"Hepatic\,Tissue"}(K_1[HLDLR])$

50. $\dfrac{d\left([HLDLRS]V_{"Hepatic\,Tissue"}\right)}{dt} = -V_{"Hepatic\,Tissue"}\left(\dfrac{K_{hldlrs}[HLDLRS]}{[HFC]}\right)$

51. $\dfrac{d\left([HSRB1]V_{"Hepatic\,Tissue"}\right)}{dt} = +V_{"Hepatic\,Tissue"}\left(\dfrac{K_{hsrb1s}[HSRB1S]}{[HCE]}\right)$

$-V_{"Hepatic\,Tissue"}(K_1[HSRB1])$

52. $\dfrac{d\left([HSRB1D]V_{"Hepatic\,Tissue"}\right)}{dt} = +V_{"Hepatic\,Tissue"}(K_1[HSRB1])$

53. $\dfrac{d\left([HSRB1S]V_{"Hepatic\,Tissue"}\right)}{dt} = -V_{"Hepatic\,Tissue"}\left(\dfrac{K_{hsrb1s}[HSRB1S]}{[HCE]}\right)$

54. $\dfrac{d\left([ABCG5G8D]V_{"Hepatic\,Tissue"}\right)}{dt} = +V_{"Hepatic\,Tissue"}(K_1[ABCG5G8])$

55. $\dfrac{d\left([ABCG5G8S]V_{"Hepatic\,Tissue"}\right)}{dt} = -V_{"Hepatic\,Tissue"}\left(\dfrac{K_{g5g8s}[ABCG5G8S]}{[HFC]}\right)$

56. $\dfrac{d\left([ABCG5G8]V_{"Hepatic\,Tissue"}\right)}{dt} = -V_{"Hepatic\,Tissue"}(K_1[ABCG5G8])$

$+V_{"Hepatic\,Tissue"}\left(\dfrac{K_{g5g8s}[ABCG5G8S]}{[HFC]}\right)$

57. $\dfrac{d\left([NTCPS]V_{"Hepatic\,Tissue"}\right)}{dt} = -V_{"Hepatic\,Tissue"}\left(\dfrac{K_{ntcps}[NTCPS]}{[HUBA]+[HCBA]}\right)$

58. $\dfrac{d\left([NTCPD]V_{"Hepatic\,Tissue"}\right)}{dt} = +V_{"Hepatic\,Tissue"}(K_1[NTCP])$

59. $\dfrac{d\left([BSEPD]V_{"Hepatic\,Tissue"}\right)}{dt} = +V_{"Hepatic\,Tissue"}(K_1[BSEP])$

60. $\dfrac{d\left([BSEPS]V_{"Hepatic\,Tissue"}\right)}{dt} = -V_{"Hepatic\,Tissue"}\left(\dfrac{K_{bseps}[BSEPS]}{[HCBA]}\right)$

61.
$$\frac{d([BSEP]V_{"Hepatic\ Tissue"})}{dt} = +V_{"Hepatic\ Tissue"}\left(\frac{K_{bseps}[BSEPS]}{[HCBA]}\right)$$

$$-V_{"Hepatic\ Tissue"}(K_1[BSEP])$$

62.
$$\frac{d([HACoAS]V_{"Hepatic\ Tissue"})}{dt} = -V_{"Hepatic\ Tissue"}(K_1[HACoAS])$$

63.
$$\frac{d([HACoA]V_{"Hepatic\ Tissue"})}{dt} = +V_{"Hepatic\ Tissue"}(K_1[HACoAS])$$

$$-n_{hacoa}V_{"Hepatic\ Tissue"}\left(\frac{V_f\left([HACoA][HACoA]-\frac{[HAACoA][HACoASH]}{K_{eq}}\right)}{[HACoA][HACoA]+K_M^B[HACoA]+K_M^A[HACoA]\left(1+\frac{[HCoASH]}{K_{iq}}\right)+\frac{Vf}{V_rK_{eq}}\left(K_M^Q[HAACoA]\left(1+\frac{[HACoA]}{K_{ia}}\right)+[HCoASH](K_M^P+[HAACoA])\right)}\right)$$

$$-V_{"Hepatic\ Tissue"}\left(\frac{V_{max}[HACoA][HAACoA]}{K_M^AK_M^B+[HACoA]K_M^B+[HAACoA]K_M^A+[HACoA][HAACoA]}\right)$$

64.
$$\frac{d([HAACoA]V_{"Hepatic\ Tissue"})}{dt} = +V_{"Hepatic\ Tissue"}\left(\frac{V_f\left([HACoA][HACoA]-\frac{[HAACoA][HACoASH]}{K_{eq}}\right)}{[HACoA][HACoA]+K_M^B[HACoA]+K_M^A[HACoA]\left(1+\frac{[HCoASH]}{K_{iq}}\right)+\frac{Vf}{V_rK_{eq}}\left(K_M^Q[HAACoA]\left(1+\frac{[HACoA]}{K_{ia}}\right)+[HCoASH](K_M^P+[HAACoA])\right)}\right)$$

$$-V_{"Hepatic\ Tissue"}\left(\frac{V_{max}[HACoA][HAACoA]}{K_M^AK_M^B+[HACoA]K_M^B+[HAACoA]K_M^A+[HACoA][HAACoA]}\right)$$

65.
$$\frac{d([HHMGCoA]V_{"Hepatic\ Tissue"})}{dt} = +V_{"Hepatic\ Tissue"}\left(\frac{V_{max}[HACoA][HAACoA]}{K_M^AK_M^B+[HACoA]K_M^B+[HAACoA]K_M^A+[HACoA][HAACoA]}\right)$$

$$-V_{"Hepatic\ Tissue"}\left(\frac{V_{max}[HHMGCoA]}{K_M+[HHMGCoA]}\right)$$

66.
$$\frac{d([HMV]V_{"Hepatic\ Tissue"})}{dt} = +V_{"Hepatic\ Tissue"}\left(\frac{V_{max}[HHMGCoA]}{K_M+[HHMGCoA]}\right)$$

$$-V_{"Hepatic\ Tissue"}\left(\frac{V_{max}[HMV]}{K_M+[HMV]}\right)$$

67.
$$\frac{d([HMV5PP]V_{"Hepatic\ Tissue"})}{dt} = -V_{"Hepatic\ Tissue"}\left(\frac{V_{max}[HMV5PP]}{K_M+[HMV5PP]}\right)$$

$$+V_{"Hepatic\ Tissue"}\left(\frac{\frac{V_f[HMV5P]}{K_M^S}-\frac{V_r[HMV5PP]}{K_M^P}}{1+\frac{[HMV5P]}{K_M^S}+\frac{[HMV5PP]}{K_M^P}}\right)$$

68.
$$\frac{d([HMV5P]V_{"Hepatic\ Tissue"})}{dt} = +V_{"Hepatic\ Tissue"}\left(\frac{V_{max}[HMV]}{K_M+[HMV]}\right)$$

$$-V_{"Hepatic\ Tissue"}\left(\frac{\frac{V_f[HMV5P]}{K_M^S}-\frac{V_r[HMV5PP]}{K_M^P}}{1+\frac{[HMV5P]}{K_M^S}+\frac{[HMV5PP]}{K_M^P}}\right)$$

69. $$\frac{d([HIPP]V_{"Hepatic\,Tissue"})}{dt} = +V_{"Hepatic\,Tissue"}\left(\frac{V_{max}[HMV5PP]}{K_M+[HMV5PP]}\right)$$

$$-V_{"Hepatic\,Tissue"}\left(\frac{\frac{V_f[HIPP]}{K_M^S}-\frac{V_r[HDMAPP]}{K_M^P}}{1+\frac{[HIPP]}{K_M^S}+\frac{[HDMAPP]}{K_M^P}}\right)$$

$$-V_{"Hepatic\,Tissue"}\left(\frac{V_{max}[HDMAPP][HIPP]}{K_M^AK_M^B+[HDMAPP]K_M^B+[HIPP]K_M^A+[HDMAPP][HIPP]}\right)$$
$$-V_{"Hepatic\,Tissue"}\left(\frac{V_{max}[HGPP][HIPP]}{K_M^AK_M^B+[HGPP]K_M^B+[HIPP]K_M^A+[HGPP][HIPP]}\right)$$

70. $$\frac{d([HDMAPP]V_{"Hepatic\,Tissue"})}{dt} = +V_{"Hepatic\,Tissue"}\left(\frac{\frac{V_f[HIPP]}{K_M^S}-\frac{V_r[HDMAPP]}{K_M^P}}{1+\frac{[HIPP]}{K_M^S}+\frac{[HDMAPP]}{K_M^P}}\right)$$

$$-V_{"Hepatic\,Tissue"}\left(\frac{V_{max}[HDMAPP][HIPP]}{K_M^AK_M^B+[HDMAPP]K_M^B+[HIPP]K_M^A+[HDMAPP][HIPP]}\right)$$

71. $$\frac{d([HFPP]V_{"Hepatic\,Tissue"})}{dt} = +V_{"Hepatic\,Tissue"}\left(\frac{V_{max}[HGPP][HIPP]}{K_M^AK_M^B+[HGPP]K_M^B+[HIPP]K_M^A+[HGPP][HIPP]}\right)$$
$$-V_{"Hepatic\,Tissue"}\left(\frac{V_{max}[HFPP]}{K_M+[HFPP]}\right)$$

72. $$\frac{d([HGPP]V_{"Hepatic\,Tissue"})}{dt} = +V_{"Hepatic\,Tissue"}\left(\frac{V_{max}[HDMAPP][HIPP]}{K_M^AK_M^B+[HDMAPP]K_M^B+[HIPP]K_M^A+[HDMAPP][HIPP]}\right)$$
$$-V_{"Hepatic\,Tissue"}\left(\frac{V_{max}[HGPP][HIPP]}{K_M^AK_M^B+[HGPP]K_M^B+[HIPP]K_M^A+[HGPP][HIPP]}\right)$$

73. $$\frac{d([HSQ]V_{"Hepatic\,Tissue"})}{dt} = +V_{"Hepatic\,Tissue"}\left(\frac{V_{max}[HFPP]}{K_M+[HFPP]}\right)$$

$$-V_{"Hepatic\,Tissue"}\left(\frac{V_{max}[HSQ]}{K_M+[HSQ]}\right)$$

74. $$\frac{d([H7DHDES]V_{"Hepatic\,Tissue"})}{dt} = +V_{"Hepatic\,Tissue"}(K_1[HLAN])$$
$$-V_{"Hepatic\,Tissue"}\left(\frac{V_{max}[H7DHDES]}{K_M+[H7DHDES]}\right)$$
$$-V_{"Hepatic\,Tissue"}\left(\frac{V_{max}[H7DHDES]}{K_M+[H7DHDES]}\right)$$

75. $$\frac{d([H7DHC]V_{"Hepatic\,Tissue"})}{dt} = +V_{"Hepatic\,Tissue"}\left(\frac{V_{max}[H7DHDES]}{K_M+[H7DHDES]}\right)$$
$$-V_{"Hepatic\,Tissue"}\left(\frac{V_{max}[H7DHC]}{K_M+[H7DHC]}\right)$$

76.
$$\frac{d([HDES]V_{"Hepatic\ Tissue"})}{dt} = +V_{"Hepatic\ Tissue"}\left(\frac{V_{max}[H7DHDES]}{K_M+[H7DHDES]}\right)$$
$$-V_{"Hepatic\ Tissue"}\left(\frac{V_{max}[HDES]}{K_M+[HDES]}\right)$$

77.
$$\frac{d([HLAN]V_{"Hepatic\ Tissue"})}{dt} = +V_{"Hepatic\ Tissue"}\left(\frac{V_{max}[HSQE]}{K_M+[HSQE]}\right)$$
$$-V_{"Hepatic\ Tissue"}(K_1[HLAN])$$

78.
$$\frac{d([HSQE]V_{"Hepatic\ Tissue"})}{dt} = +V_{"Hepatic\ Tissue"}\left(\frac{V_{max}[HSQ]}{K_M+[HSQ]}\right)$$
$$-V_{"Hepatic\ Tissue"}\left(\frac{V_{max}[HSQE]}{K_M+[HSQE]}\right)$$

79.
$$\frac{d([HCBA]V_{"Hepatic\ Tissue"})}{dt} = +V_{"Hepatic\ Tissue"}\left(\frac{V_{max}[HUBACoA]}{K_M+[HUBACoA]}\right)$$
$$-V_{"Hepatic\ Tissue"}\left(\frac{V_{max}[HCBA]}{K_M+[HCBA]}\right)$$
$$+V_{"Hepatic\ Tissue"}\left(\frac{V_{max}[BCBA]}{K_M+[BCBA]}\right)$$

80.
$$\frac{d([HCoASH]V_{"Hepatic\ Tissue"})}{dt} = +V_{"Hepatic\ Tissue"}\left(\frac{V_f\left([HACoA][HACoA]-\frac{[HAACoA][HCoASH]}{K_{eq}}\right)}{[HACoA][HACoA]+K_M^B[HACoA]+K_M^A[HACoA]\left(1+\frac{[HCoASH]}{K_{iq}}\right)+\frac{V_f}{V_rK_{eq}}\left(K_M^Q[HAACoA]\left(1+\frac{[HACoA]}{K_{ia}}\right)+[HCoASH](K_M^P+[HAACoA])\right)}\right)$$

81.
$$\frac{d([C3]V_{"Hepatic\ Tissue"})}{dt} = +V_{"Hepatic\ Tissue"}\left(\frac{V_{max}[C2]}{K_M+[C2]}\right)$$
$$-V_{"Hepatic\ Tissue"}\left(\frac{V_{max}[C3]}{K_M+[C3]}\right)$$

82.
$$\frac{d([C1]V_{"Hepatic\ Tissue"})}{dt} = +V_{"Hepatic\ Tissue"}\left(\frac{V_{max}[HFC]}{K_M+[HFC]}\right)$$
$$-V_{"Hepatic\ Tissue"}\left(\frac{V_{max}[C1]}{K_M+[C1]}\right)$$

83.
$$\frac{d([C5]V_{"Hepatic\ Tissue"})}{dt} = +V_{"Hepatic\ Tissue"}\left(\frac{V_{max}[C2]}{K_M+[C2]}\right)$$
$$-V_{"Hepatic\ Tissue"}\left(\frac{V_{max}[C5]}{K_M+[C5]}\right)$$

84.
$$\frac{d([C2]V_{"Hepatic\ Tissue"})}{dt} = +V_{"Hepatic\ Tissue"}\left(\frac{V_{max}[C1]}{K_M+[C1]}\right)$$
$$-V_{"Hepatic\ Tissue"}\left(\frac{V_{max}[C2]}{K_M+[C2]}\right)$$
$$-V_{"Hepatic\ Tissue"}\left(\frac{V_{max}[C2]}{K_M+[C2]}\right)$$

85. $$\frac{d([C6]V_{"Hepatic\ Tissue"})}{dt} = +V_{"Hepatic\ Tissue"}\left(\frac{V_{max}[C5]}{K_M+[C5]}\right)$$
$$-V_{"Hepatic\ Tissue"}\left(\frac{V_{max}[C6]}{K_M+[C6]}\right)$$

86. $$\frac{d([C4]V_{"Hepatic\ Tissue"})}{dt} = +V_{"Hepatic\ Tissue"}\left(\frac{V_{max}[C3]}{K_M+[C3]}\right)$$
$$-V_{"Hepatic\ Tissue"}(K_1[C4])$$

87. $$\frac{d([C9]V_{"Hepatic\ Tissue"})}{dt} = +V_{"Hepatic\ Tissue"}\left(\frac{V_{max}[C8]}{K_M+[C8]}\right)$$
$$-V_{"Hepatic\ Tissue"}\left(\frac{V_{max}[C9]}{K_M+[C9]}\right)$$

88. $$\frac{d([C7]V_{"Hepatic\ Tissue"})}{dt} = +V_{"Hepatic\ Tissue"}\left(\frac{V_{max}[C6]}{K_M+[C6]}\right)$$
$$-V_{"Hepatic\ Tissue"}(K_1[C7])$$

89. $$\frac{d([C10]V_{"Hepatic\ Tissue"})}{dt} = +V_{"Hepatic\ Tissue"}\left(\frac{V_{max}[C9]}{K_M+[C9]}\right)$$
$$-V_{"Hepatic\ Tissue"}(K_1[C10])$$

90. $$\frac{d([C8]V_{"Hepatic\ Tissue"})}{dt} = +V_{"Hepatic\ Tissue"}\left(\frac{V_{max}[HFC]}{K_M+[HFC]}\right)$$
$$-V_{"Hepatic\ Tissue"}\left(\frac{V_{max}[C8]}{K_M+[C8]}\right)$$

91. $$\frac{d([HUBACoA]V_{"Hepatic\ Tissue"})}{dt} = +V_{"Hepatic\ Tissue"}\left(\frac{V_{max}[HUBA]}{K_M+[HUBA]}\right)$$
$$-V_{"Hepatic\ Tissue"}\left(\frac{V_{max}[HUBACoA]}{K_M+[HUBACoA]}\right)$$

92. $$\frac{d([DFC]V_{"Dietary\ Intake"})}{dt} = -(K_1[DFC])$$

93. $$\frac{d([counter2]V_{"Dietary\ Intake"})}{dt} = +V_{"Dietary\ Intake"}(v)$$

94. $$\frac{d([DCE]V_{"Dietary\ Intake"})}{dt} = -(K_1[DCE])$$

95. $$\frac{d([VLDLC]V_{Blood})}{dt} = +(K_1[HCE])$$
$$-(K_{vldl}[VLDLC][HLDLR])$$
$$-V_{Blood}(K_{idlf}[VLDLC][LPL])$$
$$+V_{Blood}(K_{cetp2}[HDL2][CETP])$$

96. $\frac{d([IDLC]V_{Blood})}{dt} = +V_{Blood}\big(K_{idlf}[VLDLC][LPL]\big)$

$-\big(K_{idlu}[IDLC][HLDLR]\big)$

$-V_{Blood}\big(K_{ldl}[IDLC][HSL]\big)$

97. $\frac{d([LDLC]V_{Blood})}{dt} = +V_{Blood}\big(K_{ldl}[IDLC][HSL]\big)$

$-\big(K_{hldlu}[HLDLR][LDLC]\big)$

$-\big(K_1[LDLC]\big)$

$-\big(K_{pldlu}[LDLC][PLDLR]\big)$

$-\big(K_1[LDLC]\big)$

$+V_{Blood}\big(K_{cetp1}[HDL2][CETP]\big)$

98. $\frac{d([HDL2]V_{Blood})}{dt} = +V_{Blood}\left(\frac{V_{max}[HDL3]}{K_M+[HDL3]}\right)$

$-V_{Blood}\left(\frac{V_{max}[HDL2]}{K_M+[HDL2]}\right)$

$-V_{Blood}\big(K_{cetp1}[HDL2][CETP]\big)$

$-V_{Blood}\big(K_{cetp2}[HDL2][CETP]\big)$

$-\big(K_{rct}[HDL2][HSRB1]\big)$

99. $\frac{d([HDL3]V_{Blood})}{dt} = +\big(K_{hdl3}[PFC][LCAT][ndHDL]\big)$

$-V_{Blood}\left(\frac{V_{max}[HDL3]}{K_M+[HDL3]}\right)$

$+V_{Blood}\left(\frac{V_{max}[HDL2]}{K_M+[HDL2]}\right)$

100. $\frac{d([PLS]V_{Blood})}{dt} = -V_{Blood}\big(K_1[PLS]\big)$

101. $\frac{d([BCBA]V_{Blood})}{dt} = +\left(\frac{V_{max}[ICBA]}{K_M+[ICBA]}\right)$

$-\left(\frac{V_{max}[BCBA]}{K_M+[BCBA]}\right)$

102. $\frac{d([BUBA]V_{Blood})}{dt} = +\left(\frac{V_{max}[IUBA]}{K_M+[IUBA]}\right)$

$-\left(\frac{V_{max}[BUBA]}{K_M+[BUBA]}\right)$

103. $\frac{d([ndHDL]V_{Blood})}{dt} = +V_{Blood}(K_1[APOAI][PL])$

$-(K_{a1e}[PFC][ndHDL][ABCA1])$

$-(K_{psrb1}[PFC][ndHDL][PSRB1])$

$-(K_1[PFC][ndHDL])$

$-(K_{hdl3}[PFC][LCAT][ndHDL])$

104. $\frac{d([ndHDLC]V_{Blood})}{dt} = +(K_{a1e}[PFC][ndHDL][ABCA1])$

$+(K_{psrb1}[PFC][ndHDL][PSRB1])$

$+(K_1[PFC][ndHDL])$

105. $\frac{d([PCE]V_{"Peripheral\,Tissure"})}{dt} = +(K_{pldlu}[LDLC][PLDLR])$

$+(K_1[LDLC])$

$-V_{"Peripheral\,Tissue"}\left(\frac{V_{max}[PCE]}{K_M+[PCE]}\right)$

$+V_{"Peripheral\,Tissue"}\left(\frac{V_{max}[PFC]}{K_M+[PFC]}\right)$

106. $\frac{d([PLDLR]V_{"Peripheral\,Tissure"})}{dt} = +V_{"Peripheral\,Tissue"}\left(\frac{K_{pldlrs}[PLDLRS]}{[PFC]}\right)$

$-V_{"Peripheral\,Tissure"}(K_1[PLDLR])$

107. $$\frac{d([PFC]V_{"Peripheral\,Tissure"})}{dt} = +V_{"Peripheral\,Tissue"}\left(\frac{V_{max}[P7DHC]}{K_M+[P7DHC]}\right)$$

$$+V_{"Peripheral\,Tissue"}\left(\frac{V_{max}[PDES]}{K_M+[PDES]}\right)$$

$$+V_{"Peripheral\,Tissue"}\left(\frac{V_{max}[PCE]}{K_M+[PCE]}\right)$$

$$-V_{"Peripheral\,Tissue"}\left(\frac{V_{max}[PFC]}{K_M+[PFC]}\right)$$

$$-(K_{a1e}[PFC][ndHDL][ABCA1])$$

$$-(K_{psrb1}[PFC][ndHDL][PSRB1])$$

$$-(K_1[PFC][ndHDL])$$

$$-(K_{hdl3}[PFC][LCAT][ndHDL])$$

$$-V_{"Peripheral\,Tissue"}(K_1[PFC])$$

108. $$\frac{d([ABCA1]V_{"Peripheral\,Tissure"})}{dt} = -(K_1[ABCA1])$$

$$+V_{"Peripheral\,Tissue"}\left(\frac{K_{a1s}[ABCA1S]}{[PFC]}\right)$$

109. $$\frac{d([PSS]V_{"Peripheral\,Tissure"})}{dt} = +V_{"Peripheral\,Tissue"}(K_1[PFC])$$

110. $$\frac{d([ABCA1S]V_{"Peripheral\,Tissure"})}{dt} = -V_{"Peripheral\,Tissue"}\left(\frac{K_{a1s}[ABCA1S]}{[PFC]}\right)$$

111. $$\frac{d([PSRB1]V_{"Peripheral\,Tissure"})}{dt} = +V_{"Peripheral\,Tissue"}\left(\frac{K_{psrb1s}[PSRB1S]}{[PFC]}\right)$$

$$-V_{"Peripheral\,Tissue"}(K_1[PSRB1])$$

112. $$\frac{d([PSRB1D]V_{"Peripheral\,Tissure"})}{dt} = +V_{"Peripheral\,Tissue"}(K_1[PSRB1])$$

113. $$\frac{d([PSRB1S]V_{"Peripheral\,Tissure"})}{dt} = -V_{"Peripheral\,Tissue"}\left(\frac{K_{psrb1s}[PSRB1S]}{[PFC]}\right)$$

114. $$\frac{d([PLDLRD]V_{"Peripheral\,Tissure"})}{dt} = +V_{"Peripheral\,Tissue"}(K_1[PLDLR])$$

115. $\dfrac{d([PLDLRS]V_{"Peripheral\,Tissure"})}{dt} = -V_{"Peripheral\,Tissue"}\left(\dfrac{K_{pldlrs}[PLDLRS]}{[PFC]}\right)$

116. $\dfrac{d([ABCA1D]V_{"Peripheral\,Tissure"})}{dt} = +V_{"Peripheral\,Tissue"}(K_1[ABCA1])$

117. $\dfrac{d([P7DHC]V_{"Peripheral\,Tissure"})}{dt} = +V_{"Peripheral\,Tissue"}\left(\dfrac{V_{max}[P7DHDES]}{K_M+[P7DHDES]}\right)$

$-V_{"Peripheral\,Tissue"}\left(\dfrac{V_{max}[P7DHC]}{K_M+[P7DHC]}\right)$

118. $\dfrac{d([P7DHDES]V_{"Peripheral\,Tissure"})}{dt} = +V_{"Peripheral\,Tissue"}(K_1[PLAN])$

$-V_{"Peripheral\,Tissue"}\left(\dfrac{V_{max}[P7DHDES]}{K_M+[P7DHDES]}\right)$

$-V_{"Peripheral\,Tissue"}\left(\dfrac{V_{max}[P7DHDES]}{K_M+[P7DHDES]}\right)$

119. $\dfrac{d([PDES]V_{"Peripheral\,Tissure"})}{dt} = +V_{"Peripheral\,Tissue"}\left(\dfrac{V_{max}[P7DHDES]}{K_M+[P7DHDES]}\right)$

$-V_{"Peripheral\,Tissue"}\left(\dfrac{V_{max}[PDES]}{K_M+[PDES]}\right)$

120. $\dfrac{d([PAACoA]V_{"Periphral\,Tissue"})}{dt} = +V_{"Peripheral\,Tissue"}\left(\dfrac{V_f\left([PACoA][PACoA]-\frac{[PAACoA][PACoASH]}{K_{eq}}\right)}{[PACoA][PACoA]+K_M^B[PACoA]+K_M^A[PACoA]\left(1+\frac{[PCoASH]}{K_{iq}}\right)+\frac{Vf}{V_rK_{eq}}\left(K_M^Q[PAACoA]\left(1+\frac{[PACoA]}{K_{ia}}\right)+[PCoASH](K_M^P+[PAACoA])\right)}\right)$

$-V_{"Peripheral\,Tissue"}\left(\dfrac{V_{max}[PACoA][PAACoA]}{K_M^AK_M^B+[PACoA]K_M^B+[PAACoA]K_M^A+[PACoA][PAACoA]}\right)$

121. $\dfrac{d([PCoASH]V_{"Periphral\,Tissue"})}{dt} = +V_{"Peripheral\,Tissue"}\left(\dfrac{V_f\left([PACoA][PACoA]-\frac{[PAACoA][PACoASH]}{K_{eq}}\right)}{[PACoA][PACoA]+K_M^B[PACoA]+K_M^A[PACoA]\left(1+\frac{[PCoASH]}{K_{iq}}\right)+\frac{Vf}{V_rK_{eq}}\left(K_M^Q[PAACoA]\left(1+\frac{[PACoA]}{K_{ia}}\right)+[PCoASH](K_M^P+[PAACoA])\right)}\right)$

122. $\dfrac{d([PACoA]V_{"Peripheral\,Tissure"})}{dt} = +V_{"Peripheral\,Tissue"}(K_1[PACoAS])$

$-n_{pacoa}\cdot V_{"Peripheral\,Tissue"}\left(\dfrac{V_f\left([PACoA][PACoA]-\frac{[PAACoA][PACoASH]}{K_{eq}}\right)}{[PACoA][PACoA]+K_M^B[PACoA]+K_M^A[PACoA]\left(1+\frac{[PCoASH]}{K_{iq}}\right)+\frac{Vf}{V_rK_{eq}}\left(K_M^Q[PAACoA]\left(1+\frac{[PACoA]}{K_{ia}}\right)+[PCoASH]\left(K_M^P+[PAACoA]\right)\right)}\right)$

$-V_{"Peripheral\,Tissue"}\left(\dfrac{V_{max}[PACoA][PAACoA]}{K_M^AK_M^B+[PACoA]K_M^B+[PAACoA]K_M^A+[PACoA][PAACoA]}\right)$

123. $\dfrac{d([PACoAS]V_{"Peripheral\,Tissure"})}{dt} = -V_{"Peripheral\,Tissue"}(K_1[PACoAS])$

124. $\frac{d([PFPP]V_{"Peripheral\,Tissue"})}{dt} = +V_{"Peripheral\,Tissue"}\left(\frac{V_{max}[PGPP][PIPP]}{K_M^A K_M^B+[PGPP]K_M^B+[PIPP]K_M^A+[PGPP][PIPP]}\right)$

$-V_{"Peripaheral\,Tissue"}\left(\frac{V_{max}[PFPP]}{K_M+[PFPP]}\right)$

125. $\frac{d([PGPP]V_{"Peripheral\,Tissue"})}{dt} = +V_{"Peripheral\,Tissue"}\left(\frac{V_{max}[PDMAPP][PIPP]}{K_M^A K_M^B+[PDMAPP]K_M^B+[PIPP]K_M^A+[PDMAPP][PIPP]}\right)$

$-V_{"Peripheral\,Tissue"}\left(\frac{V_{max}[PGPP][PIPP]}{K_M^A K_M^B+[PGPP]K_M^B+[PIPP]K_M^A+[PGPP][PIPP]}\right)$

126. $\frac{d([PHMGCoA]V_{"Peripheral\,Tissue"})}{dt} = +V_{"Peripheral\,Tissue"}\left(\frac{V_{max}[PACoA][PAACoA]}{K_M^A K_M^B+[PACoA]K_M^B+[PAACoA]K_M^A+[PACoA][PAACoA]}\right)$

$-V_{"Peripheral\,Tissue"}\left(\frac{V_{max}[PHMGCoA]}{K_M+[PHMGCoA]}\right)$

127. $\frac{d([PIPP]V_{"Peripheral\,Tissue"})}{dt} = +V_{"Peripheral\,Tissue"}\left(\frac{V_{max}[PMV5PP]}{K_M+[PMV5PP]}\right)$

$-V_{"Peripheral\,Tissue"}\left(\frac{\frac{V_f[PIPP]}{K_M^S}-\frac{V_r[PDMAPP]}{K_M^P}}{1+\frac{[PIPP]}{K_M^S}+\frac{[PDMAPP]}{K_M^P}}\right)$

$-V_{"Peripheral\,Tissue"}\left(\frac{V_{max}[PDMAPP][PIPP]}{K_M^A K_M^B+[PDMAPP]K_M^B+[PIPP]K_M^A+[PDMAPP][PIPP]}\right)$

$-V_{"Peripheral\,Tissue"}\left(\frac{V_{max}[PGPP][PIPP]}{K_M^A K_M^B+[PGPP]K_M^B+[PIPP]K_M^A+[PGPP][PIPP]}\right)$

128. $\frac{d([PDMAPP]V_{"Peripheral\,Tissue"})}{dt} = +V_{"Peripheral\,Tissue"}\left(\frac{\frac{V_f[PIPP]}{K_M^S}-\frac{V_r[PDMAPP]}{K_M^P}}{1+\frac{[PIPP]}{K_M^S}+\frac{[PDMAPP]}{K_M^P}}\right)$

$-V_{"Peripheral\,Tissue"}\left(\frac{V_{max}[PDMAPP][PIPP]}{K_M^A K_M^B+[PDMAPP]K_M^B+[PIPP]K_M^A+[PDMAPP][PIPP]}\right)$

129. $\frac{d([PMV]V_{"Peripheral\,Tissue"})}{dt} = +V_{"Peripheral\,Tissue"}\left(\frac{V_{max}[PHMGCoA]}{K_M+[PHMGCoA]}\right)$

$-V_{"Peripheral\,Tissue"}\left(\frac{V_{max}[PMV]}{K_M+[PMV]}\right)$

130. $\frac{d([PMV5PP]V_{"Peripheral\,Tissue"})}{dt} = +V_{"Peripheral\,Tissue"}\left(\frac{\frac{V_f[PMV5P]}{K_M^S}-\frac{V_r[PMV5PP]}{K_M^P}}{1+\frac{[PMV5P]}{K_M^S}+\frac{[PMV5PP]}{K_M^P}}\right)$

$-V_{"Peripheral\,Tissue"}\left(\frac{V_{max}[PMV5PP]}{K_M+[PMV5PP]}\right)$

131. $\dfrac{d([PMV5P]V_{"Peripheral\,Tissue"})}{dt} = -V_{"Peripheral\,Tissue"}\left(\dfrac{\dfrac{V_f[PMV5P]}{\kappa_M^S}-\dfrac{V_T[PMV5PP]}{\kappa_M^P}}{1+\dfrac{[PMV5P]}{\kappa_M^S}+\dfrac{[PMV5PP]}{\kappa_M^P}}\right)$

$+V_{"Peripheral\,Tissue"}\left(\dfrac{V_{max}[PMV]}{K_M+[PMV]}\right)$

132. $\dfrac{d([PSQE]V_{"Peripheral\,Tissue"})}{dt} = +V_{"Peripheral\,Tissue"}\left(\dfrac{V_{max}[PSQ]}{K_M+[PSQ]}\right)$

$-V_{"Peripheral\,Tissue"}\left(\dfrac{V_{max}[PSQE]}{K_M+[PSQE]}\right)$

133. $\dfrac{d([PSQ]V_{"Peripheral\,Tissue"})}{dt} = +V_{"Peripheral\,Tissue"}\left(\dfrac{V_{max}[PFPP]}{K_M+[PFPP]}\right)$

$-V_{"Peripheral\,Tissue"}\left(\dfrac{V_{max}[PSQ]}{K_M+[PSQ]}\right)$

134. $\dfrac{d([PLAN]V_{"Peripheral\,Tissue"})}{dt} = +V_{"Peripheral\,Tissue"}\left(\dfrac{V_{max}[PSQE]}{K_M+[PSQE]}\right)$

$-V_{"Peripheral\,Tissue"}(K_1[PLAN])$

135. $\dfrac{d([EFC]V_{Excreted})}{dt} = +\left(K_{efc}[LFC][LCBA][LUBA]\right)$

136. $\dfrac{d([EUBA]V_{Excreted})}{dt} = +(K_1[LUBA])$

Section 3 Statistical analysis of parameters of EIS, CV, and DPV

Table A.5 Statistical analysis of the effect of adsorption time on parameters of EIS, CV and DPV.
Methylated DNA vs. unmethylated DNA. *p* values from one way ANOVA with Tukey post-hoc test for multiple comparisons. Green shading represents a statistically significant difference (*p*<0.05).

Time (Minutes)	R_{ct}	Peak to peak separation (CV200)	Peak to peak separation (CV50)	Peak Current (DVP)
1	0.901	1.000	0.807	1.000
2	0.912	1.000	0.957	0.640
5	0.389	0.002	0.248	0.002
10	0.304	1.000	1.000	0.077
15	0.965	0.000	0.000	0.865
20	0.408	0.000	0.000	0.018
25	0.481	0.000	0.000	0.953
30	0.000	0.000	0.000	0.000

Table A.6 Statistical analysis of the effect of rotation speed on parameters of EIS, CV and DPV.
Methylated DNA vs. unmethylated DNA. *p* values from one way ANOVA with Tukey post-hoc test for multiple comparisons. Green shading represents a statistically significant difference (*p*<0.05).

Rotation Speed (rpm)	R_{ct}	Peak to peak separation (CV200)	Peak to peak separation (CV50)	Peak Current (DVP)
0	0.051	0.002	0.033	0.000
1000	0.957	0.999	0.992	0.733
2000	0.000	0.000	0.0003	0.000
4000	0.169	0.112	0.429	0.353

Table A.7 Statistical analysis of parameters of EIS, CV and DPV for the determination of the limit of detection for methylated DNA.
Methylated DNA vs. 0nM. *p* values from one way ANOVA with Tukey post-hoc test for multiple comparisons. Green shading represents a statistically significant difference (*p*<0.05).

Concentration (nM)	R_{ct}	Peak to peak separation (CV200)	Peak to peak separation (CV50)	Peak Current (DVP)
1	0.273	0.298	0.971	0.000
10	0.000	0.000	0.000	0.000
25	0.000	0.000	0.000	0.000
50	0.000	0.000	0.000	0.000
100	0.000	0.000	0.000	0.000
200	0.000	0.000	0.000	0.000
400	0.000	0.000	0.000	0.000

Table A.8 Statistical analysis of parameters of EIS, CV and DPV for the determination of the limit of detection for unmethylated DNA.

Unmethylated DNA vs. 0nM. *p* values from one way ANOVA with Tukey post-hoc test for multiple comparisons. Green shading represents a statistically significant difference ($p<0.05$).

Unmethylated vs. 0nM	R_{ct}	Peak to peak separation (CV200)	Peak to peak separation (CV50)	Peak Current (DVP)
1	0.939	0.761	0.892	0.481
10	0.000	0.000	0.000	0.000
25	0.000	0.000	0.000	0.000
50	0.000	0.000	0.000	0.000
100	0.000	0.000	0.000	0.000
200	0.000	0.000	0.000	0.000
400	0.000	0.000	0.000	0.000

Table A.9 Statistical analysis on parameters of EIS, CV and DPV for determination of the concentration required to differentiate methylated and unmethylated DNA.

Methylated DNA vs. Unmethylated DNA. *p* values from one way ANOVA with Tukey post-hoc test for multiple comparisons. Green shading represents a statistically significant difference ($p<0.05$).

Concentration (nM)	R_{ct}	Peak to peak separation (CV200)	Peak to peak separation (CV50)	Peak Current (DVP)
1	0.996	1.000	1.000	0.107
10	1.000	0.279	0.075	1.000
25	0.009	0.000	0.816	1.000
50	0.000	0.000	0.000	0.000
100	0.000	0.000	0.000	0.000
200	0.000	0.000	0.000	0.000
400	0.000	0.000	0.000	0.000

Table A.10 Statistical analysis of parameters of EIS, CV and DPV for solutions of varying methylation.
p values from one way ANOVA with Tukey post-hoc test for multiple comparisons. Green shading represents a statistically significant difference (*p*<0.05).

R_{ct}	0%	25%	50%	75%	100%
0%		0.003	0.000	0.000	0.000
25%	0.003		0.098	0.000	0.000
50%	0.000	0.098		0.007	0.000
75%	0.000	0.000	0.007		0.001
100%	0.000	0.000	0.000	0.001	

CV200	0%	25%	50%	75%	100%
0%		1.000	1.000	0.124	0.003
25%	1.000		1.000	0.167	0.003
50%	1.000	1.000		0.168	0.003
75%	0.124	0.167	0.168		0.150
100%	0.003	0.003	0.003	0.150	

CV50	0%	25%	50%	75%	100%
0%		0.744	0.999	0.127	0.015
25%	0.744		0.590	0.602	0.095
50%	0.999	0.590		0.084	0.010
75%	0.127	0.602	0.084		0.639
100%	0.015	0.095	0.010	0.639	

DPV	0%	25%	50%	75%	100%
0%		1.000	0.018	0.005	0.000
25%	1.000		0.023	0.006	0.000
50%	0.018	0.023		0.881	0.001
75%	0.005	0.006	0.881		0.005
100%	0.000	0.000	0.001	0.005	

Table A.11 Statistical analysis on parameters of EIS, CV and DPV for the determination of the limit of detection for the EN1 amplicon from MCF-7 DNA.
MCF-7 DNA vs. 1X PBS. *p* values from one way ANOVA with Tukey post-hoc test for multiple comparisons. Green shading represents a statistically significant difference (*p*<0.05).

Fractional proportion of MCF-7 DNA	R_{ct}	Peak to peak separation (CV200)	Peak to peak separation (CV50)	Peak Current (DVP)
1/180	0.000	0.130	0.971	0.002
1/36	0.000	0.000	0.000	0.000
1/18	0.000	0.000	0.000	0.000
1/3	0.000	0.000	0.000	0.000

Table A.12 Statistical analysis on parameters of EIS, CV and DPV for the determination of the limit of detection for the EN1 amplicon from WGA DNA.
WGA DNA vs. 1X PBS. *p* values from one way ANOVA with Tukey post-hoc test for multiple comparisons. Green shading represents a statistically significant difference (*p*<0.05).

Fractional proportion of WGA DNA	R_{ct}	Peak to peak separation (CV200)	Peak to peak separation (CV50)	Peak Current (DVP)
1/180	0.000	0.165	1.000	0.044
1/36	0.000	0.000	0.000	0.000
1/18	0.000	0.000	0.000	0.000
1/3	0.000	0.000	0.000	0.000

Table A.13 Statistical analysis on parameters of EIS, CV and DPV for determination of the fractional proportion of secondary PCR product required to differentiate the EN1 amplicon from MCF-7 and WGA DNA.
MCF-7 DNA vs. WGA DNA. *p* values from one way ANOVA with Tukey post-hoc test for multiple comparisons. Green shading represents a statistically significant difference (*p*<0.05).

Fractional proportion of DNA	R_{ct}	Peak to peak separation (CV200)	Peak to peak separation (CV50)	Peak Current (DVP)
1/180	0.999	0.130	0.971	0.916
1/36	0.997	0.001	0.002	0.004
1/18	0.000	0.000	0.000	0.000
1/3	0.000	0.000	0.000	0.995

Table A.14 Statistical analysis of parameters of EIS, CV and DPV for solutions of varying methylation.
Methylated and unmethylated DNA derived from the EN1 amplicon of MCF-7 and WGA DNA respectively. *p* values from one way ANOVA with Tukey post-hoc test for multiple comparisons. Green shading represents a statistically significant difference (*p*<0.05).

R_{ct}	0%	25%	50%	75%	100%
0%		0.000	0.000	0.000	0.000
25%	0.000		0.000	0.000	0.000
50%	0.000	0.000		0.000	0.000
75%	0.000	0.000	0.000		0.000
100%	0.000	0.000	0.000	0.000	

CV200	0%	25%	50%	75%	100%
0%		0.205	0.000	0.000	0.000
25%	0.205		0.000	0.000	0.000
50%	0.000	0.000		0.314	0.000
75%	0.000	0.000	0.314		0.002
100%	0.000	0.000	0.000	0.002	

CV50	0%	25%	50%	75%	100%
0%		0.002	0.000	0.000	0.000
25%	0.002		0.001	0.000	0.000
50%	0.000	0.001		0.406	0.000
75%	0.000	0.000	0.406		0.001
100%	0.000	0.000	0.000	0.001	

DPV	0%	25%	50%	75%	100%
0%		1.000	0.170	0.000	0.000
25%	1.000		0.151	0.000	0.000
50%	0.170	0.151		0.010	0.000
75%	0.000	0.000	0.010		0.000
100%	0.000	0.000	0.000	0.000	